MSC-03742

THIRD ANNUAL EARTH RESOURCES PROGRAM REVIEW

VOLUME I
GEOLOGY AND GEOGRAPHY

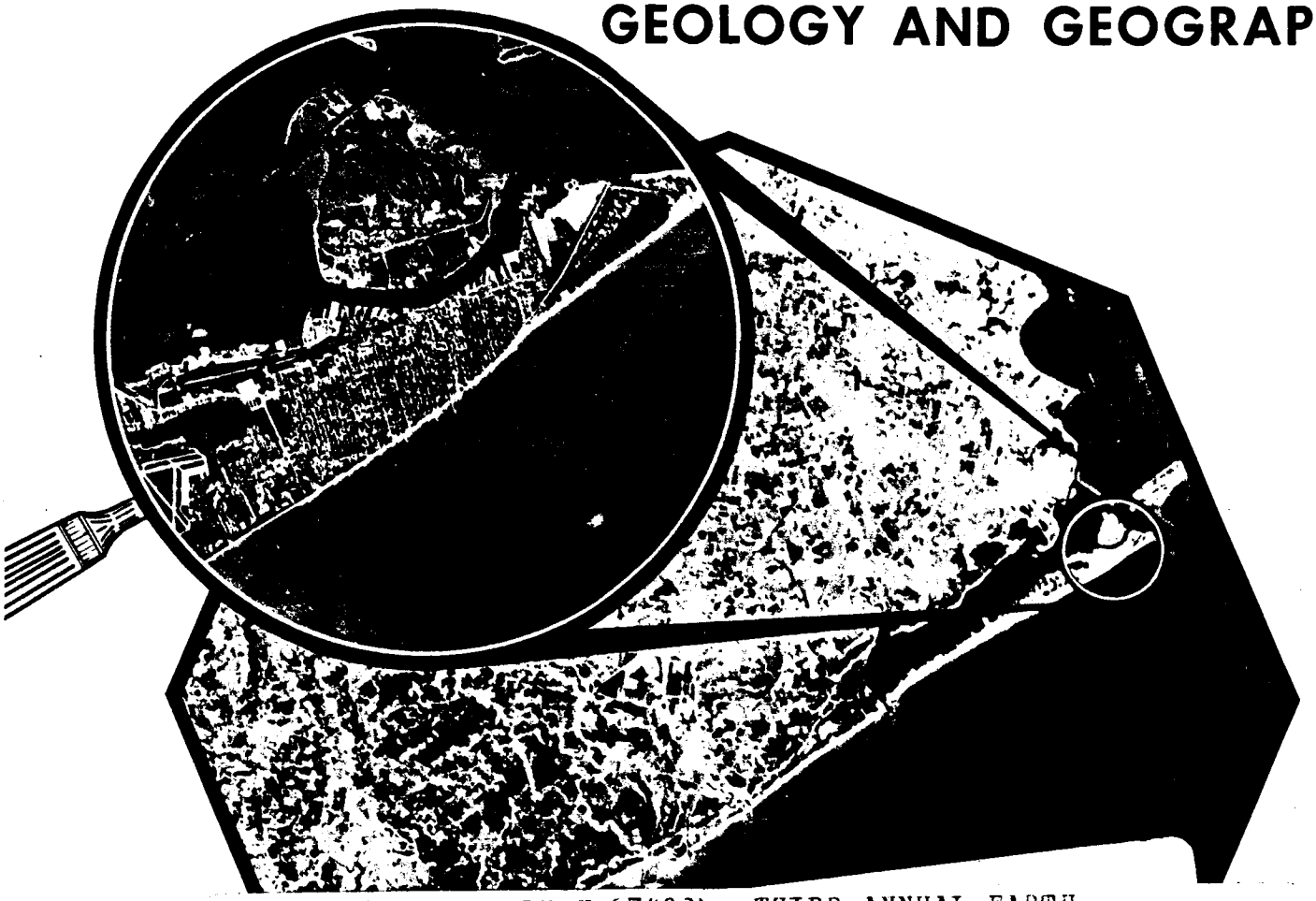

Presented at the
NASA Manned Spacecraft Center
Houston, Texas

December 1 to 3, 1970

FOREWORD

A review of various aspects of the Earth Resources Program was held at the Manned Spacecraft Center, Houston, Texas, December 1, 2, and 3, 1970. Particular emphasis was placed on the results of analysis of data obtained with the Manned Spacecraft Center and other aircraft which have contributed data to the program.

The review was divided into the disciplinary areas of Geology, Geography, Hydrology, Agriculture, Forestry, and Oceanography. Program investigators presented the results of their work in each of these areas. The material presented is published in three volumes:

VOLUME I — GEOLOGY AND GEOGRAPHY

VOLUME II — AGRICULTURE, FORESTRY, AND SENSOR STUDIES

VOLUME III — HYDROLOGY AND OCEANOGRAPHY

The review provided a current assessment of the program for both management and technical personnel. Note that the material presented represented the current status of ongoing programs and complete technical analyses will be available at a later date.

Where papers were not submitted for publication or were not received in time for printing, abstracts are used.

Color Illustrations Reproduced in Black and White

CONTENTS OF VOLUME I

CONTENTS OF VOLUME II

CONTENTS OF VOLUME III

TABLES

FIGURES

INTRODUCTORY COMMENTS ON

THE USGS GEOGRAPHIC APPLICATIONS PROGRAM

by

Arch C. Gerlach
Chief Geographer
U.S. Geological Survey
Washington, D.C.

Within the Department of the Interior, the U.S. Geological Survey's Geographic Applications Program is now in the third phase of its evolution. At the first program review, we reported progress in acquainting the Geographic profession with remote sensing technology and in stimulating considerable interest in the potentials of the resultant data applications. At the second program review, we reported on results achieved by funding selected, unsolicited research proposals from more than a score of universities, professional organizations, and commercial firms. In that way, many members of the Geographic profession acquired experience in using the new instruments and techniques. We now feel that FY 1970 marked the culmination of the exploratory phases of the Geographic Applications Program, and its shift in focus to a third phase: that of practical applications of remote sensing technology and data to current problems and operations of the U.S. Geological Survey, other Bureaus of the Department of the Interior, and other agencies engaged in related work.

This reorientation of the Geographic Applications Program has resulted in much closer coordination with the EROS Program, much more tightly defined flight requests, better control over research activities, and a new operational plan which is charted in Figure 1. The ecological approach upon which the current Geography program is largely based, requires a logically connected sequence of activities. These include INPUTS that combine: a) remote sensing data with b) multi-disciplinary spatial data from traditional sources, and c) geographic theory and techniques of environmental modeling. This third aspect of the INPUTS includes important elements of geographic knowledge of environmental conditions and human activities within study areas, which greatly expedites and adds validity to data handling and interpretation.

The combined INPUTS are then subjected to four SEQUENTIAL ACTIVITIES that involve: a) thematic mapping of land use and environmental factors; b) the dynamics of change detection; c) environmental surveillance to identify sudden changes and general trends, and d) preparation of statistical models and analytical reports. The broad objective of these SEQUENTIAL ACTIVITIES is to make the input data convertible into actions for environmental management and economic development. The immediate program GOALS on the way toward that ultimate objective, therefore, are: a) to develop a capability for rapid and reliable <u>prediction</u> of urban and regional developments, and of environmental change, b) to provide useful

information for policy formulation and management decisions, and c) to contribute to the improvement of land use and environmental quality.

Intermediate products spun off during the SEQUENTIAL ACTIVITIES of the Geographic Applications Program include: a) land use maps--such as the one of the southwestern United States at 1:1,000,000 (based on Apollo photography) completed this year by the Association of American Geographers under a USGS contract, or the map now being made at 1:250,000 of the Phoenix quadrangle area; b) an Atlas of Urban Change Detection, for which maps and taped data bases, coordinated with the 1970 census, are now being prepared for diverse urban areas included in the Census Cities Project; and c) reports synthesizing environmental quality assessments of selected areas.

An extremely significant factor in the whole Geographic Applications Program is the input of remote sensing data from high altitude aircraft and satellite platforms. Without synoptic overviews, multispectral imagery, and repetitive coverage at short time-lapse intervals, it would be impossible to achieve goals now in sight. I want to express here, on behalf of the Geographic Applications Program, our compliments to the MSC Aircraft Program on the conspicuous improvements that have been made this past year in precision of flights, quality of data, and acceleration of data delivery to investigators. I want also to take this opportunity to thank the Aircraft Program staff for their full cooperation, in every way possible, to acquire the data we have needed to carry out important steps in the current phase of the Geographic Applications Program.

Figure 2 contains a graphic summary of Geography test sites and related missions flown in FY 1970. Seventeen sites were covered for eight contractors, and 20 of the 27 Census Cities were overflown. During the year, there was a gradual decrease in the demand for the larger scale photography from low and medium altitude flights, and increasing use of the nine-sensor returns from high altitude (RB-57F) overflights that are transitional to the use of ERTS data. The dominance of RB-57F requirements during the latter part of FY 1970 is not fully reflected by Figure 2 because the 20 Census Cities are treated separately in the paper to be presented by James Wray.

For current operational efficiency, the Geographic Applications Program has been divided into four functional units dealing respectively with: 1) urban and metropolitan studies, including the Census Cities Project, the Atlas of Urban Change, and studies of the effects of urban communities on atmospheric energy; 2) regional studies, of which the Phoenix Pilot Project, the Northeast Corridor (megalopolis), the Southern California coastal zone and urbanized areas, and a portion of the Gulf Coast fit within current plans; 3) special projects, such as the MTF and Pollution studies, and concise experiments for Interior Department Bureaus, which will be reported upon by Gary North; and 4) plans and

program management, headed by Robert Alexander, Deputy Coordinator for the Geographic Applications Program.

NASA funding of projects for the Geographic Applications Program in FY 1970 was divided into four categories covered by approved Form 1122 budget requests under Task Nos. 16 (Environmental Impact), 32 (Land Use), 35 (Urban and Metropolitan Studies), and 58 (Census Studies). In FY 1971, the Environmental Impact and Census Studies were confined to urbanized areas and funded under Task 35. Task 32 was refocused from general land use studies to regional analyses that supplement Interior Department operational programs and serve as stepping stones toward the ultimate goal of using data from high altitude aircraft and satellites as a basis for national planning and policy making.

At this Third Program Review, three reports cover research under Task 35. They are by James Wray, Frank Horton, and Robert Pease, and deal respectively with the Atlas of Urban Change, Census Applications, and Energy Exchange Studies. Two reports under Task 32 will then be given by John Place and H. Grant Goodell, dealing respectively with regional studies of the Phoenix, Arizona 1:250,000 quadrangle area and Central Atlantic Coastal Zone. A third report under Task 32 has been prepared by Harry Mallon, Office of Emergency Preparedness, on "Applications of Multispectral Data to Natural Resource Inventory and Survey," but he could not be here to present it, and we do not have time to do so within the short time limits allowed each discipline this year. Consequently, we shall submit Mr. Mallon's report only for the published record of this review. Gary North will report briefly on Special Projects, jointly funded by NASA and the USDI EROS Program, including the MTF and Pollution Studies, as well as some projects undertaken by Interior Department Bureaus as part of the EROS Program. Finally, Robert Alexander will briefly summarize the reorganization and future plans for the Geographic Applications Program.

Because of the severely limited time constraints on discipline presentations at this Third Program Review, it was impractical for all of the Principal Investigators for Geographic Applications Program contracts to appear personally at this session. We have, however, arranged for James Wray to include in his report the principal achievements of Professor Simpson at Dartmouth College in preparing a land use map of metropolitan Boston, and Frank Horton to report in part on the achievements in urban analysis at Northwestern University under Professor Marble.

Without further introductory comment, I shall now introduce each speaker in the sequence listed on the program, and admonish each to limit his presentation to the scheduled time constraints in order to allow some time for discussion and to be fair to others on the program.

Geography Program Functions, Products, Clients, and Goals

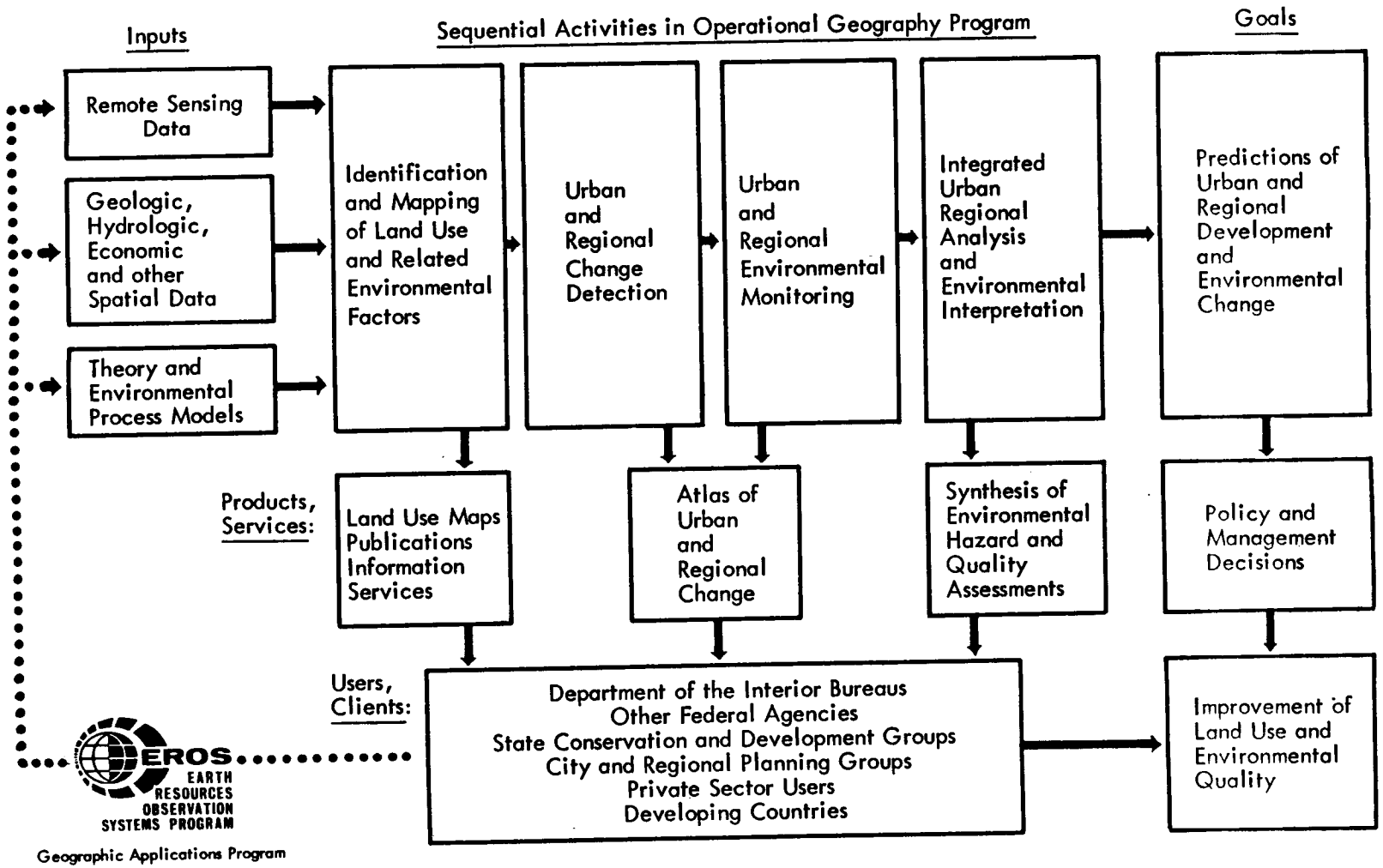

Figure 1

Aircraft Photo Missions, Geography Test Sites, FY-70

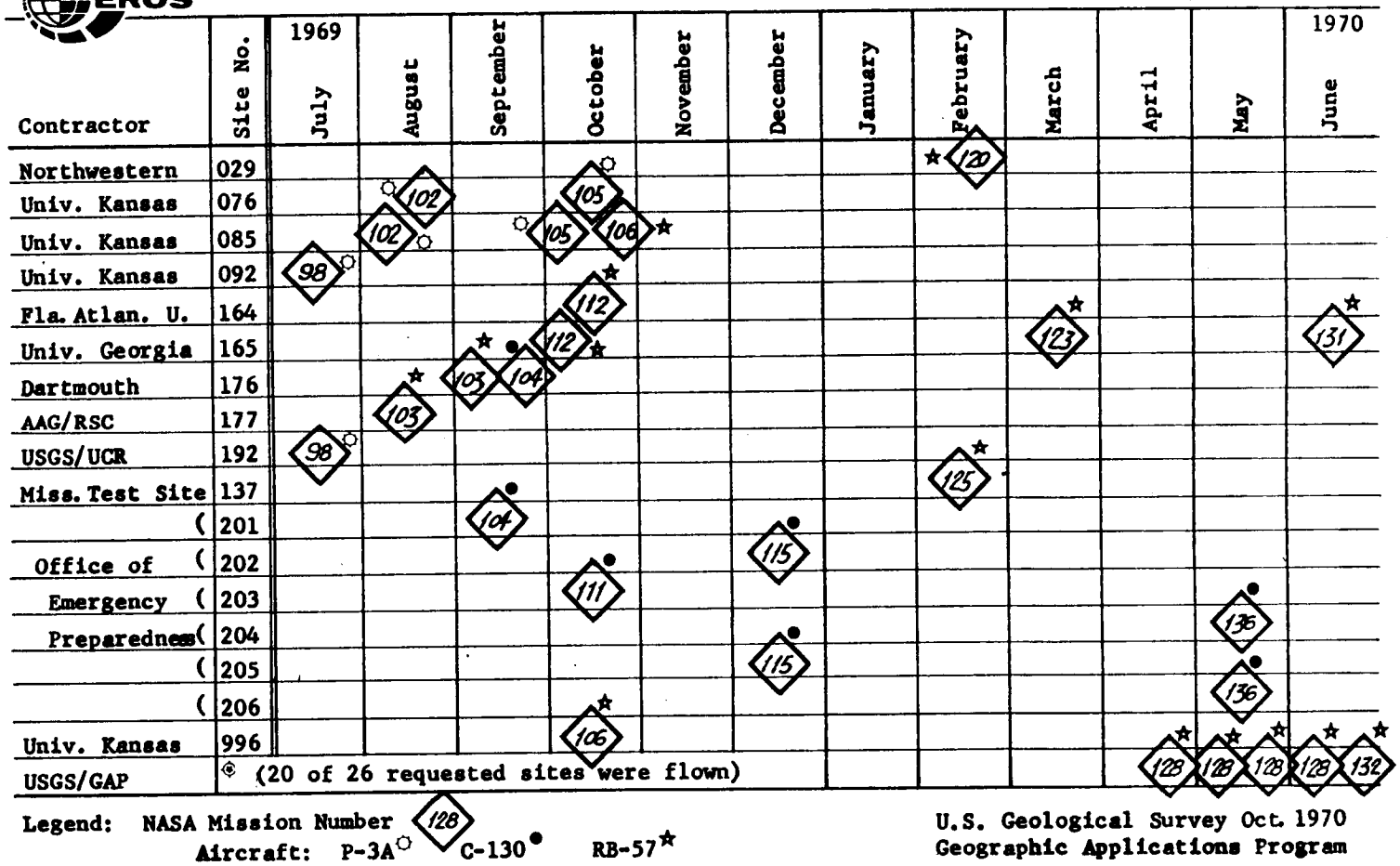

Figure 2

CENSUS CITIES PROJECT AND ATLAS OF URBAN AND REGIONAL CHANGE

by

James R. Wray
U.S. Geological Survey
Washington, D.C.

INTRODUCTION

A large segment of the USGS Geographic Applications Program is focused upon the urban applications of remote sensing. I cannot, in the time available, review all of our current urban work. However, the Program's current urban research goals can be demonstrated by an experiment on the combined use of sensors and census data, and of aircraft and spacecraft sensor platforms. Rewarding analytical experience has already been gained, and there is growing evidence that some real time uses will be realized. Early phases of this experiment received some attention as the "Census Cities Project," and one of the user oriented end-products will be a looseleaf "Atlas of Urban and Regional Change," hence, the double theme in the title of the paper.

The Census Cities Project has several related purposes: 1) to assess the role of remote sensors on high altitude platforms for the comparative study of urban areas; 2) to detect changes in selected U.S. urban areas between the 1970 census and the time of launching of an Earth-orbiting sensor platform prior to the next census; 3) to test the utility of the satellite sensor platform to monitor urban change as the 1970 census returns become available for small areas, and serve as a control for sensor image interpretation; 4) to design an information system for incorporating graphic sensor data with census-type data gathered by traditional techniques; 5) to identify and to design user-oriented end-products or information services; and 6) to ascertain what organizational capability would be needed to provide such services on a continuing basis.

All of these objectives apply also to regional problems except for scale. They imply a need to develop not only a spatial data information system, but also a methodology for detecting and interpreting change.

THE RESEARCH DESIGN

The design of the "Change Detection Experiment" is illustrated in Figure 1. In this figure each of the rectangles is a symbol representing a page in the Atlas of Urban and Regional Change, a user oriented

end-product. The horizontal rows represent steps in the research design. The vertical columns represent imagery and imagery interpretation at different times and from different sensor platforms. The experiment begins with the procurement of high altitude aircraft photography near the dates of the 1970 census for a sample of U.S. cities. From that photography a rectified mosaic is made for each city and is fitted with a rectangular coordinate system. The next step is to prepare an overlay showing the 1970 census statistical areas and their centroids. This overlay represents the interface between the census returns and the information generated from the aerial photography. The next step is to complete the land use analysis and measurement of land areas in each category and each census tract. An additional step, not illustrated in Figure 1, calls for listing the land use information for 1970 in computer-retrievable format.

When the Earth Resources Technology Satellite (ERTS) is launched in 1972, we will also receive high altitude aircraft photography over the same test sites, plus television imagery from the satellite itself. From the aircraft photography, we will make another land use analysis, but we will not need to repeat the making of a gridded mosaic or the overlay showing the census statistical areas. The new overlay will show changes detected between the 1970 land use and the 1972 land use. Besides the locational details recorded on the overlay, the new land use information will also be recorded in computer retrievable format. The 1972 land use analysis will be used as a basis for interpreting the imagery from the satellite. Thus, it will become possible to determine how well the imagery from the satellite can be used to detect the location, kind, and intensity of urban land use change between 1970 and 1972.

REMOTELY SENSED IMAGERY ACQUIRED TO DATE

Twenty-six urban test sites selected for this experiment are shown in Figure 2. A twenty-seventh test site is the Pittsburgh metropolitan area in southwestern Pennsylvania. These sites represent a ten percent rank-size sample of U.S. urban areas. Inland and coastal cities are represented and so also are most regions of the country. The preponderance of cities in the South is due to the availability of Gemini and Apollo photography for the lower latitudes. For twenty of the urban test sites, photo missions were completed during the April-to-July period when the 1970 census was being taken. Coverage is still needed for Seattle, Aurora, Midland, Tampa, West Palm Beach, Pittsburgh, and San Juan.

One of the test sites for which photography was received is the Washington Urbanized Area, NASA Test Site Number 230. Figure 3 shows the flight lines and area covered by that mission. The Washington coverage was acquired on NASA Mission 128d, June 28, 1970, with the

RB-57F aircraft flying at 50,000 feet above terrain. There were three north-south flight strips spaced about twelve statute miles apart. The diagram in the lower right corner shows the area covered by each of the cameras aboard the aircraft. The legend shows there were nine cameras, providing coverage at different scales and film-filter combinations.

Figure 4 is a diagram of the nine photo-sensors for a central frame over the Washington test site. On the left are sample frames from three metric cameras, and on the right, sample frames from six Hasselblad cameras. The cameras for the planning of the mission are the two RC-8s. Both cameras have a focal length of six inches, and produce an image scale of 1:100,000 at a flight altitude of 50,000 feet. One of these cameras has color infrared film with a minus blue filter. A portion of the RC-8 color infrared photo is shown in Figure 5. Each of the full RC-8 photos covers a square 14.2 statute miles on a side, or an area of 204 square statute miles. Photographs are taken with sixty percent overlap in line of flight and about thirty percent sidelap between flight lines. This provides stereoscopic coverage. A back-up camera is provided in the nine-inch by nine-inch film format. This is a Zeiss camera with a twelve-inch focal length lens. It procures pictures at 1:50,000 and covers a square 7.1 statute miles on a side or an area of 51 square statute miles. This camera also is loaded with color infrared film but the lens is fitted with a "D" filter. With the Zeiss camera there is edge-to-edge coverage in the line of flight, but there is a gap in coverage between flight lines.

The Hasselblad cameras all use 70 mm film. Three are loaded with black and white film, three with color film. Two of the cameras have a black and white panchromatic film, one filtered with a green filter and one with a red filter. The third contains black and white infrared film. These three cameras simulate the three television cameras which are expected to be aboard the ERTS platform. In the ERTS data handling systems these three different television images can be combined to form one false color image. The composite image is represented by the fourth camera, which contains color infrared film and the same minus blue filter used on the RC-8 cameras with color infrared film. The fifth camera contains panchromatic color film with a stronger blue filter for additional haze penetration. The sixth camera also has panchromatic film; it is filtered with a number three filter to render the scene about as you and I would see it looking through the camera sight at the time the picture was taken. Each of the Hasselblad cameras has a 40 mm focal length lens which covers about 178 square statute miles (slightly less than the RC-8 camera), producing an image scale of 1:382,000 from a flight altitude of 50,000 feet above terrain.

This same multispectral, census-contemporaneous imagery has been received for most of the urban test sites. This data base represents a truly unique opportunity for comparative urban study!

UTILIZATION OF THE IMAGERY

As called for by the research design, the first step in the analysis is the preparation of a rectified photo mosaic, fitted with a rectangular coordinate grid. Figure 6 shows a portion of the mosaic for Washington, D.C. This portion is a simulated page in the Atlas of Urban and Regional Change. The grid interval is one kilometer. The publication format will have a mosaic square 20 kilometers by 20 kilometers at 1:100,000. This square is placed to the left of the center on a page measuring 11 inches from north to south and about 14.7 inches each to west. This is the same size as one standard page used for computer printout. The right hand panel provides legend space for overprints or overlays. Pages may be bound at top or at left, or used singly, and folded into reports using conventional office stationery.

As in other experiments proposed for the Department of the Interior's Earth Resources Observation Systems (EROS), the Universal Transverse Mercator projection and rectangular coordinate system is in use, and all distances and areas are expressed in metric units. Geographic coordinates and bar scales in non-metric units will also be shown, however, and the various State Coordinate systems can be indexed for users who require them.

The UTM coordinate system will be used in several ways. It will be used to define the location of points, including the centroids of the statistical areas; to define mosaic sheetlines, thus permitting the presentation of thematic maps at multiple scales in the same publication page format; and also to provide a sheet numbering system. The squares will be used to measure distances and areas, and the grid lines provide approximate directional orientation. The square grid is an aid in image interpretation and thematic mapping compilation, and is also an aid in the training of map compilers and image interpreters. Users will reap the benefits.

The next step in the urban analysis is the preparation of an overlay showing the census statistical areas. A simulation of the census overlay is shown in Figure 7. The fine solid lines in the figure represent the census tract boundaries at the same scale as in Figures 6 and 8. The numbers represent the census tract identification. Some of the tract lines are state boundaries, county boundaries, or boundaries of incorporated cities. These delimit political areas and other "user" jurisdictions for planning and decision-making. A supplementary overlay would show additional point and line features appearing on the mosaic, or essential to its interpretation.

The next step is the analysis of area features, especially land use. This is illustrated in Figure 8, a simulated overlay or overprint

for the same area in Washington, D.C. The land use interpretation is done directly on an overlay to the color infrared photography at 1:100,000. The smallest mapping unit is a square 0.2 kilometer on each side, or four hectares, or about 11 acres. This is not much larger than the area covered by the blunt end of the color pencil used in the image interpretation. The minimum sized mapping unit is larger than the anticipated resolution cells. The legend shows the land use classification system presently being tested in the prototype analysis of the Washington test site. There are eight urban classes and five non-urban classes. Three of the classes are repeated, so there are really only ten different categories. The Urban and Non-Urban land use categories can be expanded or contracted according to the scale and minimum-size area for mapping purposes. Land ownership information garnered from "ground truth" may be shown on the supplementary overlay.

After mapping land use to the limits of the mosaic, a single boundary line is drawn around the central mass of "Urban" land uses. This is taken as the boundary of the urban area at the time of the photography. It becomes the "real estate" definition that will form the basis for comparison with other urban areas similarly delimited, or for analyzing changes in one urban area at different times.

The next step in the analysis is to measure the area of land in each land use category and to report the totals by census tract. The information for a particular time period is then stored in computer retrievable format. The land use overlays and area measurements for two different time periods will form the basis for change detection, and for the analysis of location, kind, and intensity of change.

STATUS OF CURRENT WORK

The graph in Figure 9 provides a frame of reference for reporting what the Census Cities Project has accomplished so far and what remains to be done. This figure is a graph, on which are plotted 213 U.S. Urbanized Areas having more than 50,000 population in 1960. Population is scaled on the X-axis. The Y-axis shows land area in square miles. The "Urbanized Area" is an official census delimitation of contiguous, built-up area around central cities of 50,000 or more population. Conterminous corporate municipalities, whether entirely built-up or not, are either wholly included, or wholly excluded. The minimum density is about one thousand persons per square mile. This definition is more inclusive than the corporate city; but it is less inclusive than the Standard Metropolitan Statistical Area, since the latter is comprised of whole counties. The Urbanized Area, then, is more nearly comparable to the contiguous mass of urban land use that is likely to be detected and delimited by interpretation of air photos and other sensors. Even so, a delimitation based on actual urban land use, as derived by image

interpretation, can effect more meaningful area comparison than a delimitation that may include large tracts of open unimproved land which happens to have corporate status. On the graph, the small dot in the upper left corner represents the New York Urbanized Area, with 14,000,000 persons on 1,800 square miles. The small dot in the lower right corner represents Mayaguez, Puerto Rico, with 53,000 persons on 4 square miles. Ranging between these extremes are all other urban areas. Some regional central tendencies can be discerned although they are not annotated on the graph as it is reproduced here. The Census Cities test sites are represented by the larger dots and are identified in the diagonal legend. This reads from left to right in population rank order and comprises roughly a ten percent sample. A similar model, refined by land use delimitation and regional interpretation, will be one result of our experiment. It will be used to estimate inter-censal population and to project the cost of analyzing land use in all U.S. urban areas.

Land use analysis is underway on the three largest urban test sites. The decision to begin with these was independent of their size rank. In FY 1970, high altitude, multispectral photographic coverage of the Boston area (Site 176) was twice flown for the Dartmouth College contract. Mission 103, September 1969, operated at 60,000 feet and Mission 128, July 1970, operated at 50,000 feet. During the summer of 1970, and beginning before Mission 128 was completed, the Dartmouth research team, headed by Professor Robert B. Simpson, mapped ten categories of land use for approximately 1,600 square miles of eastern Massachusetts. This includes much more than just the Boston Urbanized Area. Land use areas have been measured for nearly 600 census tracts. Summaries for the 1970 land use analysis by census tract are already in computer format. For a sample area, an experimental digital land use map, with area measurements, has also been computerized. The gridded photo mosaic for Boston has been completed by the U.S. Geological Survey. Meanwhile, for the Washington test site, the gridded photo mosaic has been finished and is now being prepared for publication. It will be presented on nine pages in the Atlas of Urban and Regional Change. Land use has been mapped for nearly half of the 1,200 square miles. The Metropolitan Washington Council of Governments, a potential user of this systems of change detection, is collaborating in this work. For all Urbanized Areas, the Bureau of the Census has provided preliminary data for the 1970 delimitations. Our own delimitations, based on analysis of 1970 land use, will be compared with the 1970 census returns when data by census tract become available.

Work is also underway for the the San Francisco test site, and negotiations are underway for analysis of two smaller urban areas. We aim to have some of these pilot studies essentially completed by late spring, 1971. At that time, we will expose this work to critical review by urban scientists and by prospective management "users." We were fortunate to receive the census-contemporaneous photography for twenty of our test sites. Funding for the current fiscal year, however, would

not allow completion of the analysis of even the five areas underway had not reinforcements been provided after the work was begun. Both Federal and local interest is keen, and getting keener.

In all on-going work special attention is being given to the identification of urban environmental problems which can be studied by spatial analysis--including the use of remote sensors. And we are giving attention to the identification and direct involvement of prospective users in the applications of remote sensing techniques to the solution of environmental problems.

There are two allied concerns which are also on our agenda. One is development of a methodology for urban change detection. The other is design of a spatial data information system that combines remote sensing data with other data for use in change detection, and then in the analysis and interpretation of change. These concerns will be discussed in another paper.

Change Detection Experiment

Geographic Applications Program — EROS EARTH RESOURCES OBSERVATION SYSTEMS PROGRAM

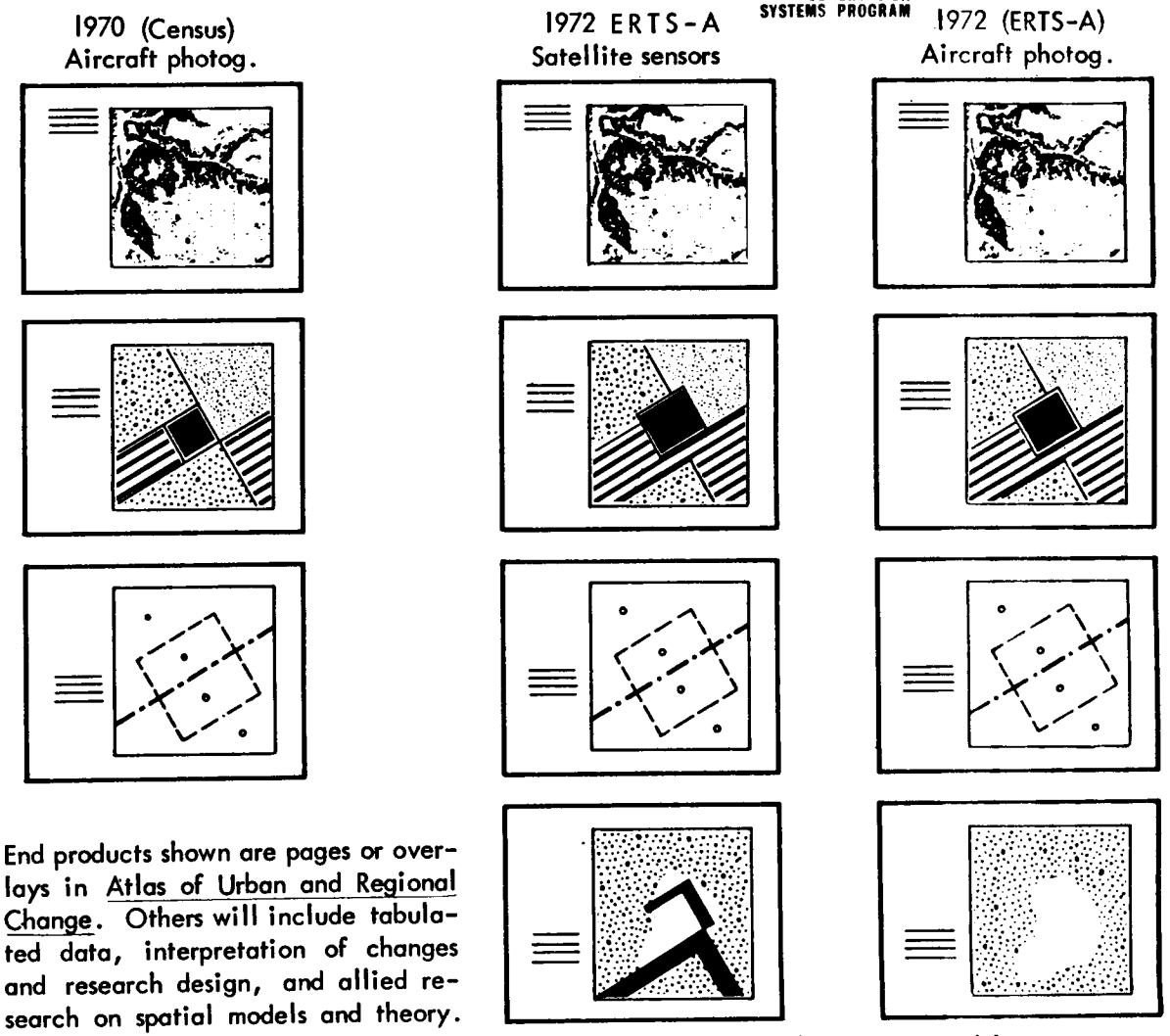

End products shown are pages or overlays in Atlas of Urban and Regional Change. Others will include tabulated data, interpretation of changes and research design, and allied research on spatial models and theory.

U.S. Geological Survey April 1970

Figure 1.- Steps and sensor components in urban change detection experiment.

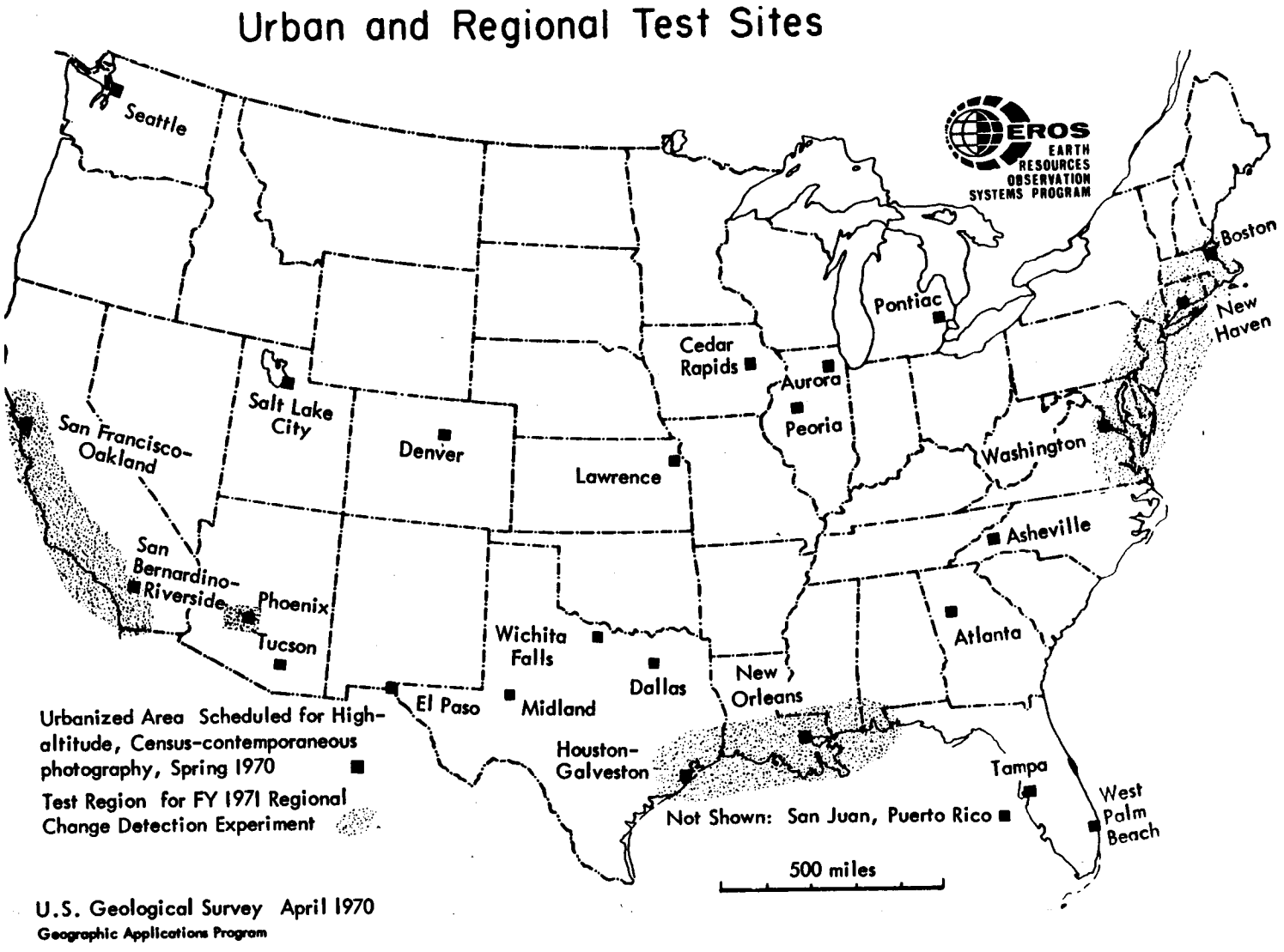

Figure 2.- Map showing urban and regional test sites.

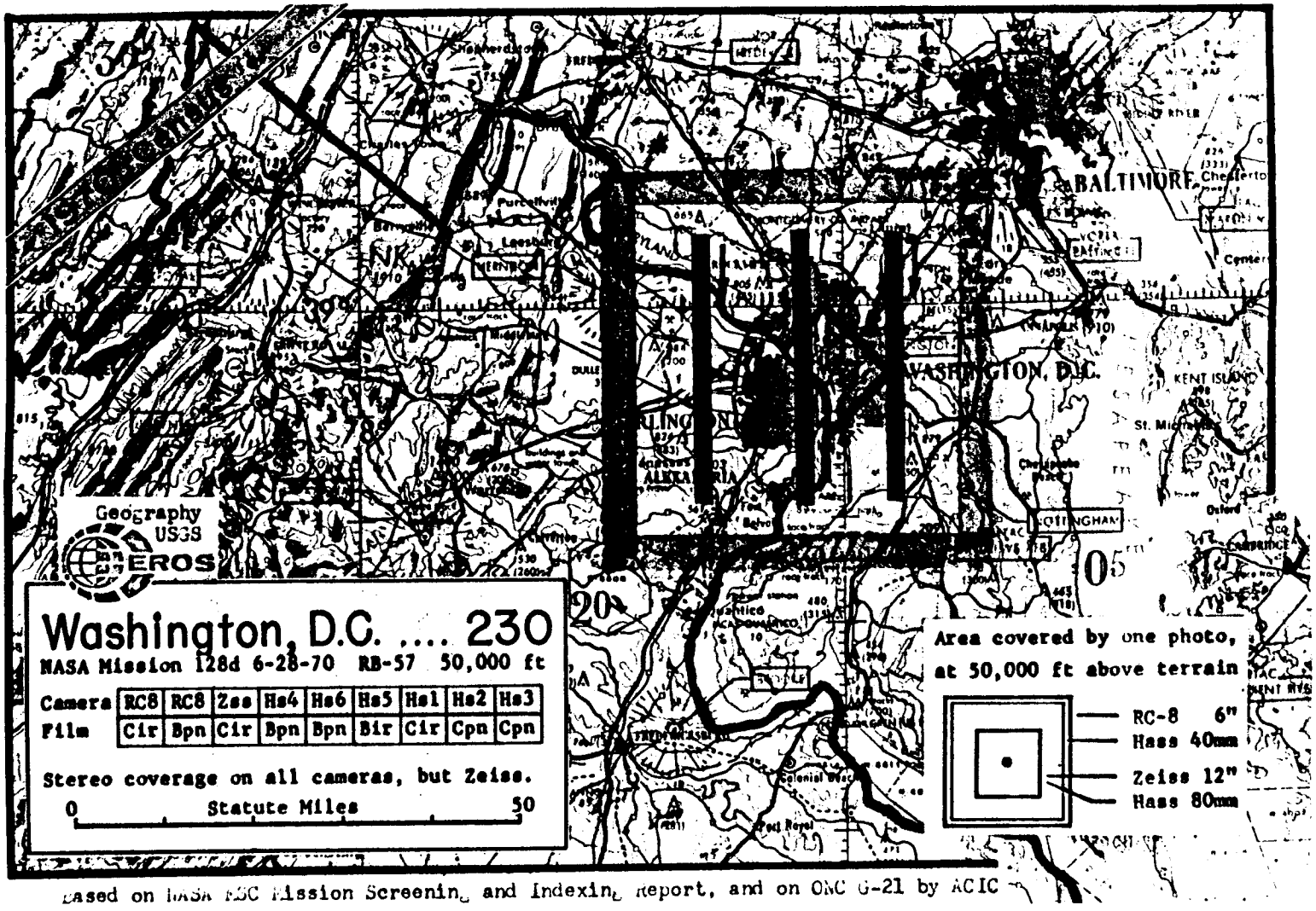

Figure 3. - Map showing flight lines and sensor coverage area, Mission 128, Washington, D.C.

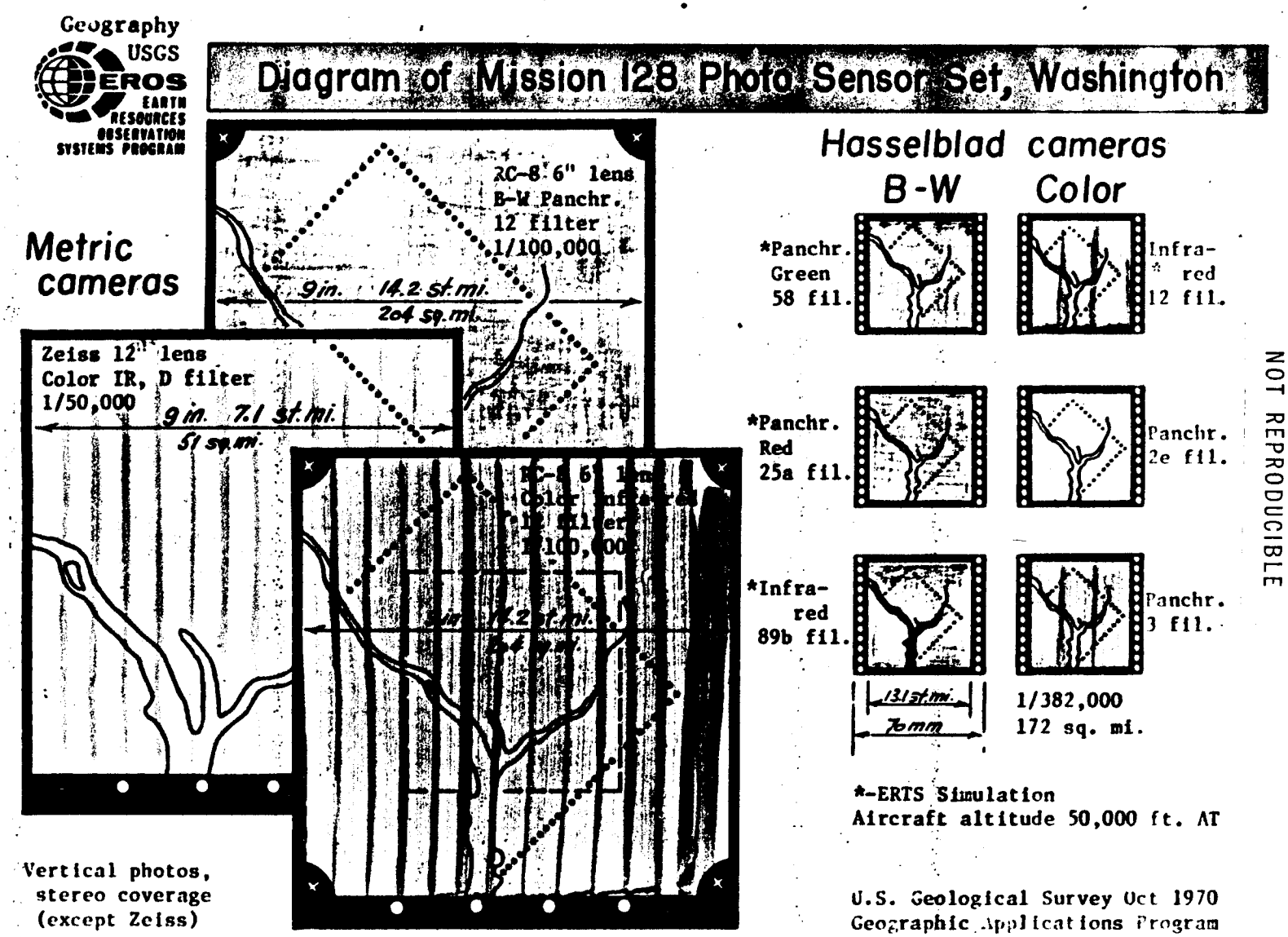

Figure 4.- Diagram of photo sensor set, one frame per camera, Mission 128, Washington, D.C.

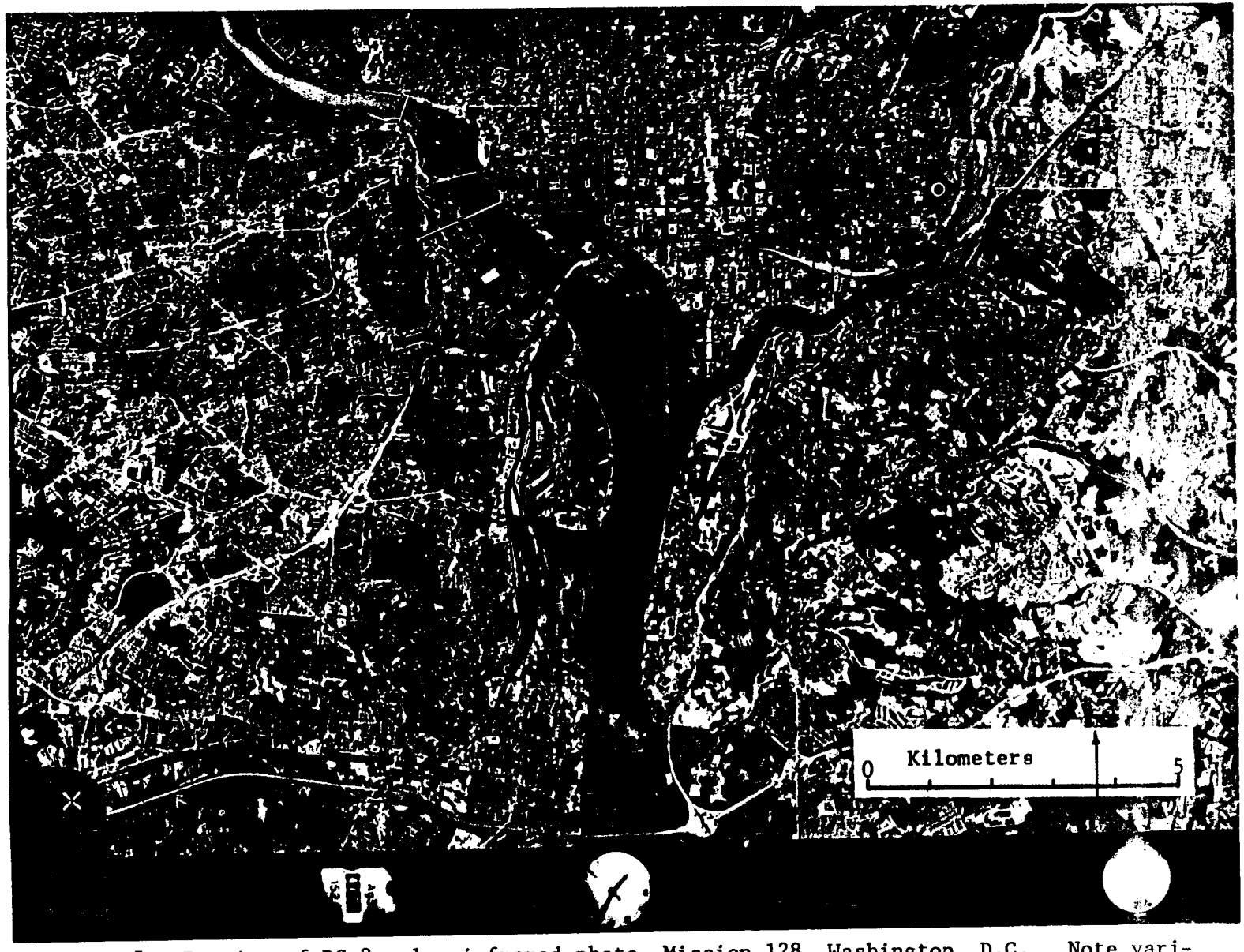

Figure 5.- Portion of RC-8 color infrared photo, Mission 128, Washington, D.C. Note variation in density of vegetation cover within the urban area as well as at its periphery.

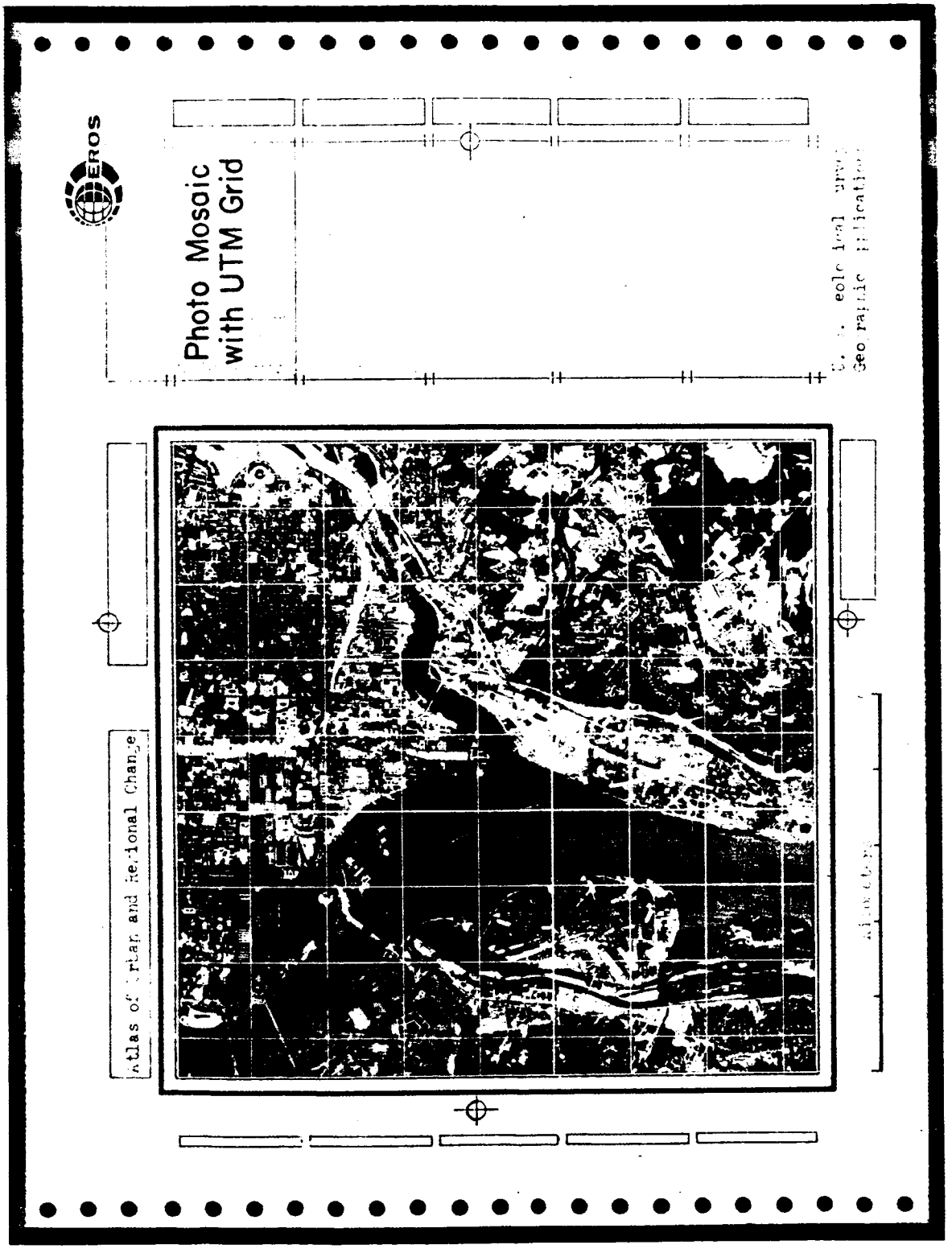

Figure 6.- Atlas of Urban and Regional Change, simulated page with gridded photo mosaic.

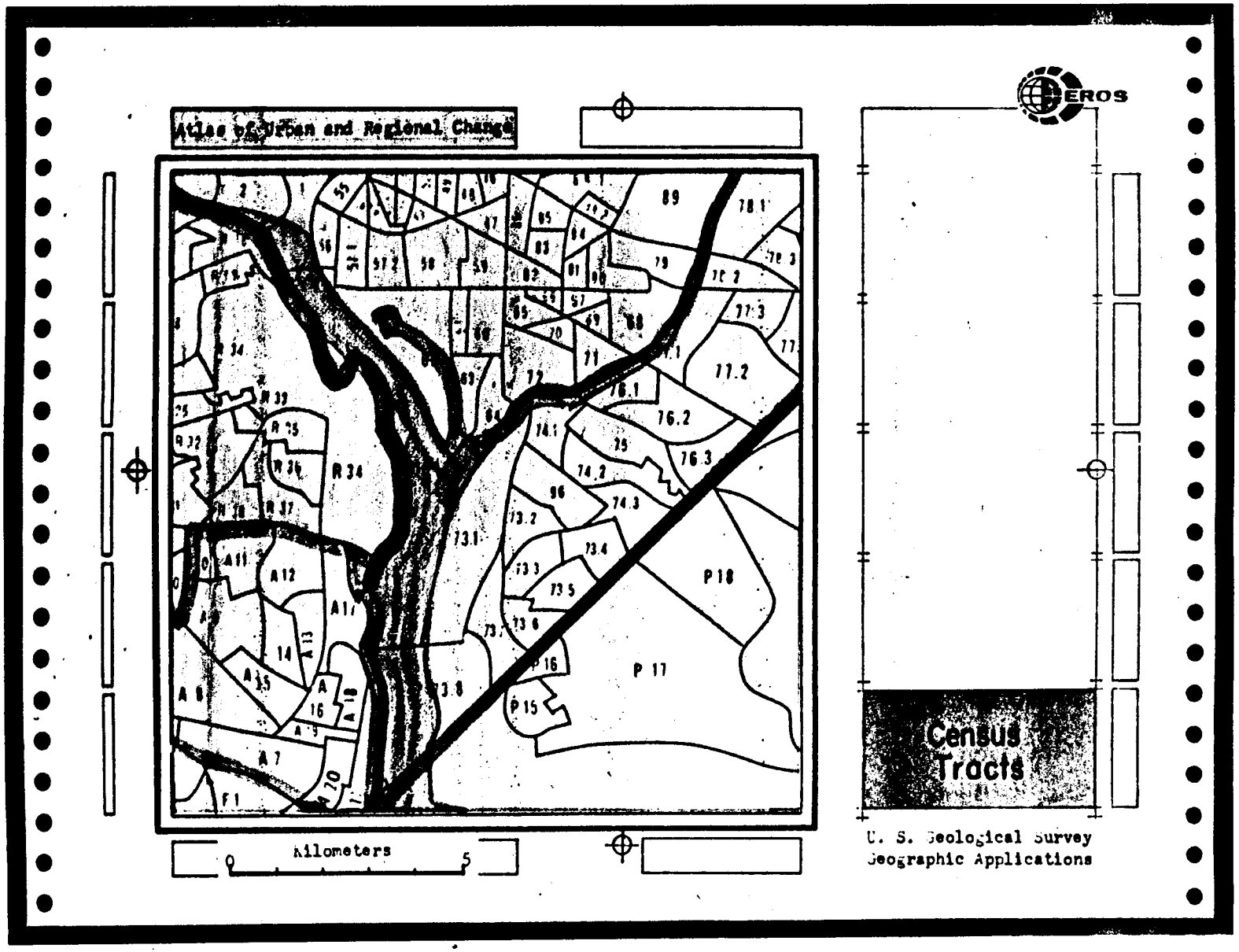

Figure 7.- Atlas of Urban and Regional Change, simulated page with Census Tract boundaries.

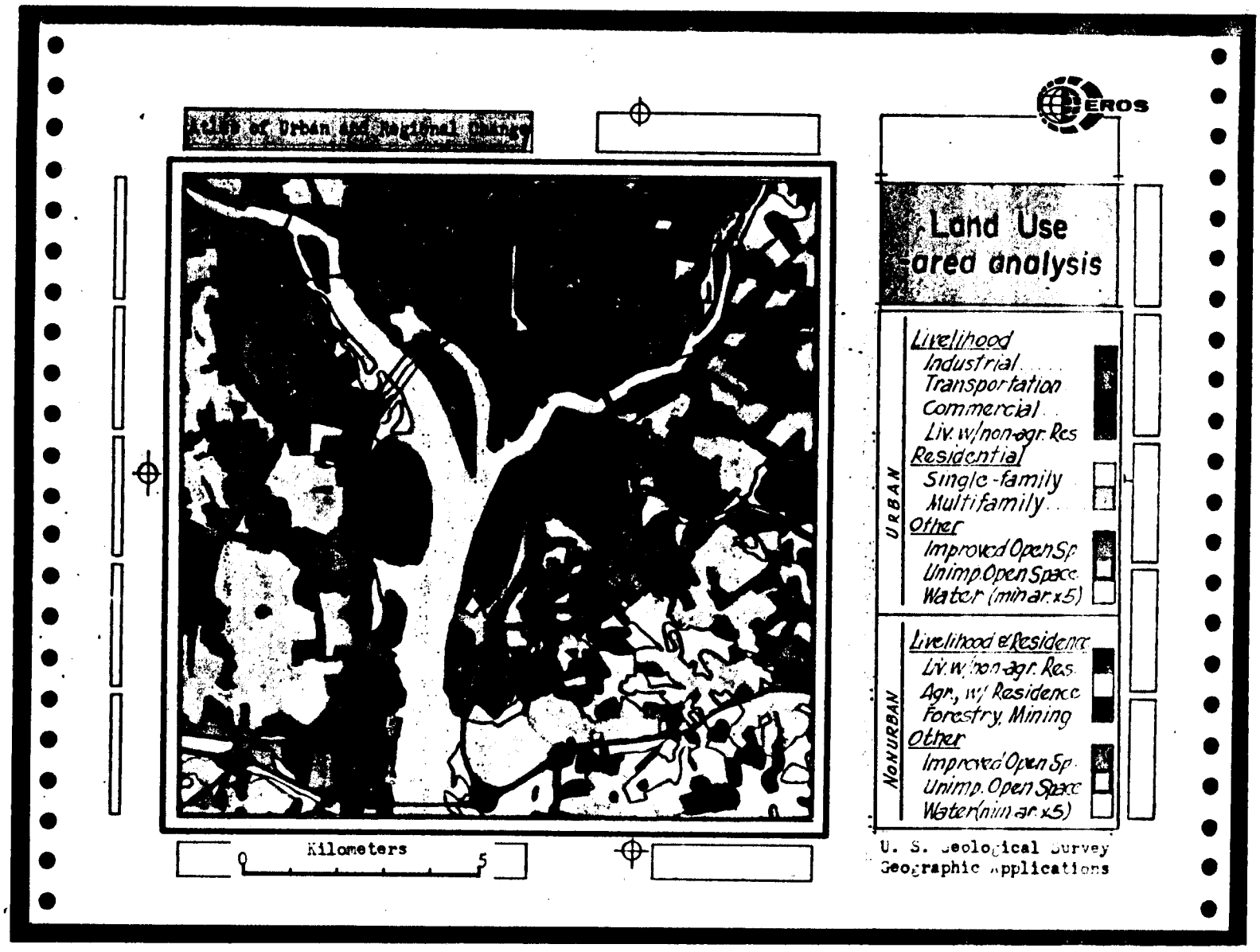

Figure 8.- Atlas of Urban and Regional Change, simulated page with land use interpretation compiled directly over the color infrared photo.

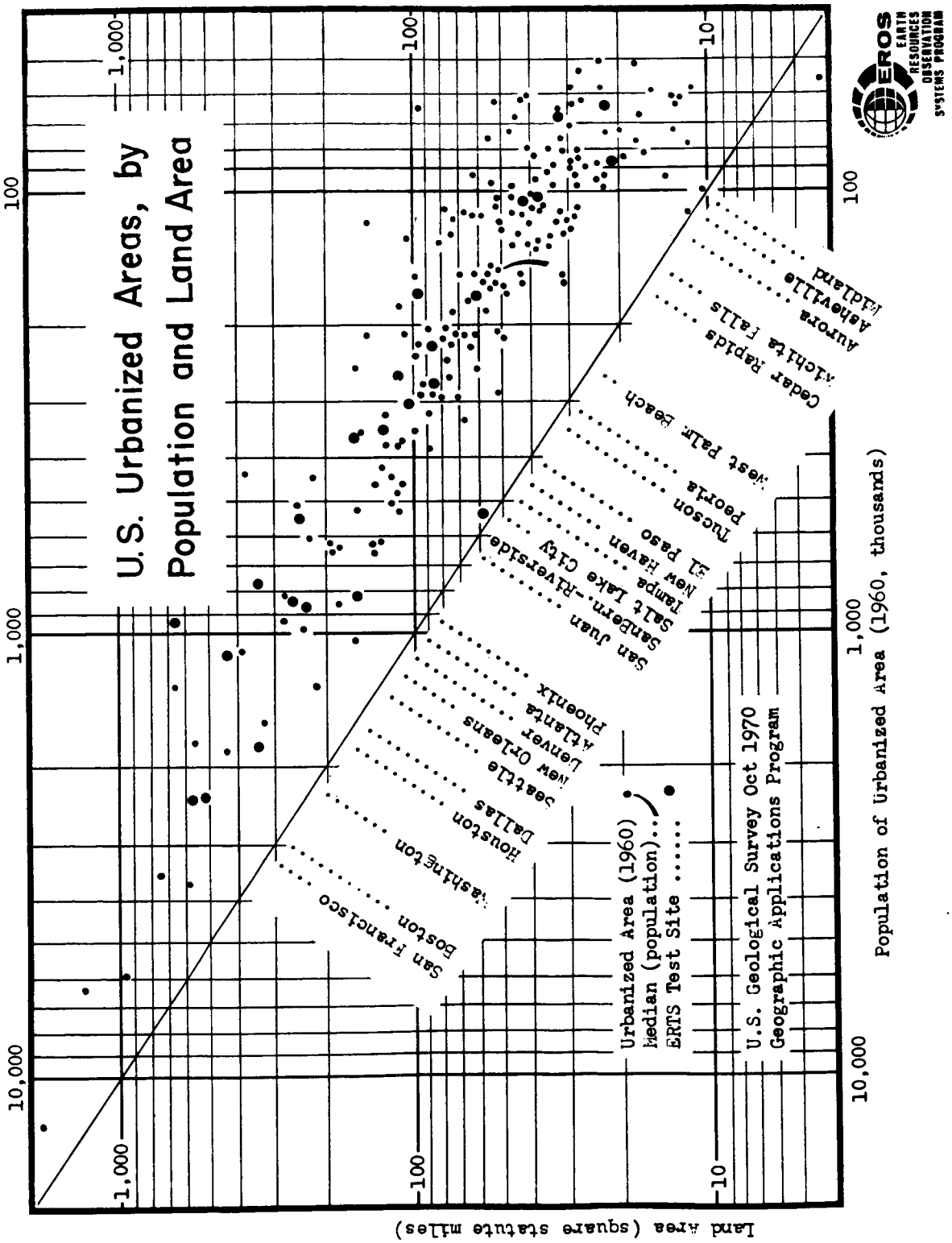

Figure 9.- U.S. Urbanized Areas, 1960, by Population and Land Area. Note ERTS test sites.

THE APPLICATION OF REMOTE SENSING TECHNIQUES TO SELECTED INTER AND INTRA URBAN DATA ACQUISITION PROBLEMS

by

Frank E. Horton
Institute of Urban and Regional Research
University of Iowa
Iowa City, Iowa

This paper will discuss two separate research endeavors: (1) research completed in the Geography Department at Northwestern University and (2) research currently being conducted at the Institute of Urban and Regional Research, University of Iowa.

RESEARCH COMPLETED AT NORTHWESTERN UNIVERSITY

Research directed toward identifying the utility of remote sensing techniques to urban data acquisition problems in several distinct areas has been completed at Northwestern University. These research endeavors include a comparison of remote sensing systems for urban data collection, the extraction of housing quality data from aerial photography, utilization of photographic sensors in urban transportation studies, urban change detection, space photography utilization, and an application of remote sensing techniques to the acquisition of data concerning intra-urban commercial centers. Much of this work has been reported elsewhere and at prior meetings or is not specifically related to NASA aircraft or spacecraft generated photography.[1] Since a final report will be available shortly, the first portion of the paper will focus on three of the several experiments carried out under the direction of Dr. Duane F. Marble at Northwestern University.[2]

An Extension of Previous Housing Quality Studies

The first experiment was an extension of a housing quality study completed previously in the United States. Its purpose was to evaluate techniques developed in various cities in the United States as to their applicability in a cross-cultural context.

The imagery consisted of 9 x 9 transparencies, both color and color infrared obtained at an altitude of 5,000 feet over San Juan, Puerto Rico. It should be pointed out that high reflection areas were over-exposed, filter combinations on the infrared lens resulted in monochromatic transparencies, certain frames were badly out of focus apparently as a result of defective motion compensation and the generally smaller structures and more crowded conditions in San Juan combined to make observations of ground truth variables per se at the parcel level impossible. However, these factors did not completely preclude block level evaluation. Ultimately, six variables were generated from the imagery:

1. total area,
2. percent area with live vegetation,
3. percent area not covered by roofs,
4. a ratio of area to number of houses,
5. perimeter, and
6. a width-length index.

These data were subjected to a principal components analysis and a statistical grouping routine was applied to the components scores, both rotated and unrotated, and in combinations of numbers from one to six. The results indicated that the experiment was generally unsuccessful due to poor resolution qualities of the imagery. Thus, the success or failure of the procedure as defined in previous studies, particularly the Los Angeles study, is not a pertinent question in this case.[3]

Residential Dynamics

Utilizing a variety of scale and resolution imagery generated by NASA as well as other sources, a preliminary analysis of the study of urban dynamics, or more appropriately in this case residential dynamics, was completed.[4]

The residential change detection analyses were performed using three different sets of imagery taken over Phoenix. The first was Apollo 9 color photography with subsequent color transformations as well as simulated orbital 70 mm. photography from Mission 120. Both of these sources primarily provided gross dimensions of urbanization, i.e., urban land, idle land, agricultural land, and major cultural features such as expressways.

The second set of photography was generated by the RB 57 overflight. This imagery included color, black and white, and black and white infrared as well as 70 mm. photography at scales of 1-60,000 and 1-100,000. The 1-60,000 scale photography allowed for a four part classification of the state of housing developments which included:

1. pre-construction,
2. partial construction,
3. almost completed with roof elements in place,
4. finished and landscaped.

The final set of black and white imagery at the scale of approximately 1-30,000 was provided by Landis aerial surveys. This imagery provided for a housing construction classification using six classes which included:

1. undeveloped,
2. cleared,
3. foundation is defined,
4. vertical structured,
5. roofed, and
6. landscaped.

The results of this research which utilized straight forward photo-interpretation techniques, indicate several useful findings. Low resolution, high altitude photography is suitable for examining large urban areas, as Phoenix in this case, where there is a rapid lateral change in the city's ground occupants. For cities on the eastern seaboard, for instance, which have exhausted most available land within their political boundaries and which are consequently changing vertically rather than horizontally, the straight forward photo-interpretation described here will probably not suffice.

Reliable measures of imaging frequency are obtainable and can be determined once the rate of change is determined. The real problem is the detection of a substantial initial change in the urban environment. In the absence of regular interval remote imagery, this information must be obtained from some other data source. Using remotely sensed imagery it is necessary to seek out some basic datum which can reasonably be supposed to be indicative of contemporary urban change. The street pattern would seem to be suitable within this framework. The evidence in this study shows that it is without doubt possible to detect areas of great change within the urban configuration, to monitor it and to derive measurements of the dynamics of change. The present available ranges from the frequent low level, high resolution study, offering instant change detection and precise details of the process to the high altitude, low resolution study offering only the grossest measures of change over extensive periods.[5]

The Identification of Intra-Urban Commercial Centers and their Functional Makeup

The third project discussed here was primarily directed toward the identification of intra-urban commercial centers and their functional makeup.[6] Two sets of imagery for Phoenix were utilized. The 1-60,000 black and white imagery, mentioned previously and the 1-23,000 black and white photography provided by Landis aerial surveys. The two objectives of the study were identification of commercial centers and the identification of characteristics of commercial centers which were identified:

Given the type of imagery utilized in the study, it is clear that commercial centers can be identified. However, when proceeding to evaluate the functional makeup of the centers from variables derived from imagery we are somewhat restricted. In the main, it would appear that large or first order centers are capable of being defined, while lower order centers have overlapping functional mixes. The general problem is one of defining appropriate breaks in a functional continuum. That is, the basic premise that centers can be conveniently grouped into different orders of functional complexity is only partially valid. Ten variables were chosen to represent criteria appropriate for disaggregating the total number of centers into their appropriate hierarchical position. These variables were as follows:

1. distance to the center from the central business district,
2. distance to the center to the nearest commercial center,
3. distance to the center to the nearest center of equal or greater size,
4. a subjective rank ordering of centers on the basis of building size,
5. a subjective rank ordering of centers on the basis of arterial street size,
6. distance of the center from the nearest industrial facility,
7. number of homes within half of a mile of the commercial center,
8. number of lanes of automobile traffic on arterial streets passing the center,
9. size of buildings in the commercial center, and
10. size of parking lot in the commercial center.

Not all ten of these variables could be retrieved from both data sets; only the first six were acquired from both the large and small scale photography. An important finding was that the relative difference in precision from the changes in the scale of photography, indicated that 1-60,000 photography would suffice for this analysis. Distinctive functional characteristics of the centers could be identified using the variable set previously mentioned. Variation did occur with respect to the correct assessment of several minor functions. These minor functions and the misallocation which occurred because of them would indicate that further research with respect to which functions can accurately be assessed is necessary. However, this experiment does add further credence to the contention that socio-economic variables can be derived from variables related primarily to the physical environment.

RESEARCH CURRENTLY UNDERWAY AT THE INSTITUTE OF URBAN AND REGIONAL RESEARCH, UNIVERSITY OF IOWA

The final portion of this paper will focus on the work being conducted at the Institute of Urban and Regional Research at The University of Iowa. Two basic research themes are being explored at Iowa: (1) the first focuses on the systematic evaluation of variable extraction for urban modeling and planning at several different scales, and (2) the second centers on the derivation of models for identifying and predicting

economic growth and change within a regional system of cities.

Intra-Urban Research

In order to systematically reach the goals which are implicit in both of the research themes listed above, the Institute of Urban and Regional Research is currently pursuing three research aims, the first of these is to evaluate the capability of photographic sensors at various scales to replicate an existing land use file used by the Washington, D.C. Council of Governments in their planning endeavors. The second objective is to evaluate at various scales the utility of photographic sensors in estimating population and dwelling units for small areas within cities. The third objective is to evaluate our ability to extract data from low resolution space photography which is important to the understanding and planning of large scale urban systems and their change over time.

In the first project land use data compiled and used by the Washington Council of Governments is being used as reference data. NASA imagery generated by the RB 57, on Mission 128, which includes color infrared transparencies at a scale of 1-50,000 and 1-100,000, and 70 mm. photography at a 1-400,000 scale, in the June 1970 flight over Washington, D.C. is being used as raw data by the Iowa researchers. Additional photography from a variety of sources was used to put together an imagery set at a scale varying from 1-11,500 to 1-13,500. Therefore land use definition from all four scales can be evaluated. The land use classification used by the Washington, D.C. Council of Governments includes:

1. residential,
2. industrial/storage,
3. education,
4. transportation/communication/utilities,
5. consumer services,
6. offices,
7. institutional,
8. public assembly,
9. parks and recreation, and
10. underdeveloped and resource uses.

The only data set completely evaluated to date is the 1-11,500 to 1-13,500. While a variety of discrepancies were noted between the Washington, D.C. Council of Governments data file and those emanating from the 1-11,500 to 1-13,500 photography, many of the errors were oriented toward differences in land use definition.[7] Currently work is proceeding on the 1-50,000 scale photography using the same classification and will proceed to the 1-100,000 and 1-400,000 imagery shortly.

The second phase of the study concentrates on estimating population and dwelling unit information by census tract. It is based on the same imagery provided for the Washington, D.C. area mentioned previously. However, only the 1-50,000, 1-100,000, and the 1-400,000 scale imagery will be evaluated. In a broader context, socio-economic variables such as population and dwelling units could also be estimated by including lag variables in the analysis, i.e. the counts of population and dwelling units which were derived at an earlier point in time such as those developed by the Census; change variables, i.e. monitoring the number of persons moving into and out of an area, or the number of dwelling units constructed and demolished, etc.; and imagery derived variables, i.e. those variables which can be measured directly or indirectly from imagery. In order to pursue this line of research an urban change detection model has been formulated which includes first a vector of imagery derived variables and secondly a vector of lag variables. The following is a tentative listing of dependent variables which presumably can be specified as a function of the variables extracted directly or indirectly from imagery and the lag variables to be used in the investigation in the Washington, D.C. area:

1. population,
2. number of households,
3. number of housing units,
4. number of single family units,
5. number of two family units,
6. number of multiple family units, and
7. population density.

The imagery derived variables to be analyzed include:

1. total land area,
2. predominantly residential land area,
3. net residential land area,
4. number of single family structures,

5. number of multi-family structures,
6. distance to CBD,
7. central city or suburban,
8. predominant land use,
9. density of single family structures,
10. density of multi-family structures, and
11. age of predominant proportion of the census tract.

The lag variable set includes:

1. population,
2. number of households,
3. number of housing units,
4. number of single family units,
5. number of two family units,
6. number of multi-family units, and
7. population density.

The model described above will be calibrated and tested by standard statistical techniques.[8] For calibration, the dependent variables will be taken from the 1970 Census data. Data acquired from the imagery will be used as the independent variables for testing purposes. Some data from the 1960 Census will be evaluated as to their usefulness as lag variables. Two classes of models will be calibrated: (1) the first for estimating variables in suburban tracts, and (2) a model for estimating variables in central city tracts. As was the case with land use, one of the objectives of this investigation is to evaluate information gains and losses due to scale differences as well as capability to define population and dwelling unit variables.

Inter-Urban Research Activities

The preliminary focus of the systems of cities study has been on evaluating the quality of information which can be extracted from imagery taken from space platforms.[9] Both subjective and automatic interpretation techniques are being evaluated utilizing Apollo 9 photography of the Atlanta, Georgia region. This portion of the project will be combined with other studies denoted in the remote sensing literature to define the confidence with which researchers and operational planners can expect from this data source. Sections and portions of the study will involve the development and application of models of urban spatial structure to

determine important characteristics of the spatial ordering of the hierarchy of cities found within the study region.

Analysis of the utility of microdensitometers and a new optical scanning device developed at the University of Pennsylvania and its application in identifying the extent and attributes of urban systems within a regional context is currently underway. Through the application of inferential statistics, it is expected that settlement size coefficients will be developed, change in built-up areas and regional changes in built-up areas will be defined, and the relationship between area and population size and functional complexity will be specified. Various graphic tools for the planning process will be generated. These include maps of the observed areas, maps of computed areas, and maps of the differences. Also to be completed are maps of changes in built-up areas, percent of urbanized area map, and the development of maps and other cartographic materials to identify population density declines and urban population throughout the region. Using this information as a foundation, a full scale regional central place model will be constructed which can be used in identifying central place hierarchies, predicting settlement size changes, and specifying the potential and probable changes in the location of industrial development, as well as secondary and tertiary activities.

CONCLUSION

Both from the research completed at Northwestern University and that being carried on at the Institute of Urban and Regional Research, University of Iowa, the emphasis is being placed on urban dynamics or urban change detection. This denotes a relatively new element important in all phases of current urban related remote sensing research endeavors. That is, an ability to detect change over time. While in their simplest form, change detection systems would evaluate data acquired in the first time period and data acquired in the second time period in order to discern changes, more sophisticated methods could and should be evaluated. Generally, this area of research might fall under the general rubric of information systems.

Issues to be resolved in the general area of geographic information systems based on remote sensing inputs are: (1) compatibility with the operational needs of the host of interested public agencies at the local, regional, federal, and international level, (2) the integration of urban and regional information systems requirements, (3) the setting of urban and regional information systems into a national or international program of land use or environmental monitoring, (4) specific recommendations for hardware and software systems. In addition, to these considerations there is the general problem of the development of imagery analysis procedures designed to automatically define changes which are occurring in metropolitan regions. In other words, if one bit of information did not change between the two observation points, it is unnecessary to re-collect that information. Automated change detection systems are clearly a necessary step. If experiments in urban and regional analysis are to be successfully translated into operational programs, a continuous concern for the development of automated systems of retrieval and manipulation must continue. All urban and regional related experiments should be conducted with a clear understanding of the kinds and types of management information system in which remote sensing inputs will ultimately reside.

REFERENCES

1. Moore, Eric G. (1971) "Applications of Remote Sensing to the Classification of Areal Data at Different Scales: A Case Study in Housing Quality." Forthcoming in Remote Sensing of Environment; Horton, Frank E., and Marble, Duane F., "Housing Quality in Urban Areas: Data Acquisition and Classification Through the Analysis of Remote Sensing Imagery." Proceedings, Second Annual Earth Resources Program Review, National Aeronautics and Space Administration.

2. Marble, Duane F., and Horton, Frank E., Remote Sensing as Data Sources for Urban Research and Planning: Final Report. Remote Sensing Laboratory, Northwestern University, Evanston, Ill., (forthcoming).

3. Moore, Eric G., "Application of Remote Sensors to Analysis of Housing and Population Characteristics in Urban Areas," in Marble and Horton, op. cit., Ref. 2.

4. Rawlings, Gerald R., "Applicability of Remote Sensing Imagery to Urban Change Detection," in Marble and Horton, op. cit., Ref. 2.

5. Ibid.

6. Horton, Frank E., and Campbell, John, "The Application of Remote Sensing Techniques: The Identification of Intra-Urban Commercial Centers," in Marble and Horton, op. cit., Ref. 2.

7. Schmitt, Robert P., Land Use Data Acquisition Via Photographic Sensors: An Operational Test. Technical Report No. 1, Remote Sensing Project, Institute of Urban and Regional Research, University of Iowa, October, 1970.

8. Dueker, Kenneth J., "Estimating Population and Dwelling Units from Imagery." Position Paper #1, Intra-Urban Studies, Remote Sensing Project, Institute of Urban and Regional Research, University of Iowa, November, 1970.

9. Rushton, Gerard, and Hultquist, Nancy, Remote Sensing Techniques for Evaluating Systems of Cities: A Progress Report. Technical Report No. 2, Remote Sensing Project, Institute of Urban and Regional Research, University of Iowa, November, 1970.

CLIMATOLOGY OF URBAN-REGIONAL SYSTEMS

by

Robert W. Pease
Department of Geography
University of California
Riverside, California

Urbanized areas now dominate many regional complexes. A major problem for which remote sensing methods appear to provide a better answer is the measurement of the impact of urban areas upon regional land-atmosphere energy exchange systems. During the past fifteen months significant progress has been made in mating remote sensing techniques to urban energy climatology using data secured during the BOMEX experiment by the NASA Earth Resources Aircraft Program. Cooperation by the Earth Observation group has aided immeasurably in interpretation and calibration of the information used.

Today climate is being analyzed in terms of energy systems. Absorption of solar energy and the radiation of energy from the terrestrial surface are parts of energy budgets which can be analyzed by measuring the energy exchanges that are taking place. Most commonly measured are radiant fluxes, the shortwave energy from the sun and the interchange of longwave radiant energy between the surface and overlying air. A measurement from which useful inferences can be made is the balance of incoming to outgoing radiant energy flows, or "net radiation." A long-term net radiation deficit, for example, indicates that energy is being transferred from surface to air by non-radiant means such as transpiring plants, whereas a long-term surplus indicates the transportation of non-radiant energy into the area of concern. A change in this balance toward a consistent surplus is fundamental to the existence of cities as "heat islands" within their respective regions as the energy sinks of living plants are diminished and a great deal of non-solar energy is liberated which sooner or later must be emitted from the urban surface.

The mating of remote sensing techniques to urban-regional energy climatology is desirable because of certain characteristics of the urban surface.

(1) It is highly three-dimensional. Streets between rows of buildings become "thermal canyons" with many of the characteristics of the blackbody cavity of Kirchhoff. Radiant energy, absorbed and re-emitted repeatedly between building walls, results in almost total absorption of solar and atmospheric inputs despite albedos and emissivities of surfaces. An observer at street level, using traditional radiation measuring instruments, is within the cavity structure and,

although he may be able to sense well the environment around him, he cannot assess the energy contribution to the open air over the city as well as can measurements made from above.

(2) The urban surface is a mosaic of smaller surfaces, each with its own radiant and thermal properties. A ground observer must attempt to extrapolate his point observations into a spatially complex system by assigning proportionality to the many types of surfaces he measures. This is an almost impossible endeavor without an airborne perspective. The new generation of mechanical-optical imaging scanners capable of self-calibration, such as the RS-14 flown by NASA, automatically demarcates and measures characteristics of the many small surfaces that make up the urban mosaic. In the RS-14 image in Figure 1, both the urban mosaic and the urban-rural interface of Houston show well, imaged solely by the energy they are emitting in the thermal spectral band.

(3) Urban patterns of radiant exchange are constantly changing during diurnal and annual cycles. Relative radiant states may reverse between day and night. Blacktop is a good reservoir for solar energy, for example, and may not become as hot during the day as poorly conducting dry soil. This is apparent on Figure 1 when one compares the cleared areas in the non-urban lands with the apparent radiation temperatures of the freeway and city streets. Had we a view of the same area made late at night, the pavement would be the warmer of the two. Thus there is reason to believe that synoptic maps of radiant exchange and thermal states may be of greater value in the analysis and monitoring of urban energy phenomena than maps laboriously compiled from statistical averages of difficult-to-obtain data collected at street level. Synoptic maps now have been made successfully with data rapidly acquired aloft with the RS-14 scanning radiometer.

A brief account of the results derived from the Barbados data will best suffice to show progress made to date in the use of remote methods for monitoring and mapping radiation. Logistics of the experiment and initial attempts at cross-calibration between ground and airborne instruments on Barbados during the overflights were described in the last program review. The following, therefore, will be confined to the reduction of the data to maps of radiant emission.

Data came from MSC in the form of photographic transparencies of the output of the 8-14 micron channel of the RS-14 for selected flightlines over the island (Figure 2). A portion of a flightline that extended eastward from the seacoast across the northern edge of Bridgetown to rural areas inland was selected for the mapping

experiment. The scan image was augmented by a graphical profile of radiation temperatures measured by a Barnes PRT-5 radiation thermometer, also mounted on the P3A sensing airplane. The trace of the profile was located by computerized methods upon 9 x 9 metric photos made during the flight. Fortunately, this trace passed through the primary ground calibration target.

The initial problem was to relate transmittances of the scan image to surface radiance. This was accomplished with the aid of a transmission densitometer by measuring the transmittances of ground targets, the radiation temperatures of which had been observed during the imaging overflight. With a positive image, transmittance was used rather than density to avoid an inverse relationship. Sea-surface radiance was used to anchor one end of an appropriate conversion curve (Figure 3) and land calibration targets the other in order to make the graphical plot shown as curve A.

To make isoline maps that would show meaningful patterns of terrestrial radiation, it was necessary to generalize the minute patterns of the scan image, particularly over the urban area. To accomplish this, the image was divided into a matrix of choropleth cells one centimeter square or close to one-half kilometer square on the ground. A silicon cell device with an area equal to a matrix cell was first calibrated to the densitometer as shown in curve B and was then used to integrate each cell transmittance. The matrix, superimposed upon the scan image, and derived averaged transmittances are shown on the left-hand side of the composite of Figure 4. With the aid of a computer, slope equations for curve B of Figure 3 then converted the averaged cell transmittances to radiances as shown in the next matrix. Mapping involved the use of the centroids of the choropleth cells as control points from which to plot the desired isolines. Maps in other radiation terms were made in the same manner and appropriately all showed the same radiation patterns.

The RS-14 has built-in calibration sources which give the instrument a self-calibration potential. The radiance received aloft by the instrument, however, is not the same as the radiance emitted by the surface target being imaged. Intervening air, even in the 8-14 micron water vapor window, both attenuates the surface signal and adds an energy component of its own. Realization of the full potential of the RS-14, then, necessitates that the error induced by the atmosphere

be systematized in order that a correction without elaborate ground controls be carried out. For the Barbados data, this has been accomplished by using a gray-window model for the intervening air expressed by the equation:

$$I_z = \epsilon[E_{bb}(\bar{T})] + (1-\epsilon)\ I_o$$

where (I_z) is the radiance at the sensor, (I_o) the radiance of the surface target, $[E_{bb}(\bar{T})]$ the blackbody equivalent of the mean temperature of the intervening air column, and epsilon the effective emissivity of the air column in the spectral band being sensed. When values for sensor and surface radiance (I_z and I_o) are known from instrument readout and ground calibration and a mean air temperature has been established, the effective emissivity of the air, or epsilon in the equation, can be determined. This value permits the mathematical computation of surface radiances (I_o) for all values of sensor radiance (I_z) which in turn permits plotting a correction curve (Figure 5) that will fit all parts of the scan image if the intervening air is considered to be relatively homogeneous.

Although at the time of the Barbados flight the internal calibration sources of the RS-14 were not deemed to be working properly, Victor Whitehead of the Earth Observation Program systematized the error and obtained image vs radiation temperature values which, when corrected for the effects of the atmosphere by the foregoing equation, corresponded closely to values derived from ground calibration targets.

Certain characteristics of the relationships just described may in the future significantly reduce the amount of ground calibration necessary. The slope of the correction curve is equal to the reciprocal of the air transmissivity ($1/1-\epsilon$) and can thus be set by a single ground calibration which permits determination of the effective air emissivity in the spectral band being utilized. The position of the curve with respect to the I_z axis of the graph is established by the fact that the curve must intersect a line of equal value at a radiance equal to the blackbody equivalent of the mean temperature ($\bar{T}$) of the intervening air column. Further, according to Beer's Law, the transmissivity of the air is also equal to the natural log base (e) to the minus (ku) power where (k) is the absorption coefficient of the spectral band of concern and (u) the optical depth of the intervening air in gram-centimeters squared of precipitable water. Thus the slope of the correction curve is also equal to $1/e^{-ku}$, a relationship which should permit setting the slope without the aid of ground controls,

solely from atmospheric data, when more knowledge has been collected regarding absorption within the water vapor window. Elimination of ground controls may be particularly important when the system is applied to earth-viewing satellites with a thermal sensing capability, such as ERTS-B.

Future progress in achieving an ability to remotely monitor urban-regional energy budgets must follow two paths. First, the sensing capability must be extended to include fluxes other than terrestrial longwave emission. Investigation this past summer indicates that surface albedos can feasibly be determined photographically or perhaps better by the use of a silicon sensor for channel 1 of the RS-14. With ground pyranometers to assess solar input, the addition of albedo measurements may make possible the construction of synoptic maps of net radiation, adding this valuable analytical tool to radiation analysis.

The second path of improvement is the application of the methods developed from data acquired in the single flight over tropical Barbados to a sequence of flights over a midlatitude city in the United States. Derived maps can show patterns of both diurnal and annual change for a variety of phenomena related to radiant exchange. Houston has been chosen as the test city for this next phase of the experiment. First, probably in April, will be an initial sequence of four flights with additional sensors to sample a diurnal period. This sequence logically should be followed by similar diurnal sequences at other seasons to demonstrate annual change in patterns.

The continuing effort is a logical preliminary to work with ERTS-A and B. Houston will become a "pre-calibrated" target for calibrating ERTS instruments. Previously acquired knowledge pertaining to the target city will be augmented by aircraft and ground truthing at the time or times of satellite passage. Present planning calls for establishment of several automatic platforms around the city which will transmit at least daily records of selected surface radiation information to ERTS for subsequent retrieval.

If we are successful in quantifying ERTS outputs for Houston, attempts will then be made to apply the methods to 26 other urban-regional complexes without resorting to ground truth.

ERTS-A will have sensors that permit only analysis of temporal change in albedos. With a thermal scanning channel on ERTS-B, more complete energy exchange analyses will be attempted, analyses which will use the broad regional perspective hopefully obtainable from a satellite.

As Outcalt has broadly stated, "... a reasonable programme goal is the prediction of the effects of land-use manipulation on the climates of urban areas." To this I add, "... and on the regional climates which urban areas help to create." At this point, a path toward an operational capability begins to take shape. By the endeavors of this program it is hoped we can gain the ability to monitor rapidly urban-induced changes in the climatic aspects of man's environment.

REFERENCES

Outcalt, Samuel I. (1970) "A Plan for Urban Climatology within the Geographic Applications Branch, USGS, Interior," Geographic Applications Program Discussion Paper, June, 1970.

Pease, Robert W. (1970) Mapping Terrestrial Radiation Emission with the RS-14 Scanner, Technical Report 4, U. S. Department of Interior Contract 14-08-0001-11914, July, 1970.

Figure 1.- An image made with the RS-14 scanning radiometer in the 8-14 micron spectral band showing an urban-rural boundary near Houston. It is readily apparent that the overall energy contribution from the urban surface is greater than from the rural. Light areas in the rural surface appear to be excavations which expose loose dry soil. Also to be noted, the pavement surfaces do not have as high radiation temperatures as the dry soil. Image made on NASA Mission 130.

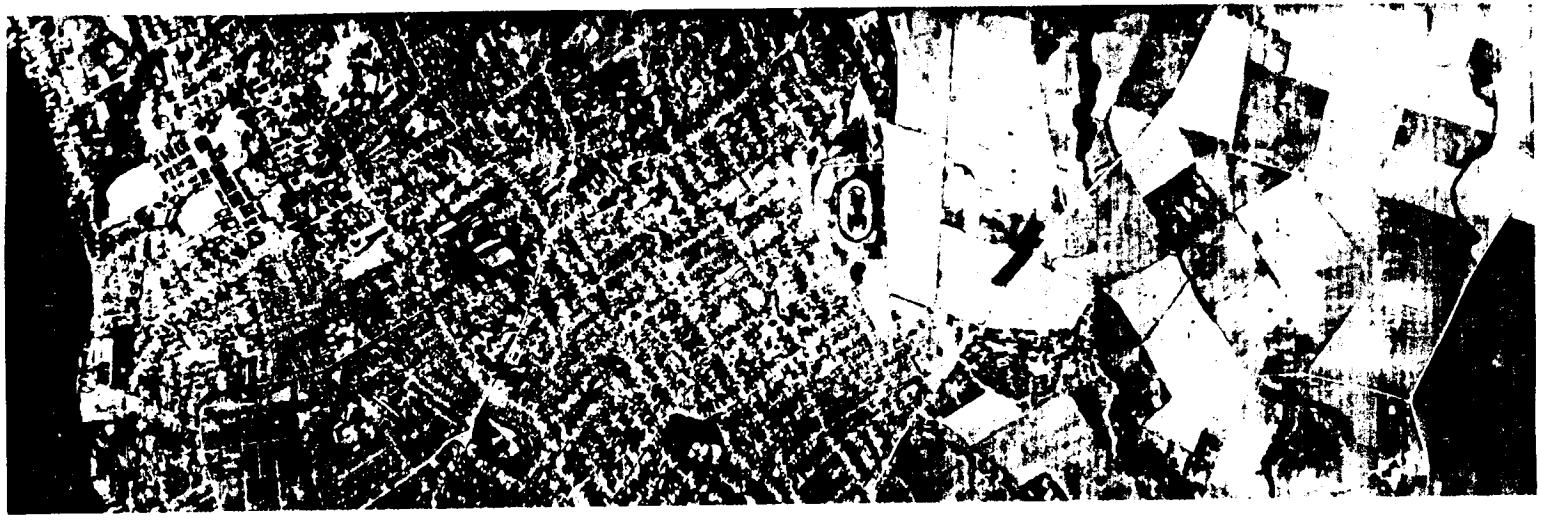

Figure 2.- The RS-14 image of the portion of the Barbados flight-line used in the radiation mapping experiment. The urban areas on the left-hand side of the image (west) are northern suburbs of Bridgetown. Land sites for which radiation temperatures were measured during the sensing overflight are in the "warm" fields east of the stadium. The sea surface was also used as a calibration reference. Image made on NASA Mission 98.

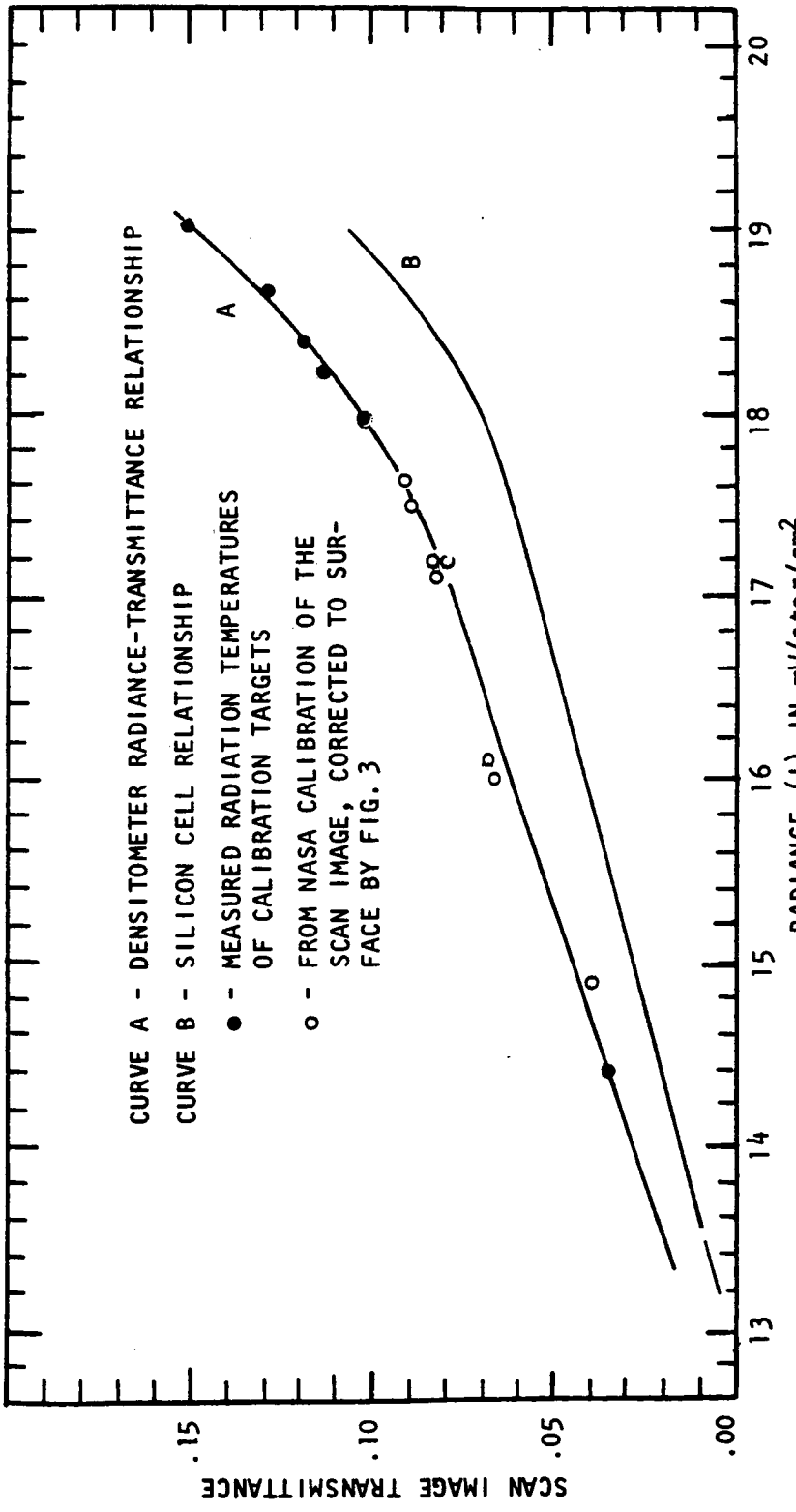

Figure 3.- Transmittance-radiance relationships for the transparency of the RS-14 scan image used in the mapping experiment.

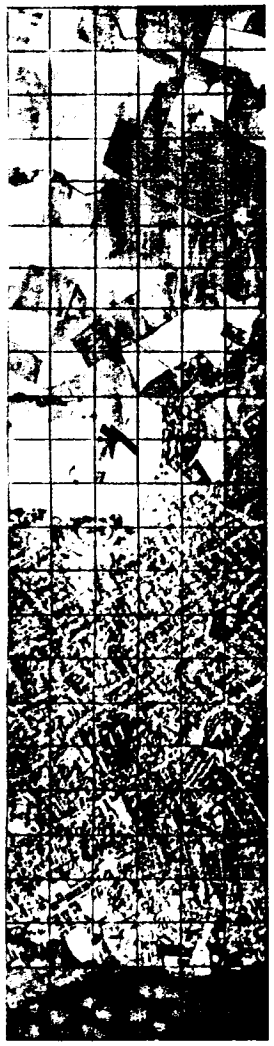

(a) Scan image of the map area with matrix grid superimposed.

AVERAGED CELL TRANSMITTANCES

.050	.048	.040	.024	.020	.034	
.054	.062	.070	.045	.027	.042	
.043	.057	.056	.030	.036	.025	
.054	.058	.029	.020	.017	.019	
.064	.040	.023	.022	.014	.018	
.055	.042	.029	.031	.021	.019	
.038	.038	.054	.038	.023	.023	SUGAR CANE FIELDS
.057	.034	.032	.045	.048	.037	
.042	.050	.036	.043	.032	.023	
.043	.049	.042	.036	.030	.029	
.070	.070	.046	.048	.034	.028	RURAL
.067	.083	.080	.058	.035	.023	URBAN
.042	.049	.053	.048	.030	.023	
.034	.046	.044	.048	.034	.025	
.033	.035	.038	.035	.032	.024	
.029	.039	.039	.037	.032	.033	
.032	.038	.032	.028	.033	.028	
.032	.038	.030	.036	.032	.028	BRIDGETOWN
.039	.040	.050	.028	.031	.026	
.047	.042	.051	.035	.031	.027	
.050	.060	.071	.064	.040	.037	
.056	.078	.082	.075	.054	.043	
.049	.032	.029	.043	.039	.026	SEA LAND
.021	.019	.020	.021	.021	.022	

(b) Matrix of choropleth cells with average transmittance values determined from image transparency by a silicon cell integrating device.

RADIANCE (mW/ster/cm^2)

16.65	16.50	15.90	14.70	14.40	15.45	
16.95	17.55	18.15	16.28	14.93	16.05	
16.13	17.18	17.10	15.15	15.60	14.78	
16.95	17.25	15.07	14.40	14.12	14.33	
17.70	15.90	14.63	14.55	13.95	14.25	
17.03	16.05	15.08	15.23	14.48	14.33	
15.75	15.75	16.95	15.75	14.63	14.63	SUGAR CANE FIELDS
17.18	15.45	15.30	16.28	16.50	15.68	
16.05	16.65	15.60	16.13	15.30	14.62	
16.13	16.57	16.05	15.60	15.15	15.08	
18.15	18.15	16.35	16.50	15.45	15.00	RURAL
17.93	18.44	18.34	17.25	15.53	14.63	URBAN
16.05	16.58	16.86	16.50	15.15	14.63	
15.45	16.35	16.20	16.50	15.45	14.78	
15.38	15.53	15.75	15.53	15.30	14.70	
15.08	15.82	15.83	15.68	15.30	15.37	
15.30	15.75	15.30	14.96	15.38	15.00	
15.30	15.75	15.15	15.60	15.30	14.96	BRIDGETOWN
15.83	15.90	16.65	15.00	15.23	14.85	
16.42	16.05	16.73	15.53	15.23	14.93	
16.65	17.40	18.03	17.70	15.90	15.67	
17.10	18.27	18.41	18.17	16.95	16.13	
16.58	15.30	15.08	16.13	15.83	14.85	SEA LAND
14.48	14.33	14.44	14.44	14.48	14.51	

(c) Matrix of choropleth cells with transmittances converted to radiances by using equations derived from curve B of Figure 3.

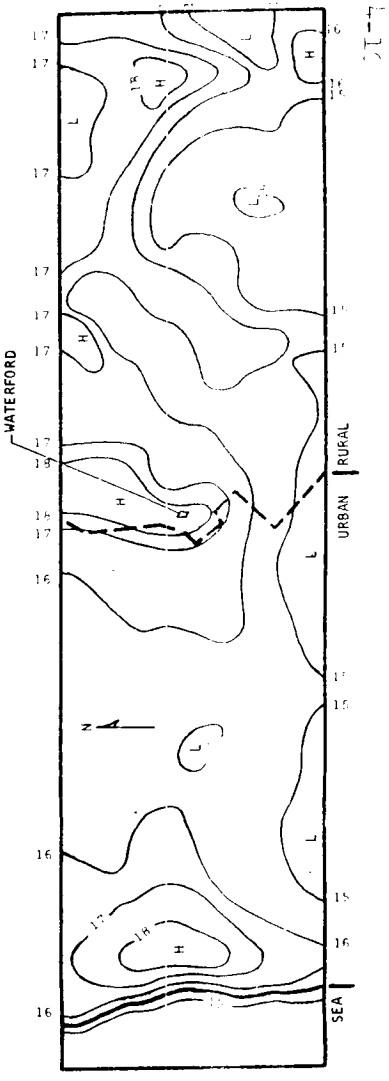

(d) Finished isoline map showing surface radiance in mW/ster/cm^2, made by using the centers of matrix cells as control points for the line plotting.

Figure 4.- The sequence of steps followed in making the maps of radiant emission.

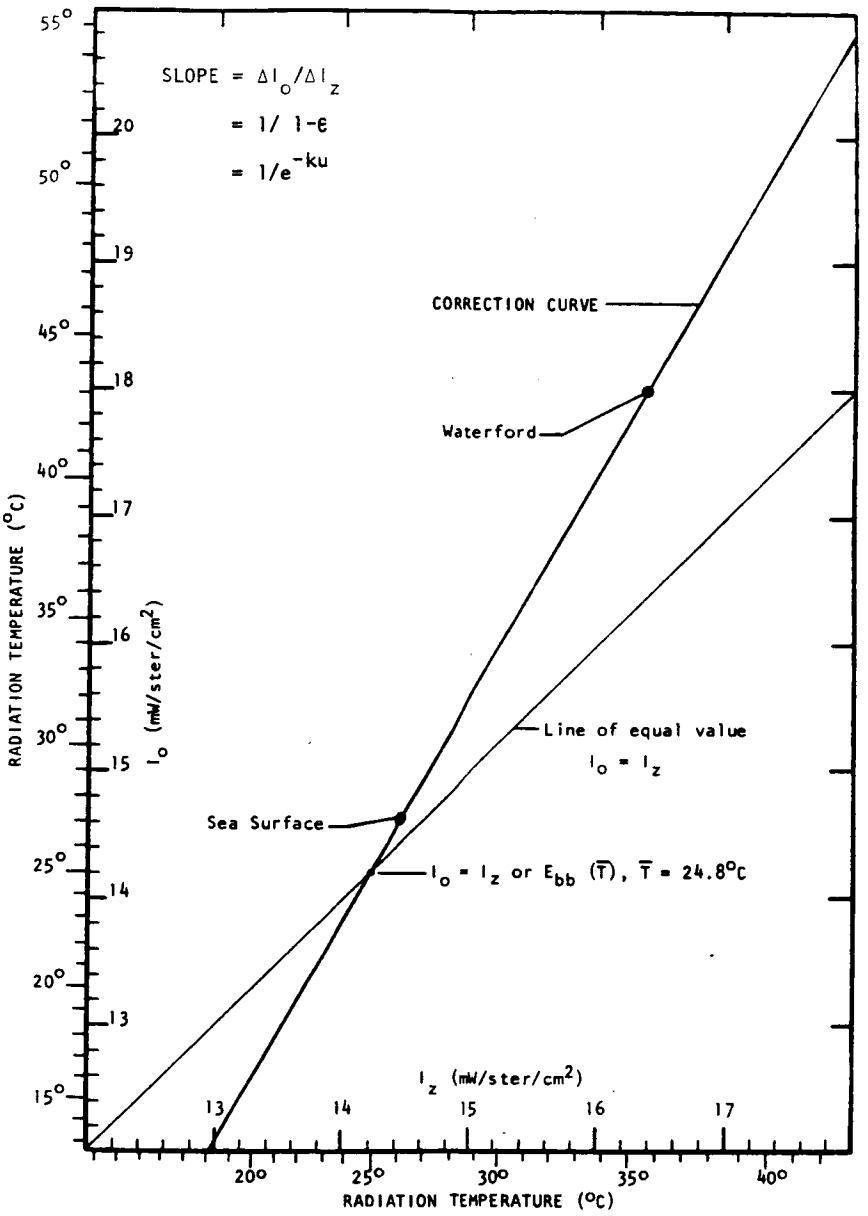

Figure 5.- Graph for correcting radiance values received aloft at the sensor to target radiances. The slope of the correction curve can be determined empirically by calibration targets or by use of one of the slope equations in the upper left-hand corner. The curve must pass through a point on a line of equal value where $I_o = I_z$ at the equivalent blackbody radiance for the mean temperature of the air intervening between the target and sensor.

REGIONAL LAND USE STUDIES

by

John L. Place
U.S. Geological Survey
Washington, D.C.

INTRODUCTION

Many agencies are concerned with land use trends, forecasts, and decision-making with respect to highly competitive and often incompatible demands from special interest groups. These decision-making and planning agencies often lack the data they need for valid judgments. Traditional techniques for land use data collection, mapping, and updating on a national or even regional scale are not satisfactory because:

1. They are too slow--the information is out-of-date by the time it is collected and mapped.

2. They are too fragmentary--state and local agencies collect data for limited areas, leaving many holes in the coverage desired by Federal agencies.

3. The data differ in scales, categories, interpretations, and data collected and, hence, cannot be integrated meaningfully.

It is the plan of the Geographic Applications Program to find a way to use remote sensing technology and data from instrumented satellites and high altitude aircraft to map land use on a current national basis, to monitor changes and trends, and to create statistical models which can be manipulated to demonstrate the probable effects of proposed land use and of environmental changes over large areas.

In the absence of coverage for the whole United States, or existence of a fully operational plan for using such data if they existed, we plan first to use a single 1:250,000 scale topographic map quadrangle area as a pilot study, then to progress to larger regions and to the testing of samples in other parts of the United States. When data become available from either ERTS-A or from high altitude aircraft, we could be ready to undertake land use analysis of the entire United States.

The high quality of the color infrared photographs taken of Arizona during the Apollo 9 mission, as exemplified in Figure 1, has led to the selection of the Phoenix quadrangle for our pilot study. Its low latitude and characteristically clear skies have favored Gemini and Apollo photography. Furthermore, we have, in past years, sponsored research in this area through contracts with Northwestern University and with the Association of American Geographers. And most recent, the Arizona ecological test site is being developed for interdisciplinary study.

PROCEDURES

The USGS Topographic Division already has made a photo map of the Phoenix quadrangle, using this nearly vertical Apollo photo of the Phoenix area, mosaicked with another overlapping it on the west. Since the rectified photo mosaic already existed, it was used as the base on which to compile the land use map. These photos also provided the best complete coverage available for the entire quadrangle. From the space photos, small areas of more intensive use, such as settlements or croplands, can be detected. For these spot areas, larger scale aircraft photos were obtained to aid precise land use measurements on the Apollo photomap base.

The aircraft photographs were of types that could be expected to exist for any quadrangle of the United States. For example, Department of Agriculture photo mosaics were used for the major cropland districts. Likewise, it was reasonable to use, for Phoenix, the NASA color infrared photos taken for the USGS Census Cities Project in May of this year. The Apollo underflights, which covered strips across the quadrangle, and the NASA photos for the University of California's agricultural study near Phoenix will be used to check and evaluate the initial land use map. Ideally, we would use very high altitude aircraft photography to plot land use, supplemented by data from additional current sources, and then update the results with ERTS-A. Since high altitude aircraft coverage was not available for the entire quadrangle, we used the Apollo photos plus larger scale photography from traditional sources and field investigations.

It was found that the Apollo photos and the aircraft photos complimented each other in several ways. The confusion caused by different sun angles in the agricultural study mosaic was cleared up by the space photo, and cropland boundaries were easier to define. Also, the urban residential fringe for Phoenix was difficult to delimit on aircraft photos because of the nearly random scattering of housing developments outside of the city. However, with this Apollo photo, one can distinguish the "forest from the trees."

Even with supplementary information, it was necessary to keep the land use categories simple. Dr. James Anderson of the University of Florida, in cooperation with the Commission on Remote Sensing of the Association of American Geographers, produced a generalized land use classification system designed specifically for our problem. We did not attempt to identify crops, only the boundaries of cropland and the distinction between tree and non-tree crops. We also indicated such changing patterns as highways, airports, forest or mineral exploitation, recreation areas, and settlements of different sizes. The one large urban area, Phoenix, was mapped in four categories: residential, commercial,

industrial, and open. To provide the four-way classification for Phoenix, the most recent land use map, two years old, was obtained from local planners. This information was then updated using the aircraft photos.

Not only was pertinent governmental data obtained for the Phoenix area, but some field mapping was done as well, mostly as a check on accuracy. In some cases, cropland was shown on the Apollo photo in spots where aircraft photos were not available. A field check was made to determine whether or not any orchards or groves of trees were present.

When the map is completed, the land use data will be aggregated to rectangular grid points spaced 1,000 meters apart on the Universal Transverse Mercator projection, and read into a computer data bank. The Phoenix quadrangle alone contains nearly 20,000 grid points. Other identifiers attached to each grid point will be latitude and longitude and codes for state, county, census tract, river basin, and land ownership. The code for land ownership indicates whether the land falls under the jurisdiction of the Forest Service or the Bureau of Land Management, or the State, or private ownership, etc. Maps of each of these identifiers already have been prepared to fit the quadrangle and are ready for reading into a computer.

DISCUSSION

The resulting computer model will be used for statistical analyses and for printing out updated maps automatically. The data bank can be updated rapidly and changes detected by the computer. In this experiment, a careful check will be made of several change detection procedures being tested. It is important that we obtain complete photo coverage of the quadrangle next year, so that the change detection processes can be tested.

The greatest value of such a map and computer model will stem from frequent, at least seasonal, updating of land use inventories covering large areas. It would be of much greater value if a large region, such as the entire Gila River drainage area, could be covered, rather than merely one quadrangle.

Land use maps of this type, and the statistical models produced therefrom, will provide current, large area information not presently available to planners and decision-makers at the Federal, regional, and state levels.

OTHER REGIONAL STUDIES

We plan to experiment with regional land use mapping elsewhere, not just in the arid southwest. We hope to perform more fully integrated regional studies, in addition to making automated land use maps and data bases. These other regions are shown in stippled patterns on the map in Figure 2. They presently consist of the Atlantic seaboard between North Carolina and Boston, the Gulf Coast from Houston to Biloxi, and the California coast between San Francisco and San Diego. These sites will give us a chance to study problems relating to the growth and merging of cities in a megalopolis, the disappearance of open spaces, monitoring the quality of our environment, and the management and development of resources.

During the past fifteen months, the NASA RB-57 aircraft has photographed two geography test sites in the southeastern U.S. Because of the high cost of travel and briefness of the reports, the principal investigators at those sites have permitted me to describe briefly the progress of their research projects, both emphasizing regional land use, and thus relating to my in-house study of regions.

In August of last year, the RB-57 aircraft photographed an area in eastern Tennessee around Knoxville. The principal investigators at this site were Dr. Richard Witmer and Dr. Robert Peplies of the East Tennessee State University. They have used these photos to evaluate: 1) forest resources, 2) the influence of land forms on land use planning, and 3) the relationship between transportation routes and population distribution.

In addition, they have used color infrared photos from the Apollo 9 mission--such as the one shown in Figure 3--to study vegetation patterns in northern Alabama. It was found that improvements could be made to existing vegetation maps; that is, boundaries between certain types of forests could be delimited more accurately using such space photos. It was also determined that the tonal and textural differences seen in the photo allowed identification of the general size of farms and provided some measure of population density. The final report has been prepared in draft form and will be available shortly.

In October 1969 and March and June of this year, the RB-57 aircraft photographed a geographic test site extending from Orlando, Florida, south to Lake Okeechobee, as shown on the map in Figure 4. Research conducted here was under the direction of Dr. Merle Prunty of the University of Georgia, and involved a study of the intentional burning of vegetation, particularly tropical grasslands. Film types used included Ektachrome, black and white infrared, and color infrared. The principal objective

of the three flights was to gather data for: 1) evaluation of various scales of images and to compare their utility for revealing vegetation burns, 2) analysis of seasonal burn patterns, and 3) comparison of the utilities of various types of photography; for example, Ektachrome versus color infrared.

Color infrared photography, taken with the Zeiss camera with 12-inch focal length, was extremely useful. Recent burns are discernable on the RC-8 photographs at the scale of 1:120,000, but the Hasselblad photos at 1:240,000 are almost unusable for the identification of changes in vegetation caused by fire.

In the seasonal comparison, late winter proved to be the most favorable time for burn studies.

In the comparison of color infrared image qualities, film type 8443 was found superior to S0117 for burn pattern recognition. Imagery exposed at an altitude of above 60,000 feet tended to register a bluish "haze," which reduced the quality of the color infrared signatures. Color infrared film still proved to be of greater value than either color Ektachrome or panchromatic in burn studies.

A final report on these findings is being prepared at the University of Georgia and is expected to be completed soon.

CONCLUDING REMARKS

To summarize, what we need from the NASA Aircraft Program is complete, high altitude photo coverage of the Phoenix quadrangle to update the present land use map and to test the concept of automatic change detection using very high altitude photography. Additional high altitude photography will be needed eventually for the other regional test sites.

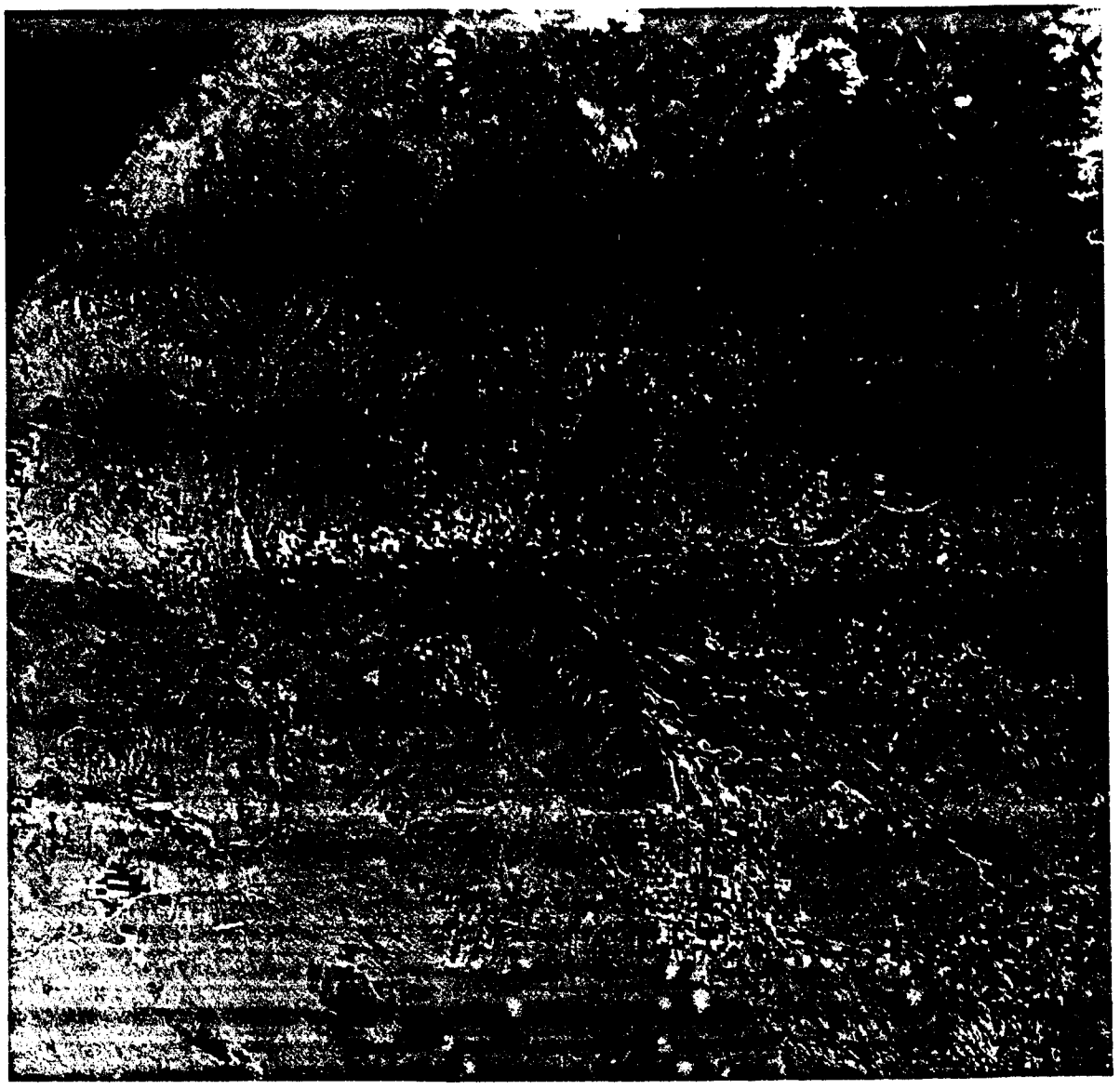

Figure 1 - Apollo 9 photo of central Arizona using color infrared film

Figure 2 - Urban and Regional Test Sites

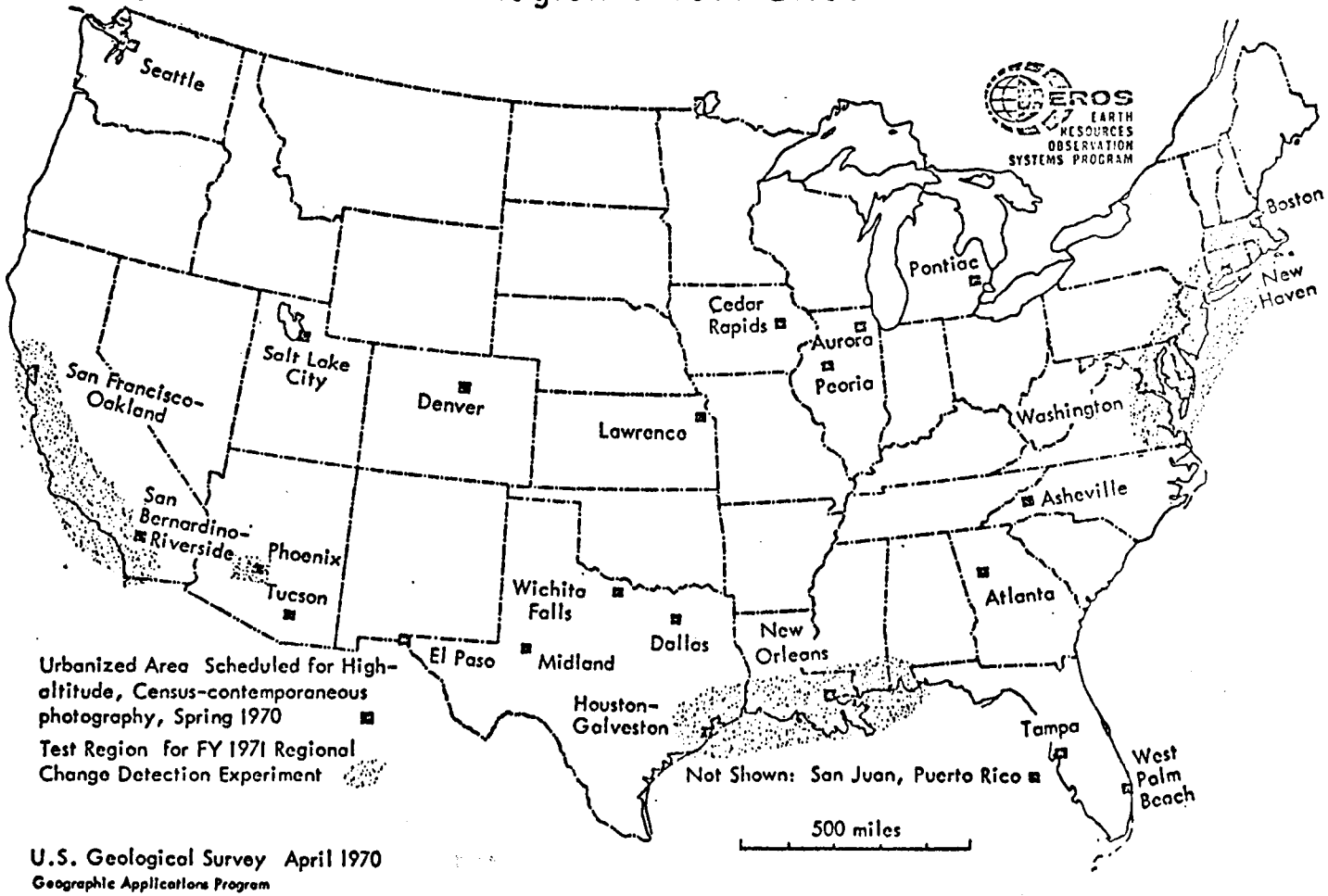

Figure 3 - Apollo 9 (3/69) photo of Alabama using color infrared film

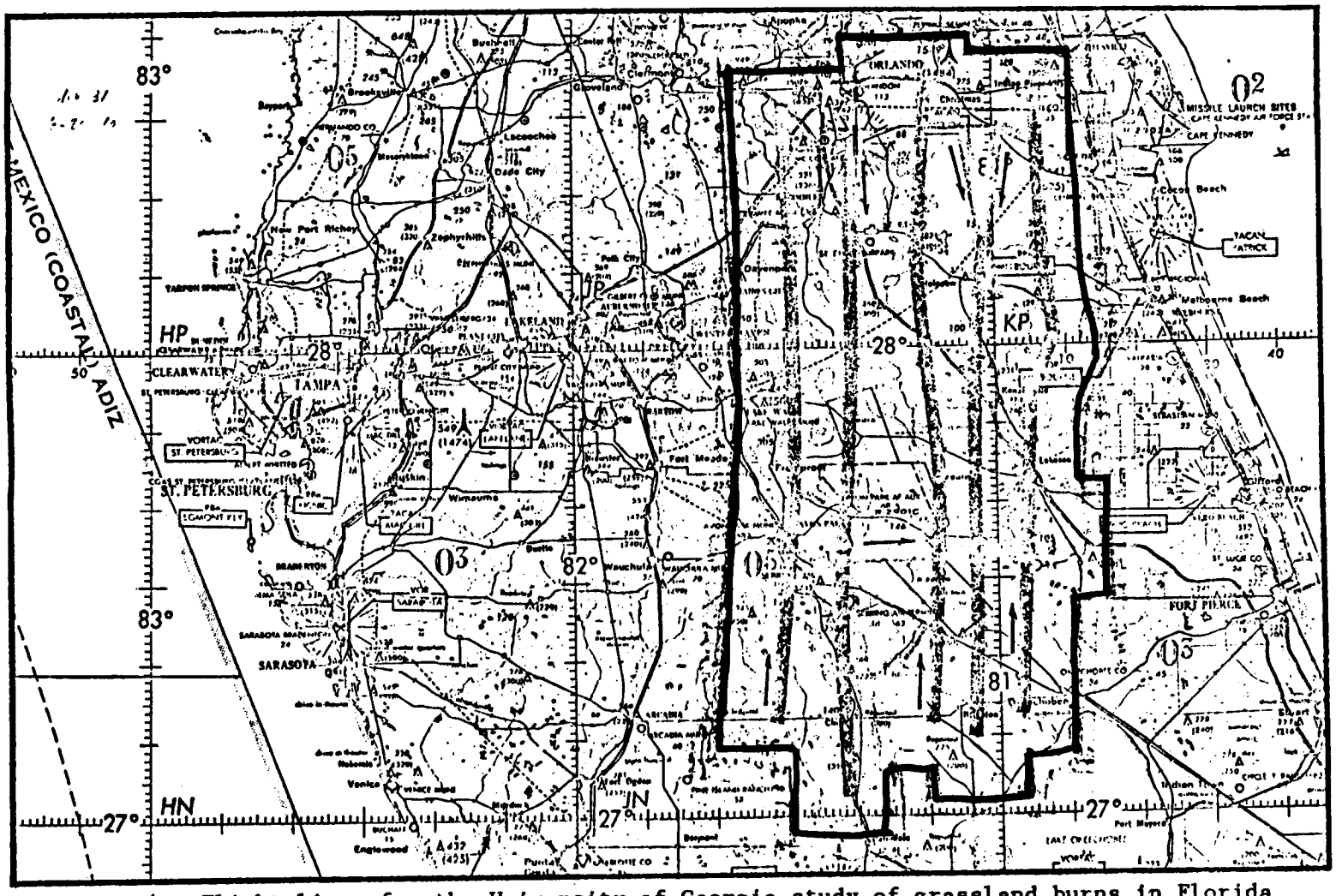

Figure 4 - Flight lines for the University of Georgia study of grassland burns in Florida

ENVIRONMENTAL APPLICATION OF REMOTE SENSING METHODS TO COASTAL ZONE LAND USE AND MARINE RESOURCES MANAGEMENT

by

H. G. Goodell
Department of Environmental Sciences
University of Virginia
Charlottesville, Va.

INTRODUCTION

Man and his culture have placed tremendous stress on environmental systems and dynamics by his unchecked use of land and resources. These strains are perhaps greatest in the environments of coastal megapolis where the shock of urban impact, virtually unmanaged, barely understood, and scarcely forecast has been in many instances almost fatal. In these areas resource allocation and environmental management have been historically based on extrapolations on past patterns of land use and from forecasts of short term economic gain, but with minimal realization for the long term social cost. If resource utilization is to be optimized and environmental degradation checked, much deeper insight into the dynamics of human ecology is required. This necessitates a reevaluation of the entire social/biophysical ecosystem. At the heart of such a system are those local, regional, state, interstate and federal government agencies charged with evaluating, planning, regulating and enforcing resource allocation. It is an *a priori* assumption that a knowledge of biophysical environmental systems is a necessity to social decision making, yet it is acknowledged that the current status of comprehension of environmental systems is minimal and that the cultural contributions to such systems are either generally ignored or universally deplored. Neither viewpoint is logically defensible. This paper is the first report from an investigatior designed to probe these interrelationships. It is funded through the Geographic Applications Program, U.S. Geological Survey. The author acknowledges his colleagues on this investigation with deep appreciation and absolves them of guilt by association: D. Adams, L. Grosenick, T. Hadd, M. Nichols, W. Reed, and C. Woolheater.

USER ANALYSIS

The Central Atlantic coastal zone was selected as a diversified environmental model of man/environmental interactions because it provides

examples of all levels of urbanization over a wide span of biotopes: from the densely populated southern margin of the northeast urban corridor to the estuaries, the rural salt marshes, sounds, barrier islands of eastern Virginia and North Carolina (Fig. 1). The potential impact of remote sensing will be tested on this model for the following:

1) the inventory and description of environmental systems at all geometric levels;

2) the monitoring of environmental dynamics at all temporal scales;

3) the identification and modeling of environmental processes for prediction of environmental change; and

4) the decision making processes for land use, resources allocation; and environmental management.

The word environment as used above includes all aspects of human ecology in its broadest connotations.

The evaluation has required the assembling of an interdisciplinary task force of social and natural scientists to probe the nature and basis of decision making at all levels of government, the present patterns of land use and resource allocation, the systems by which man's culture interacts with his environment, and the processes and dynamics of environmental change. The initial efforts of the task force have been two-fold:

1) to appraise the structure of state regional and local governmental agencies from the aspect of function and responsibility so as to assess the present data base for environmental decision making; and

2) to establish environmental baselines against which the dynamics of naturally and culturally induced environmental change can be measured.

THE DECISION MAKERS

It was apparent early in the investigation that while substantial overlap existed in functional activity between many agencies some functions were abnegated by all agencies. In addition, it was soon realized that the data-base used for planning is usually inadequate both in content and in time-reference. While there is a general agency awareness of the possible heavy implications of federal and state environmental legislation that required the preservation and even the improvement of environmental quality in spite of advancing urbanization and industrialization, there is little comprehension of possible environmental consequences which

might stem from decisions of agencies that have here-to-fore been environmentally immune. There is practically no agency with such immunity today. Therefore, while the need for environmental data-bases has broadened immensely, there remains almost a total lack of basis for the recognition of environmental status, analysis and prediction even among agencies which have had a background of working with natural systems.

Eighteen governmental agencies of the State of Virginia responsible for fifty programs, almost all of which have environmental and/or resource allocation responsibilities, yielded an array of 205 agency defined data catagories that are actually used in decision making. Each of these data catagories was evaluated in terms of the application of one or more of seven types of current remote sensing:

1) aerial photography - black and white

2) aerial photography - color

3) aerial photography - color infrared

4) thermal infrared scanning

5) radar

6) ERTS satellite photography

7) other

Data Needs

Inasmuch as with few exceptions there was little knowledge about the nature or potential of remote sensing, demonstration kits consisting of photography at scales of 1:10,000; 1:36,000; 1:60,000 and 1:120,000 were used in interviews with agency personnel. Only 58 of the 205 data catagories seemed susceptible to some form of remote sensing, yet if remote sensing is to make a meaningful contribution to the decision making process, it must be capable of either supplementing or substituting for existing data sources, as well as to demonstrate a capability of providing new data or a new dimension of data here-to-fore unrecognized. Most of these 58 data catagories would be satisfied by black and white photography at a scale of 1:10,000. Only 19 of the 58 catagories seem to offer high potential application of several varieties of sensing:

1) Types and acreage of crops and vegetation - botanical geography

2) Subsurface earth composition

3) Location and character of surface natural characteristics

4) Location and character of surface cultural characteristics

5) Soil types and distribution

6) Flood plain data

7) Stream profiles

* 8) Effluent discharge locations

9) Effluent characteristics

10) Shellfish (mariculture) locations

11) Potential shellfish (mariculture) growing areas

12) Land use data

13) Locations and dimensions of watersheds, watercourses and flood plains

14) Locations of piers, docks, and pipelines

*15) Water temperature

16) Location of scenic river sites

*17) Water turbidity

*18) Erosion by type of land use

*19) Location and surveying of areas proposed for dredging

These 19 data catagories as agency defined boil down to a single catagory: Surface characteristics, natural and cultural, and their status and distribution, in other words inventory. There are some obvious data catagories that deal with environmental quality and have high potential for remote sensing that are absent from the data array:

1) Air quality

2) Water quality

3) Estuarine and coastal circulation

4) Construction erosion

5) The results of catastrophic events

These data bits together with those marked with an asterisk (*) require sensing on time scales shorter than annual.

THE BASE LINE

The entire Central Atlantic Coastal (Mission 144 Test Site 244) zone was blocked sensed in late September under low streamflow and rainfall and low wave power conditions using multispectral photography, infrared scanning, and radar imagery at 60,000 ft. It will be sensed again in spring under high water and wave power conditions. Ground truth in the form of water samples, photography and map annotation was obtained from as many as three helicopters and a single light plane which underflew the high altitude aircraft. Historical NASA and other agency photography has been obtained and will in some areas afford a kinetic scale against which to formulate environmental dynamics.

The question of the optimal temporal scale of sensing would seem to be a function of the kinetics and geometric scale of the system under observation. These appear to range in time scale from hours through days, months, and years; and geometric scales from less than one-tenth of a square mile to more than 1000 square miles. For example, it is obvious that for much cultural planning, annual inventory at large photo scales is sufficient. On the other hand, estuarine circulation studies essential for the location of power plants or sewer outfalls require study at small sensing scales and with frequent repetition.

The best understood natural processes are those of small geometric scale (easily observable) on a short time scale; those about which least is known are of large scale at any time scale (in these cases dynamic modeling is resorted to and the geometric and/or temporal scales are adjusted to manageable and measurable quantities). Significant errors may accrue through studying large-scale processes by non-synchronous small-scale photography. For example, it is impossible to study sediment/water interactions over a tidal cycle (hourly time scale) in a fairly large estuary, or along a one-hundred-mile beach unless photographs are at hand which cover the area essentially synchronously. In this case large-scale photography becomes a necessity. Any large geometric scale process which occurs at short time scales requires large scale imagery (Table 1).

It seems likely that most processes leading to environmental degradation can occur at short time scales but at multiple geometric scales (Table 2). Dangerous pollution processes generally begin to make themselves felt on intermediate geometric scales but at many time scales. Finally, the shorter the time scale, the faster need be the response time. That is, the quicker the photography need be in the hands of the users.

SUMMARY

There is little question in the minds of most of the task force that remote sensing from high altitude aircraft and even satellites will afford a powerful and ultimately indespensible tool in inventory and planning. It is also of little doubt that repetitive low to medium altitude photography will be essential for the study of environmental dynamics, and to document the cultural impact of man on his environment.

TABLE 1

Aerial Photographic Capabilities

Geometric Scale (up to)	Temporal Scale (up to)					
	Hour	Day	Week	Month	Year	10 Years
1/10 mile	L	L	L	L	L	L
1 mile	M	M	M	M	M	M
10 miles	H	H	H	M	M	M
100 miles	S	S	H	H	M	M
1,000 miles	-	S	S	S	S	S

L = Low altitude up to 5,000'

M = Medium altitude 5,000 - 20,000'

H = High altitude 20,000 - 100,000'

S = Satellite

TABLE 2

Possible Functions Using Remote Sensing

Geometric Scale (up to)	Temporal Scale (up to) Hour	Day	Week	Month	Year	10 Years
1/10 mile	E, H	E, H	E, H	E, H	E, H	E, H
1 mile	E, H	E, H	E, H	E, H	E, H, I	E, H, I
10 to 1,000 miles	E, H, Po	E, H, Po	E, H, Po	E, H, Po	E, H, Po, I, Pl	E, H, Po, I, Pl

E = Erosion

H = Hydrology (includes circulation)

Po = Pollution

I = Inventory (includes status and land use)

Pl = Planning

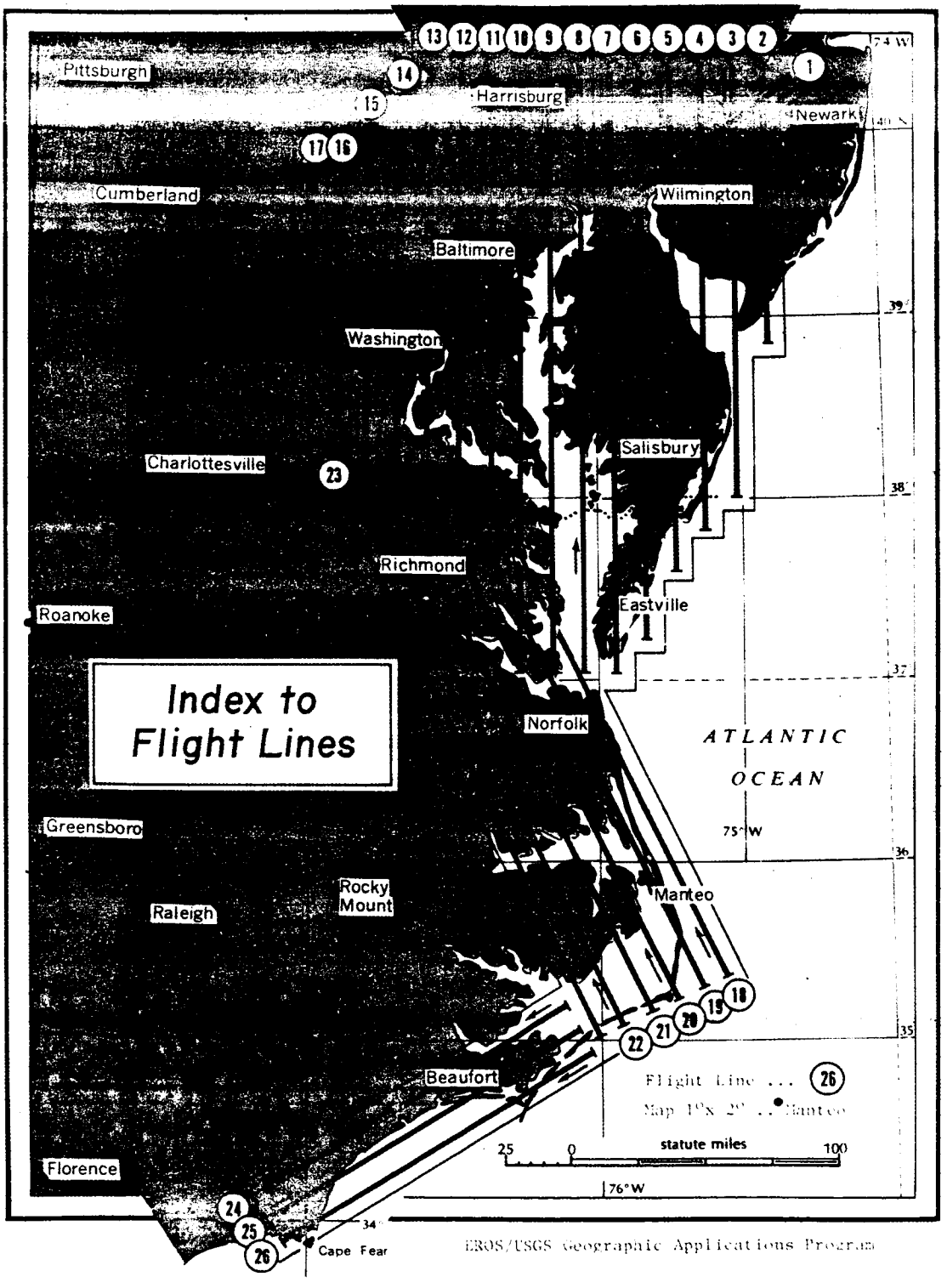
13 12 11 10 9 8 7 6 5 4 3 2 1
74 W
Pittsburgh
14
15
Harrisburg
Newark
17 16
Cumberland
Wilmington
Baltimore
39
Washington
Salisbury
Charlottesville
23
38
Richmond
Eastville
Roanoke
37
Index to Flight Lines
Norfolk
ATLANTIC OCEAN
75°W
Greensboro
36
Rocky Mount
Raleigh
Manteo
18 19 20 21 22
35
Beaufort
Flight Line ... 26
Map 1°x 2° ... Manteo
25 0 statute miles 100
Florence
76°W
24 25 26
34
Cape Fear
EROS/USGS Geographic Applications Program

Figure 1

EXPERIMENTAL APPLICATIONS OF MULTISPECTRAL DATA TO NATURAL RESOURCE INVENTORY AND SURVEY

by

Harry J. Mallon
Office of Emergency Preparedness
Executive Office of the President
Washington, D.C.

INTRODUCTION

The primary purpose of the Office of Emergency Preparedness (OEP) experimental research in this phase of work has been to examine the feasibility of using multispectral, color, color infrared, thermal infrared imagery and related ground data to recognize, identify, determine and monitor the status of mineral ore and metals stockpiles. An attempt has been made to identify valid, unique spectral signatures of such materials for possible use under a wide variety of environmental circumstances. Consequently, research emphasis during 1970 has been upon the analysis of the multiband imagery from the various film-filter combinations, using density analysis techniques.

PROCEDURES

Six sample sites were selected to provide samples of different materials and their spectral differences. Site selection was also governed by the presence of similar or identical materials at different locations. Arrangements were made through the USGS Geographic Applications Program and NASA Manned Spacecraft Center at Houston for instrumented aircraft overflights at altitudes of 4,000; 8,000; and 20,000 ft. between 1000 and 1500 hours, local time, between May and August 1969. Instrumentation included two RC-8 cameras with Aerial Ektachrome and Ektachrome infrared film; multiband imagery using Plus X Aerographic Film in three cameras exposing in the 400-500 mu, 500-600 mu, and 600-700 mu ranges, and one camera using Aerographic infrared film to be exposed in the near infrared. Thermal IR imagery was requested in the 8-14 u range.

Arrangements were also made with General Services Administration personnel to collect ground data at these test sites at times (or close to) of overflight.

The following data were collected:

1. Site 201, Mission 104, Sept. 14, 1969 at 1756-1813 G.m.t. (Rec'd. 2-13-70)

Aircraft instruments:

Three Hasselblads (40 mm); 2402 film; filters 25A, 47B, 58B

One Hasselblad (40 mm); 5424 film; filter 89B

One RC-8; film SO-117

One RC-8; film 2448

Reconofax IV Scanner 8-14 u.

Quality: Color very good; multiband B/W and B/W IR very dense; Recon IV not useable.

Ground Team:

Physical dimensions of material piles; length, width, height, slope angles. Temperature readings of materials in place and of surrounding air envelope. Color slide transparencies.

2. Site 202, Mission 115, Dec. 2, 1969 at 1912-1946 G.m.t. (Rec'd. 2-13-70)

Aircraft instruments:

Essentially the same instruments and data; one RC-8; film SO-397 (vice 2448).

Quality: Color IR excellent; aerial color fair to good; multiband imagery good; Recon IV imagery not useable.

Ground Team: Same data.

3. Site 203, Mission 111, Oct. 14, 1979 at 1536-1632 G.m.t. (Rec'd. 2-13-70)

Aircraft instruments:

Essentially the same instruments and data; RS 7 IR Scanner vice Recon IV.

Quality: Color IR fair to good (underexposed at 20,000 ft.); color fair to good (some camera malfunction); multiband B/W fair to good; B/W IR fogged; RS-7 much improved over Recon IV (static at 20,000 ft.). Best data at 4000 ft.

Ground Team: Same data.

4. Site 204, Mission 136, May 27, 1970 at 1404-1503 G.m.t. (Rec'd. 6-22-70)

Aircraft instruments:

Essentially the same instruments and data; Hasselblads with film types 2402 and 5424; Recon IV vice RS-7 scanner.

Quality: All data good and useable. Recon IV imagery very good, possible side uses.

Ground Team: Same data.

5. Site 205, Mission 115, Dec. 2, 1969, at 1750-1803 G.m.t. (Rec'd. 2-13-70)

Aircraft instruments: Same instruments and data as for Site 202.

Quality: Same comment.

Ground Team: Same data.

6. Site 206, Mission 136, May 27, 1970, at 1513-1615 G.m.t. (Rec'd. 2-13-70)

Aircraft instruments: Same instruments and data as for Site 204.

Quality: Same comment as for Site 204. Data extremely good at all altitudes; color seems best at 4000 ft.; at that altitude, the flight run just caught edge of target area.

Ground Team: Same data.

ANALYSIS AND DISCUSSION

All imagery collected were examined on a comparative basis over multiple light table arrays. Optimal color, color IR frames were selected for analysis, presentation to OEP materials management, reports, and for use as initial inputs of remote sensing data to supplement specific resource materials data files.

The piles of materials chosen for this investigation were bauxite, chromite, manganese, and lead. They were selected because of their anticipated different spectral responses. Because of a lack of comparative data on lead, it will not be reported on at this time.

The aerial color film presents these tested materials (bauxite, manganese, and chromite) generally in their expected tonal values. The color infrared does so also, but in a more startling way. Some insight is required to recognize what one is looking for as well as some understanding of the colors rendered by the films - particularly the color IR.

For example, the pinks, coral, and reds of the bauxite ores appear in the same relative values in aerial Ektachrome film. On the color infrared film, however, these same colors appear in corresponding shades of green. Refer to Figs. 8 and 9 respectively for this contrast. Dark gray and black substances such as chromite and manganese ores appear generally as one would expect on both types of film but with enhanced contrast on the color infrared.

The piles of bauxite, manganese, and chromite were located and centered on the frames of the multiband imagery, and scan lines for microdensitometric analysis were delineated. The lines were so drawn that two to three density lines along the longitudinal axis of each pile could be run. Where possible, lines were chosen along the top, the bright side, and the shaded side.

Average values of the microdensity data were determined for each filter, film, altitude, scan line, and ore material combination. These values were then plotted against the corresponding average filter wavelength. Figures 2 through 7 and 10 through 11 represent the results of this work.

Chromite

This ore is very dark in color, almost coal-black. It possesses a different texture, crystalline banding structure, and hardness than manganese (also coal-black). Micro-D traces were run on three separate piles which are illustrated in the four multiband frames of Fig. 1. The multispectral plots shown in Figs. 2 and 3 are fairly close in density values and shape, almost congruent. The data shown in Fig. 4 is incomplete; however, a "family" resemblance is seen with the other two curves.

Bauxite

Bauxite is a hydrated aluminum oxide--amorphous and lumpy. It is variably colored pink to dark coral. The multispectral plots for this material are shown in Figs. 5, 6, and 7; and represent the appearance of three different piles of the ore at three different locations. Fairly good agreement appears in the curves in Figs. 5 and 6. There is much less agreement with either of these two in the data shown in Fig. 7. Reasons are uncertain. Some bauxite is imported from Jamaica, some from Surinam, and some from other areas. It is possible that we may be seeing these differences as functions of variations in compoisition, moisture content, conditions of the data gathering, and many other factors. In all cases, it is noted that the reddish color of the ore is emphasized in the density cut by the red filter combination.

Manganese

This ore is also a very dark material. The "step-like" curves of the multispectral plots are shown in Figs. 10 and 11. Data from two

different piles located in two different areas are represented. There are strong differences in the shapes and values of these curves. However, one sees some similarities for an optimistic judgment to suggest a common family resemblance and a possible common spectral response. The diminution of the density values with increasing altitude is presumably due to the accumulative effects of haze and so on.

General

Altitudes flown, as previously noted were 4000 ft., 8000 ft., and 20,000 ft.. In all curves, the multispectral data seems consistent for any one pile of material at all three altitudes.

Comparison with work done by Colwell and associates (see reference No. 8) indicates fairly good agreement by visual comparison of black and white frames taken with red, green, blue, and infrared filters of the tonal values of similar colored substances.

Some questions have been raised relative to the microdensitometric traces inasmuch as the work was done on first generation duplicate positive transparencies rather than on the original film itself. Reruns on the original negatives are being considered and requests for the material on one or two sites will be forthcoming if deemed necessary. It is anticipated, however, that the relative shapes of the curves should not be significantly altered, though the density values may shift.

Analysis of the ground data using the measured pile dimensions and comparison with the results of stereo-comparator computation of the amounts of material in the piles remains to be done. The writer is optimistic about expected results from this phase of work.

A computer analysis of portions of the microdensitometric data has been initiated. However, it, too, is not available for reporting on at this time. Samples of the density run of the bauxite data were selected for this analysis, and it is with much interest that the results are awaited.

CONCULSIONS

In general, the field data, both aerial and ground, were satisfactory and useable. Equipment malfunction and inadvertent missing of some of the target piles (located at edges of flight lines) decreased the total data content; in one case (Site 203) to preclude detailed analysis. However, in the overall, there has been sufficient data to work with, to permit the drawing of several conclusions, to speculate on others, and to eliminate still others from further consideration at this time.

The results definitely confirm that aerial survey methods readily lend themselves to the programmed surveillance of certain natural resource materials. It is entirely feasible to note and record status, changes in physical appearance, location, layout, and to inventory (with limits) assorted materials within the same general storage facilities.

Identification of some of these substances should be entirely possible from an interpretation of the imagery alone. However, in most cases, the combination of reliable field reports plus the imagery would render identification a relatively simple task. Color, toning, sloping, and other observable associated features aid in this respect. In addition, it should also be possible to arrive at quantitative estimates of stocks of materials visible in the photography. Weathering, erosion, growth of vegetation, and other changing factors are observable and would prove useful in augmenting data from ground sources in reporting on status and condition.

The color films are excellent and reliable sensors, preferable in many cases to black and white. Color contains so much more information. The principal drawback is the higher processing cost (time as well as expense). Few government facilities in the Washington, D.C. area can handle large quantities of color work. However, in smaller amounts, the additional information content would more than warrant the extra cost.

The spectral signature investigations are interesting, but at this time, not conclusive. It remains perhaps the most intriguing area of investigation in this series of analyses. The investigation for useful and unique spectral signatures of different materials of these types has been relatively lightly treated. In this analysis, the several piles of materials observed show interesting spectral patterns. The microdensitometry data and filter wavelength plots show spectral relationships which lend support to our initial speculations. On the basis of this initial work, some common reflectance characteristics for given materials seem to be evident. However the body of data is lean (one mission, one date, one time, one set of weather conditions, etc.), and relatively simple analytical procedures were used. Additional data at different conditions of time and date are needed and will be requested.

The data from the thermal infrared scanners were examined. There seems to be no unique thermal response observable, hence the usefulness of this sensor for further investigations in this connection is considered limited. However, some very interesting thermal variations of down-stream hydro-electric dam effluent were observed, which obviously have application in river/stream pollution investigations.

Recommendations have been made in-house for further and extended use of color, color IR, and (on a selective basis) multiband imagery for follow-up materials surveys and analyses. These data obtained on a

periodic basis (say annually) will enable managers of these stocks to improve materially their data position with respect to making the requisite judgments and decisions relative to this program. Examination is presently being given to possible extention of this work as an additional investigation within the ERTS-A and B experiment.

REFERENCES

1. Bonau, U., 1967, Application of photography to the survey of cross-profiles: Vermess. -Techn., Berlin, v. 15, no. 3, pp. 90-92.

2. Henderson, H.L. and Jacoby, H., 1960, Stockpile measurements by automatic data recording and electronic computation: Photogrammetric Engineering, v. 26, no. 1, pp. 54-59.

3. Marschall, G., 1966, Determination of earthwork quantities by terrestrial photogrammetry: Eisenbahningenieur, Frankfort a M., v. 17, no. 1, pp. 9-13.

4. Massa, W.S., 1958, Inventory of large coal piles: Photogrammetric Engineering, v. 24, no. 1, pp. 77-81.

5. Pierson, W.R., 1959, The validity of stereophotogrammetry in volume determination: Photogrammetric Engineering, v. 25, no. 1, pp. 83-84.

6. Sutti, J., 1965, Volume determination on the basis of a point-by-point plotting with a stereocomparator: Geod. a Kartogr. Obzor, Praha, v. 11, no. 8, pp. 197-199.

7. Young, H.E., 1955, Photogrammetric volume determination of huge pulpwood piles: Canadian Surveyor, v. 12, pp. 536-542.

8. Colwell, R.N., Draeger, W.C., Lent, J.D., Thorley, G.A., 1966, A multispectral photographic experiment based upon statistical analysis of spectrometric data: A report of research performed under NASA Grant NGR/05-003-080.

9. Fritz, N.L., 1967, Optimum methods for using infrared-sensitive color film: Photogrammetric Engineering, v. 32, no. 10, pp. 1128-1138.

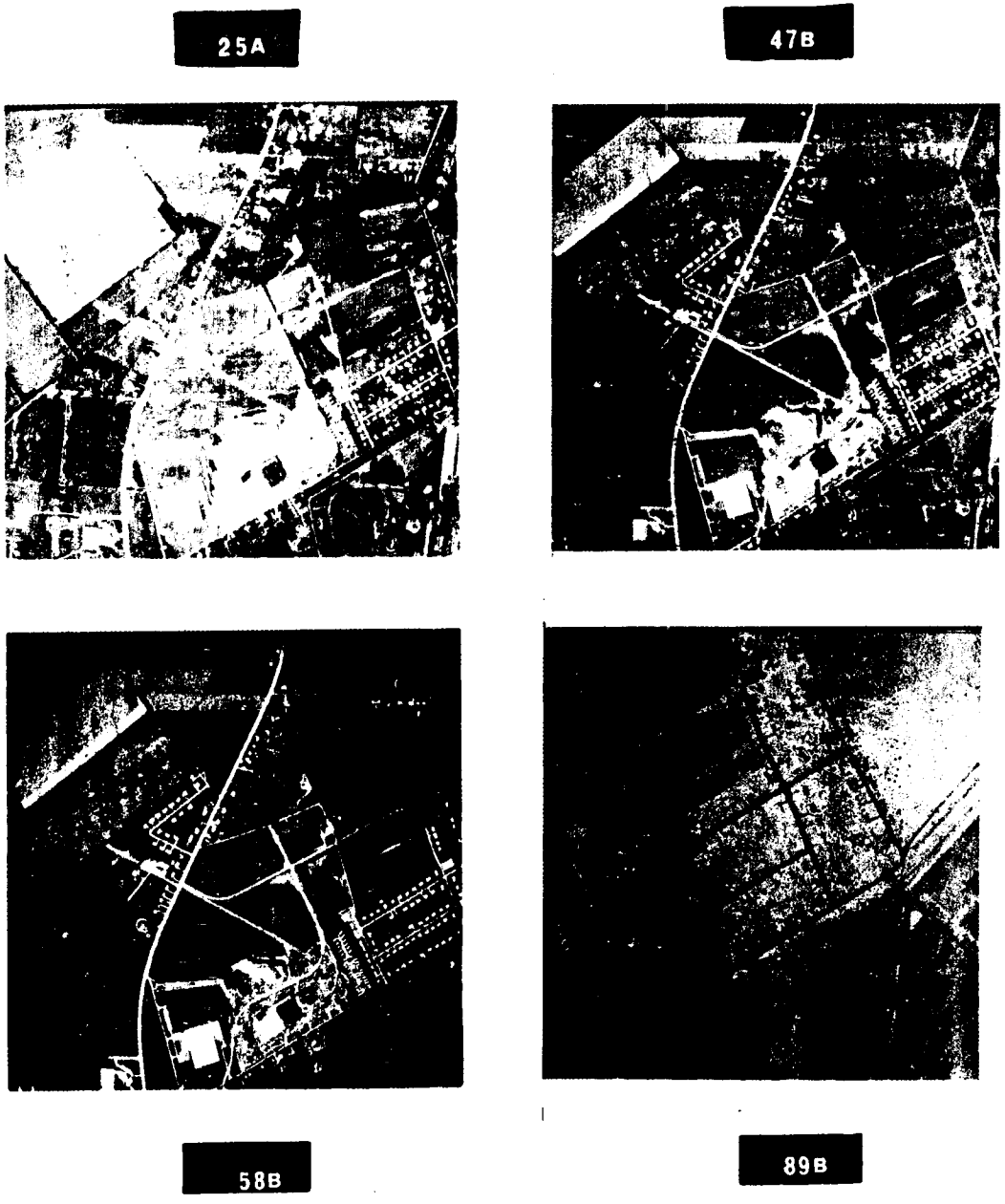

Multiband Views of piles of chromite ore.

Figure 1

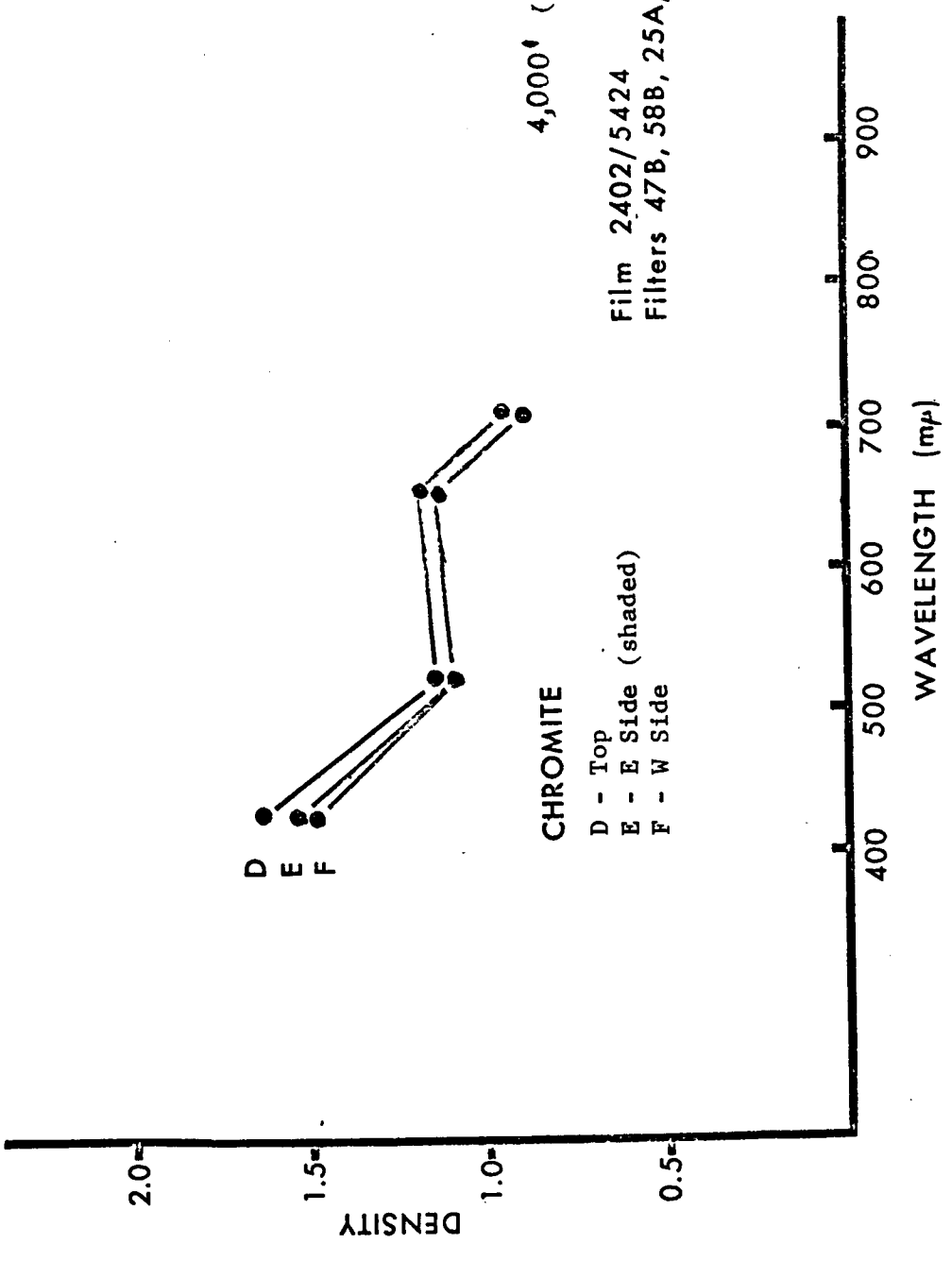
4,000' (altitude)
Film 2402/5424
Filters 47B, 58B, 25A/89B
CHROMITE
D - Top
E - E Side (shaded)
F - W Side
D
E
F
DENSITY
2.0
1.5
1.0
0.5
400
500
600
700
800
900
WAVELENGTH (mμ)

Figure 2

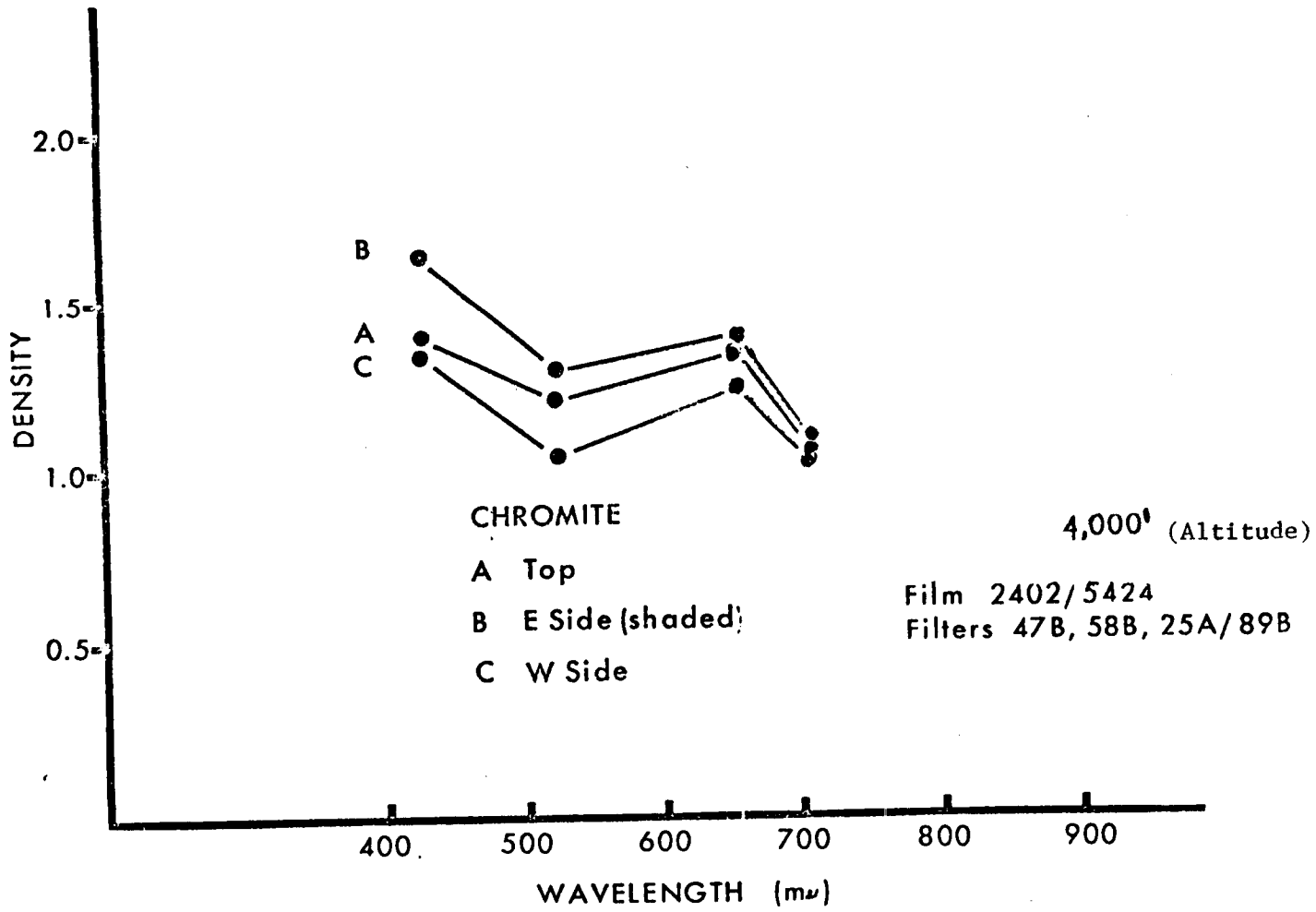
2.0
1.5
1.0
0.5
DENSITY
B
A
C
CHROMITE
A Top
B E Side (shaded)
C W Side
4,000' (Altitude)
Film 2402/5424
Filters 47B, 58B, 25A/89B
400
500
600
700
800
900
WAVELENGTH (mμ)

Figure 3

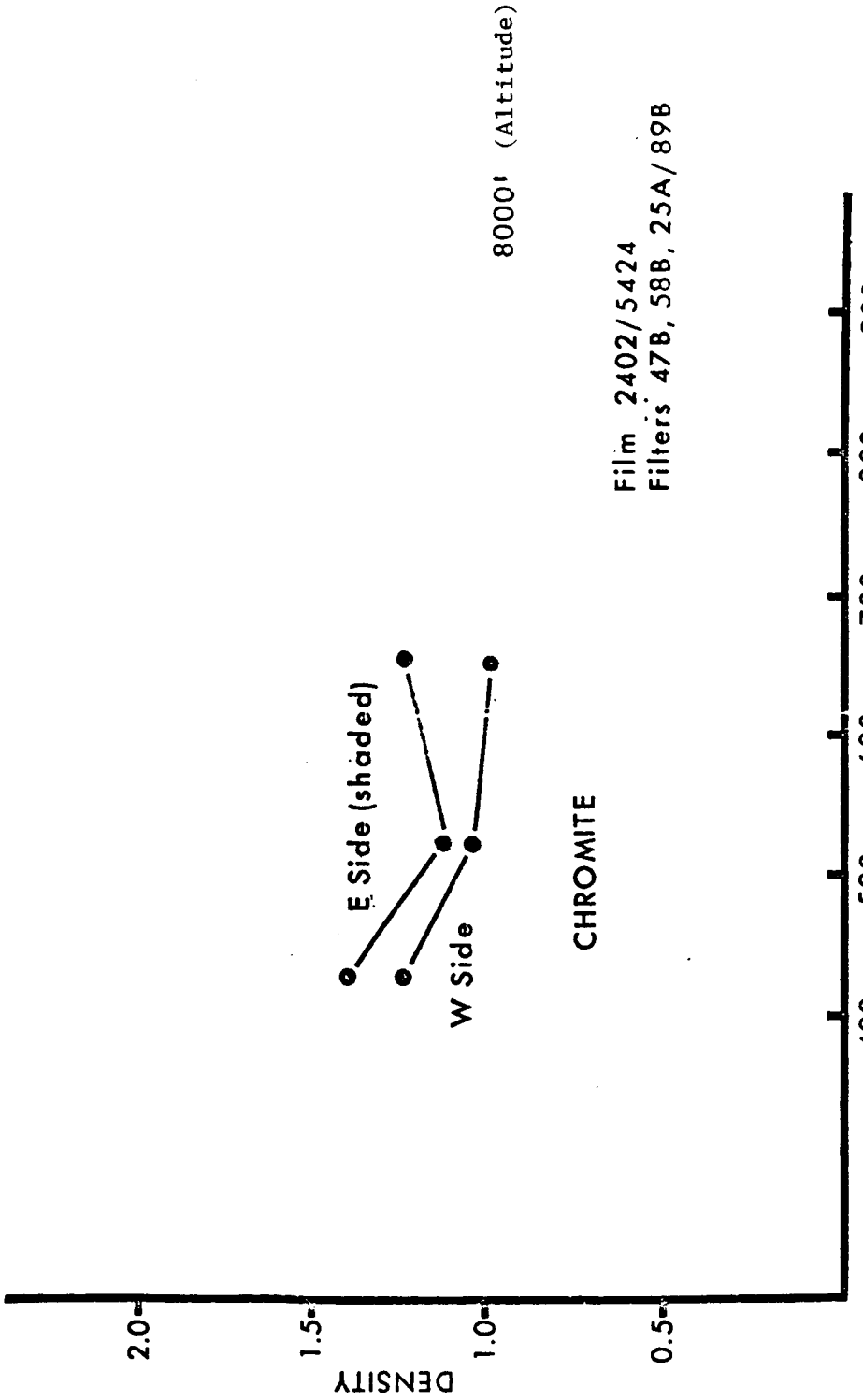
8000' (Altitude)
Film 2402/5424
Filters 47B, 58B, 25A/89B
CHROMITE
E Side (shaded)
W Side
DENSITY
2.0
1.5
1.0
0.5
400
500
600
700
800
900
WAVELENGTH (mμ)

Figure 4

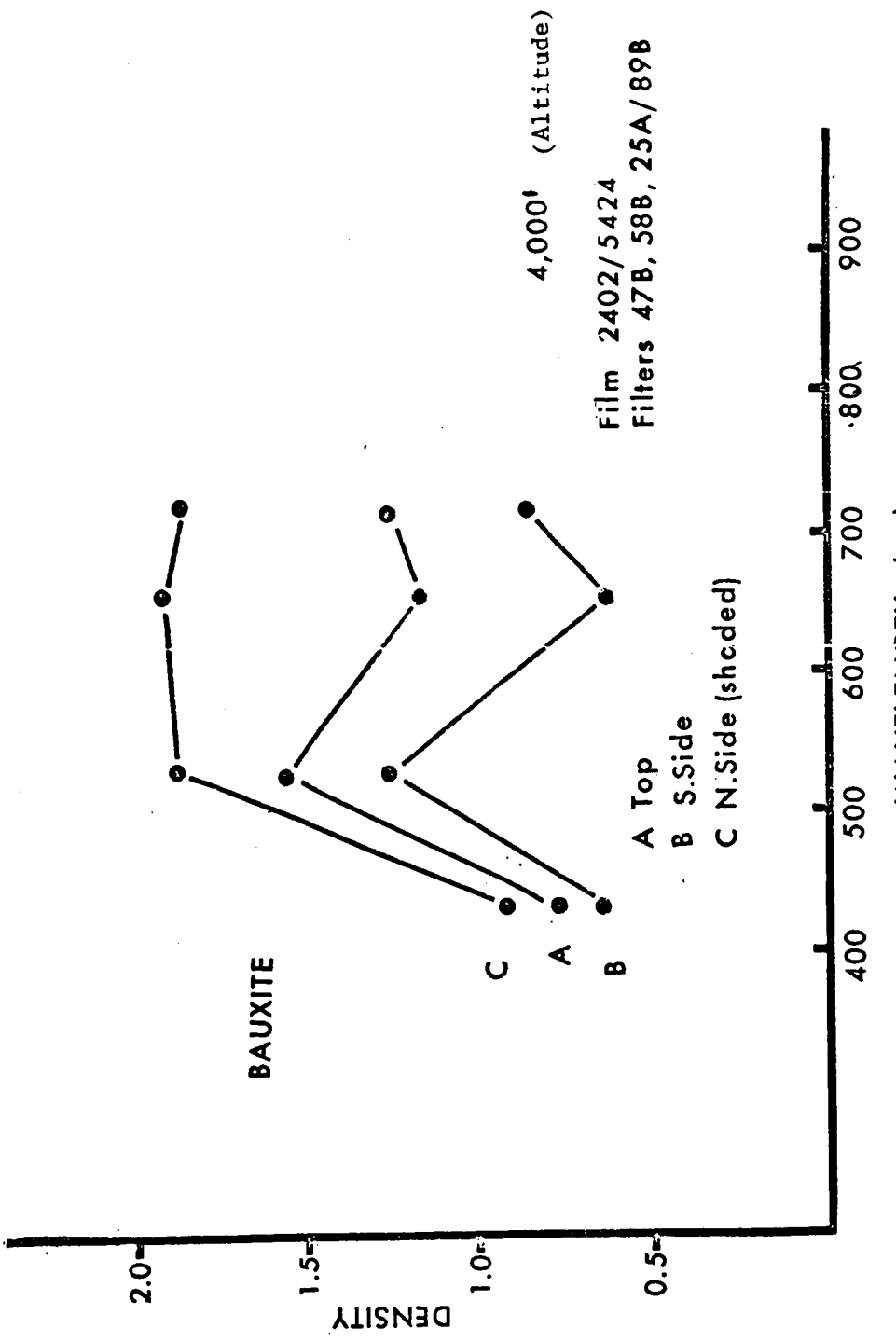
BAUXITE
4,000' (Altitude)
Film 2402/5424
Filters 47B, 58B, 25A/89B
A Top
B S.Side
C N.Side (shaded)
DENSITY
2.0
1.5
1.0
0.5
400
500
600
700
800
900
WAVELENGTH (mμ)
A
B
C

Figure 5a

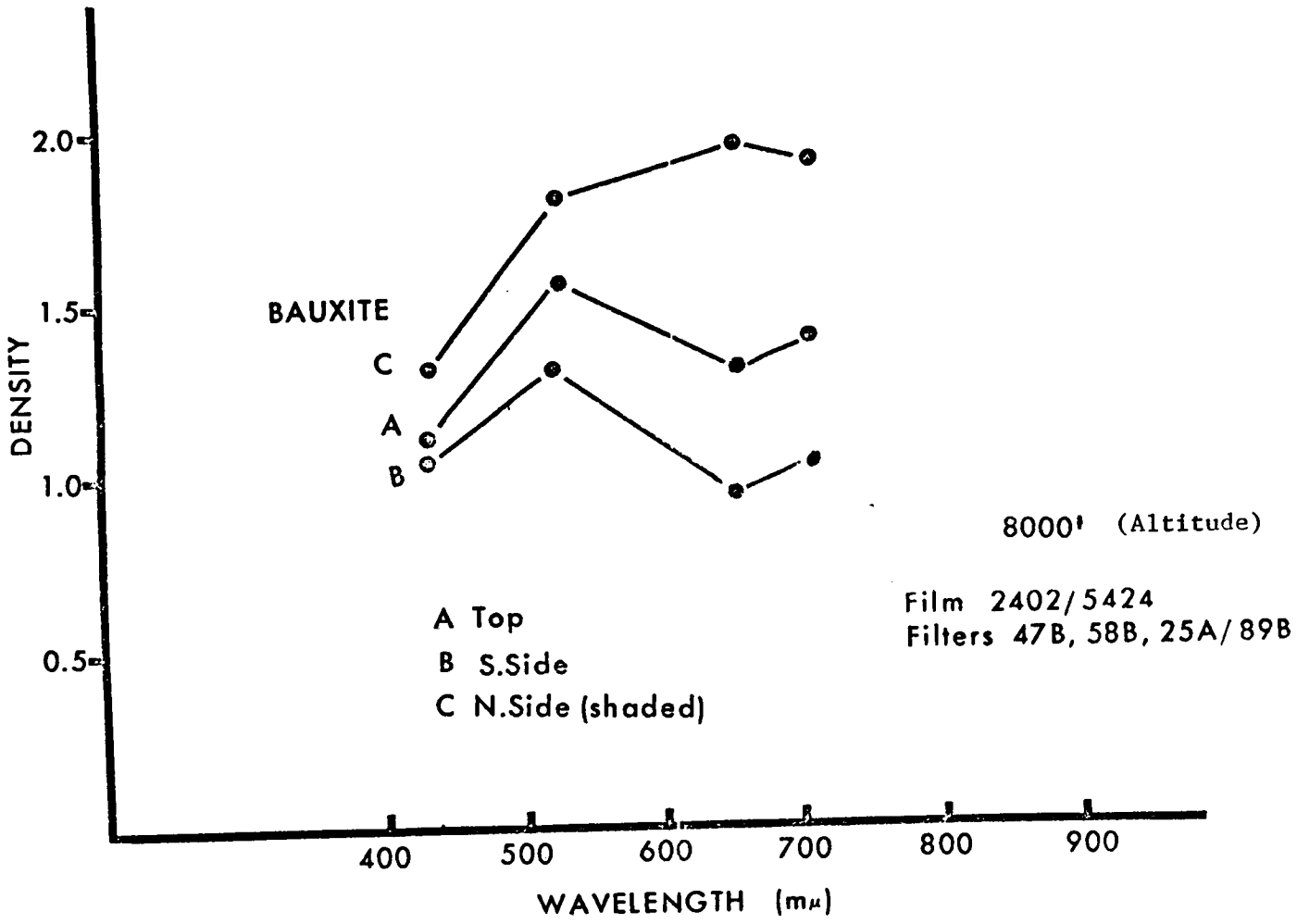
2.0
1.5
1.0
0.5
DENSITY
BAUXITE
C
A
B
8000' (Altitude)
A Top
B S.Side
C N.Side (shaded)
Film 2402/5424
Filters 47B, 58B, 25A/89B
400
500
600
700
800
900
WAVELENGTH (mμ)

Figure 5b

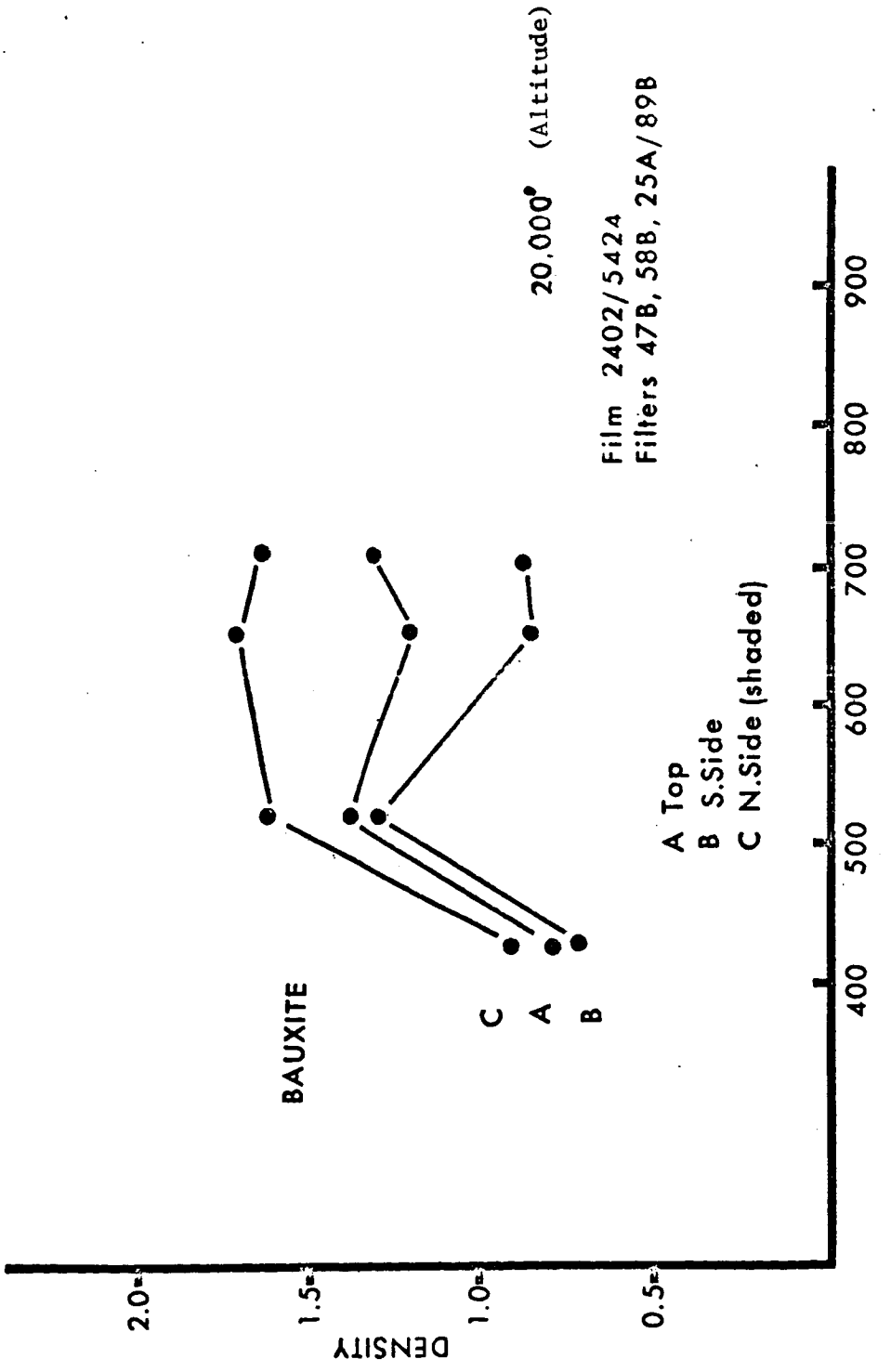
20,000' (Altitude)
Film 2402/5424
Filters 47B, 58B, 25A/89B
A Top
B S.Side
C N.Side (shaded)
BAUXITE
C
A
B
DENSITY
2.0
1.5
1.0
0.5
400
500
600
700
800
900
WAVELENGTH (mμ)

Figure 5c

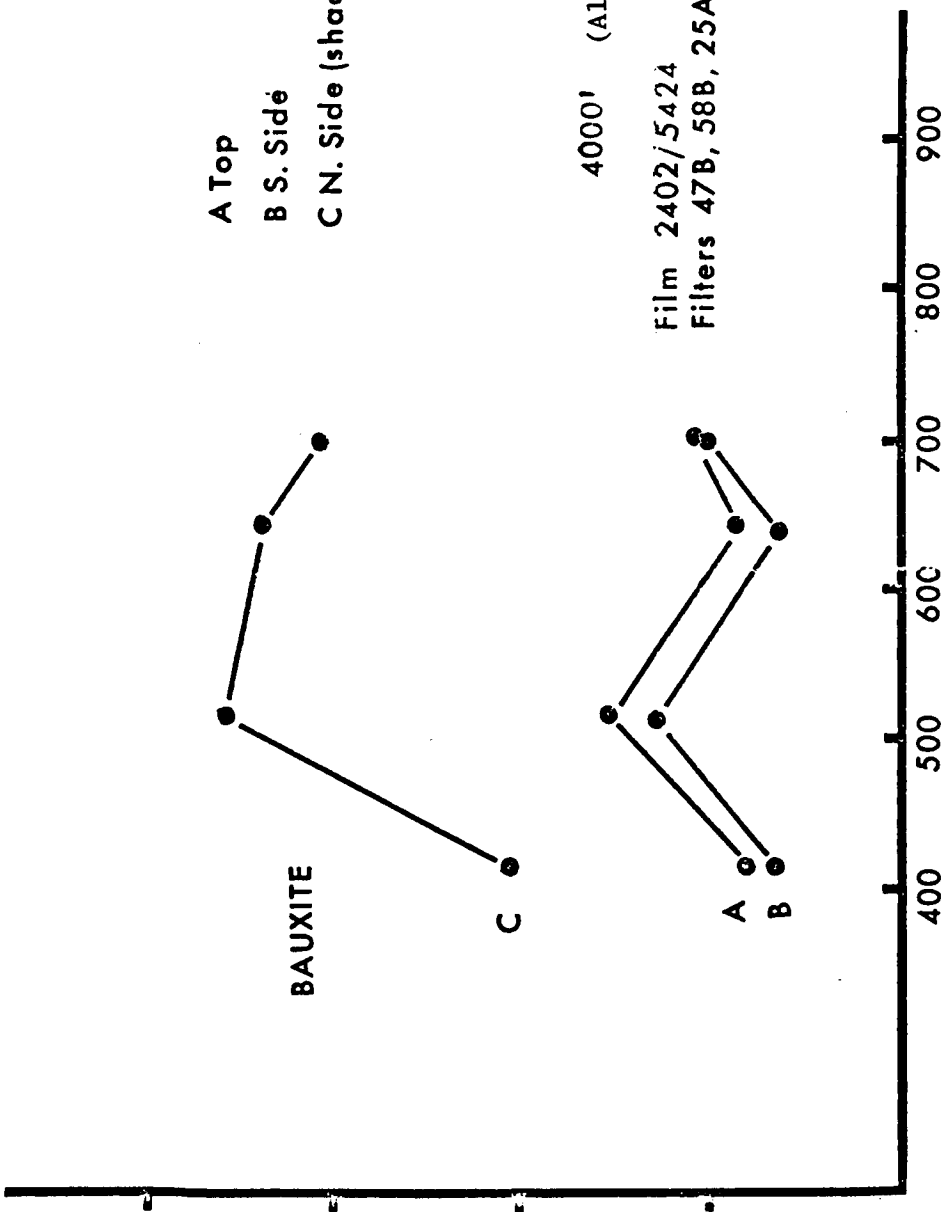
A Top
B S. Side
C N. Side (shaded)
4000' (Altitude)
Film 2402/5424
Filters 47B, 58B, 25A/89B
BAUXITE
C
A
B
DENSITY
2.0
1.5
1.0
0.5
400
500
600
700
800
900
WAVELENGTH (mμ)

Figure 6a

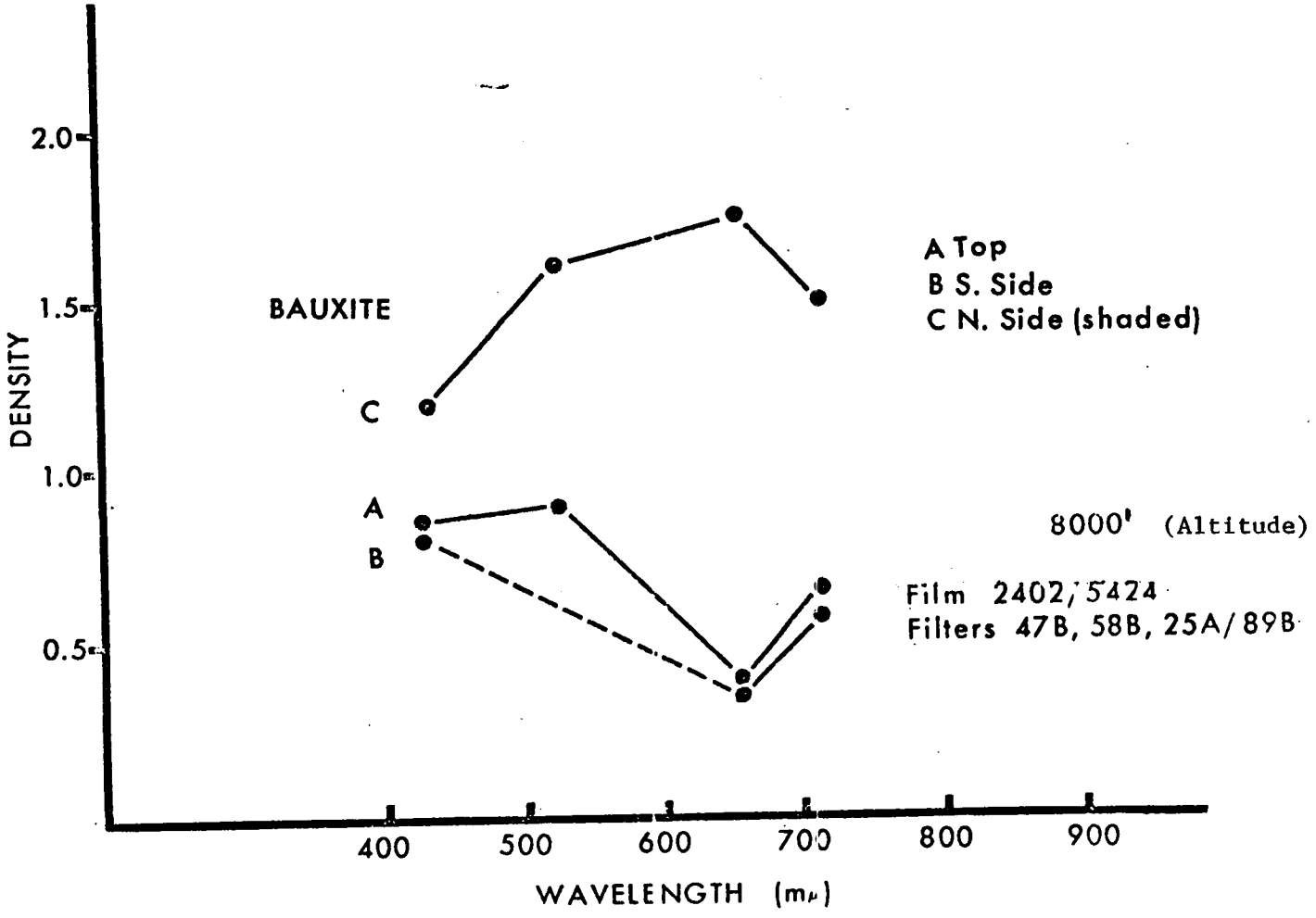
2.0
1.5
1.0
0.5
DENSITY
BAUXITE
C
A
B
A Top
B S. Side
C N. Side (shaded)
8000' (Altitude)
Film 2402/5424
Filters 47B, 58B, 25A/89B
400
500
600
700
800
900
WAVELENGTH (mμ)

Figure 6b

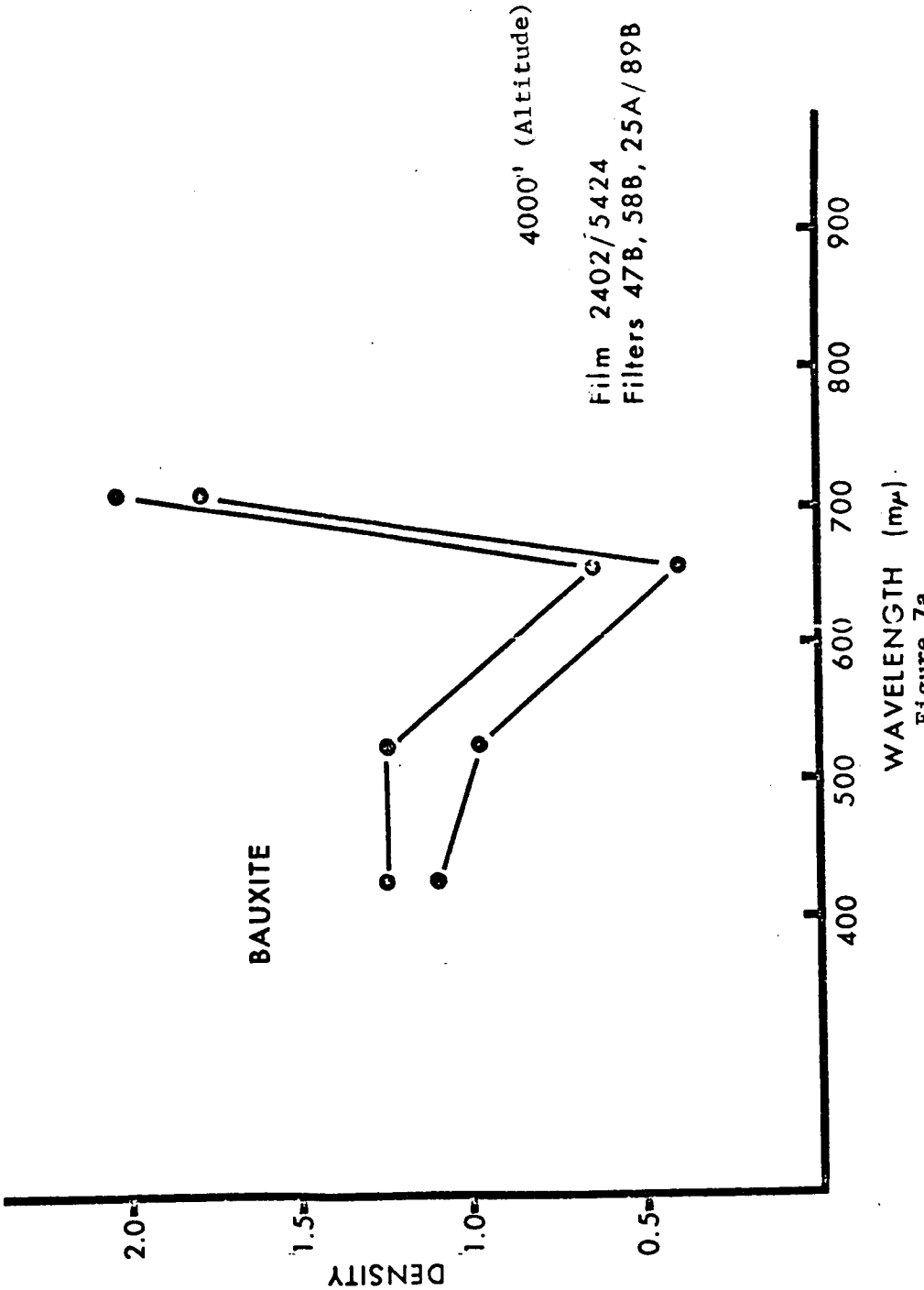
4000' (Altitude)
Film 2402/5424
Filters 47B, 58B, 25A/89B
BAUXITE
DENSITY
2.0
1.5
1.0
0.5
400
500
600
700
800
900
WAVELENGTH (mμ)

Figure 7a

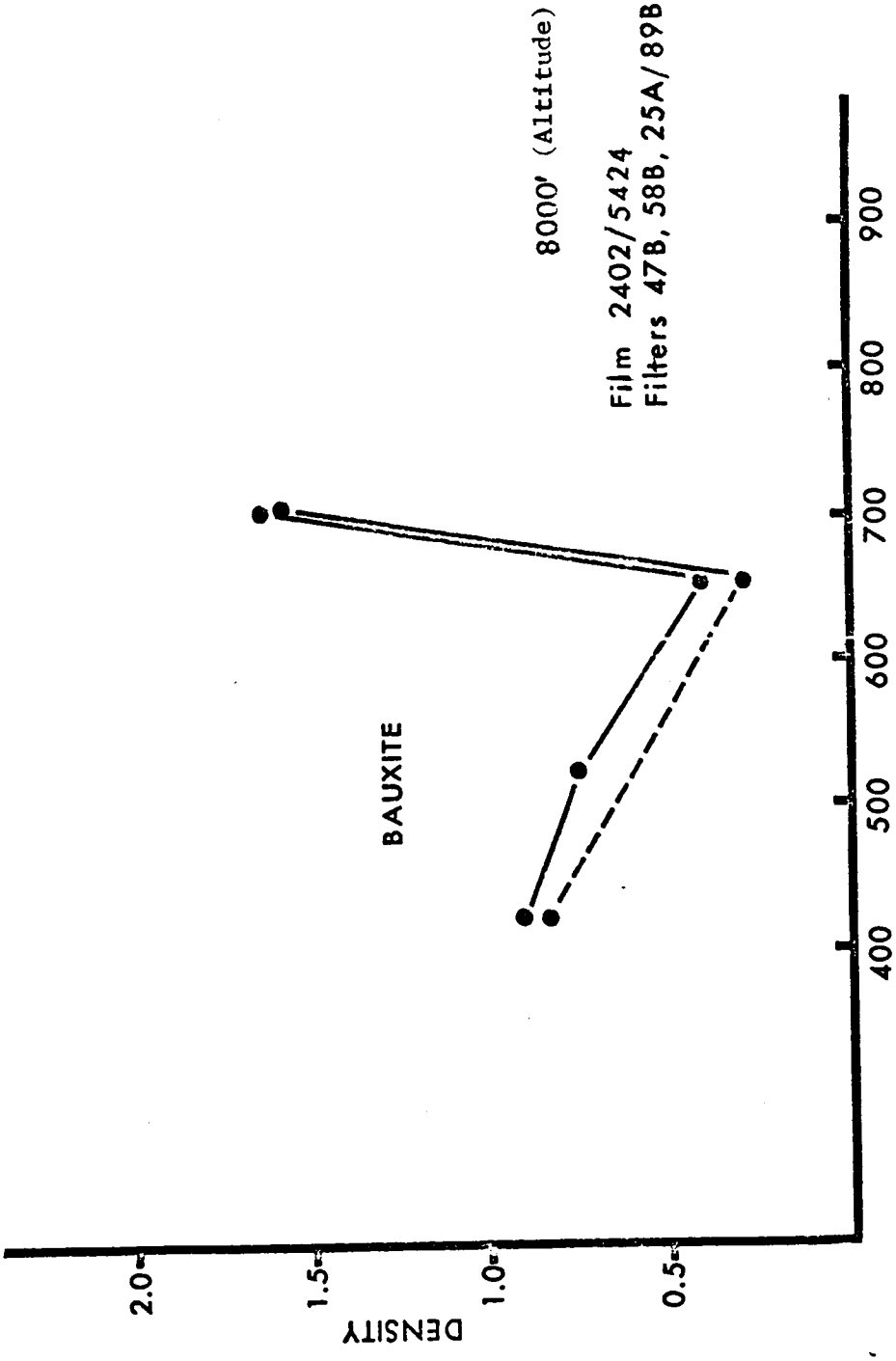
8000' (Altitude)
Film 2402/5424
Filters 47B, 58B, 25A/89B
BAUXITE
DENSITY
2.0
1.5
1.0
0.5
400
500
600
700
800
900
WAVELENGTH (mμ)

Figure 7b

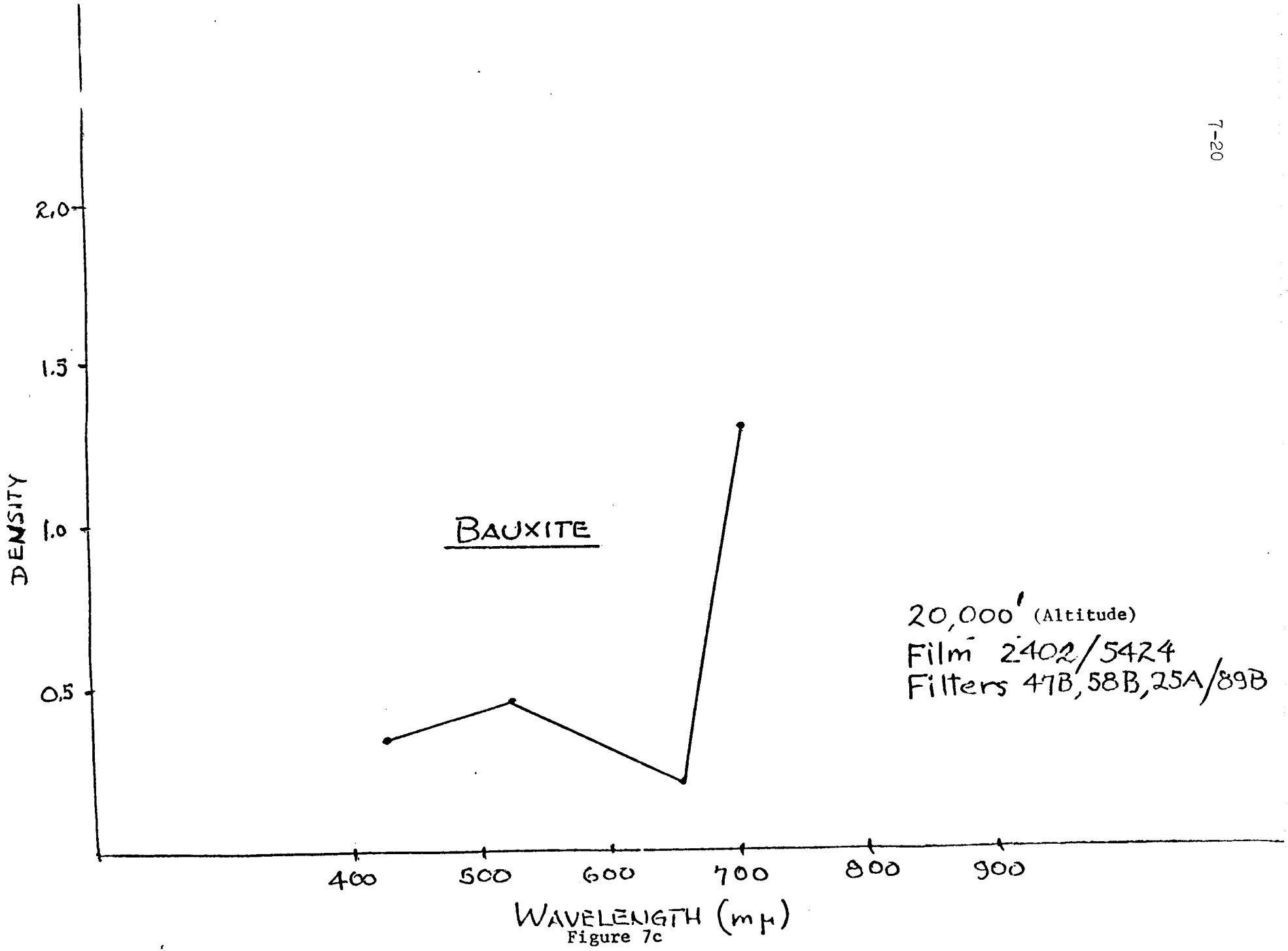
2.0
1.5
1.0
0.5
DENSITY
BAUXITE
20,000' (Altitude)
Film 2402/5424
Filters 47B, 58B, 25A/89B
400
500
600
700
800
900
WAVELENGTH (mμ)

Figure 7c

Fig. 8
Bauxite - Aerial Ektachrome

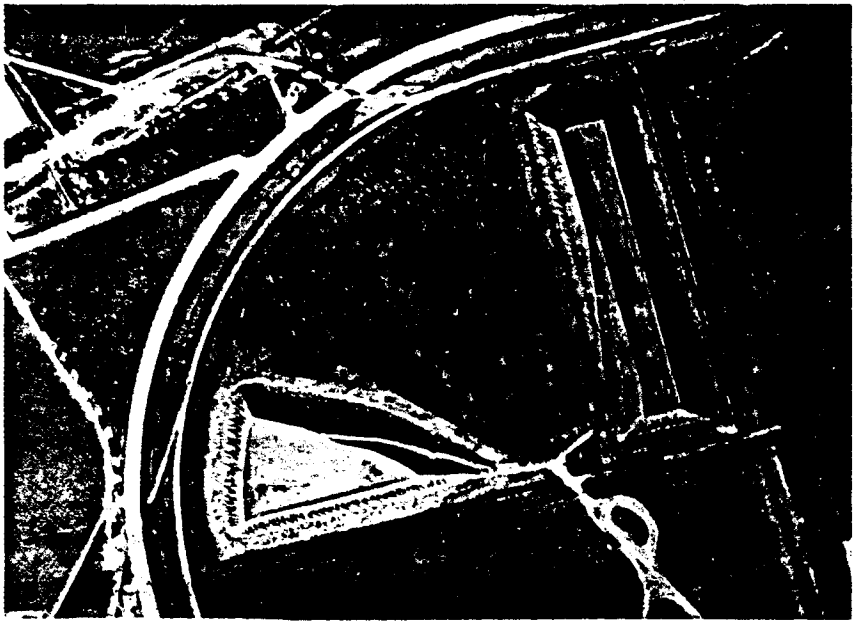

Fig. 9
Bauxite - Color Infrared

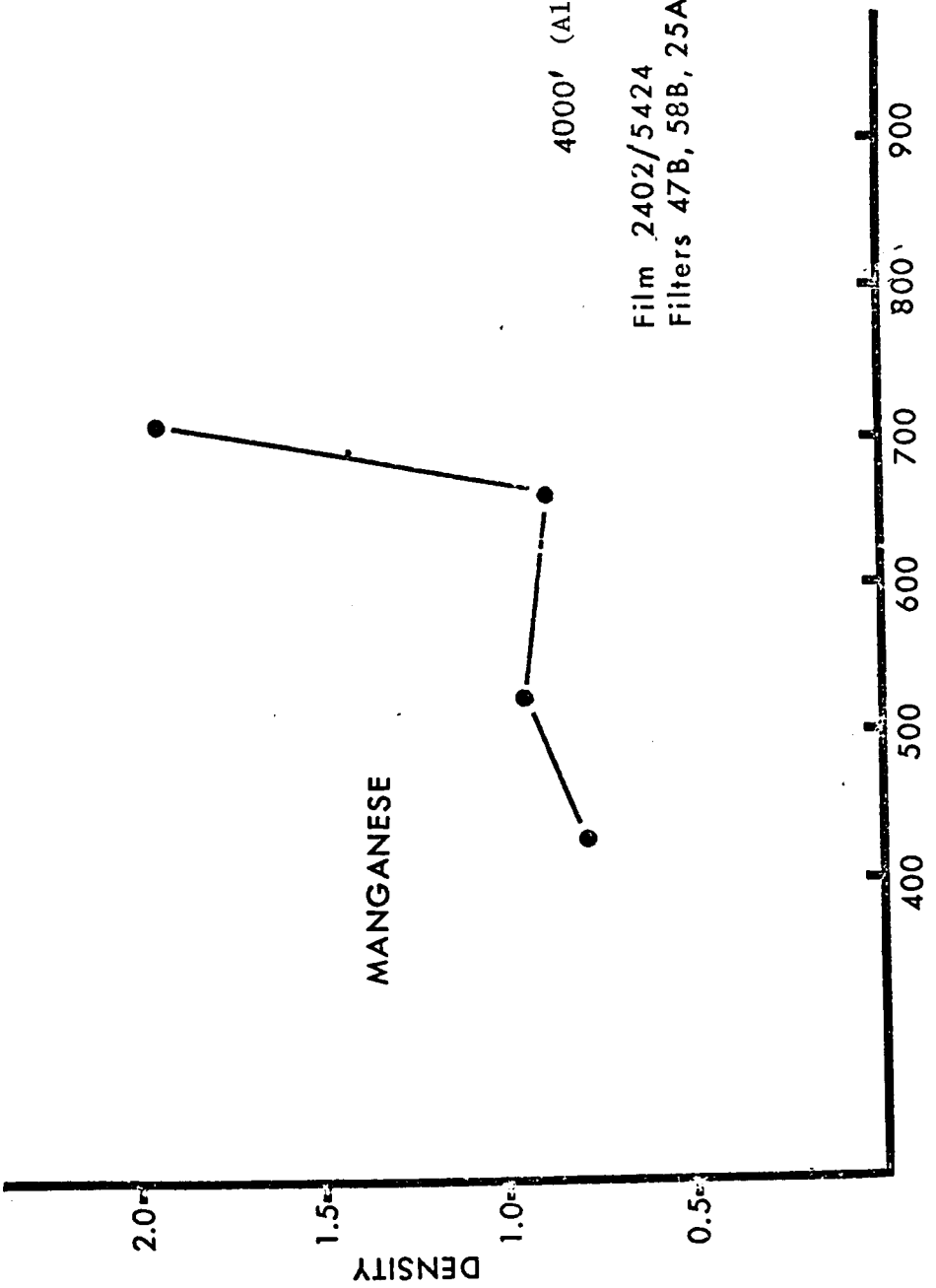
4000' (Altitude)
Film 2402/5424
Filters 47B, 58B, 25A/89B
MANGANESE
DENSITY
2.0
1.5
1.0
0.5
400
500
600
700
800
900
WAVELENGTH (mμ)

Figure 10a

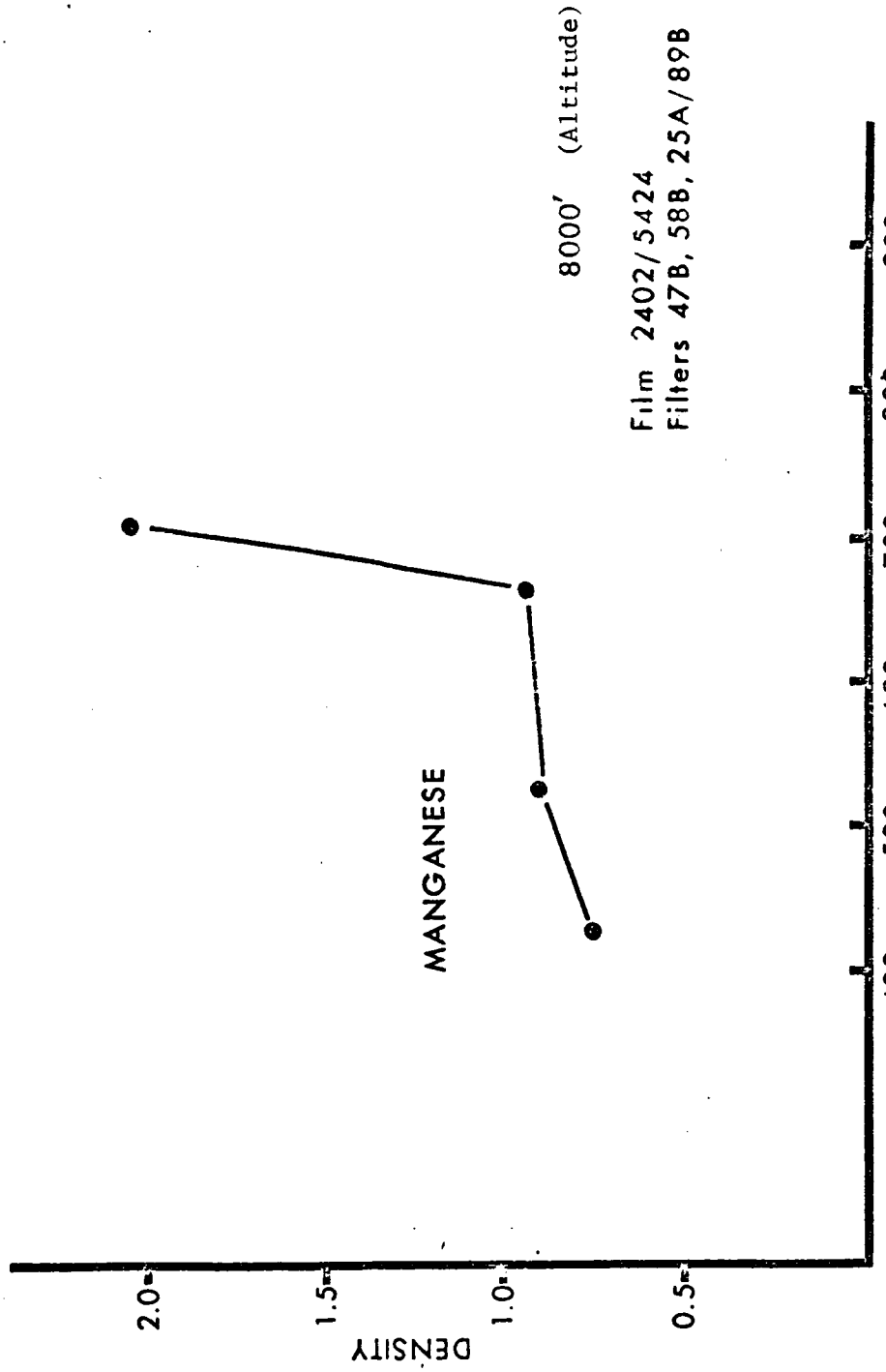
8000' (Altitude)
Film 2402/5424
Filters 47B, 58B, 25A/89B
MANGANESE
DENSITY
2.0
1.5
1.0
0.5
400
500
600
700
800
900
WAVELENGTH (mμ)

Figure 10b

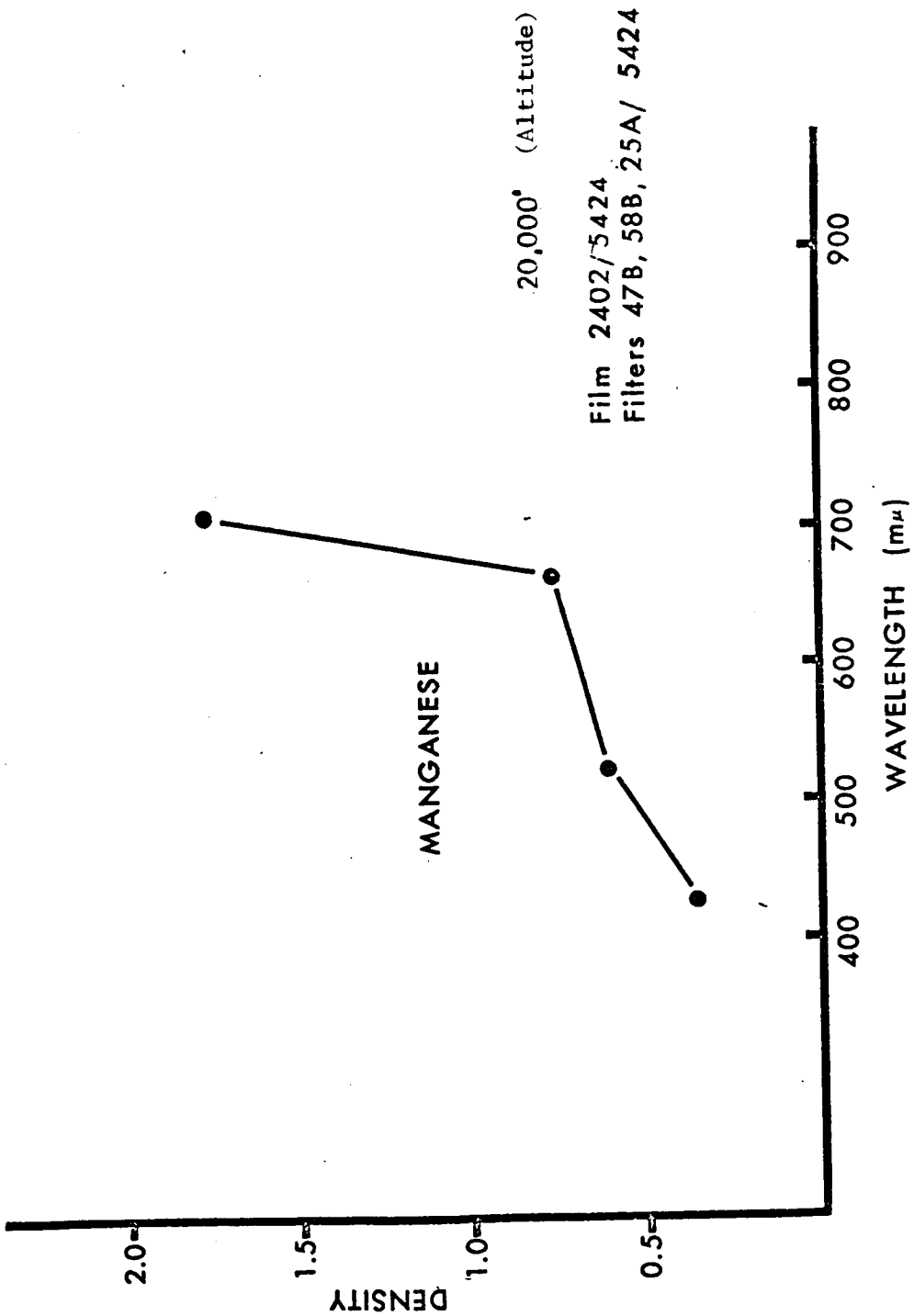
MANGANESE
20,000' (Altitude)
Film 2402/5424
Filters 47B, 58B, 25A/ 5424
DENSITY
2.0
1.5
1.0
0.5
400
500
600
700
800
900
WAVELENGTH (mμ)

Figure 10c

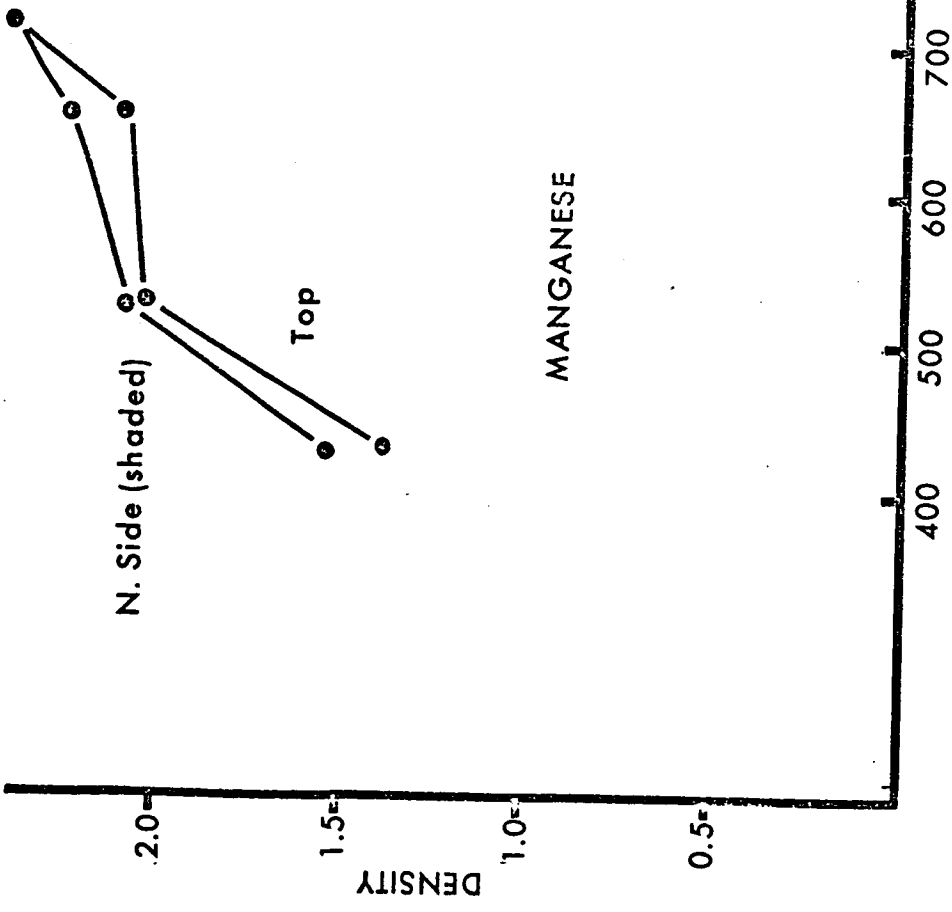
4000' (Altitude)
Film 2402/5424
Filters 47B, 58B, 25A/89B
MANGANESE
N. Side (shaded)
Top
DENSITY
2.0
1.5
1.0
0.5
400
500
600
700
800
900
WAVELENGTH (mμ)

Figure 11a

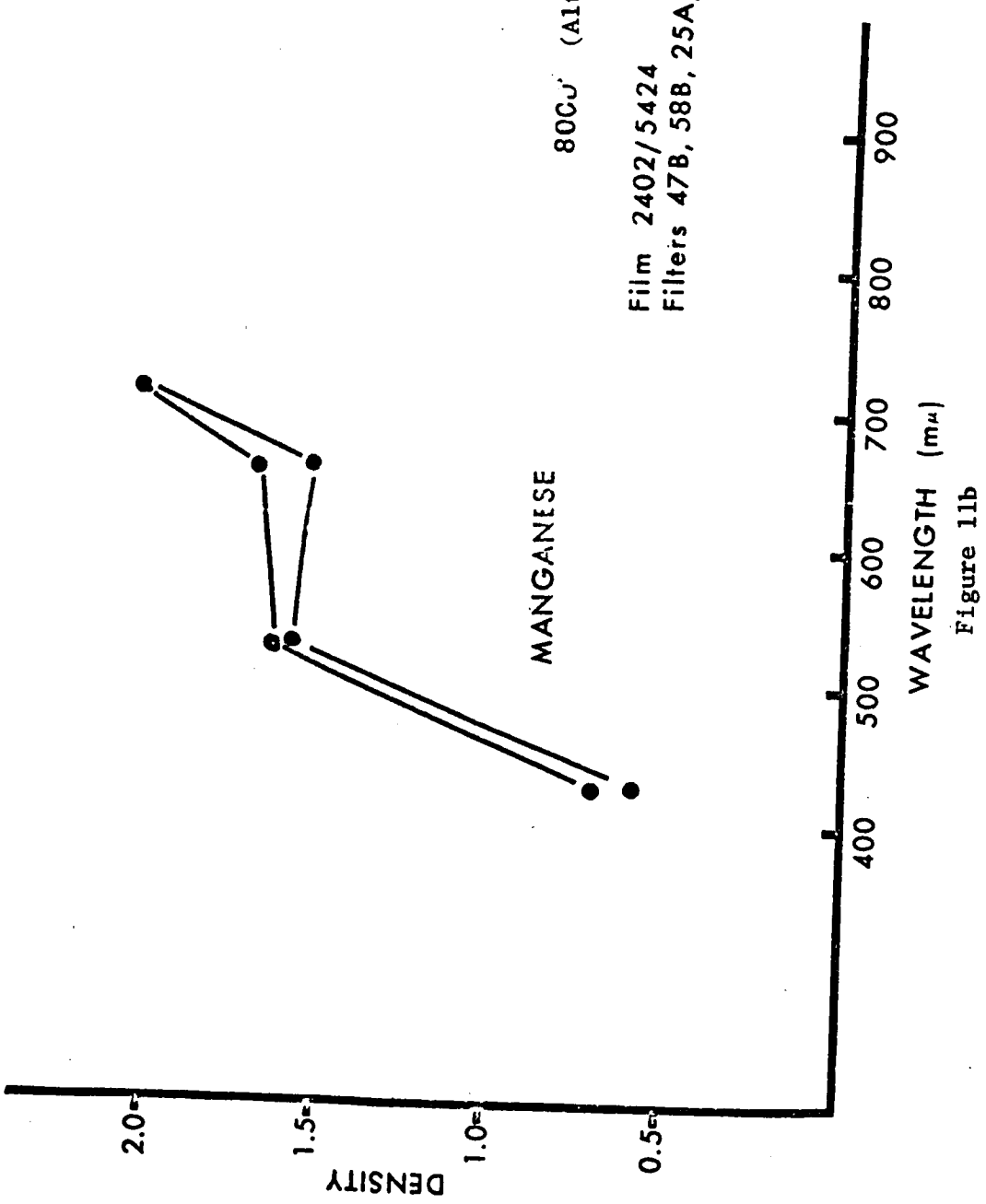
8000' (Altitude)
Film 2402/5424
Filters 47B, 58B, 25A/89B
MANGANESE
DENSITY
2.0
1.5
1.0
0.5
400
500
600
700
800
900
WAVELENGTH (mμ)

Figure 11b

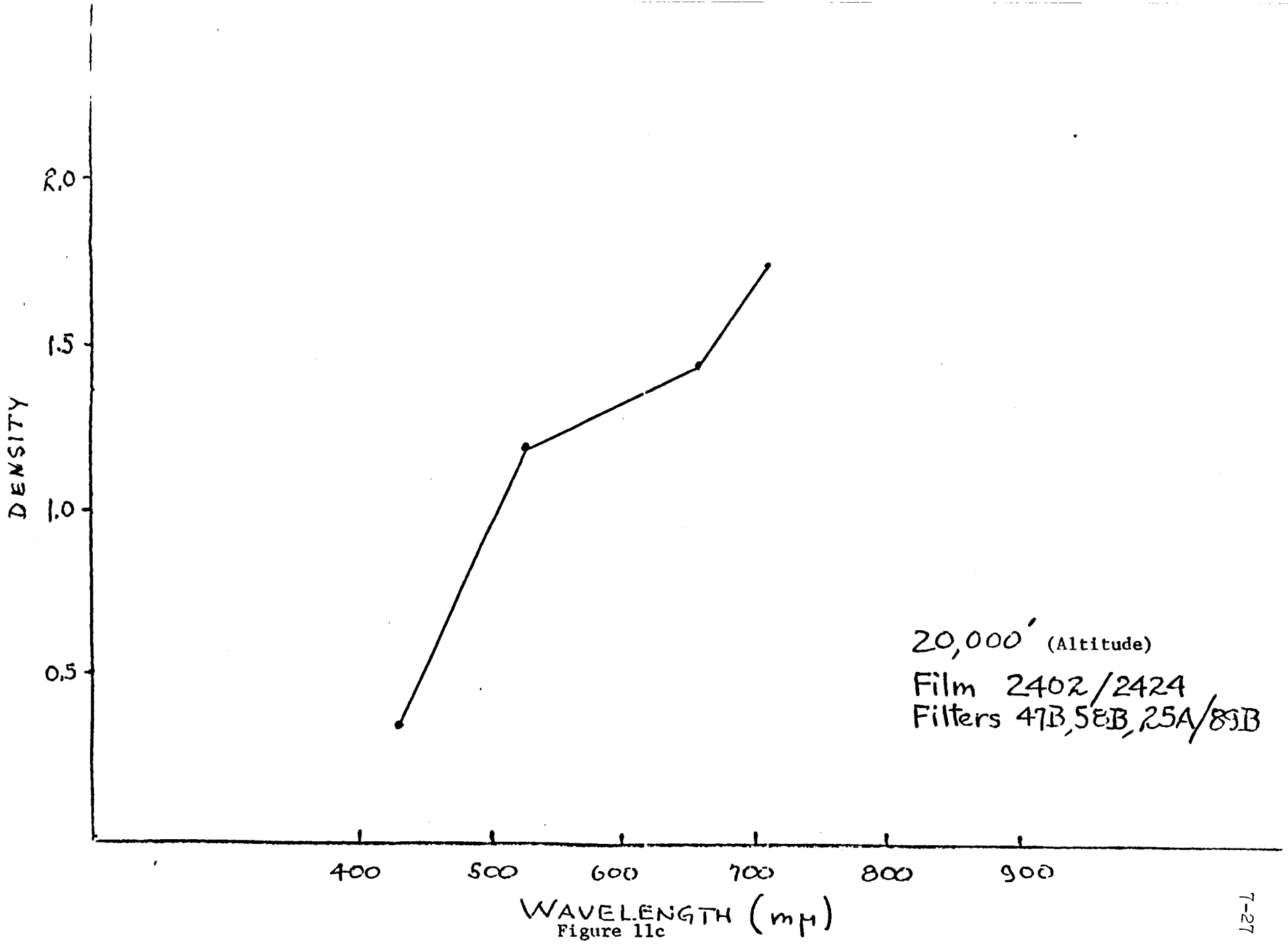
2.0
1.5
1.0
0.5
DENSITY
400
500
600
700
800
900
WAVELENGTH (mμ)
20,000' (Altitude)
Film 2402/2424
Filters 47B, 58B, 25A/89B

Figure 11c

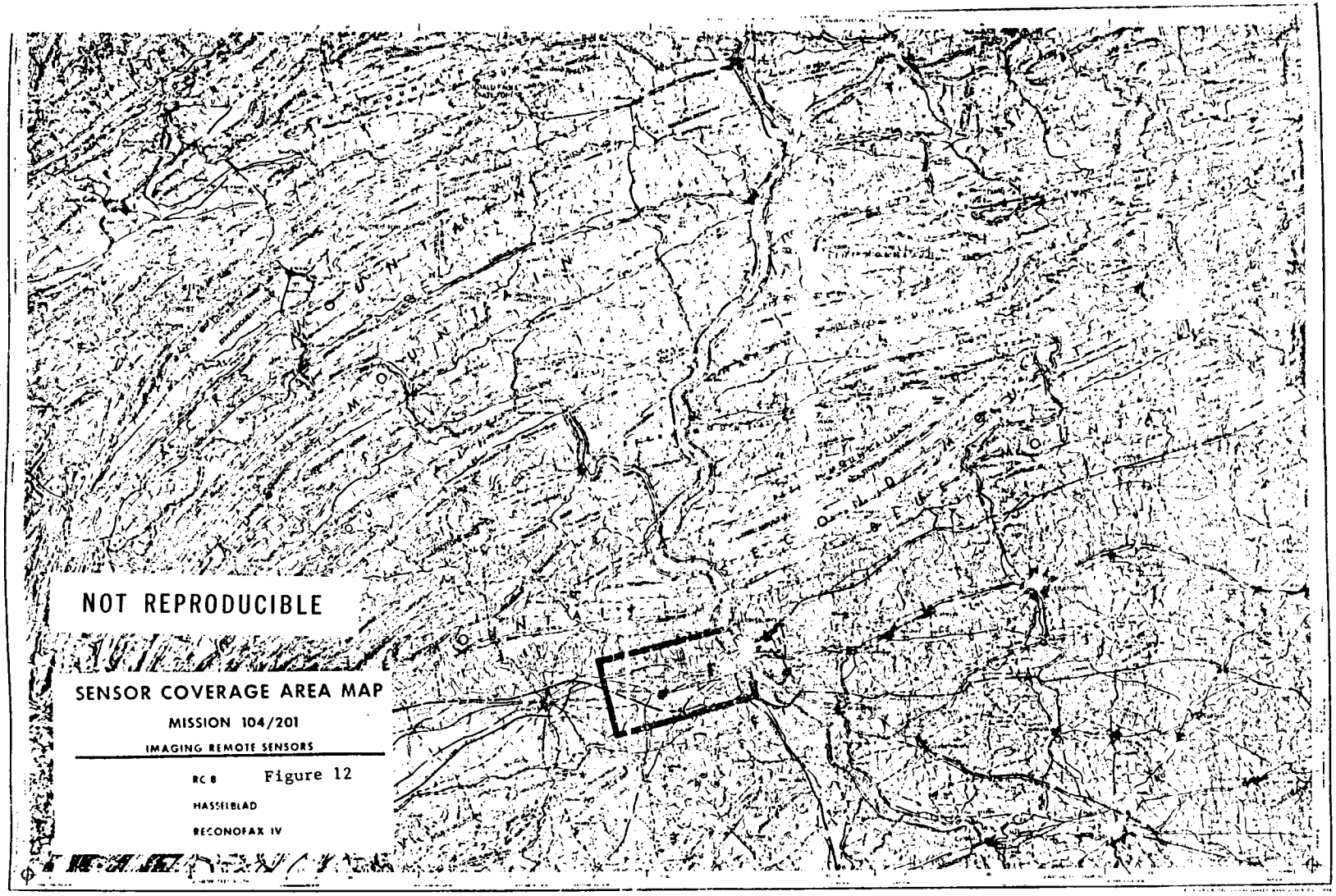
NOT REPRODUCIBLE
SENSOR COVERAGE AREA MAP
MISSION 104/201
IMAGING REMOTE SENSORS
RC 8
HASSELBLAD
RECONOFAX IV
Figure 12
BOSTON
RICHMOND

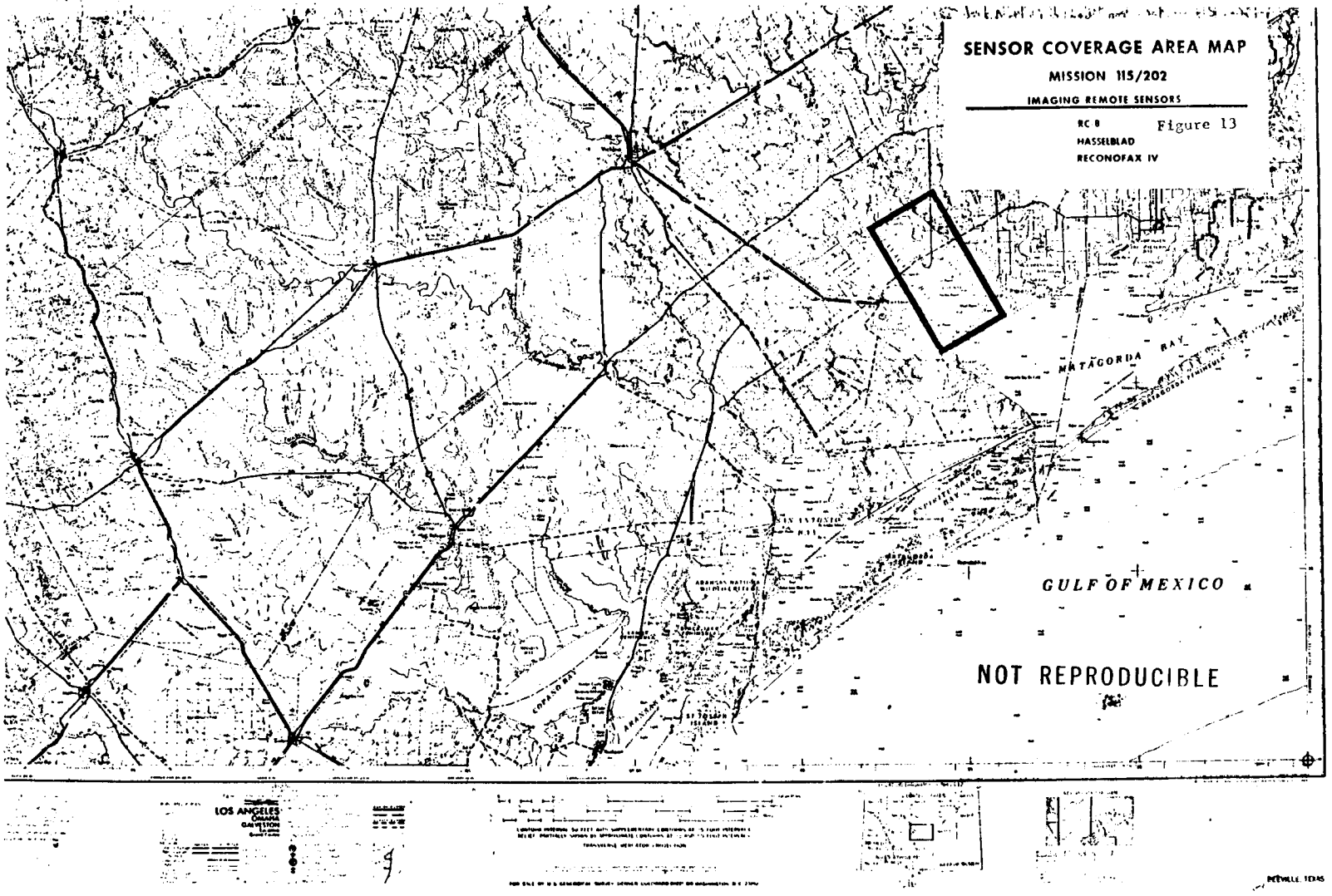

Figure 13

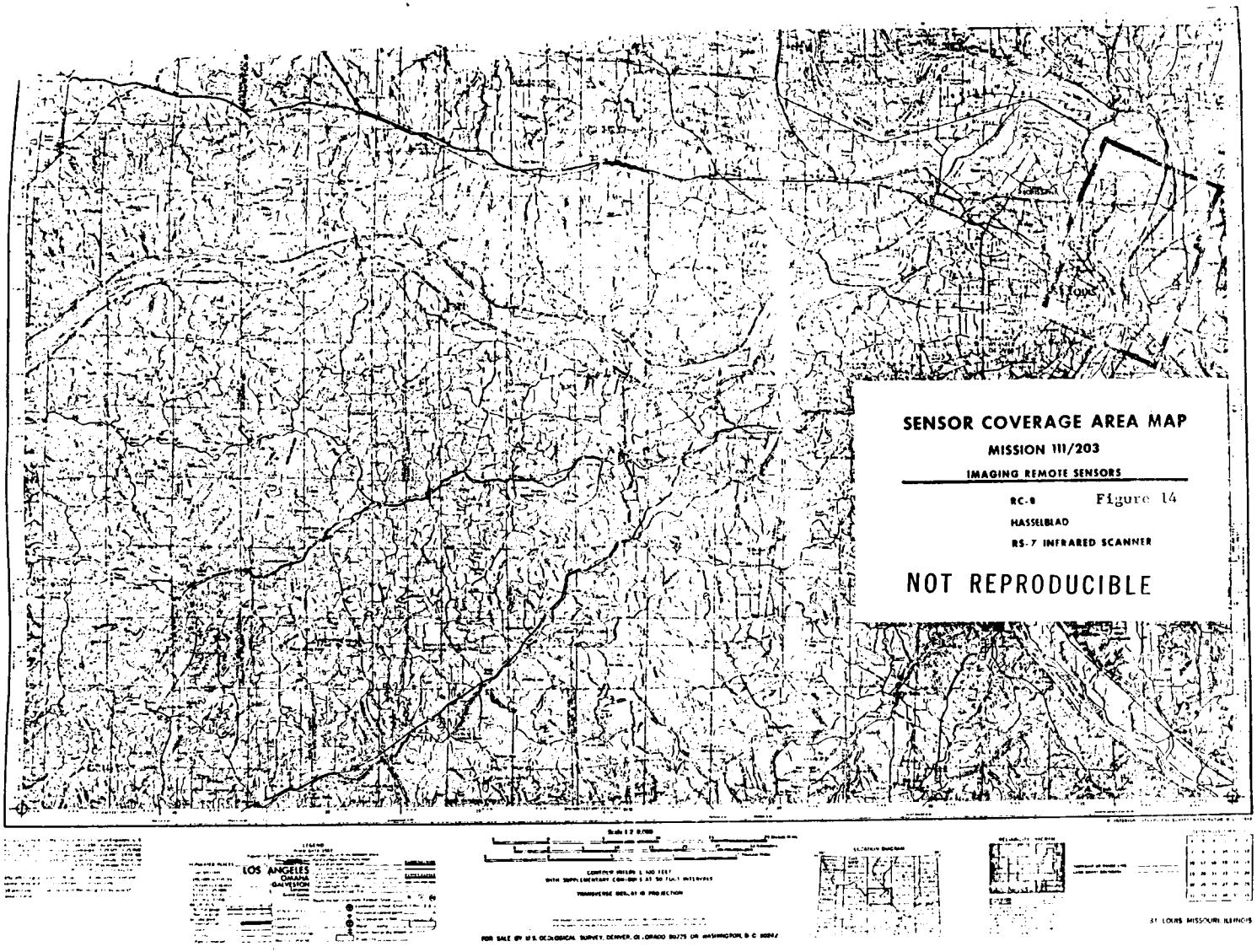
SENSOR COVERAGE AREA MAP
MISSION 111/203
IMAGING REMOTE SENSORS
RC-8
HASSELBLAD
RS-7 INFRARED SCANNER
NOT REPRODUCIBLE
LOS ANGELES
ST. LOUIS MISSOURI ILLINOIS

Figure 14

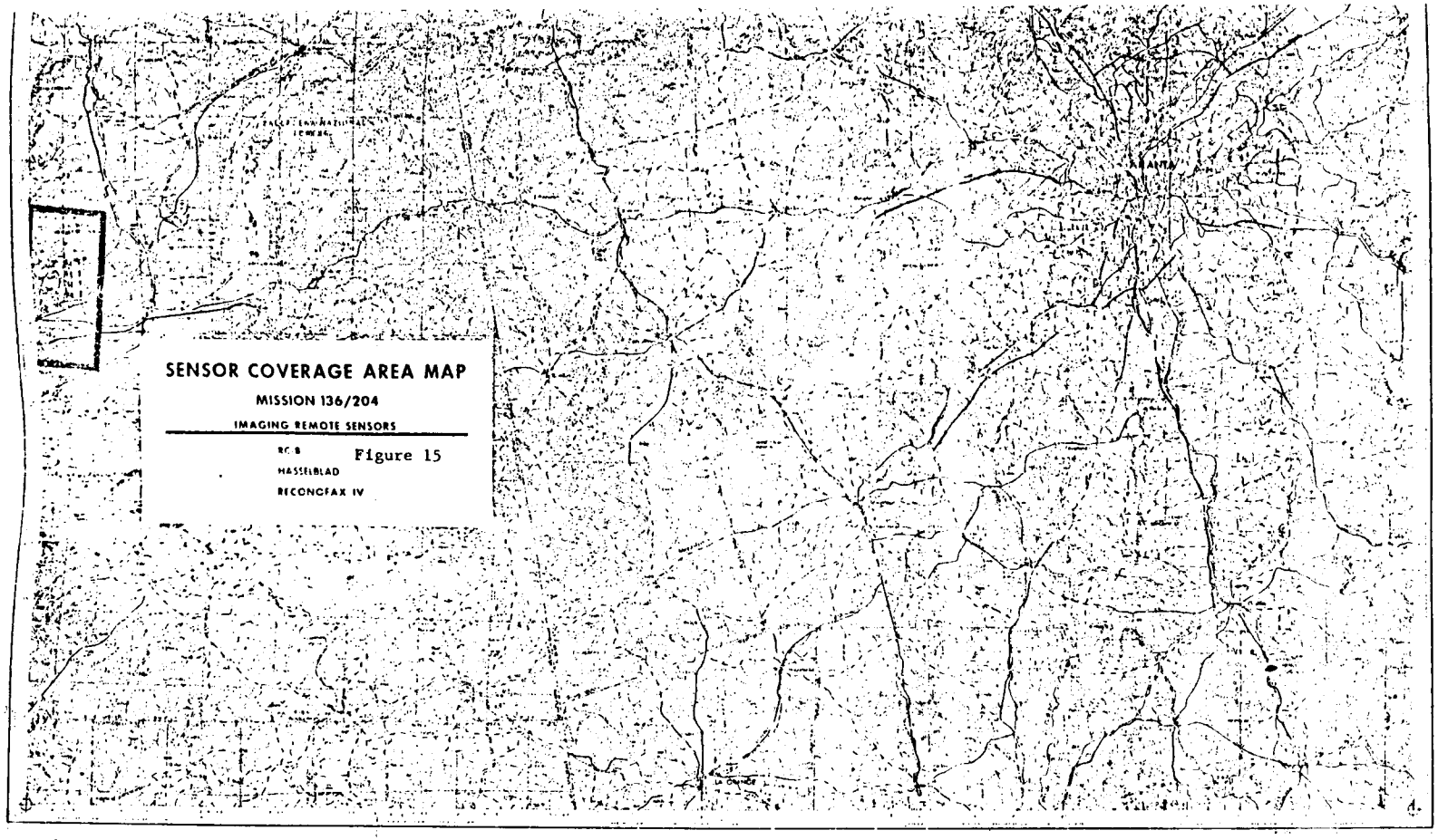

Figure 15

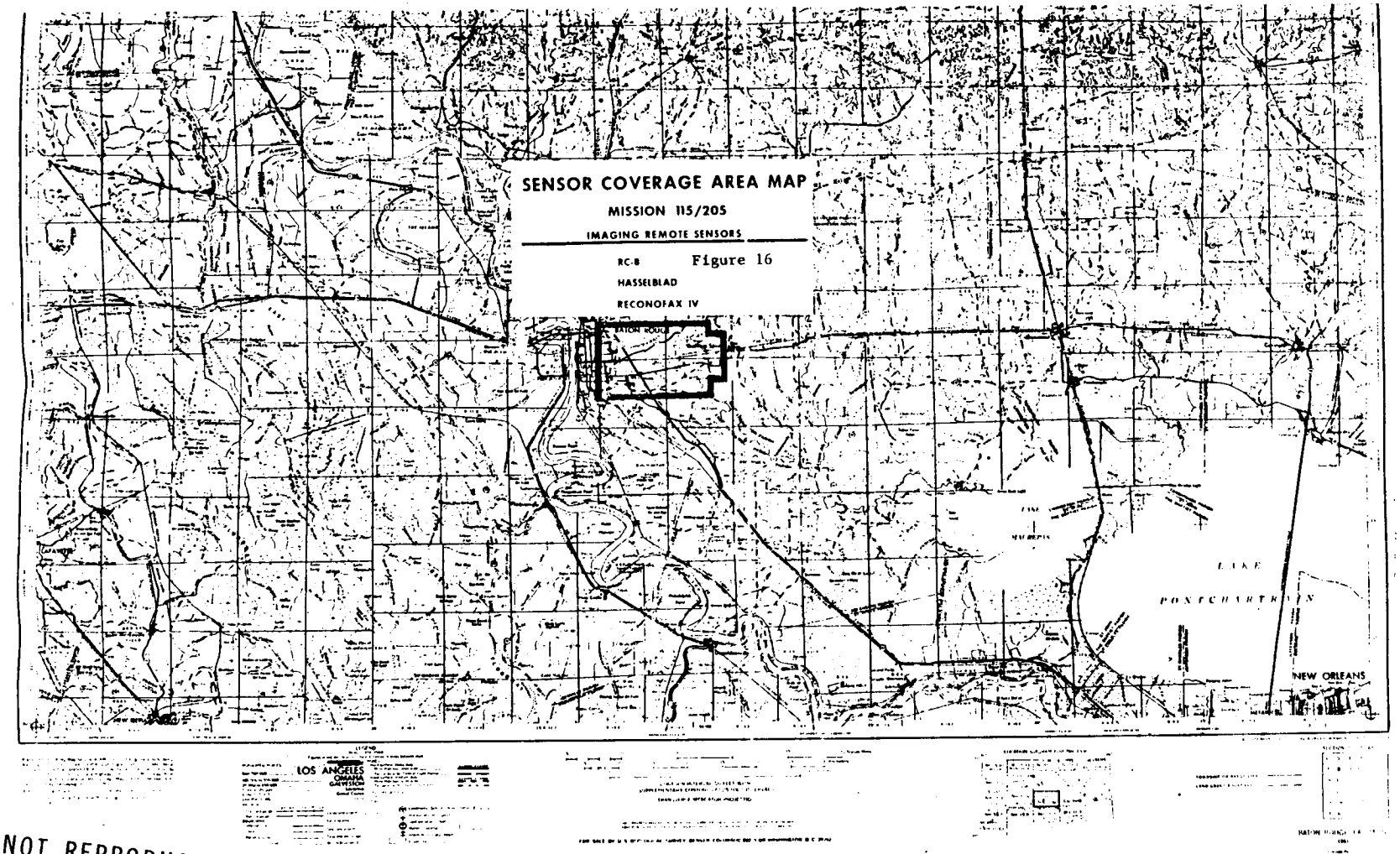

NOT REPRODUCIBLE

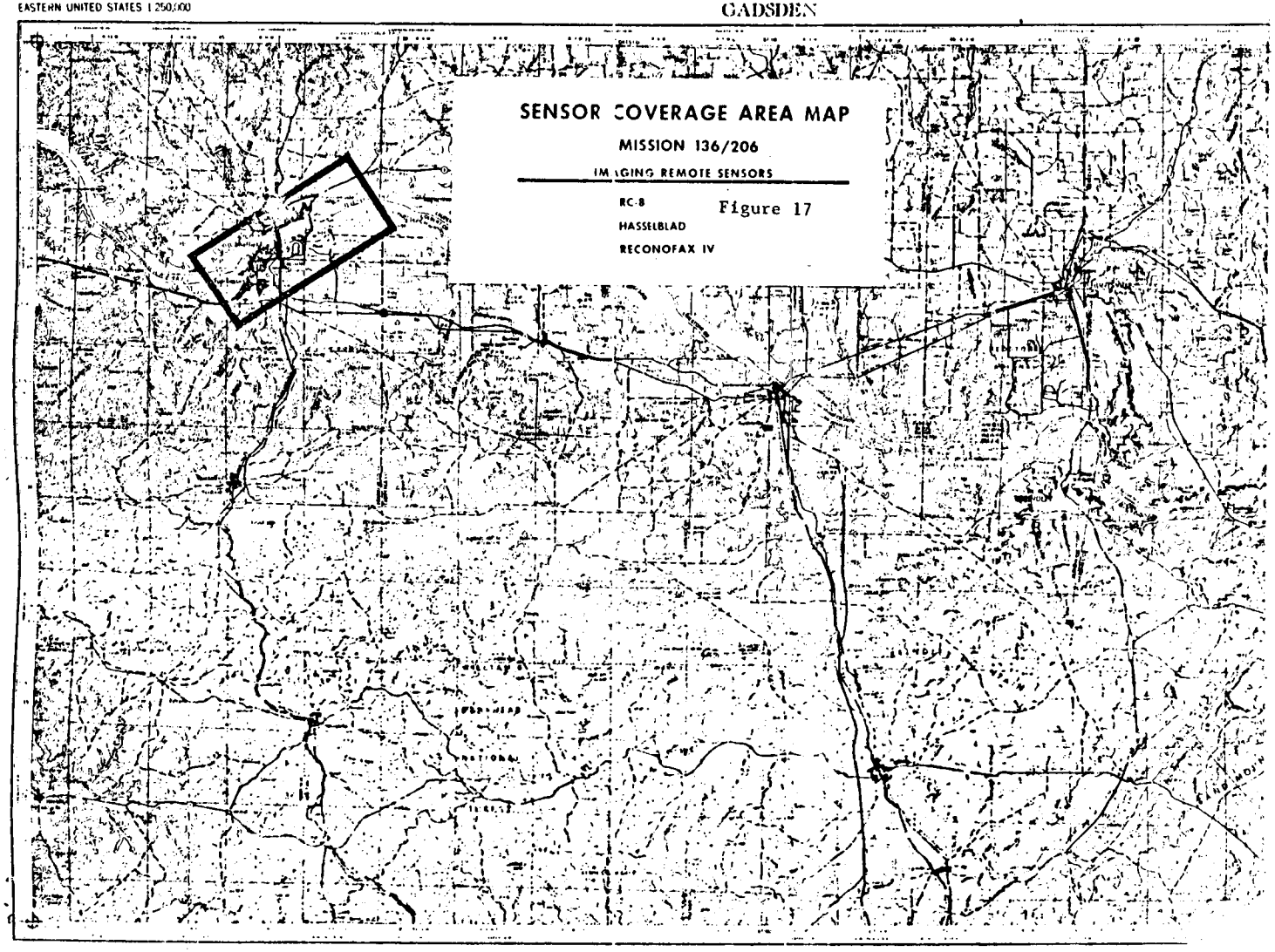

Figure 17

SPECIAL PROJECTS OF THE GEOGRAPHIC APPLICATIONS PROGRAM

by

Gary W. North
U.S. Geological Survey
Washington, D.C.

INTRODUCTION

The U.S. Geological Survey's Geographic Applications Program (GAP) is designed primarily to study problems of environmental imbalance arising from rapid urbanization, changes in land use, and the depletion of natural resources. Most of these studies are based on the analysis of remote sensor data provided through the NASA Earth Resources Aircraft Program at the Manned Spacecraft Center in Houston, Texas.

In 1970, a Special Projects group was established to undertake short-term, in-house studies and to work with representatives from other Bureaus of the Department of the Interior to start pilot research projects based on the use of remotely sensed data. This effort is being accomlished through the Geography and Human-Cultural Resources Working Group of the Interior Department's Earth Resources Observations Systems (EROS) Program, and is coordinated by the Survey's Chief Geographer.

To date, two studies have been undertaken; one has resulted in the publication of a report entitled "Environmental Conditions and Resources of Southwestern Mississippi," and the second is nearing completion in the form of a report entitled "Remote Sensing of Environmental Pollution." In addition to these studies, several remote sensing projects have been, or soon will be, started in the National Park Service, Bureau of Outdoor Recreation, Bureau of Land Management, and Bureau of Indian Affairs.

MISSISSIPPI TEST FACILITY STUDY

In February 1970, the Geographic Applications Program was asked by NASA to prepare a rapid and up-to-date study of environmental factors pertaining to NASA's Mississippi Test Facility (MTF) in southwestern Mississippi. Because of the impending phaseout of the Saturn V engine testing by NASA at MTF, it had become necessary to consider alternative uses for the Facility and surrounding region. It was felt that remotely sensed data could be used as a principal data source for the study and that its use would demonstrate the value of using this type of data in regional studies.

Procedure

On February 4, 1970, a multidisciplinary team of scientists met to plan the effort which was to be completed in 28 days. An outline of pertinent environmental factors was drafted and people were assigned to pull together information on their specific topic. Assistance was requested from the National Atlas staff, USGS regional offices, several Gulf Coast universities, and several Interior Bureaus, particularly Outdoor Recreation. Discussions were then held with Mr. Jackson Balch, NASA MTF Director, and with other NASA officials involved in deciding the future of MTF.

By the end of the first week's effort to collect data, it became quite clear that additional current data were needed. Most maps of the area were out-of-date, and complete coverage of the area at constant large scales did not exist. Photography of the area was available from NASA's Earth Resources Data Center in Houston, but it did not completely cover the area, and the Department of Agriculture coverage was dated 1952. Therefore, on February 12, a mission request was submitted by phone to the Manned Spacecraft Center from NASA Headquarters in Washington, D.C. for high altitude RB-57F coverage of the area.

Following submission of the mission request, the RB-57F aircraft was ferried to Houston from Kirkland Air Force Base, New Mexico, and on February 15, 1970, the GAP Principal Investigator arrived in Houston to assist in planning the mission. The area selected for photo coverage had been delineated by studying the Apollo VII photography taken in October 1968. The mission called for nine-camera coverage from 60,000 feet of approximately 2,100 square nautical miles of area around MTF.

The flight took place on February 17, 1970, following two days of delay due to weather conditions. The mission, involving eight 60 nautical mile, east-west flight lines, took 4.7 hours and provided coverage of 3,000 square nautical miles. The only problem encountered during the flight was that the northern-most flight line was flown five nautical miles too far north due to a target tracking problem with the onboard television viewfinder. This did not adversely affect the coverage, however, and the mission was considered a success.

During the overflight, the GAP Principal Investigator collected 35 mm color and color infrared oblique photographs of the area from a NASA provided helicopter. He was accompanied on the flight by a regional planner from the Atlanta office of the Bureau of Outdoor Recreation, who was also surveying and photographing the area for the express purpose of making recommendations on its recreational potential.

To complete the on-site work at MTF, the Survey's Chief Geographer visited the area to talk with politicians, bankers, planning groups, MTF staff members, local officials, etc., in order to gain a better

understanding of the whole region and to collect on-site data related to its environmental conditions and economic potentials.

On February 18, 1970, the Principal Investigator returned to Houston to review the photographic data. Special provisions had been made for quick photo processing and all data were available twelve hours after the aircraft returned on February 17. The flight produced the following data:

1. RC-8 black and white and color infrared, metric camera coverage at a scale of 1:120,000.

2. Zeiss color infrared coverage at a scale of 1:60,000.

3. Six Hasselblad cameras coverage in black and white, color and color infrared at scales ranging from 1:110,000 to 1:220,000.

Analysis

By February 20, 1970, all of the RB-57F photographic data had been reproduced and returned to Washington, D.C. At this point copies of the data were given to the disciplinary specialists working on the project. Maps were updated, soil boundaries were checked, a color infrared mosaic was made, etc. From the mosaic a five-category land use interpretation was derived. It was, in turn, compared with the results of a similar effort performed on a black and white mosaic made from the 1952 Department of Agriculture photography by the Survey's Branch of Special Maps. Land use changes were displayed in multiple overlay form for comparative purposes and illustrated the impact of the Facility on the area. Among results of the analysis which were quite obvious, were the expansion of the urban centers, the addition of new interstate highways, and the increase in agricultural activity northeast of MTF. Others, however, required closer examination, such as the change from agriculture to urban housing, and changes in drainage caused by urbanization.

Report Preparation

During the initial planning phase of the MTF study it had been decided to use remote sensing data as the graphic base for displaying such information as well as for analysis. Thus, the report was designed to contain a minimum amount of text and a large number of pictures, maps, and graphics based on the data.

The report is in four specific sections. The first, and most important section, presents in chart form and discusses nineteen suggested uses for the Facility. Each suggestion is evaluated against sixteen environmental factors, and each of these factors is rated as having a conducive, satisfactory, or negative influence on each possible use.

Following this section is a discussion of the role of remote sensing in the study and the results of the comparative land use analysis. The third section of the report contains a description of MTF and the supporting Slidell, Louisiana, Computer Center, and the environmental information arranged under the following subject headings:

A. Geology and Mineral Resources	G. Agriculture and Forestry
B. Geothermal Energy	H. Fish, Wildlife and Pests
C. Soils	I. Population
D. Vegetation and Terrain	J. Transportation
E. Water	K. Outdoor Recreation
F. Climate	L. Esthetic Qualities

The fourth section contains a list of available photography of MTF; an annotated bibliography of reports relating to the southwestern Mississippi area, and three special inserts which are folded into an envelope at the end of the report. These include: a modified topographic map with five-foot contours, a black and white enlargement of the Apollo VII photograph of the area, and a 1:120,000 scale black and white mosaic.

Results

The complete collection of photography used in the study constitutes a significant indicator of both prominent and subordinate features of the area. Geologists used the photography to plot the cheniers (old beach ridges), and to update older geologic maps. Hydrologists studied the Pearl River basin, moisture distribution for the area, water quality, and leakage potentials of the MTF sewage lagoons. A significant new agricultural experiment was discovered within the buffer zone; on one helicopter photo the story of the lumbering industry was recorded; the population and agricultural statistics can be seen in their spatial relationships on the change detection overlays; the areas suitable for outdoor recreation were identified on the mosaic; and areas for hunting, fishing, boating, etc., are now more easily seen when placed on the photographically updated base map. Even areas subject to fire damage or pests were first determined by use of the photography. Especially significant was the photographic description of the physical and economic destruction that took place during Hurricane Camille in August 1969.

Additional remote sensor data would have been helpful in the interpretation that was accomplished. Thermal infrared and side-looking radar imagery of the area would have been useful. The radar might have helped in mapping the drainage and water distribution to a greater

extent, and in providing a better synoptic view of the surface structure. With some geothermal activity located south and west of the Mississippi coast, it is possible that infrared imagery might have detected some thermal anomalies near the site. Nevertheless, the photography from the RB-57F overflight provided an excellent base and proved to be adequate for the regional study.

On March 4, 1970, the final draft of the report was submitted in ten copies to NASA Headquarters for review. Within a few days a request was received for 100 additional copies, and one of the original reports was photocopied to meet that request. At this point a decision was made to submit the report to NASA Headquarters for a limited press run of 1,500 copies. In July, however, because of the amount of color reproduction and the critical demand for the report, the job was turned over to the Government Printing Office (GPO). Of 12,000 copies of the report being printed, 10,000 will be placed on public sale for $2.25 from the Superintendent of Documents, U.S. Government Printing Office, Washington, D.C. 20402 under the revised title: "Environmental Conditions and Resources of Southwestern Mississippi."

ENVIRONMENTAL POLLUTION

Following completion of the Mississippi Test Facility Report, NASA Headquarters suggested that the Geographic Applications Program undertake a study which would summarize the remote sensing of pollution. In April 1970, a meeting was held at the Geological Survey with representatives of the EROS Program and other Interior Bureaus to decide what form the study should take and what the major objective would be. It was decided that a largely pictorial report would be prepared to illustrate the capabilities of various remote sensing devices to detect, identify, monitor or determine the effects of environmental pollution. In addition, it was decided that the report should attempt to demonstrate which pollutants can be monitored from spacecraft, high and low altitude aircraft, and ground based platforms. It was also felt that the report should include examples of any special processing, enhancement or analysis techniques used in connection with remote sensing data.

Procedure

During April and May 1970, the GAP Principal Investigator and one assistant began canvassing the remote sensing community for possible inputs to the report. Phone contacts and/or visits were scheduled with 40 of the major aerospace and sensor producing industries, 15 universities and foundations, and 38 governmental agencies or programs. In each case, the contacted individual or group was asked whether they had ever collected remote sensing data of any environmental pollutant and, if so, could they send us the best example of the results. From these requests over 500 specific data inputs were received.

Analysis

In June 1970, analysis and screening of the pollution data began. Two additional part-time Survey employees were assigned to assist in completing the report. The text is largely limited to explanatory captions for the maps, photographs, and other illustrations. The report is divided into three major and seven minor sections. The major sections are entitled "Land, Air, and Water," and the minor sections are designed to contain the following information:

A. An introduction containing the abstract, credits, table of contents, etc.

B. A perspective discussing the general situation and problem of environmental pollution.

C. A discussion of remote sensing technology and instrumentation.

D. A case study of what one major aerospace firm has done in the field.

E. A five-dimensional matrix showing goals, objectives, problems, sensor selection, and platforms.

F. A brief discussion of the establishment of an environmental index.

G. A list of the names and addresses of all contributors, plus pertinent flight information for each selected photograph.

Within the three major sections, an attempt was made to collect data involving all categories of pollution. More than 50 specific topics are covered, ranging from junk yards to ship stack contrails and from cattle feed lots to radiation. In each case illustrations are provided as evidence of the remote sensing capability. The report also shows how man is using the land, air, and water around him in a positive and/or negative way. Thus, such things as improperly located housing developments are included, since they tend to degrade an environment that is not capable of supporting them in the first place.

Report Preparation

In December 1970, a preliminary draft of the final report entitled "Remote Sensing of Environmental Pollution" was completed and submitted to NASA Headquarters for review. It contained 62 photographic plates containing more than 125 illustrations. The report should be useful to resource managers, public officials, planners, scientists, and environmental decision makers. Completion of the report may be expected in January 1971, but definite arrangements concerning its reproduction and distribution have not yet been made.

DEPARTMENT OF THE INTERIOR BUREAU ACTIVITIES

To increase the effectiveness of remote sensing projects within the Department of the Interior's Bureaus, the Geographic Applications Program staff, in cooperation with other members of the EROS Geography and Human-Cultural Resources Working Group, has begun to work closely with Bureau staffs in organizing and managing remote sensing projects. It is hoped that by working directly with Bureau personnel, their interest will be stimulated to seek additional ways to employ remotely sensed data in the solution of their own resources problems. This procedure also makes it possible to provide much needed assistance to the Bureaus in preparing experiment definitions for the use of Earth Resources Technology Satellite (ERTS) data which is scheduled to become available in 1972.

Project proposals are being developed in the National Park Service (FNP), Bureau of Outdoor Recreation (BOR), Bureau of Indian Affairs (BIA), the Bureau of Land Management (BLM), and the Bureau of Sports Fisheries and Wildlife (FSF).

The National Park Service is planning operations in two areas, archeology and the natural sciences. In the area of archeology, projects are being initiated to test remote sensing capabilities over areas in the southwest, over and around Fort Stanwix in Rome, New York, and over various areas where underwater shipwrecks and ruins are known to be present. In the natural sciences area, projects may soon be started to study land use and the environmental impact of development in and around various parks, as well as studies of plant and tree diseases.

The Bureau of Outdoor Recreation is initiating several contracts for research to test the feasibility of using remote sensing data for national, state, and regional recreation planning, as well as for monitoring site use and studying the recreation needs of developing urban areas.

The Bureaus of Land Management and Indian Affairs will undertake a joint effort to demonstrate how remote sensing can be used to help solve some of the problems involved in forest and range management. The Bureau of Indian Affairs may also undertake preparation of a Mississippi Test Facility type of report on several Indian reservations throughout the United States. In turn, the Bureau of Land Management is considering a land use and environmental impact study of the lower Colorado River valley.

Finally, the Bureau of Sports Fisheries and Wildlife will be investigating how remote sensing data can be used to monitor the impact on wildlife of environmental changes.

In all of these Bureau projects, the use of already acquired remote sensing data has been stressed since it is available and is less expensive to acquire than having new flights. Once feasibilities have been demonstrated to decision makers in the Bureaus, additional projects will be initiated and ERTS-A and B proposals will be expanded.

GEOGRAPHY PROGRAM, DESIGN, STRUCTURE AND OPERATIONAL STRATEGY

by

Robert H. Alexander
U.S. Geological Survey
Washington, D.C.

INTRODUCTION

Each of the geography papers presented at the NASA Third Program Review is part of a carefully designed program structure. The purposes of this summary are to point up the common thread of the other geography presentations; to show how they are tied together, and to outline the essential elements in the structure of the Geographic Applications Program. The geography papers are linked both conceptually and programmatically. Conceptually, they are linked by a unity of subject matter, which is land use and its environmental impact. Programmetically, they are part of a structure which connects new scientific knowledge gained from the use of the remote sensors with necessary actions by institutions and client-sponsors to make the new knowledge useful in solving environmental problems having to do with land use.

The total program is designed to move systematically toward a capability to incorporate remote sensing data into operational systems for monitoring land use and related environmental change. The major problems being addressed by the Geography Program are those of environmental imbalance arising from rapid urbanization and other dramatic changes in land use. These overall problems translate into working level problems of establishing the validity of various sensor-data combinations that will best obtain the regional land use and environmental information. The Program goal is to better understand, predict, and assist policy makers to regulate urban and regional land use changes resulting from population growth and technological advancement. In short, we intend to see that the new remote sensing data gets used to help arrange and locate ourselves on the surface of this planet so as to be assured of a high quality environment.

REGIONAL ENVIRONMENTAL SYSTEMS CONCEPT

The central concept with which we are attempting to guide the Geographic Applications Program is called the regional environmental systems model. According to this concept, what the remote sensor sees in a given regional setting is a pattern of land use and landscape arrangement which

is in turn the result of processes in underlying environmental subsystems. This is illustrated in Figure 1 where the top portion of the diagram shows the remote sensor or sensor systems looking down upon a regional landscape scene. The sensor system utilizes the entire spectral variety present in the scene that is necessary for the environmental data-gathering. The lower portion of the diagram represents the regional environmental subsystems which simultaneously affect the landscape pattern seen by the remote sensor.

These regional subsystems are traditionally the domain of discipline specialists. The geophysical subsystem encompasses those elements of the environment pertaining to the solid Earth; such as geologic structure, lithology, rock mechanics, seismicity, sedimentation, geomorphology, soils, etc. The hydrological subsystem refers to elements involving ground water, streams, lakes, wetlands, oceanic and estuarine factors, and glaciers. The biological subsystem includes plants and animals, particularly the so-called "natural" vegetation and the man-modified vegetation, for example, agricultural crops. The climatological subsystem involves near-surface atmospheric phenomena, air-mass dynamics, and energy exchange. Adding to the effects of these subsystems on the physical environment are the workings of the socio-economic subsystems, which include man himself and his works such as culture, demography, population dynamics, migration, health, and so forth.

All of these subsystems operate through processes that produce the patterns the remote sensor registers. To understand land use and the processes that produce it, the observer needs more, however, than the sum of the contributions of the individual discipline specialists. He needs to get inside of the relationships that connect the discipline subsystems and look at the cross-disciplinary processes that operate to affect land use. A basic assumption of the Geographic Applications Program is that an understanding of these processes is essential to the design of an effective remote sensing, data-gathering system for land use and environmental monitoring.

ENVIRONMENTAL PROBLEM-SOLVING STRATEGY

The regional environmental systems concept is put to work within the Geography Program in the context of a problem-solving strategy, which is illustrated in Figure 2. The center column of this figure illustrates the path now followed for the solution of environmental problems without the adequate information that could be provided by the remote sensors.

In the democratic system, we assume that the motivating force behind the attempt for a solution to environmental problems is the individual's perception of those problems, and his wish to improve the situation resulting from the problems. These are problems that he confronts regularly,

or may confront unexpectedly. He finds he is not able to cope with them as an individual because they are "systems" problems--that is, problems that have arisen from an imbalance in a complex of interconnecting parts, a complex which does not respond to the intervention of an individual acting alone. They are problems like traffic jams, air that is practically unbreathable, an occasional disastrous storm, flood or landslide, or other catastrophe. Being unable to cope with them as an individual, the citizen turns to some responsive institution, whether it be a local, state, or Federal agency, to help alleviate the problem. The center line of the chart represents the response by the institutions; i.e., the present system of providing a solution or a recommendation with insufficient knowledge of the environmental systems involved, and a policy decision, action, or inaction which may or may not alleviate the perceived environmental problem.

The loops on the left and right-hand sides of the diagram in Figure 2 represent the improvements that can be added to this problem-solving system by means of remote sensing data. On the left is illustrated the new scientific inputs obtained from better understanding of the environment itself. First, we examine the regional environmental systems themselves and try to understand what processes are operating on them and within them to produce environmental and land use patterns that cause the problems. To understand the workings of these environmental systems, we rely upon development of ecological models. These ecological models are simplified representations of the cross-disciplinary or subsystems processes used to help explain what the environment is doing, so that we can learn how to predict, and eventually control, the land use systems that develop. The ecological models which are sought for understanding land use relationships are of two types. The first, which might be called "vertical" models, describe processes operating through more than one of the environmental subsystems and explain or predict some factor related to land use at a given locality. The second, which might be called "horizontal" models, govern the spatial distribution of changes in land use or other environmental processes, such as the growth and expansion of an urbanized area, the migration of a portion of the population, and the geographic spread of air pollution over an area. Ecological models generate data requirements, including requirements for remote sensor data. Thus, the role of remote sensing is seen in its proper perspective vis-a-vis the solving of environmental problems.

In summary, then, ecological models are systems models stressing processes and dynamics in the environment. They are of two types: 1) models dealing with connections among regional environmental subsystems and the resulting land use, and 2) spatial process models governing geographic changes in land use and environmental response. Ultimately, it is hoped that these models will encompass the fundamental energy and mass transactions in the man-land ecosystem, and that remote sensing data can help to provide key inputs.

PHASES IN THE GEOGRAPHIC APPLICATIONS PROGRAM DEVELOPMENT

Portrayed on the right-hand column of the diagram in Figure 2 are the new institutional inputs occasioned by the remote sensing data gathering systems. A first requirement is a new grouping of users for efficiency in sharing remote sensing data. These users are of two types: 1) existing agency users, and 2) new client-sponsors for new synoptic environmental data that can be provided by remote sensing systems. The mechanism for carrying the remote sensing data systems from the new user groupings to the development of operational remote sensing programs is through the setting up of demonstration projects, which are regional test site operations involving all potential users of the remote sensing data from both public and private sectors, who are present in the test region. In the Geographic Applications Program, 27 urban and 4 regional test sites in the United States have been planned. The locations of these sites have been mentioned elsewhere in this program review. Upon completion of the demonstration of feasibility of using remote sensing data in the demonstration projects, the development of new operational systems will be undertaken. These will require new geographic information systems for handling and channeling the great quantities of resulting environmental data into the hands of the users. Finally, we can expect that urban and regional analysis and environmental monitoring centers may be set up as the program becomes operational with systematic inputs of remote sensing data from satellites and aircraft. It is expected that urban and regional environmental monitoring will feed back and improve the quality of decisions about our environment as illustrated by the non-directional feedback loops in the diagram in Figure 2.

For purposes of organizing program elements and projecting the development of each into a future operational activity, the Geographic Applications Program may be presently defined to consist of three tasks: 1) urban land use dynamics, 2) regional land use dynamics, and 3) land use climatology. The urban and regional tasks also encompass investigations of environmental consequences, other than climatological, of land use patterns and practices. The three tasks are separated by dashed rather than solid lines in the Program Development Chart (Figure 3) to emphasize the close relationships and interconnections among them. The various elements of the Geographic Applications Program are thus not just thrown together as a miscellaneous collection of activities. They are, rather, assembled to constitute tightly-connected parts of a single system of Earth-surface phenomena confronting the new remote sensing observational programs--phenomena pertaining to the human use of the land and the environmental consequences of that use.

The three Program Tasks are projected into the future in phased steps which are depicted in a highly condensed fashion in Figure 3. The phases progress from aircraft experiments conducted in a few pilot cities

and regions, to a larger sample of cities and regions representing different environmental situations, to an operational capability for monitoring and eventually predicting land use and related environmental change.

The ingredients required to achieve Program goals are listed in Figure 4: 1) improved ecological models to understand the underlying environmental processes and to guide the collection and use of remote sensing data; 2) a responsive and flexible remote sensing data source, based on both aircraft and satellite systems; 3) the collaboration of present and future user institutions which will employ the information systems necessary to carry the remote sensing data into the heart of the decision-making processes; and 4) broad support for the Geographic Applications Program concept which integrates the effort into a single coordinated attack and provides for all the required connecting links from research to operational problem-solving.

Environmental Systems Concept

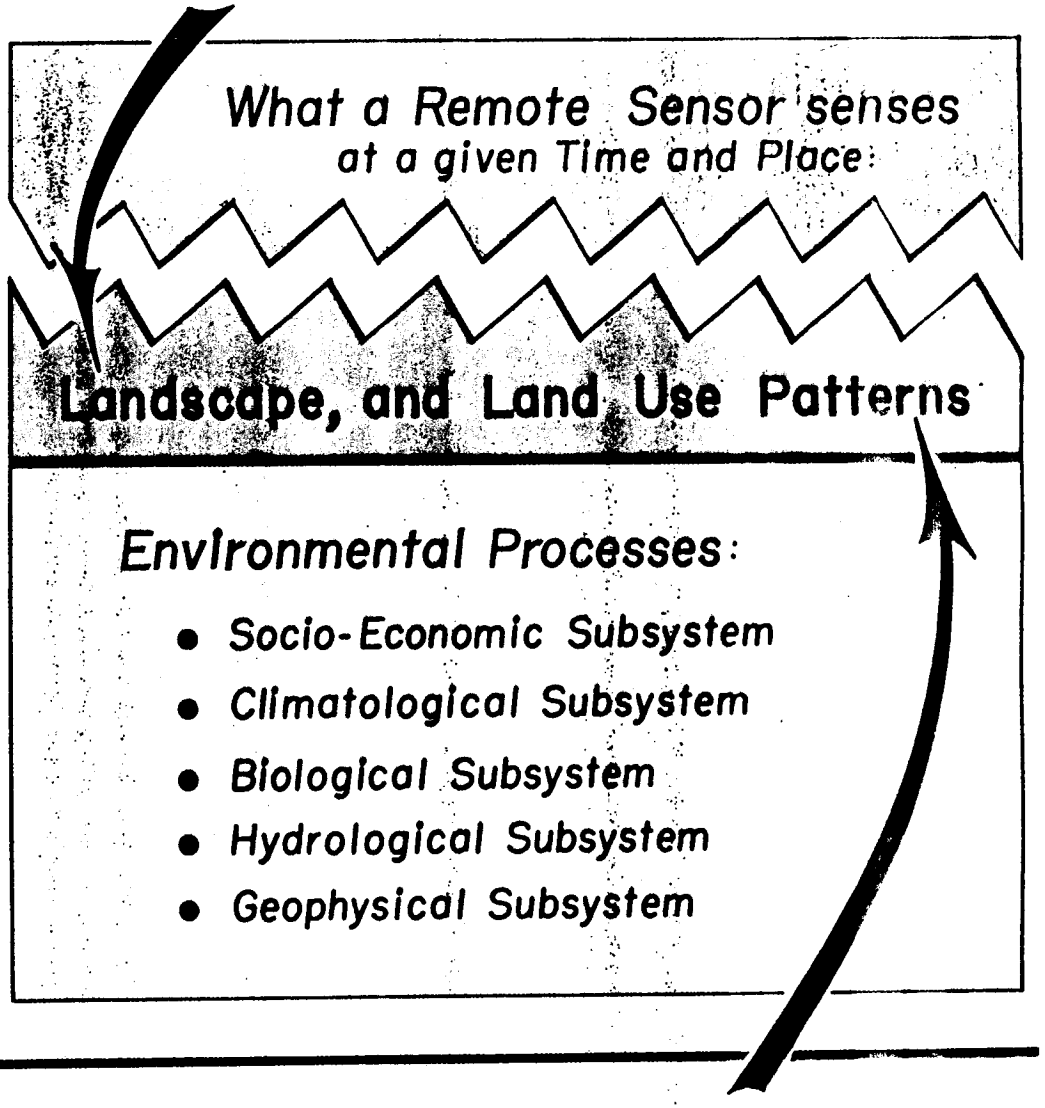

Geography
USGS
EROS
EARTH RESOURCES OBSERVATION SYSTEMS PROGRAM

Figure 1

Environmental Problem-Solving Strategy

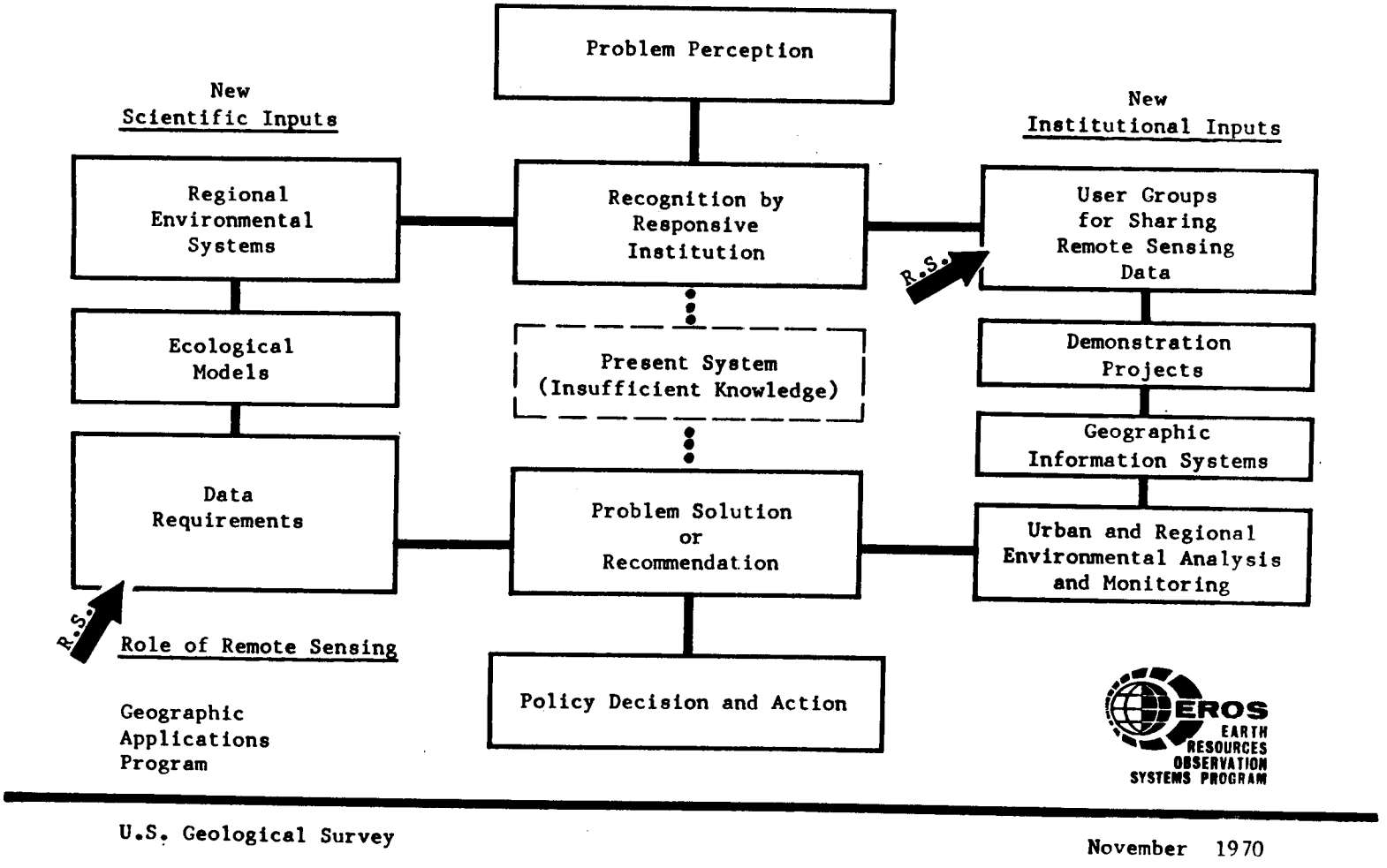

U.S. Geological Survey

November 1970

Figure 2

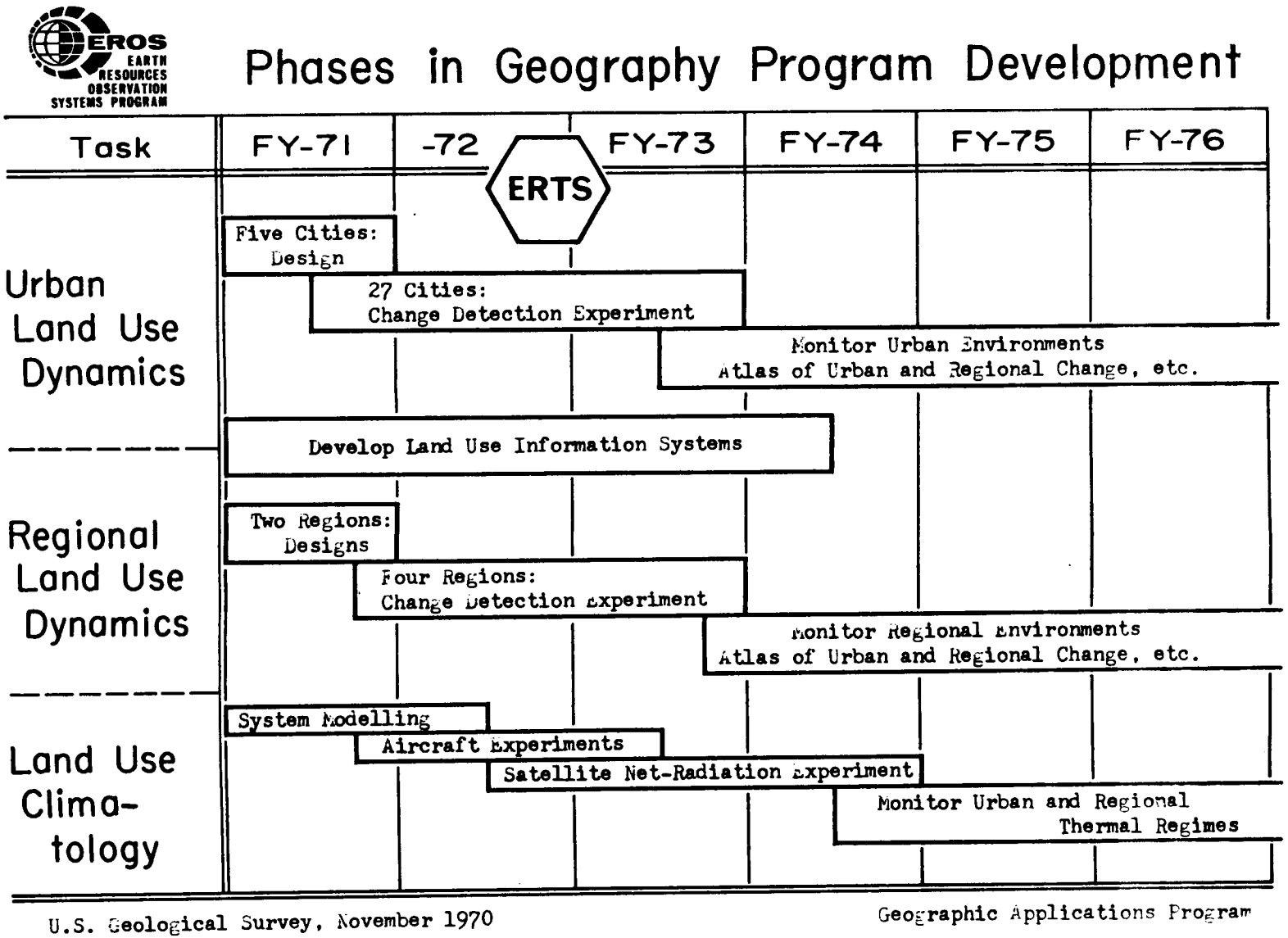
EROS
EARTH RESOURCES OBSERVATION SYSTEMS PROGRAM
Phases in Geography Program Development
Task
FY-71
-72
ERTS
FY-73
FY-74
FY-75
FY-76
Urban Land Use Dynamics
Five Cities: Design
27 Cities: Change Detection Experiment
Monitor Urban Environments
Atlas of Urban and Regional Change, etc.
Develop Land Use Information Systems
Regional Land Use Dynamics
Two Regions: Designs
Four Regions: Change Detection Experiment
Monitor Regional Environments
Atlas of Urban and Regional Change, etc.
Land Use Clima-tology
System Modelling
Aircraft Experiments
Satellite Net-Radiation Experiment
Monitor Urban and Regional Thermal Regimes
U.S. Geological Survey, November 1970
Geographic Applications Program

Figure 3

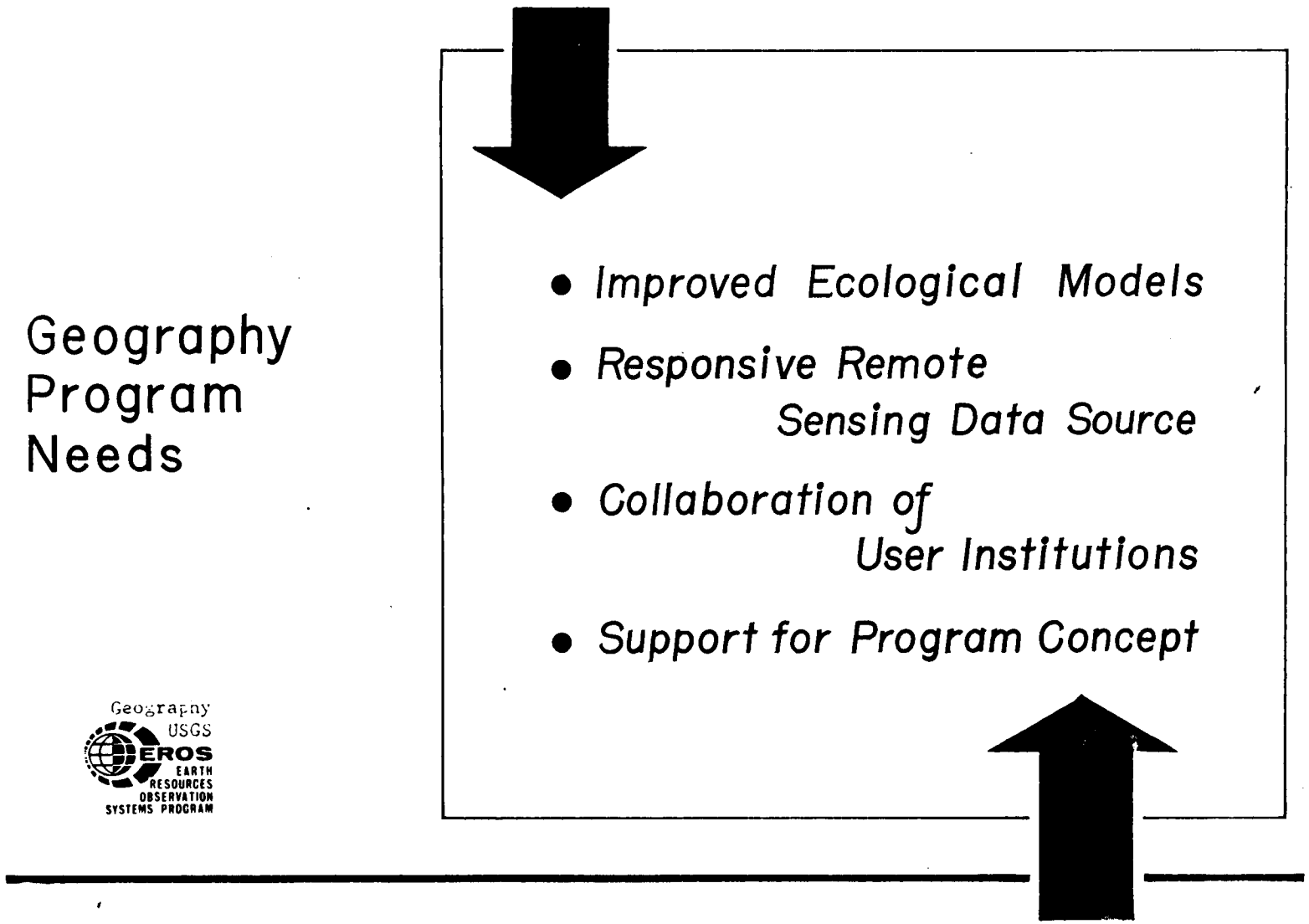
Geography
Program
Needs
• Improved Ecological Models
• Responsive Remote Sensing Data Source
• Collaboration of User Institutions
• Support for Program Concept
Geography
USGS
EROS
EARTH RESOURCES OBSERVATION SYSTEMS PROGRAM

Figure 4

PREPROCESSING OF MULTISPECTRAL DATA AND SIMULATION OF ERTS DATA CHANNELS TO MAKE COMPUTER TERRAIN MAPS OF A YELLOWSTONE NATIONAL PARK TEST SITE[1, 2]

by

Harry W. Smedes
U.S. Department of the Interior
Geological Survey
Denver, Colorado
and
Margaret M. Spencer and Frederick J. Thomson
Institute of Science and Technology
Ann Arbor, Michigan

INTRODUCTION

In conventional multispectral techniques for making terrain maps by computer, areas of a scene are classified on the basis of the similarity of their spectral radiance signature to that of training areas representing the classes to be recognized. Such techniques assume that all objects of a given class have substantially the same spectral radiance. Previous studies (Smedes and others, 1969, 1970) of a Yellowstone National Park test site (fig. 1) and unpublished data proved this assumption invalid, because such factors as shadows, variations in topography, and scanner look angle cause errors in classification.

The present study tested the possibility of improving the accuracy of classification by preprocessing the spectral data. We used the following transformations with the data from the University of Michigan 12-channel scanner spectrometer (table I):

1. Ratio transformations
   (a) Ratio of each channel to the sum of all channels
   (b) Ratio of adjacent channels
   (c) Ratio of the difference to the sum of adjacent channels
2. Transformation using a normalized scan-angle function.

---

[1]Publication authorized by Director, U.S. Geological Survey.

[2]Work performed in cooperation with the National Aeronautics and Space Administration.

The normalized scan-angle function transformation resulted in the most accurate classification. Technique 1.(a) was the best of the ratio transformations.

The University of Michigan data were used to make terrain maps of the area by the following techniques:

A. Preprocessing by scan-angle function transformation, using the computer-selected best set of three channels.
B. Preprocessing by ratio transformation, using the specified Earth Resources Technology Satellite (ERTS) data channels simulated by fitting the spectral response of each of the 12 University of Michigan channels to the ERTS data channels by a set of weighting coefficients.

By use of a simple technique during printout, the maps were produced in color.

CONVENTIONAL TECHNIQUES

Studies with Purdue University (Smedes and others, 1969, 1970) produced computer maps showing the distribution of eight terrain classes in a test site in Yellowstone National Park, which occupied 12 square miles and had a topographic relief of 1,800 feet. The classes were bedrock, vegetated bedrock rubble, talus, glacial till meadows, glacial kame meadows, forest, bog, and water. In addition, shadows were mapped. Accuracy of mapping was about 85 percent.

The conventional techniques of multispectral classification and mapping used for those studies assume uniform radiance in each class regardless of where it occurs in the scene. Those studies, and analog computer studies with the University of Michigan, proved the assumption wrong because of such factors as cloud shadows, haze, variations in topography, and changes in scanner look angle. These factors degrade the accuracy of classification based on spectral signatures, in both analog and digital tests. Accuracy was improved by selecting multiple training sets for each class, each set effective over a short segment of the scan line. However, this lengthened the preparation and computer-processing time.

For some classes, the signatures from each training area could satisfactorily be combined to make a single composite signature (fig. 2). For other classes, this resulted in too large a standard deviation and too much overlap with signatures from other classes (fig. 3). As a result, some classes had to be treated as two or more separate classes depending on their scan-angle position. Although recognized separately,

these classes were combined during the printing stage by assigning them the same map symbol.

Nonuniform radiance along scan lines is illustrated in the analog computer displays (fig. 4) of the entire test area. For example, when training areas of the forest class were selected only along the south side of the area, the computer recognized forest only along that side, as shown by the black areas in the top strip of figure 4. This, and similar data from other classes made it clear that the misclassification was due to the scanner look angle. When the scanner looked south, it saw the shaded sides of trees, and when it looked north it saw the maximum back-reflection from the terrain. Topographic slope accentuated this phenomenon. Only by training along the south side, middle, and north sides could the analog computer recognize and map the complete distribution of the forest class, as shown on the lower strip of figure 4, where at least 98 percent of the forest class was recognized.

Basically, the procedure for both analog and digital techniques involved the following steps:

1. Selecting a training area.
2. Making a map of the entire area, based on the spectral signatures from the training areas.
3. Checking this map against the control data to see where the computer map was inaccurate.
4. Repeating step 1 by selecting a training area in the region of error.
5. Repeating steps 2 and 3.
6. Repeating steps 1, 2, and 3 until sufficient training areas have been selected to make an accurate map.

Obviously this procedure is cumbersome and has the following disadvantages:

A. The preparation and processing of data were slowed by the complexity of the recognition process.
B. Considerable manipulation of the data is required to get good results.

PREPROCESSING TECHNIQUES

Preprocessing of the data to compensate for reflectance variations with scan angle was studied using digital computer programs developed by the University of Michigan.

In a way, shadows and topography pose similar problems in that they affect the total level of irradiance. North-facing slopes and shadows

reflect less light back to the sensor, lowering the total level, whereas south-facing slopes reflect more light, raising the level. However, in both cases, the ratio of observed (recorded) spectral radiance in two spectral channels is independent of variations in the level of radiance.

Variations in irradiance due to topography and scan angle may be corrected for by dividing by functions of the scan angle. The variations in total level of irradiance can be corrected for by using various ratio preprocessing techniques.

A normalized scan-angle function transformation resulted in the most accurate classification for this particular set of data. The best of the ratio preprocessing transformations was the one based on the ratio of the channels to the sum of all channels. Preprocessing allowed the use of a single training area for each class of objects anywhere in the field of view. It shortened the preparation and computer-processing time, gave more accurate results, and, in places, enabled areas under cloud shadow to be classified as to the correct terrain class. Circular reasoning was eliminated and manipulation of data drastically reduced.

RATIO TRANSFORMATIONS

Three ratio preprocessing techniques, previously reported by Kriegler and others (1969), employ the fact that if the scene radiance varies, this variation is present in all spectral channels. Ratios of channel signals, therefore, will show less[1] variation with scene changes than will the signals themselves.

One disadvantage inherent in ratio preprocessing is that for N original channels of data, there are only N-1 independent channels of transformed data; so one channel is lost. The 12th channel was eliminated in our studies.

These ratio transformations have been previously used for preprocessing the scanner-spectrometer data to reduce illumination variations and extend signatures. The transformations are:

A. Ratio of the difference to the sum of adjacent channels. The new transformed first channel is $\frac{2-1}{2+1}$; and the new 11th channel is $\frac{12-11}{12+11}$; hence there can be no new transformed 12th channel, so one channel is lost.

[1] In shadow areas, the shorter wavelengths will be affected more than the longer because of scattering.

B. Ratio of adjacent channels. The new transformed first channel is $\frac{2}{1}$, and the new 11th channel is $\frac{12}{11}$. Again, there can be no new transformed 12th channel, so one channel is lost.

C. Ratio of each channel to the sum of all channels. The new transformed first channel is $\frac{1}{\Sigma}$, and so forth. In this case, although it appears that no channels have been lost (the new N^{th} channel is $\frac{N}{\Sigma}$), none of the new transformed channels is independent of the remaining channels, since $1-\Sigma$ (N-1) transformed channels=the N^{th} transformed channel.

All three of these ratio transformations were studied for use on the Yellowstone Park data. The last transformation (C) was the best of the ratio transformations (table II) for preprocessing these data, and therefore was used for the recognition processing.

SCAN-ANGLE TRANSFORMATION

One of us (M.M.S.) assumed and subsequently confirmed that the variations in scene radiance in each spectral channel were functions of scan angle; the functions can be determined by analyzing the variation of spectral signature of one or more classes of objects distributed along the scan line. Enough information must be available to locate samples of a given class of objects at various scan angles; thus, more knowledge of the scene is required for this preprocessing technique than for the ratio preprocessing.

If the ratio of spectral radiances of two classes as a function of scan angle is constant, then a single correcting function can be derived which can be assumed will be valid for all data in each spectral channel for all classes. This assumption is equivalent to assuming that the bi-directional reflectance variations (as a function of scan angle) of different classes are the same. A universal function to correct for scan angle for each channel is obtained by normalizing the function of signal output versus scan angle for any one class at some particular scan angle.

Figure 5 shows the variation of output with scan angle for one spectral channel in the forest, bog, and till training areas. In this example, an output of 0.8 could be interpreted as any one of the three classes depending on the scan angle. Figure 6 shows the same data after the scan-angle transformation. Now the classes are clearly separated, and a radiance value of 0.8 could be interpreted only as till. The wide variation with scan angle in mean value of spectral signature of each training class at different scan angles has been eliminated.

Figure 7 shows a segment of the terrain map made by scan-angle function transformation. The symbols and colors are explained in figure 9.

RECOGNITION PROCESS

The Michigan computer program[1], like that of Purdue (Smedes and others, 1969, 1970), uses a supervised training program involving maximum-likelihood decision for selecting the best spectrometer channels and closely similar techniques for digitizing the data of the analog magnetic tapes.

We calculated the probability of misclassification using the preprocessing techniques described above. The results, summarized in table II, indicate that use of the normalized scan-angle function transformation results in the lowest probability of misclassification. Hence, that transformation was used in making the recognition map of figure 7. The symbols used to designate the different terrain classes are shown in figure 9.

TERRAIN CLASSES AND NUMBER OF TRAINING AREAS USED

Cloud shadows were recognized in addition to eight classes of terrain.

Class	Number of Training Areas
Glacial till meadow	4
Glacial kame meadow	1
Bedrock exposure	3
Talus	3
Vegetated bedrock rubble	3
Forest	4
Bog	4
Water	1
Cloud shadow	1
Total: 9 classes	24 training areas

These 24 areas for the 9 classes were identified from ground control data. For those classes with only one training area, the spectral signature was obtained directly from the data. For those classes with more than one training area, signatures were combined statistically. The variance of the statistically combined signature is a function both of the variances of the individual signatures (the small oval areas of

[1]A CDC-1604 computer with 32K bytes (8 bits per byte) of core storage was used. The computer language was FORTRAN IV. An IBM-1401 computer was used for peripheral work and for printing the maps in color.

figs. 2 and 3) and of the difference of means of these individual signatures (the separation of the black dots in figs. 2 and 3). Similarly, the covariance of the combined signature equals the covariances of the individual signatures and the cross-product terms of the difference of means of the individual signatures. The combined signature is a function of the mean difference (separation) of the individual means (figs. 2 and 3).

The preprocessing technique is successful if, for any one class, wide separation of mean spectral signature in different training areas (cf. fig. 3) is much reduced (cf. fig. 2).

LIKELIHOOD RATIO FOR RECOGNITION

The statistical decision criterion for classification defines a decision rule that utilizes a likelihood-ratio test. This test is applied to each data point, where each data point has n parameters corresponding to the n channels of spectral data. The decision rule states that this data point is classified as a particular class depending on the outcome of the likelihood-ratio test. If there are two classes the likelihood-ratio test is as follows:

$\frac{f(C_1)}{f(C_2)} > 1$; then the data point is recognized as originating from class C_1

where

$f(C_1)$ is the multivariate Gaussian probability density function for class C_1.

When there are n classes, there would be n(n-1) ratios to compute. The rule for recognizing a particular class is that when the following n-1 ratio tests are satisfied simultaneously,

$\frac{f(C_i)}{f(C_j)} > 1$; then the data point is recognized as originating from class C_i.

for $j = 1 \ldots n$
$i \neq j$.

The likelihood-ratio test for n classes is then equivalent to recognizing the class whose probability density function is greater than the probability density functions for the other classes.

The "no recognition" category, which occurred in the recognition processing, is a result of having an upper limit test on the value of

the exponent in the probability density function of each of the classes. The exponential limit is used to eliminate those data points which have low probability of belonging to the class being recognized. First, the maximum-likelihood-ratio test is performed, and the class to be recognized is that with the greatest probability density function. Next, the exponent limit test is applied; if the values of the exponent of the class to be recognized exceed this limit, the point is not recognized (rejected).

CHANNEL SELECTION

It is important to choose the best channels for distinguishing classes. In general, terrain can be accurately classified using only a few of the 12 available spectrometer channels, if the proper combination of channels is selected for each class. At the University of Michigan, a digital computer program has been written to select the best spectrometer channels for likelihood-ratio recognition. The program inputs are the signatures of the classes to be recognized and the weights to be placed on the probability of misclassifying each pair. The use of weights allows the optimum channel choice to be biased in favor of one or more pairs of classes, as with Purdue's program.

The channel selection is started by picking the best channel out of the group of N channels. Then this first choice is tested with each of the remaining N-1 channels for the best combination of two channels, and so forth. Not all possible channel combinations are tested by this ordered selection scheme; it is assumed that the best two channels are the best channel plus an additional one. The criteria for best channel or combination of channels are based on the lowest average probability of misclassification. If there are C classes then C(C-1) probabilities of misclassification are to be averaged. The probability of misclassification is the probability of picking class, C_1, given class, C_2.

The average probabilities of misclassification for the original spectrometer channels under the normalized scan angle function transformation are given in table II. The three selected channels were 5, 12, and 2.

CRITERION FOR CHOICE OF RATIO PREPROCESSING TECHNIQUES

All nine combined signatures were used to compare the performance of the three ratio preprocessing techniques for three channels. The ratio preprocessing transform selected was the one with the lowest average probability of misclassifying each pair. The results are shown in table II.

The transformation based on the ratio of each channel to the sum was used in the preprocessing because its average probability of misclassification is the lowest. The third channel choice was computed for this transformation. The sequence of channels selected for the first transformation is channels 1, 5, and 10, which correspond to the 1st, 5th, and 10th original channels divided by the sum of the 12 original channels.

SIMULATIONS OF ERTS DATA CHANNELS

The purpose of this part of the investigation was to simulate the ERTS-A spectral channels, using the same data as before, to assess their accuracy in classifying the same scene in Yellowstone National Park. The spectral response of each channel of the ERTS scanner and Return Beam Vidicon (RBV) cameras was simulated by a weighted addition of spectrometer channel signals. The same ratio preprocessing technique was used both on the simulated ERTS data channels and on the original spectrometer channels in order to compare all three spectrometer systems. The average probability of misclassification for each of the two simulated data sets was compared with the average probability of misclassification for the original spectrometer channels. The best two channels were selected from the original 12 channels and from the ERTS 4-channel scanner, because the RBV camera system had only two channels after the ratio transformation, owing to the inherent N-1 loss described above.

SIMULATION TECHNIQUE

Specifications for the spectral responses of the ERTS sensors (L. Goldberg and O. Weinstein of NASA Goddard, oral commun., 1970) were used to construct nominal spectral sensitivity curves. The detailed spectral response of each spectrometer channel (Larsen and Hasell, 1968) was fitted graphically to the specified ERTS data, using a technique described by Nalepka (1970). Weighting coefficients (table III) were then assigned to each spectrometer channel to simulate the ERTS data. Further corrections for peak sensitivity variations in each photomultiplier were determined from radiance standard lamp data.

The signatures of the training areas were obtained for both the ERTS scanner and the RBV camera system, and combined signatures were obtained for the classes that had more than one training area. The average probability of misclassification was computed for the three transformed channels of the ERTS scanner data and for the two transformed channels of RBV camera data. The average probabilities of misclassification are given in table II for comparison with original spectral data using a ratio transformation and the normalized scan angle function transformation.

The three preprocessed ERTS scanner channels were used in recognition processing. The recognition map is shown in figure 8. The symbols and colors used to designate the classes are shown in figure 9.

COMPARISON OF RESULTS

The purpose of this study of preprocessing was to represent each terrain class by a statistical signature and to use the likelihood-ratio test for recognition processing. To do this, we preprocessed the multi-channel spectral data. Four techniques were tried; two of the techniques were eliminated before final recognition processing because their average probabilities of misclassification were too high. The choice of the number of channels--three--to be used in the recognition process was not based on getting best results but rather, because the simulated ERTS scanner data would result in a 3-channel system, on preprocessing with ratio transformation. All three recognition techniques could then be compared. Accuracy of terrain classification was evaluated in the training areas for the three techniques. The combined training areas constitute 1.82 percent of the total map area. The results of these evaluations are summarized in table IV.

In comparing the accuracy of maps made using preprocessing with those made without preprocessing (Smedes and others, 1969, 1970), the following generalizations are valid:

For the computer-selected best set of channels, using scan-angle transformation:
BOG, KAME, WATER, and VEGETATED ROCK RUBBLE were as accurate or slightly more accurate:
FOREST, TILL, and BEDROCK were distinctly more accurate.
These maps are more accurate than those made without preprocessing, in spite of far fewer training areas (24 versus 187) and fewer channels used (3 versus 4); moreover, they required less preparation and computer time.

The preprocessed simulated ERTS data gave poor results for three classes--BEDROCK, TALUS, and SHADOWS. However, bedrock and talus are basically exposures of blocks of rock, the blocks in talus simply having moved down slope a short distance, and the two units are actually gradational. If these two units are combined, the accuracy rises to values comparable to those of other classes, for nearly 18 percent of the bedrock was misidentified as talus, and nearly 28 percent of the talus was misidentified as bedrock.

The apparently poor performance of the ERTS data for shadows (71 percent) is misleading because 10 percent of the training area was identified as forest, which is the true terrain unit that was in shadow.

This indicates that, because of preprocessing and in spite of a shadow signature as part of the training sets, the simulated ERTS data channels can "see" through the shadow better than can other recognition techniques.

CONCLUSIONS

Analysis of the training sets shows that the normalized scan-angle function transformation produced better results than those obtained from the best ratio transformation but was more specialized in that it corrected only for the tendency of the terrain to reflect sunlight to the scanner in different amounts at different angles. Rugged topography could still degrade recognition locally.

Another linear transformation of the normalized scan-angle transformed data would eliminate anomalies parallel to the flight line. One such anomaly might be a persistent topographical feature. One area north of the river in the Yellowstone Park test site data may show such an anomaly. An investigation of four classes in this area indicates that their reflectance was stronger than those from the same materials at the same scan angle but occurring farther west along the flight line. These classes are BEDROCK, TILL, FOREST, and WATER. Therefore, after the normalized scan-angle function transformation, the reflectance from these four classes would still be greater. This investigation shows that the signal level for the whole region north of the river should have been uniformly reduced. This would have been equivalent to a regional correction based on the flight line coordinate.

Preprocessing of data results in more accurate maps, requires fewer training areas (hence less preparation and computer time), and enables much of the area formerly classified as shadow to be classified as to actual terrain type. Use of a simple technique enabled the computer to print the map in color.

ERTS data channels were more closely simulated than in previous tests made without preprocessing (Smedes and others, 1969, 1970). Spectral resolution is reduced because the broad spectral band width is more closely simulated. But preprocessing appears to compensate for the loss of resolution, resulting in maps of comparable accuracy, with the advantage of having correctly classified areas in shadow. Scan-angle preprocessing of ERTS data will undoubtedly produce more accurate maps because all four rather than just three of the four channels can be used.

REFERENCES CITED

Kriegler, F. J., Malila, W. A., Nalepka, R. F., and Richardson, W., 1969, Preprocessing transformations and their effects on multispectral recognition: Proc. Sixth International Symposium on Remote Sensing of Environment, v. 1, p. 97-131.

Larsen, L. M., and Hasell, P. G., 1968, Calibration of an airborne multispectral optical sensor: Michigan Univ., Willow Run Laboratories, Tech. Rept. ECOM-00013-137, September 1968.

Nalepka, R. F., 1970, Investigation of multispectral discrimination techniques: Michigan Univ., Willow Run Laboratories, Rept. No. 2264-12-F, January 1970.

Smedes, H. W., Pierce, K. L., Tanguay, M. G., and Hoffer, R. M., 1969 [1970], Digital computer mapping from multispectral data, and evaluation of proposed Earth Resources Technology Satellite (ERTS) data channels, Yellowstone National Park; Preliminary Report: in Second Annual Earth Resources Aircraft Program Status Review, v. 1, Geology and Geography, p. 3-1 to 3-37.

Smedes, H. W., Pierce, K. L., Tanguay, M. G., and Hoffer, R. M., 1970, Digital computer terrain mapping from multispectral data: Jour. of Spacecraft and Rockets, v. 7, no. 9, p. 1025-1031, September 1970.

Smedes, H. W., Pierce, K. L., Tanguay, M. G., and Hoffer, R. M., 1970, Digital computer terrain mapping from multispectral data, and evaluation of proposed Earth Resources Technology Satellite (ERTS) data channels, Yellowstone National Park; Preliminary Report: in AIAA Earth Resources Observations and Information Systems Meeting, AIAA Paper No. 70-309, 18 p.

TABLE I.- WAVELENGTH BANDS OF THE UNIVERSITY OF MICHIGAN 12-CHANNEL SCANNER SPECTROMETER USED IN THIS STUDY

Channel number	Wavelength band μm	Channel number	Wavelength band μm
1	0.40-0.44	7	0.55-0.58
2	.44- .46	8	.58- .62
3	.46- .48	9	.62- .66
4	.48- .50	10	.66- .72
5	.50- .52	11	.72- .80
6	.52- .55	12	.80-1.00

TABLE II.- AVERAGE PROBABILITY OF MISCLASSIFICATION FOR DIFFERENT PREPROCESSING TRANSFORMS, AND CHANNELS USED (SHOWN IN PARENTHESES)

		Channels used and probability of misclassification		
		Best channels	Two best channels	Three best channels
Ratio transformations of original scanner data.	$\frac{n}{\Sigma}\left(\frac{1}{\Sigma}, \frac{5}{\Sigma}, \frac{10}{\Sigma}\right)$	(1) 0.08799	(1+5) 0.03718	(1+5+10) 0.02554
	$\frac{n}{n-1}\left(\frac{12}{11}, \frac{10}{9}\right)$	(11) .17856	(11+9) .08678	
	$\frac{n-1}{n+1}\left(\frac{12-11}{12+11}, \frac{10-9}{10+9}\right)$	(11) .18614	(11+9) .09066	
Normalized scan-angle function transformation of original scanner data.	(5, 12, 2)	(5) .06960	(5+12) .01529	(5+12+2) .00865
Ratio transformations of simulated ERTS data channels.	$\frac{n}{\Sigma}$ (using simulated ERTS scanner data channels; see table III)	.10133	.03923	
	$\frac{n}{\Sigma}$ (using simulated ERTS RBV camera data; see table III)			.03544

TABLE III.- WEIGHTING COEFFICIENTS FOR SIMULATING ERTS SENSORS WITH ORIGINAL SCANNER SPECTROMETER DATA

Michigan Spectrometer channel number	ERTS 4-channel scanner and RBV cameras	Weighting of Michigan channels
5	Channel 1	0.68
6		.86
7		.98
8		.70
8	Channel 2	.74
9		.96
10		.72
11	Channel 3	1.00
12	Channel 4	1.00
4	Camera 1	.72
5		.82
6		.95
7		.86
9	Camera 2	.94
10		.59
11	Camera 3	1.00

TABLE IV.- ACCURACY OF RECOGNITION IN TRAINING AREAS, USING DIFFERENT PREPROCESSING OF ORIGINAL SPECTROMETER DATA AND SIMULATED ERTS SCANNER DATA

Category	Percentage of training areas classified correctly		
	Normalized scan-angle transformation	Ratio transformation $\frac{\text{channel n}}{\text{channels}}$	Simulation of ERTS scanner using ratio transformation $\frac{\text{channel n'}}{\text{channels}}$ [1]
Bedrock	96.7	80.8	47.7
Talus	91.9	81.0	63.1
Vegetated Rock Rubble	94.4	91.9	95.3
Glacial Kame	100	93.3	94.7
Glacial Till	98.6	74.4	89.0
Forest	97.0	88.8	85.5
Bog	95.0	92.7	88.9
Water	94.7	94.7	93.4
Shadows	97.4	91.8	71.3
Average percentage of correct recognition	96.2	87.7	81.0
Average percentage of incorrect recognition	3.4	11.6	18.4
Average percentage of no recognition	0.4	0.7	0.6

[1] n' indicates the simulated ERTS channel, which is a non-linearly weighted summation of several original spectrometer channels (see table III) and does not correspond to n, which represents the non-weighted original spectrometer channel (table I).

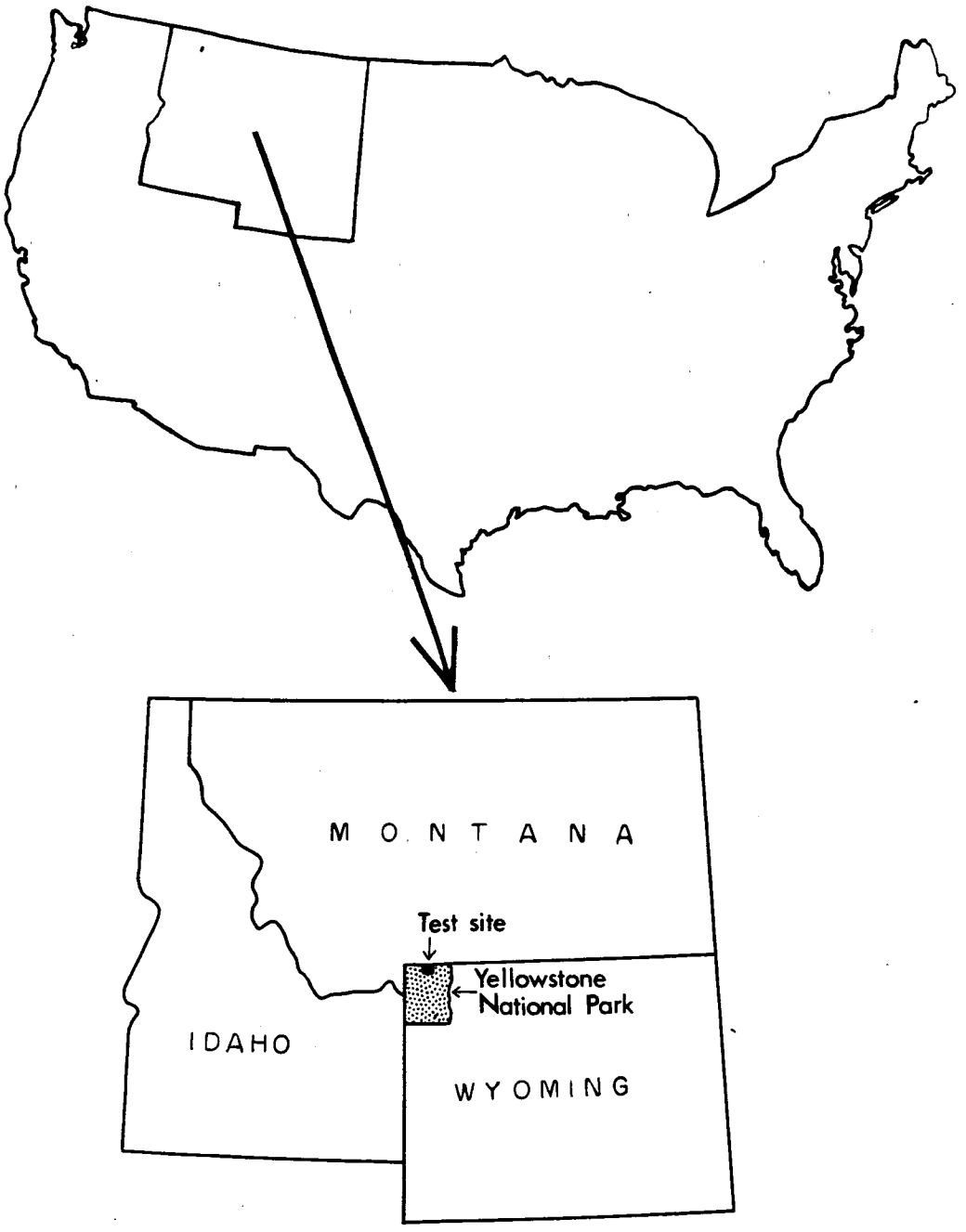

Figure 1.- Index map showing location of terrain mapping test site in Yellowstone National Park.

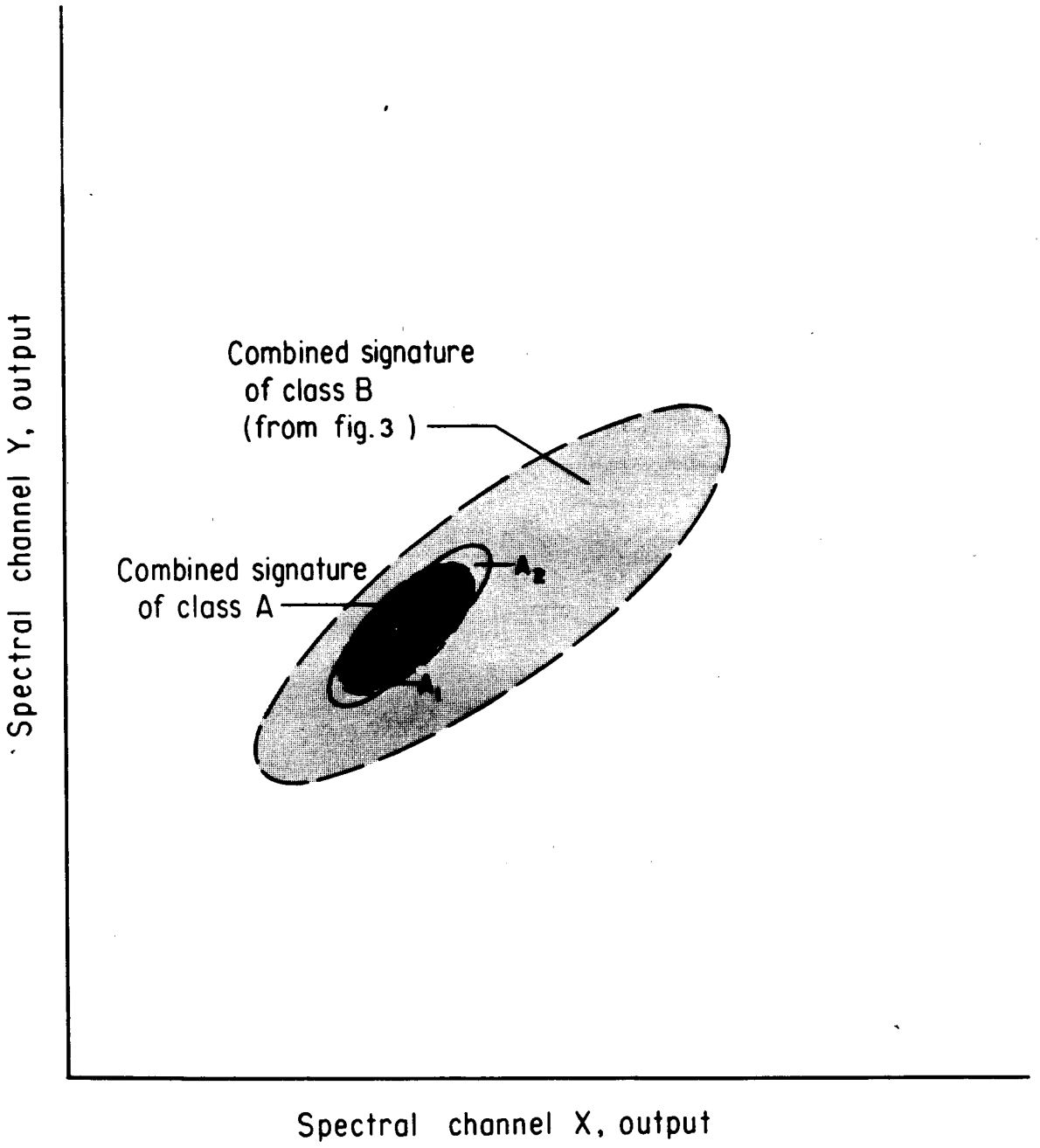

Figure 2.- Combined spectral signature of a class (A) where the means of the signatures from different training areas are close and the signatures overlap. Signatures from two training areas are outlined with solid line and labelled A_1 and A_2. Their means are shown by black dots. The combined signature of class A is outlined by dashed line. Its mean is shown by a cross.

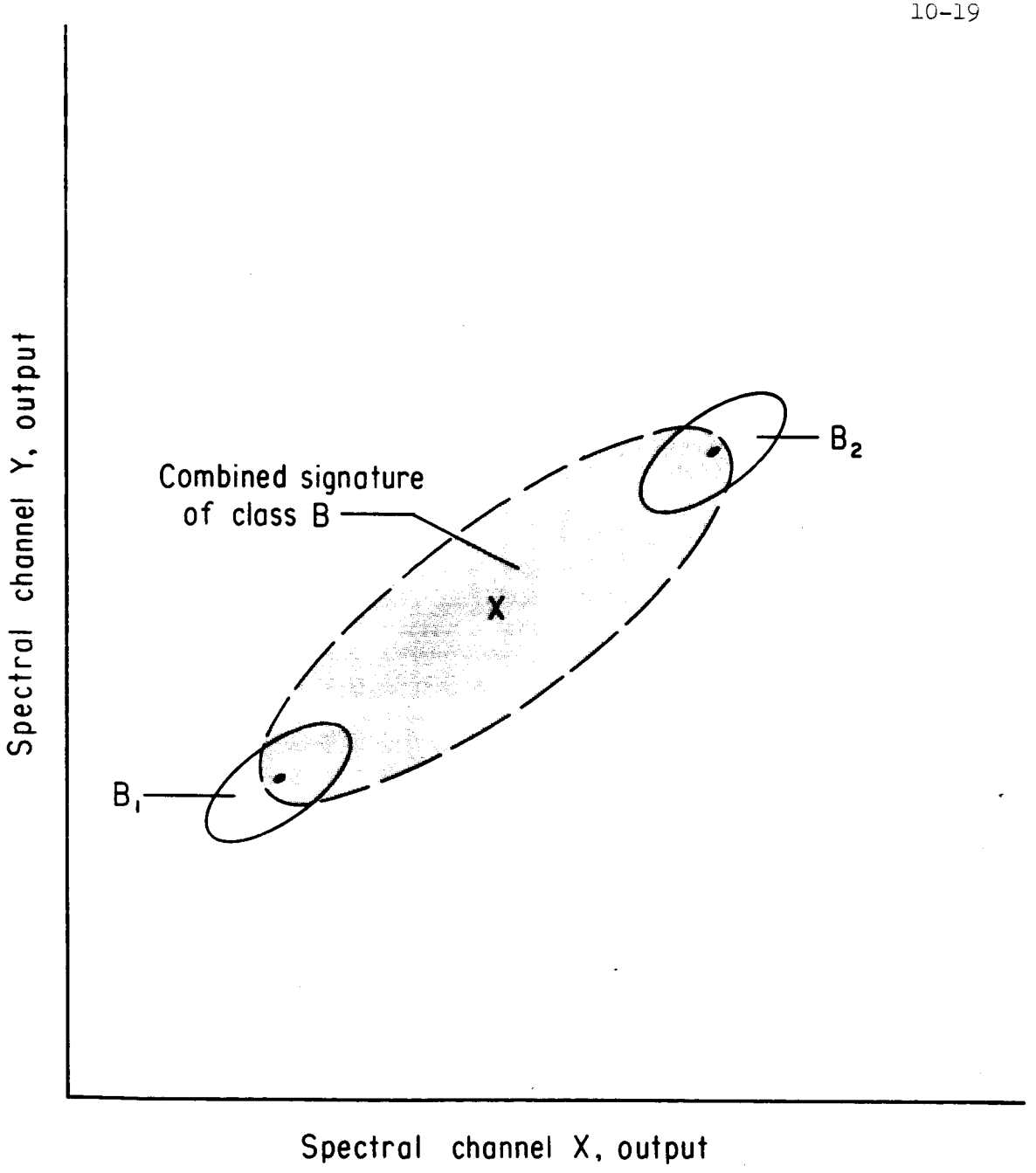

Figure 3.- Combined spectral signature of a class (B) where the means of the signatures from different training areas are widely separated and the signatures do not overlap. Signatures from two training areas are outlined with solid line and labelled B_1 and B_2. Their means are shown by black dot. The combined signature of class B is outlined by dashed line and is shaded. Its mean is shown by a cross. This combined signature would incorrectly include all elements of class A of figure 2.

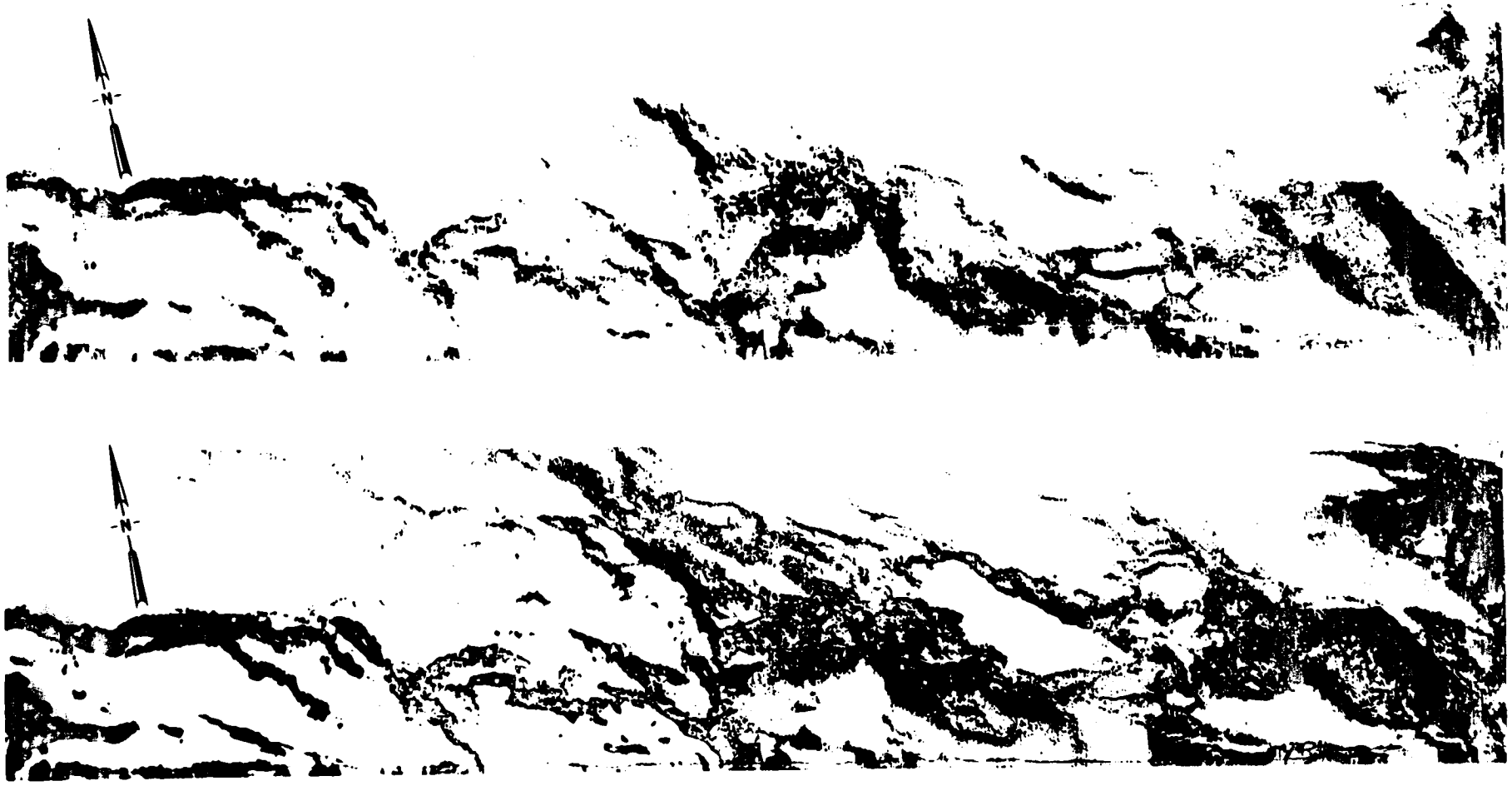

Figure 4.- Analog computer display of forest recognition over entire test site. Forest areas are shown as black. Top strip was made by selecting training areas only along the south side of the test area; bottom strip was made by selecting training areas along the south side, middle, and north side of the test area.

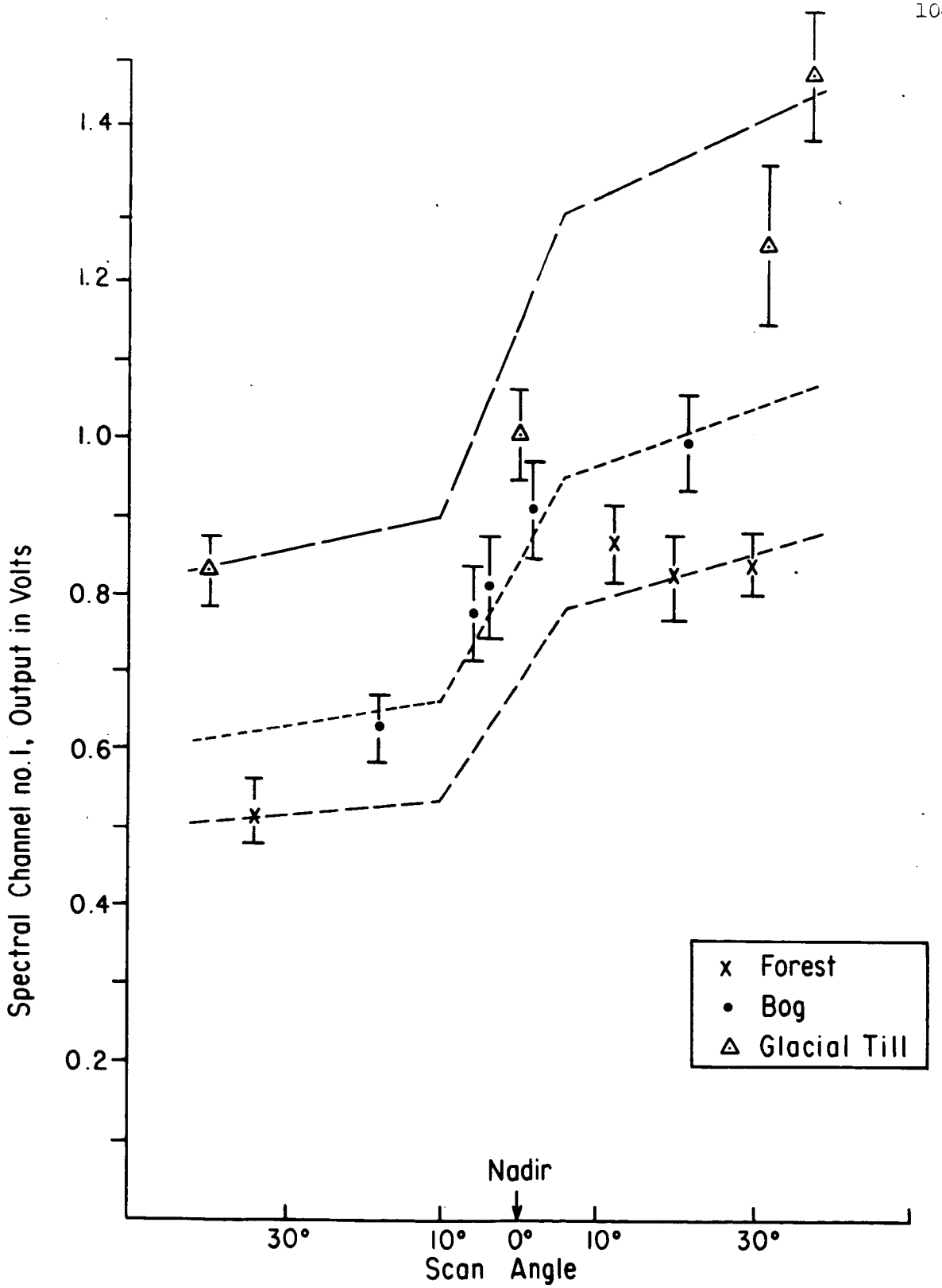

Figure 5.- Spectral channel output (radiance) versus scan angle for three terrain classes. The symbol for each training area is placed at the mean value which is centered on a bar two standard deviations long. Mean values of combined signatures are indicated by broken lines. The total length of the scan is about 2 miles, or less than 1 percent of that to be covered by the ERTS scanner and camera system.

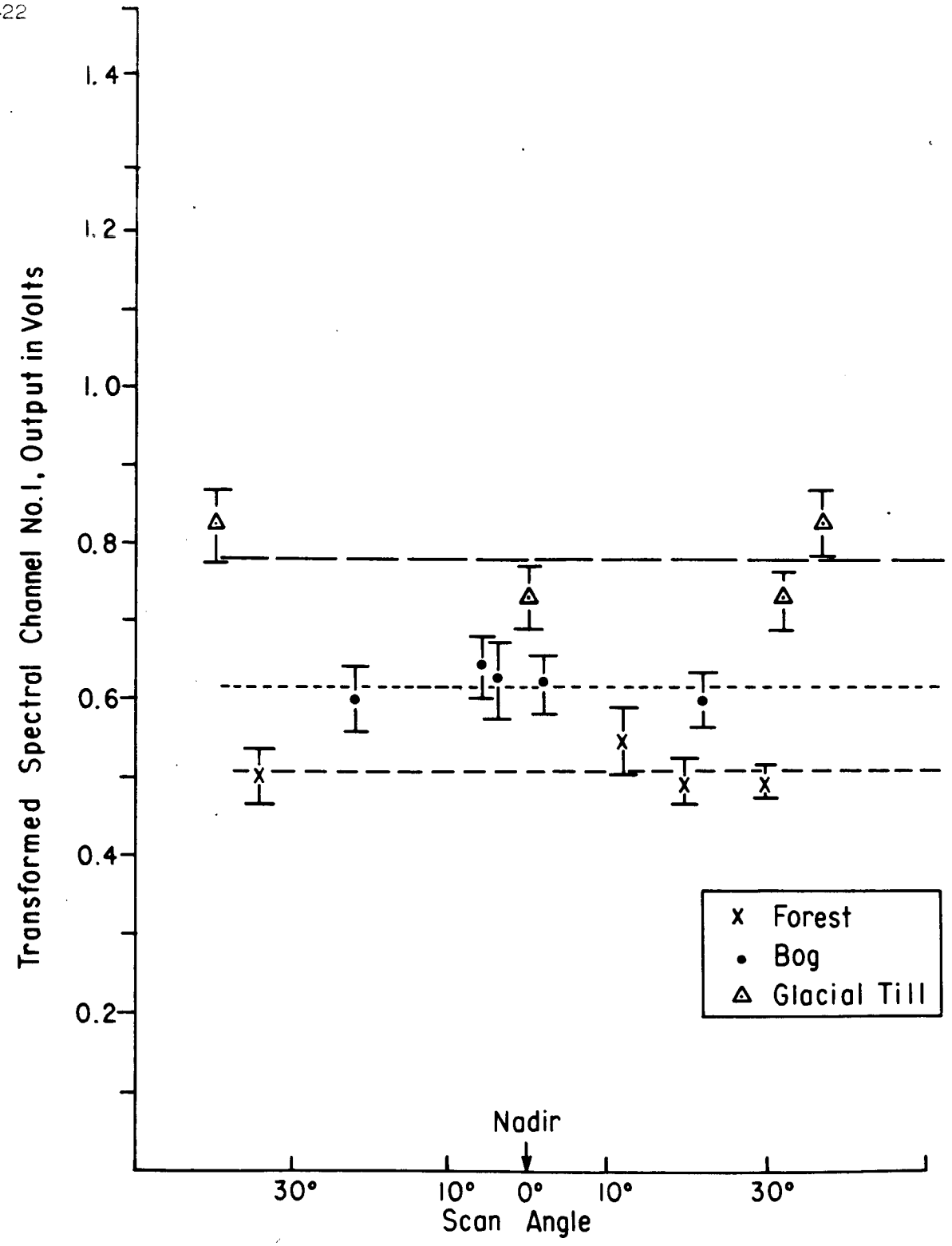

Figure 6.- Transformed spectral channel output (radiance) versus scan angle for the same three classes as in figure 5. Annotations are the same as in figure 5.

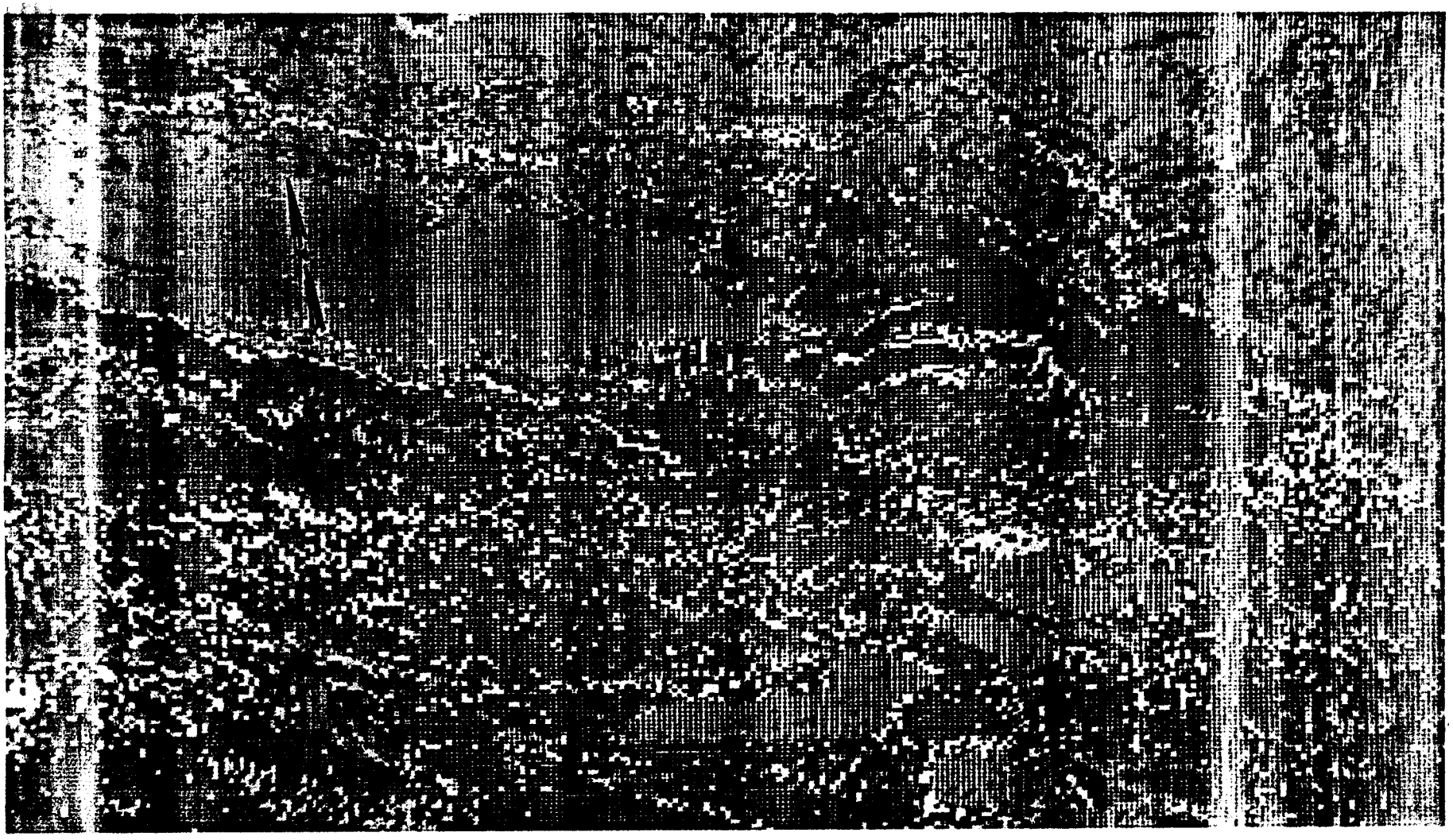

Figure 7.- Segment of terrain map made with the University of Michigan digital computer classification programs with preprocessing by scan-angle function transformation using channels 2, 5, and 12. The overall accuracy is about 86 percent. Symbols used to designate the terrain classes are shown in figure 9.

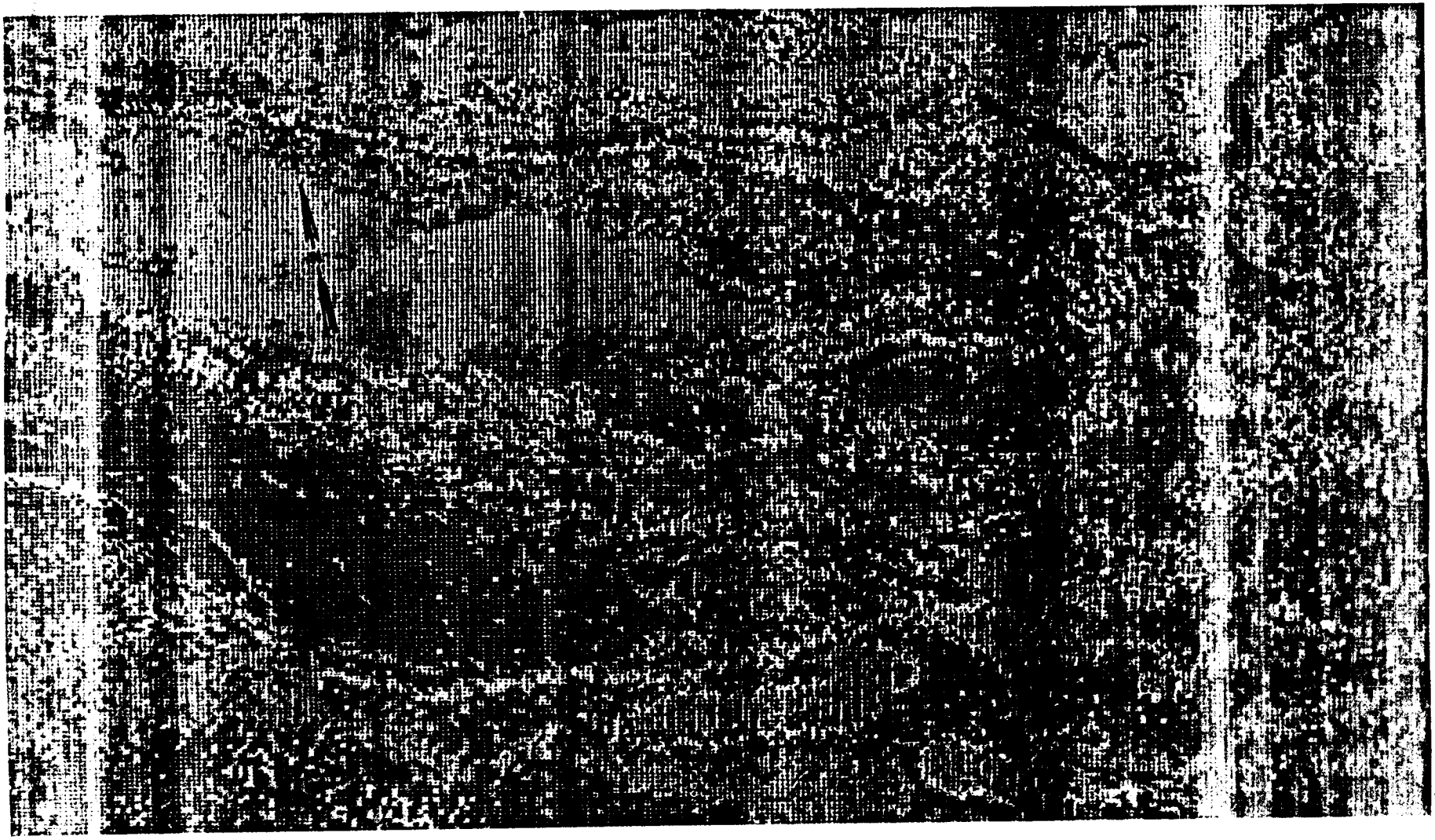

Figure 8.- Segment of terrain map made with the University of Michigan digital computer classification programs with preprocessing by ratio transformation using simulated data of the ERTS 4-channel scanner. The overall accuracy is about 83 percent. Symbols used to designate the terrain classes are shown in figure 9.

Material	Color				
	Blue	Red	Green	Black	White
Bog			*		
Forest			▒		
Glacial Till		▒			
Glacial Kame		*			
Bedrock	▒				
Vegetated Rock Rubble	*				
Water				▒	
Talus				*	
Cloud				·	
Not Classified					No Symbol

Figure 9.- Symbols and colors used to designate the terrain classes on the maps of figures 7 and 8. Because of the photographic reduction, the different symbols may not be distinguishable. Their effect is to produce a light and a dark shade of each color.

LINEAR GEOLOGIC STRUCTURE AND MAFIC ROCK DISCRIMINATION AS DETERMINED FROM INFRARED DATA*

By

T. W. Offield, L. C. Rowan, and R. D. Watson
U.S. Geological Survey,
Denver, Colorado 80225

ABSTRACT

Data from NASA flights over U.S. Geological Survey test sites in Montana-Wyoming and Oklahoma provide excellent examples of the value of infrared photographs and images for use in geologic investigations. Color-infrared photographs of the Beartooth Mountains, Montana, uniquely show the presence and distribution of mafic dikes and amphibolite bodies. Lineaments that cross grassy plateaus and that can be seen in other photographs commonly can be identified as mafic dikes only by the marked contrast between the dark rocks and the red vegetation in color-infrared photographs. Some amphibolite bodies in granitic terrane can also be detected by infrared photography and their contacts can be accurately drawn because of the enhanced contrast of the two types of rock in the near-infrared. Reflectance measurements made in the field for amphibolite and granite show that the granite is 25-50 percent more reflective in the near-infrared than in the visible region. The scene contrast resulting from this difference is further enhanced in color-infrared because atmospheric scattering is less than in the visible region of the spectrum.

Thermal-infrared images of the Mill Creek, Oklahoma, test site provide information on geologic faults and fracture systems not obtainable from photographs. Faults appear as thermal anomalies where thermally contrasting rocks are juxtaposed or where water is concentrated in the fault zones. The width of water-rich broken zones along the faults is revealed more exactly than in photographs. Subtle stripes that cross rock outcrop and intervening soil areas and that probably record water distribution in rock features are also shown on infrared imagery.

---

*Publication authorized by the Director, U.S. Geological Survey.

INTRODUCTION

Data from NASA aircraft flights over U.S. Geological Survey test sites in Montana-Wyoming and Oklahoma provide excellent examples of the value of infrared photographs and images for use in geologic investigations. The data offer some unique information for photogeologic analysis, permitting discrimination of mafic rock and definition of linear structures not possible or not easily done from data in the visible region of the spectrum. Consideration of reflectivity and thermal properties of rocks, soils, and vegetation clearly indicates the kinds of contrast between surface units that are of particular advantage for many geologic studies.

MAFIC-ROCK DISCRIMINATION

Color-infrared photographs taken in midmorning at about 16,600 m above the Beartooth Mountains in Montana-Wyoming provide better definition of ground features than do color photographs taken at the same time. This is a well-known advantage of infrared photography: filtering eliminates the blue portion of the spectrum where scattering is excessive, and as a result "haze penetration" is greater than in the visible region of the spectrum. A more important advantage, however, is that reflectance differences of vegetation and some rocks (see discussion below, and fig. 3) in the near-infrared result in greater scene contrast than is observed in color photographs.

Figure 1 provides a comparison of color-infrared and color photographs of a grassy plateau surface on the Beartooth Mountains. Linear features across the surface can be seen in both photographs, but most of those that are mafic dikes can be identified as such only in the color-infrared picture (fig. 2a). For this area, the advantage of color-infrared primarily and very simply rests in the fact that the mafic rocks are dark and the surrounding grass is red. The scene contrast is striking and results in the definition of the dikes; in color photographs the whole scene is generally green. (Note: the color photographs in figures 1 and 2 were not filtered and exposed for optimum fidelity of scene color, but the advantage of color-infrared for contrasting adjacent materials is, nevertheless, valid.) Dike trends are important in this area, because they are determined by fractures developed in the early geologic history [1, 2] and hence provide a key to early structural deformation.

Elsewhere in the Beartooth Mountains, amphibolite and other dark rocks occur as folded layers within light-colored granitic rocks. Delineation of the amphibolite is generally sufficient to define the main

structural features in the area [3, 4]. The contrast of dark amphibolite against light granite is apparent to any ground observer and would be expected to be obvious in color photographs. It is not obvious, however, in available high-altitude color pictures. One such amphibolite mass shown in figure 2 can be poorly discriminated in the color photograph (fig. 2b) *if* the observer knows it is there; it is more easily discerned and its contact with adjacent granite can be drawn in some detail in the companion color-infrared photograph (fig. 2a). Accurate discrimination of amphibolite across the whole area, however, requires stereoscopic coverage (ideally at more than one solar-illumination angle) for distinguishing reflectance differences from topographic effects, because areas sloping away from the sun, owing to shadow, appear similar to the amphibolite.

Reflectance measurements in the field demonstrate the advantage of photographs in the near-infrared over those in the visible region. Spectral reflectance differences were calculated for the amphibolite in figure 2 and two different areas in the adjacent granite. Measurements were made with an Instrument Specialties Company (ISCO) spectroradiometer, referenced to a fiberfrax standard and normalized to remove effects of slope and solar altitude. Sample areas were approximately 60 cm in diameter and measurements were made in midmorning. Figure 3 shows the two comparisons of amphibolite with slightly different granitic rocks; reflectance differences were determined at 0.05 μm intervals from 0.4 μm to 0.9 μm. The curves for the two sets of measurements permit comparison of the percent difference in reflectance (ΔR) between amphibolite and granite across the spectral bands of color-infrared and color films. Both curves show the amphibolite-granite reflectance difference to be significantly greater at the midpoint of the color-infrared film range than at the midpoint of the color film range. Such differences are highly useful in visual identification studies, given the well-known capability of the eye to discriminate extremely subtle color differences.

LINEAR STRUCTURE DISCRIMINATION

At another test site, near Mill Creek, Oklahoma, in the Arbuckle Mountains, photographs (fig. 4) taken in midafternoon at 6,500 m above terrain also show the advantage of color-infrared over color. The haze penetration characteristic of color-infrared results in significantly sharper definition of outcrops and, particularly, of rock layering. In addition, the red appearance of vegetation makes the drainage pattern more obvious than on color film and especially points up the presence of three fault zones, as indicated on figure 4. These linear zones are conspicuous because vegetation in the fault zone area has greater density and more vigor, and hence a higher reflectance than the adjacent vegetation. This, in turn, can reasonably be inferred to indicate greater

concentration of ground water in the zones. If the area was not known geologically, faults could be identified by the combination of linearity and inferred presence of ground water. For such structural features, color-infrared film consistently should be more useful than color film, because moisture loss reduces plant reflectance in the near infrared long before change in the visible can be observed [5]. Reflectance contrast between moist zones and drier surroundings is added to the generally enhanced scene contrast and the clearer definition of features provided by color-infrared film.

A nighttime thermal-infrared image (8-14 μm) (fig. 5) taken in winter shows the same fault zones to be relatively cold, confirming the supposition that the zones are water-rich. Daytime thermal-infrared images taken the previous day (fig. 6, for example) do not show the zones to be temperature anomalies. Similar images (not shown) taken in summer at a drier time show the zones as slight anomalies at morning, afternoon, and predawn and reflect seasonal changes in moisture content of the ground, vegetation albedo and evapotranspiration, and insolation effects.

Figure 6 shows the presence of relatively broad cool areas which are intricately lineated, mainly NE-SW; the most conspicuous of these areas is shown in the bottom part of the image. These cool zones are probably areas of relatively high evaporative cooling at midafternoon. This characteristic of thermal-infrared images should be useful in defining areas of differing surface moistures and as a means of discriminating soil units. The lineations, to a large extent, match bedrock joint traces but are much more continuous, clearly crossing areas of soil cover between outcrops. They are not limited to the cool areas, but occur throughout the area. These lineations may reflect patterns of soil moisture controlled by fracture systems in the underlying bedrock, but they may also reflect subtle effects of topography, density differences, and cumulative insolation. If the lineations are related to soil moisture that is influenced by geologic structure and if simi- features can be found in other regions, knowledge of their pattern and the intensity of their development could be useful in geochemical prospecting. More work is planned to determine the nature of the lineations.

Thermal-infrared images of the Mill Creek test site also show faults on a larger scale, owing to the juxtaposition by faulting of units that have different outcrop characteristics and rock thermal properties. (Compare with geologic map [6].) Figure 7 shows the fault blocks on a thermal image (fig. 7a) and a high-altitude photograph (fig. 7b). The high-altitude photograph shows the blocks better than does a mosaic of low-altitude photographs, because it provides a single, synoptic view. However, parts of the boundary faults, as well as rock-type variations within the blocks, show more clearly on the infrared image.

This is a daytime infrared image; for other areas a nighttime image might provide better discrimination of rock units, depending on the thermal contrast produced by differences in albedo, thermal inertia, and heating cycle.

APPLICATION TO SATELLITE OBSERVATIONS

The advantages of increased scene contrast that high-altitude color-infrared photographs display as a result of haze penetration, vegetation discrimination, and rock and soil reflection differences apply equally to photographs and to images from space. The effect of atmospheric scattering on space photographs will not be appreciably more than that observed from 18,000 m altitude, and so the principal difference between the data shown here and space photographs will be system resolution. For the ERTS system, nominal resolution is about 80 m, but linear features as small as 30 m wide can probably be detected if they contrast sufficiently with surrounding terrain. This means that features as small as the fault zones in figure 4 can be detected and probably identified in ERTS reconstituted color-infrared images. ERTS multiband imagery, therefore, will be of interest to geologists working at quadrangle scale; and where available for little-known regions, it will be invaluable for detailed reconnaissance study.

Nominal resolution of the thermal-infrared images to be obtained by ERTS-B is about 250 m, but again linear features smaller than that will be detectable. Such features as the fault blocks shown in figure 7 should be readily visible in ERTS thermal images. Many rock units will be discriminable because of thermal and reflective properties which contrast with those of adjacent units. Daytime images will be useful in many instances, but nighttime images will add data of great importance and must be secured if the full potential of ERTS-B for geologic investigations is to be realized.

REFERENCES

1. Spencer, E. W., 1959, Fracture patterns, pt. 2 of Geologic evolution of the Beartooth Mountains, Montana and Wyoming: Geol. Soc. America Bull., v. 70, no. 4, p. 467-508.

2. Prinz, Martin, 1965, Structural relationships of mafic dikes in the Beartooth Mountains, Montana-Wyoming: Jour. Geology, v. 73, no. 1, p. 165-174.

3. Larsen, L. H., Poldervaart, Arie, and Kirchmayer, Martin, 1966, Structural homogeneity of gneisses in the Lonesome Mountain area, pt. 7 of Geologic evolution of the Beartooth Mountains, Montana and Wyoming: Geol. Soc. America Bull., v. 77, no. 11, p. 1277-1291.

4. Casella, C. J., 1969, A review of the Precambrian geology of the eastern Beartooth Mountains, Montana and Wyoming, in Igneous and metamorphic geology--A volume in honor of Arie Poldervaart: Geol. Soc. America Mem. 115, p. 53-71.

5. Heller, R. C., 1970, Imaging with photographic sensors, in Remote sensing, with special reference to agriculture and forestry: Natl. Acad. Sci., p. 35-72.

6. Ham, W. E., McKinly, M. E., and others, 1954, Geologic map and sections of the Arbuckle Mountains, Oklahoma: Oklahoma Geol. Survey, scale 1:72,000.

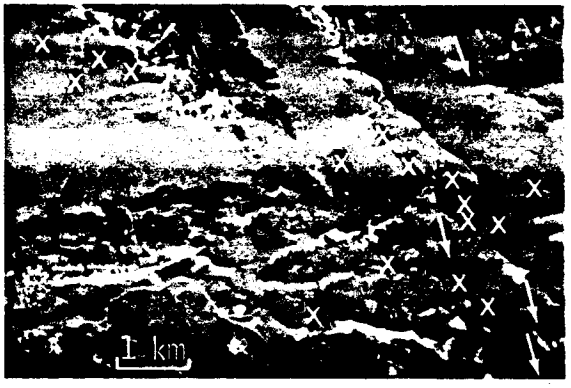

(a) Ektachrome-IR SO-117 with 0.500 μm filter.

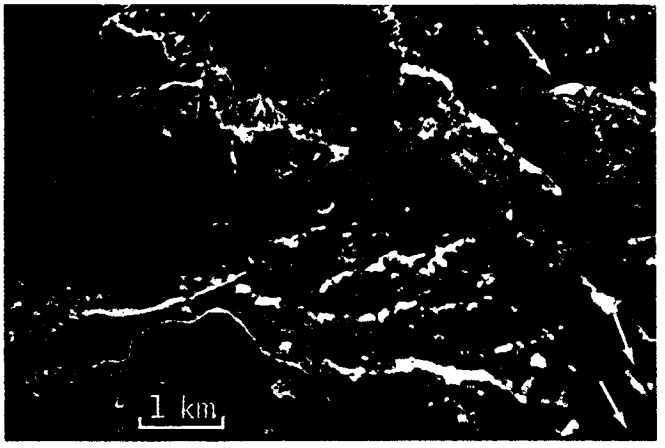

(b) Ektachrome 2448 with HF-3 and AV filters.

Figure 1. Beartooth Mountains, Montana-Wyoming (RC-8 cameras, altitude above terrain approximately 16,600 m; mid-morning). Arrows indicate mafic dikes identifiable in both pictures, X's indicate mafic dikes identifiable only in color-infrared. North toward left side of figures.

(a) Ektachrome-IR SO-117 with 0.500-μm filter.

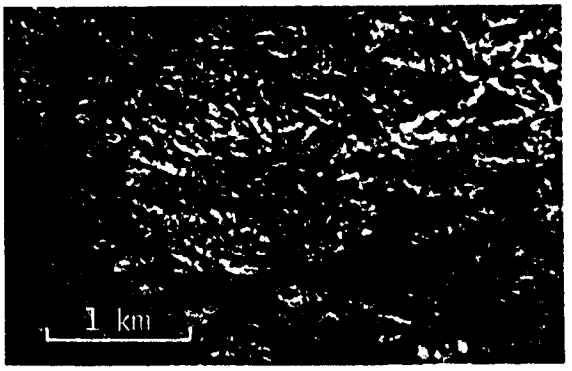

(b) Ektachrome 2448 with HF-3 and AV filters.

Figure 2. Beartooth Mountains, Montana-Wyoming (RC-8 cameras, altitude above terrain approximately 16,600 m; midmorning). Black line (fig. 7a) outlines amphibolite body in granitic terrane. North toward right side of figures.

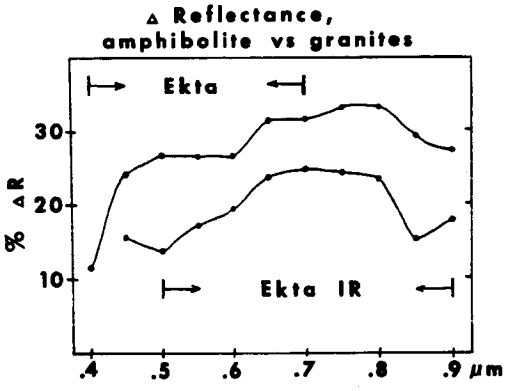

Figure 3. Comparison of amphibolite and granite (two samples); midmorning reflectance.

(a) Ektachrome-IR 2443 with 0.500 μm filter.

(b) Ektachrome SO-397 with AV filter

Figure 4. Fault zones near Mill Creek, Oklahoma (RC-8 cameras, altitude above terrain approximately 6,000 m; midafternoon). F, fault zone. North at top of figures.

Figure 5. Predawn thermal-infrared (Reconofax IV, 8-14 μm, altitude above terrain 1,500 m) image showing fault zones (F) near Mill Creek, Oklahoma, as cool (dark) anomalies. North at top of figure.

Figure 6. Afternoon thermal-infrared (Reconofax IV, 8-14 μm, altitude above terrain 1,500 m) image showing cool (dark) areas (near bottom of figure), northeast-trending thermal linears, and fault zones near Mill Creek, Oklahoma. North at top of figure.

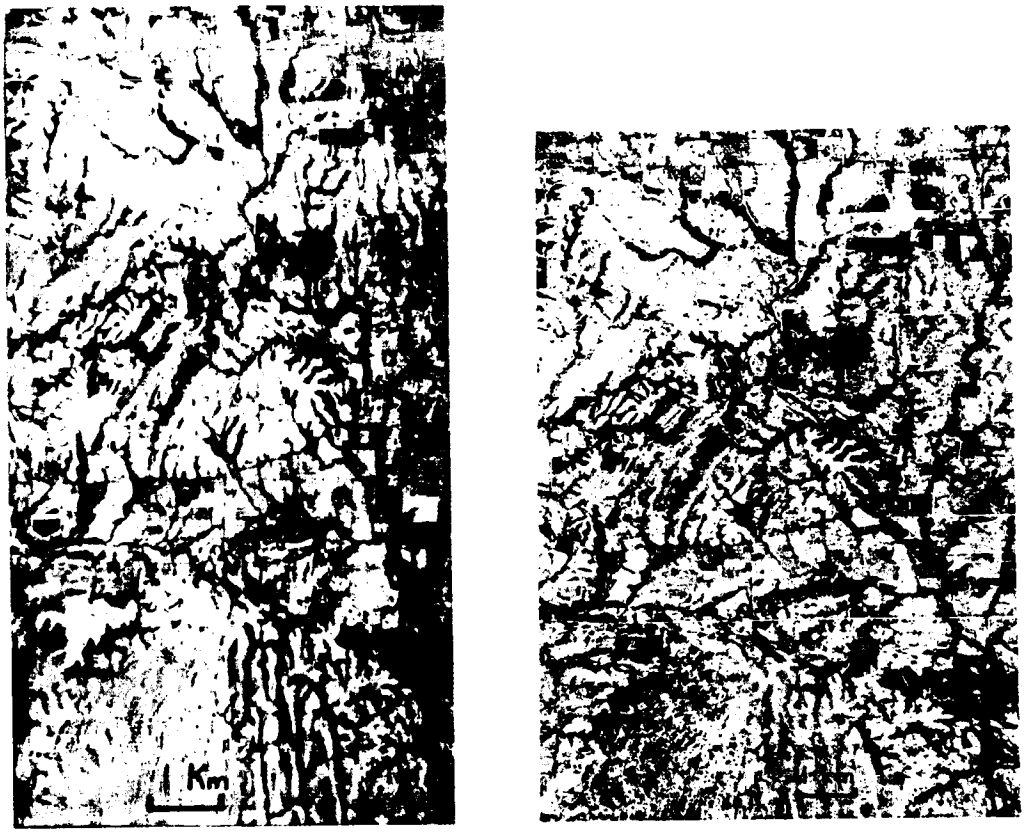

(a) Daytime thermal-infrared (RS-14, 8-14 μm, altitude above terrain 3,000 m) image.

(b) Daytime photograph reproduced from Ekta-chrome SO-397 (RC-8 camera, AV filter, altitude above terrain approximately 17,000 m).

Figure 7. Fault blocks near Mill Creek, Oklahoma. North at top of figures.

MULTISPECTRAL ANALYSIS OF LIMESTONE, DOLOMITE, AND GRANITE, MILL CREEK, OKLAHOMA*

BY

L. C. Rowan and Kenneth Watson
U.S. Geological Survey
Denver, Colorado 80225

ABSTRACT

Spectral-reflectance and thermal-emission data were collected at the Mill Creek, Oklahoma, test site during NASA missions 132 and 133 in June 1970. These data were collected by three aircraft flown several times during the diurnal cycle at altitudes of 150 to 17,000 m above mean terrain. This report deals with the spectral reflectance of the main rock types of the site--limestone, dolomite, and granite --as determined from the data collected by the University of Michigan 12-channel multispectral scanner during mission 133 and from thermal-infrared images recorded during mission 132 on an RS-7 scanner from 17,000 m above terrain.

Reflectances for selected areas of limestone, dolomite, and granite were calculated by referring scanner detector voltages of the selected areas to detector voltages of reflectance panels placed along one flight line recorded at 0900 hrs. from 150 m above terrain. Between 0.42 and 0.70 μm, the order of mean reflectance is dolomite, limestone, and granite. Between 0.70 and 0.80 μm, limestone is markedly more reflective than the dolomite and granite. These spectra are in reasonably good agreement with ground-level measurements, except that the airborne reflectance spectra are at a coarser scale and include the effects of vegetation and soil.

In November 1970, a preliminary "rock-recognition map" was automatically generated using data collected at 0900 hrs. from 900 m above terrain. Although the limestone and dolomite in the map area appear similar on black-and-white and color photographs, the discrimination provided by the map is reasonably accurate. Misidentification occurred in areas of unusually high dolomite reflectivity, which were misidentified as limestone, and in areas of rubbly limestone which were misidentified as dolomite. Additional computer processing should eliminate most of these errors.

---

*Publication authorized by the Director, U.S. Geological Survey.

High-altitude (17,000 m above terrain) thermal-infrared (10-12 μm) images of the Mill Creek test site show, in spite of 30-40 percent cloud cover, regional folds and faults distinguished by the presence of thermally contrasting materials. Linear and curvilinear structural features two to three times smaller than the nominal 17 m resolution can be detected, which suggests that narrow geologic features might be detectable on ERTS-B thermal-infrared images.

INTRODUCTION

The Mill Creek test site (178) is in the Arbuckle Mountains in south-central Oklahoma (fig. 1). Detailed remote-sensing studies were conducted in the eastern part of the site (fig. 2), particularly southwest of the village of Mill Creek.

In 1968, investigations were begun in the Mill Creek area by the U.S. Geological Survey. The main objective of these studies was to determine criteria for the delineation and identification of rock types by their reflection and emission characteristics. Mathematical modeling techniques were used to define the important physical variables, to determine the relation of the variables to the rock composition and hence to use the variables in rock unit discrimination, and to predict the optimum time and level of confidence with which other areas might be explored with remote-sensing techniques.

The Mill Creek test site consists mainly of folded and faulted Paleozoic limestone and dolomite and jointed and faulted Precambrian granite [1]. The area is well suited for detailed remote-sensing studies, because exposures are excellent, topographic relief is low, and access is good. Perhaps equally important is the fact that the main rock types are representative of rocks that underlie large percentages of the Earth's land surface. In addition, the degree of prior geologic understanding of this area gained through our studies and those of other workers [1, 2, 3, 4] is relatively high.

This report discusses the preliminary results of missions 133 and 132 flown in June 1970 and the impact of these results on previous findings. This report will deal mainly with reflectance data collected by means of the University of Michigan 12-channel multispectral scanner during mission 133. Three lines were flown by the University of Michigan aircraft at 0900, 1200, and 1500 CDT (Central Daylight Time) at altitudes of 150, 900, and 3000 m above mean terrain. The following discussion will be limited to analysis of reflectances computed from measurements made at 0900 CDT from 150 m and to a preliminary "rock-

recognition map" prepared from voltage data recorded along line 1 at 0900 CDT from 900 m. During mission 132, thermal-infrared images were obtained from about 17,000 m above mean terrain, and a few comments will be made concerning these data.

REFLECTANCE STUDIES

Analysis of multiband photographs of the Mill Creek area and of ground-level reflectance measurements by R. D. Watson (unpub. data) suggested that the limestone, dolomite, and granite might be discriminable through analysis of reflectance measurements. Multispectral analysis has been previously applied in the discrimination of terrain units in the Yellowstone National Park area [5]. Reflectances also are required to determine albedos for the thermal modeling techniques being used in our studies [6].

That photographs are of very limited value for discrimination of the main rock types in the Mill Creek area is demonstrated by the black-and-white photograph (fig. 3) obtained in September 1969 (mission 105). This generalized geologic map (fig. 3) shows the distribution of limestone, dolomite, and granite, as well as two faults and one of the flight lines to be discussed later. Note that the limestone and dolomite are difficult to distinguish on the basis of reflectance alone, and that the granite and limestone appear to have almost identical reflectances. Although multiband photographs of the area are an improvement over broad-band black-and-white and color photographs, they are uncalibrated and are complicated by the numerous limitations of film for quantitative analysis [7].

In order to determine the reflectances of the limestone, dolomite, and granite, scanner detector voltages recorded on magnetic tape were converted to reflectances by use of calibration panels of known reflectance placed on the ground along line 1.

Figure 4 shows the mean reflectance spectra for limestone, dolomite, and granite measured in the 12 channels at 0900 hrs. from 150 m above terrain. Between 0.42 and 0.70 μm, the order of rocks showing increasing reflectance is dolomite, limestone, and granite. Between 0.70 and 0.80 μm, the limestone is markedly more reflective than the dolomite and granite. These spectra are in reasonably good agreement with ground-level measurements made by R. D. Watson, except that the airborne spectra are complicated by influences of soil (R. D. Watson and L. C. Rowan, unpub. data).

Although the standard deviations of the voltages used to generate the reflectances are fairly large, the means appear to be consistent with the results at the other flight times, and they provide important information for the mathematical modeling of the thermal properties of the three rock types.

ROCK-RECOGNITION MAP

In November 1970 a preliminary "rock-recognition map" was automatically generated by means of data collected from 900-m altitude at 0900 CDT along part of line 1. The area along line 1 is of special interest because of the intricate relationship of limestone and dolomite. Along the trace of line 1 from east to west are limestone, a narrow band of dolomite, limestone, a thick sequence of dolomite, and then limestone (fig. 5). Vegetation, mainly grass, occupies the areas of nonexposure, and no significant difference is apparent from one rock type to another. The locations of the trace of line 1 and the calibration panels are also shown (fig. 5).

Although the limestone and dolomite along line 1 appear on the photograph (fig. 5) to be similar, their discrimination shown on the rock-recognition map (fig. 6) is reasonably accurate. For example, the main areas underlain by limestone just east of the road and to the west of the western limit of the dolomite are portrayed mainly as limestone. The accurate location of outcrops in the area is of special importance to a geologist, because a map on which they are located can be used as a guide to the most critical areas for ground study.

Steps preliminary to preparation of the map were selection of small training areas for study of limestone and dolomite and the computation of the signal voltage in each channel for each data point in the area. The mean and standard deviations of the limestone and dolomite voltages were then computed, and the channels with the most significant statistical differences were selected for discrimination of rock types: channels 10, 11, 1, 5, 2, and 7 (see fig. 4) were used in preparation of this map.

Two types of misidentification occurred: (1) Moderately reflective dolomite was confused for limestone, and (2) limestone rubble and vegetation at the edges of limestone outcrops were misidentified as dolomite. Training areas for the moderately reflective dolomite and rubbly limestone were not used in processing the recognition map, and we believe that analysis using areas which are representative of these conditions will significantly improve the identification process.

In summary, the important preliminary results are (1) the determination of relative reflectances for limestone, dolomite, and granite, and (2) automatic preparation of both a "rock-recognition map" for limestone and dolomite and a very accurate outcrop map.

HIGH-ALTITUDE THERMAL-INFRARED IMAGES

During mission 132, which was flown simultaneously with part of mission 133, thermal-infrared images (10-12 μm) of the Mill Creek test site were recorded from approximately 17,000 m above terrain. Although the area was 30-40 percent covered by clouds, thus reducing thermal contrast as well as obscuring some areas, these images contain considerable geologic information. The fact that spatial resolution of thermally contrasting linear features is significantly higher than nominal 18.5 m resolution has important implications concerning the geologic utility of thermal-infrared images obtained from satellites.

Regional folds and the northwest-trending Reagan fault are conspicuous on the high-altitude black-and-white photograph of the eastern and central part of the site shown on figure 7. These structural features are apparent on the thermal-infrared images shown in figure 8 owing to the presence of thermally contrasting units. In most places, the contrast can be correlated with vegetation distribution; but in a few areas, the rocks have thermal properties sufficiently different to produce the thermal contrast. For example, granite outcrops are anomalously warm (fig. 8a); this brightness is consistent with data secured from lower altitudes [6]. Water-rich fault zones are more readily identified on the thermal-infrared image (fig. 8a) than on the photograph obtained at approximately the same time, because these zones were anomalously cool at this time. The cool zone extending north from Mill Creek is where a rain-shower occurred just prior to this flight.

Perhaps of more significance than the specific contrast on these images is that, as mentioned, thermally contrasting linear and curvilinear features as small as 6-7 m can be detected. The scanner used to obtain these images, an RS-7, has a 1-milliradian instantaneous field of view which provides a nominal ground resolution of 17 m at the nadir from 17,000 m. These relations suggest that features two to three times smaller than the calculated 215-m ground resolution for the ERTS-B thermal band might be detected. If this were true, it would be possible to observe many local, as well as regional, structural, and stratigraphic features on ERTS-B thermal-infrared images.

REFERENCES CITED

1. Ham, W. E., 1949, Geology and dolomite resources, Mill Creek-Ravia area, Johnston County, Oklahoma: Oklahoma Geol. Survey Circ. 26, 104 p.

2. _____1950, Geology and petrology of the Arbuckle limestone in the southern Arbuckle Mountains, Oklahoma: Yale Univ. unpub. Ph. D. dissert., 162 p.

3. Ham, W. E., McKinley, M. E., and others, 1954, Geologic map and sections of the Arbuckle Mountains, Oklahoma: Oklahoma Geol. Survey, scale 1:72,000.

4. Ham, W. E., and others, 1969, Regional geology of the Arbuckle Mountains, Oklahoma: Oklahoma Geol. Survey Guidebook 17, 52 p.

5. Smedes, H. W., Spencer, Margret, and Thompson, Frederick, 1971, Preprocessing of multispectral data and simulation of ERTS data channels to make computer terrain maps of a Yellowstone National Park test site, in NASA Third Annual Earth Resources Program Review: Houston, Tex., Natl. Aeronautics and Space Adm., this volume.

6. Watson, K. D., 1971, A thermal model for analysis of infrared images, in NASA Third Annual Earth Resources Program Review: Houston, Tex., Natl. Aeronautics and Space Adm., this volume.

7. Pohn, H. A., 1964, A systematic program of photoelectric and photographic photometry of the moon, in Astrogeologic studies--Annual progress report, July 1, 1963, to July 1, 1964: U.S. Geol. Survey open-file report, p. 79-83 [1965].

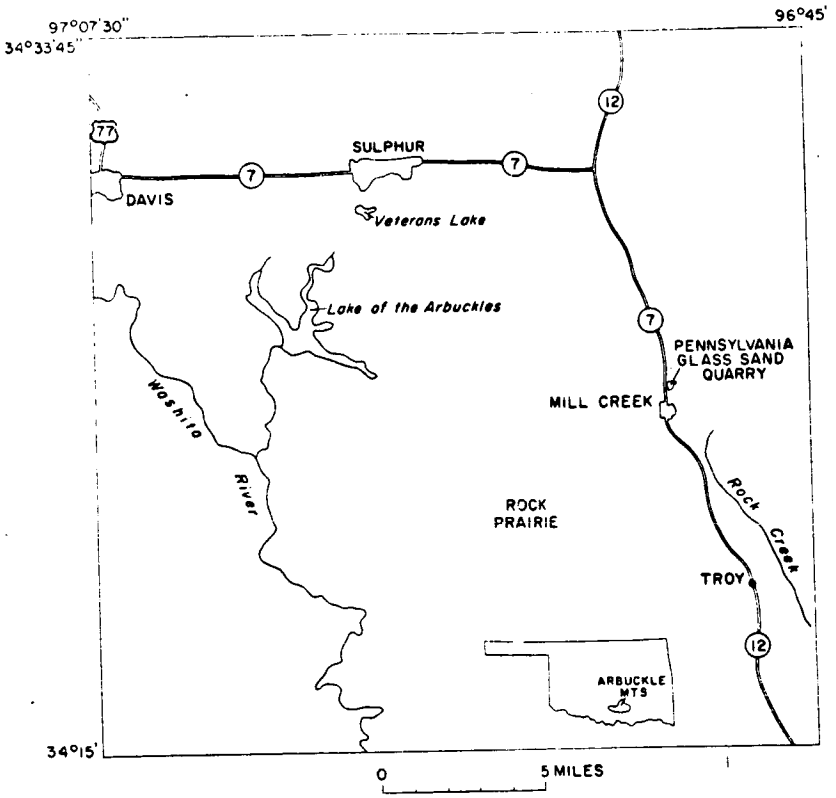

Figure 1. Index map of Oklahoma showing the location of the Mill Creek test site.

Figure 2. Photograph showing the eastern part of the Mill Creek test site. Areas of limestone (L), dolomite (D), and granite (G). North at top. Prepared from Ektachrome positive transparency obtained from 17,000 m above terrain.

Figure 3. Photograph of the area southwest of Mill Creek, Oklahoma, showing the distribution of main rock types. Areas of limestone (L), dolomite (D), granite (G). Faults (F), trace of flight line 1 (L1). North at top.

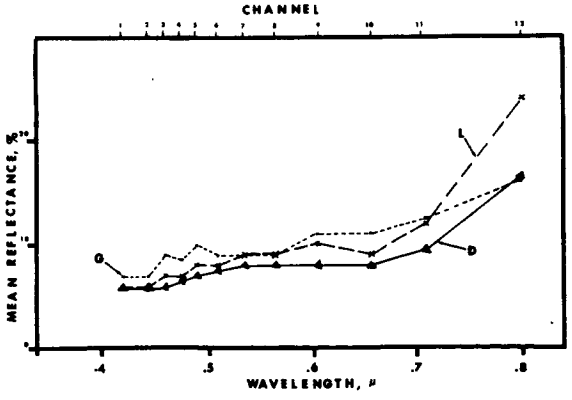

Figure 4. Mean reflectance of limestone (L), dolomite (D), and granite (G), calculated from voltages recorded at 0900 CDT from 150 m above mean terrain.

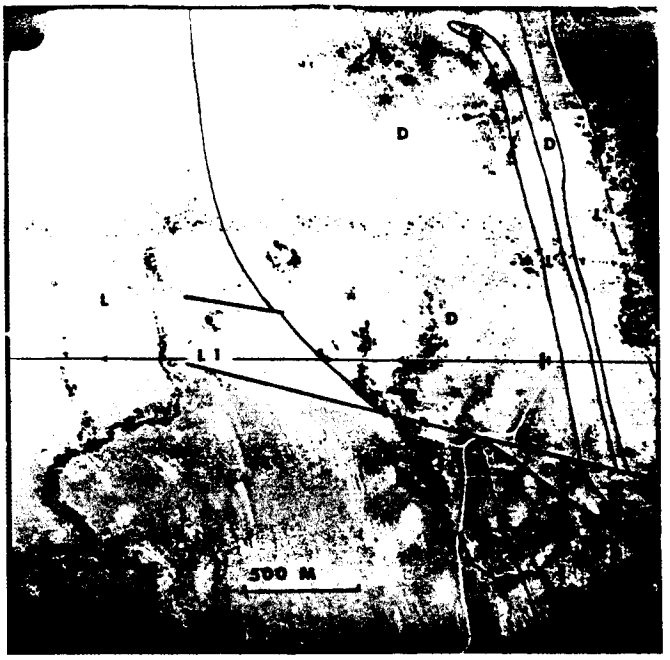

EXPLANATION

L	Limestone
D	Dolomite
SD	Sandy dolomite
	Contact
	Fault
	University of Michigan flight line 1. Arrow shows direction of flight. Short heavy lines perpendicular to flight line indicate location of calibration panels

Figure 5. Photograph of the area along line 1 showing the distribution of the main rock types. Prepared from Ektachrome positive transparency obtained in September 1969.

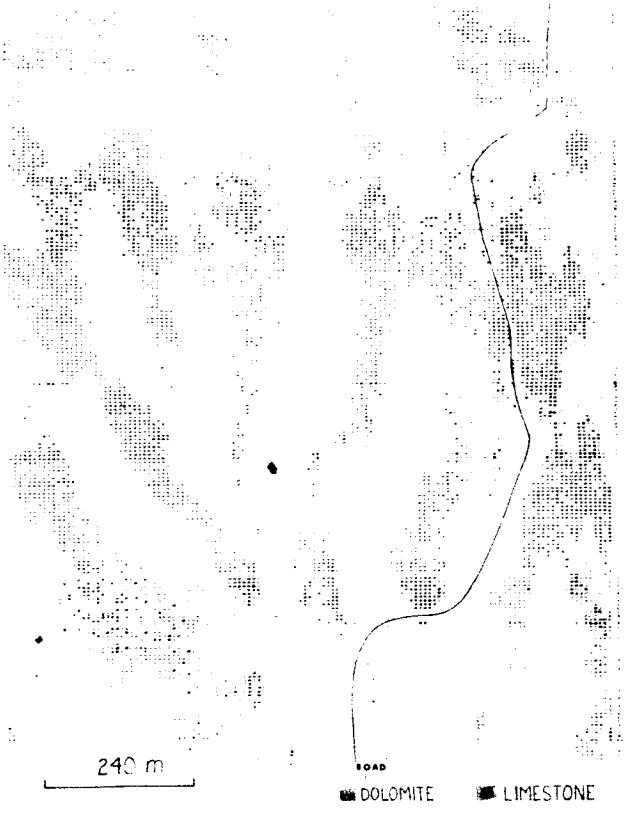

Figure 6. Rock-recognition map of area along the eastern part of line 1. The distributions of limestone (dark x's), dolomite (light x's), and vegetation (blank) were determined from voltages collected from 900 m at 0900 CDT. North at top.

Figure 7. Photograph of the eastern and central part of the Mill Creek, Oklahoma, test site showing the regional structural features and prominent granite outcrops. Photograph was prepared from an Ektachrome positive transparency obtained from 17,000 m above terrain approximately simultaneously with the thermal-infrared images shown in figures 8a and b. North at top.

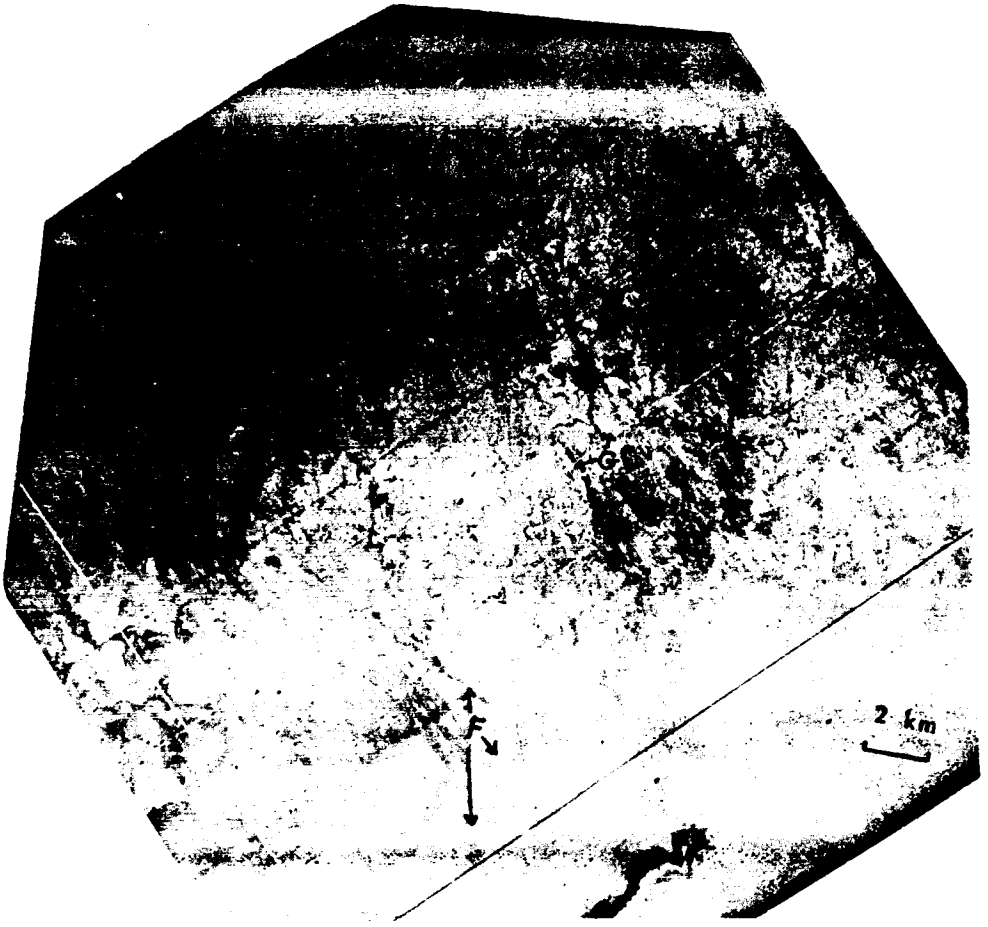

(a) Eastern part of site at 0926 CDT showing anomalously warm granite outcrops (G), water-rich and vegetated fault zones (F), and area of rain-shower (CR). North at top.

Figure 8. Thermal-infrared images of the Mill Creek, Oklahoma, site recorded with an RS-7 scanner from 17,000 m above terrain.

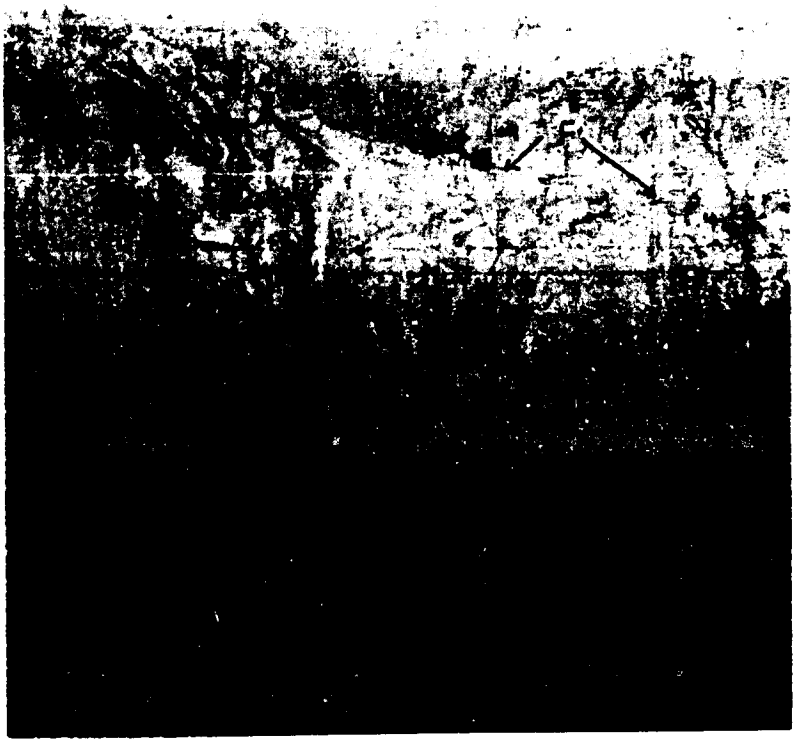

(b) Western part of site at 0912 CDT showing regional folds and the Reagan fault (F). North at top.

Figure 8. Concluded.

A THERMAL MODEL FOR ANALYSIS OF INFRARED IMAGES*

by

Kenneth Watson
U.S. Geological Survey
Denver, Colorado 80225

ABSTRACT

A mathematical model, derived from the equation of heat conduction, has been developed to assist in the interpretation of thermal-infrared images acquired from aircraft and spacecraft. The model assumes steady-state boundary conditions and, hence, it does not require that an initial temperature distribution be prescribed. The model contains the parameters of rock and soil properties (thermal inertia, albedo, emissivity), atmospheric effects (transmission, effective air temperature), site location (latitude), and season (sun's declination). The results predicted by the model provide an explanation for the thermal differences among granite, limestone, and dolomite that were recorded in the December 1968 daytime and predawn flights over the Mill Creek, Oklahoma, test site when representative thermal inertia and albedo values were used.

A second test of the model made use of data acquired during the June 1970 predawn overflight of Mill Creek. Although some features of the limestone-dolomite contrast similar to those of the first test were observed, the most striking new feature of the predawn images was the relatively warm granite outcrops. A simple model of transient heating of the ground was constructed as an extension of the overall model to examine the effects of atmospheric perturbations. Results obtained from the model are consistent with those of ground observations made at the time of the overflight. Additional flights will be necessary to evaluate more fully the transient heating hypothesis.

The development of a mathematical model for analysis of thermal-infrared images is an important step in discrimination of rock types and in the selection of optimum overflight times.

---

*Publication authorized by the Director, U.S. Geological Survey

INTRODUCTION

The interpretation of remote sensing observations that are obtained to study Earth resources is complicated by both the number and the magnitude of factors that affect the recorded signal. Mathematical models, based on scientific principles, provide a powerful technique to (1) examine correlations between selected variables, (2) test assumptions about suspected major factors, and (3) discover and analyze unsuspected factors. An effective approach is to start with observations of simple areas, analyze the results in terms of simple models, and iteratively increase the complexity of the models and the sites in a systematic manner. This approach, which I will call the "geophysical method," has been successfully applied in traditional geophysical activities; for example, seismology, gravity, and magnetism. It should be equally appropriate to the interpretation of measurements of reflected and emitted electromagnetic energy from terrain.

This approach will be explained by the demonstration of a mathematical model that was developed to assist in the interpretation of thermal infrared data. The details of the model are described elsewhere [1]. Although somewhat unsophisticated, the model has provided insight into the problems of discrimination of geologic materials from aircraft. It should be equally applicable to spacecraft observations.

THE MODEL

The model was constructed by the Laplace transform technique applied to one-dimensional heatflow to obtain an equation between surface temperature and surface flux [2]. This nonlinear equation--nonlinear because it involves radiative transfer--was then solved by conventional iterative techniques based on an initial "first guess" solution. The problem can be solved rapidly on a digital computer if sufficient care is taken to avoid convergence problems [1]. The effects of a variety of rock and soil properties, atmospheric conditions, site location, season, and topographic orientation on the diurnal surface temperature have been examined by this model. The effect of thermal inertia on the diurnal surface temperature is illustrated in figure 1. Thermal contrast is greatest about 1 hour after local noon; dawn provides the greatest nighttime thermal contrast. Note that materials of highest thermal inertia have the least diurnal temperature change and therefore will appear cooler in the daytime and warmer in the night than materials of low thermal inertia. Figure 2 illustrates the effect of albedo on the diurnal temperature. As expected, the temperature contrast is greatest during the daytime owing to insolation and is least at dawn. The effects of site

location (fig. 3) and of season (fig. 4) on the diurnal temperature are determined by the well-known dependence of insolation on latitude and sun's declination.

THE TEST SITE--INITIAL RESULTS

In December 1968, the Mill Creek, Oklahoma, test site (no. 178) was overflown as part of Mission 84 of the NASA Aircraft Earth Resources Program. As previously reported [3], a distinct contrast between limestone and dolomite that was not apparent on the daytime images was observed on the predawn thermal infrared image (fig. 5). With some variation, the granite appeared to be about the same temperature as the limestone. Field measurements in conjunction with conventional photo interpretation were used to determine albedos of the rock types [4], and thermal inertia values were computed from existing data [5, 6]; the surface temperature variation was then determined by means of the theoretical model (fig. 6). The results are reasonably consistent with the thermal images.

RECENT RESULTS

A further test of the model was conducted during June 1970 by use of thermal inertia and albedo values used in the original model to make a prediction for the temperature variation of the three materials (fig. 7). The test site was then overflown as part of the NASA Aircraft Earth Resources Program Mission 105; the resulting predawn thermal image is shown in figure 8. Although some features of the limestone-dolomite contrast are similar, it is clear that the most striking anomaly is the warm granite outcrops. This is at variance with both the model prediction and the initial predawn image.

However, on the night previous to the June aircraft overflight a very warm front moved into the Mill Creek area. To examine its potential effect on the ground temperature an extension of the model was made to include "impulsive" heating or cooling. The results were computed by the following equations, which neglect nonlinear effects.

Steady state:

$$v = v(x,t) \qquad \text{where} \qquad \frac{\partial v}{\partial t} = \kappa \frac{\partial^2 v}{\partial x^2}$$

$$\text{subject to} \qquad -K\frac{\partial v}{\partial x}\bigg|_{x\,=\,o} = F(t)$$

in which

κ = diffusivity

K = conductivity

F = flux

v = temperature as a function of depth x, and time t.

Impulse:

Let $v(x,t) = v_o(x,t) + \Delta v(x,t)$

v = final temperature

v_o = steady-state temperature

Δv = perturbed temperature due to flux ΔF

$$\frac{\partial(\Delta v)}{\partial t} = \kappa \frac{\partial^2(\Delta v)}{\partial x^2} \text{ subject to } -K\frac{\partial(\Delta v)}{\partial x}\bigg|_{x\,=\,o} = \Delta F(t)$$

therefore,

$$\Delta v(x,t) = \frac{1}{P\sqrt{\pi}} \int_o^t \Delta F(t-\tau) e^{-x^2/4\kappa t} \frac{d\tau}{\sqrt{\tau}} \qquad [7],$$

hence,

$$v(o,t) = v_o(o,t) + \frac{1}{P\sqrt{\pi}} \int_o^t \frac{\Delta F(t-\tau)\, d\tau}{\sqrt{\tau}}$$

where

P, the thermal inertia, is $\sqrt{\kappa}/K$.

The effect on the model of a nighttime impulse is illustrated in figure 9. As expected, the time of initiation of the impulse, the duration of the impulse, and the magnitude of the heat transfer are all important in determining the resultant surface temperature. Application of the impulsive heating model to the circumstances of the June 1970 flight (fig. 10) yields results which are reasonably consistent with the observed predawn image (fig. 8). As expected, the material with the lowest thermal inertia (granite)--low because of the extensive lichen cover [1]--is heated the most and becomes the warmest anomaly, and the contrast between the limestone and dolomite is reduced. It is planned to further test the model at additional sites that have a variety of rock types, insolation, and atmospheric conditions.

CONCLUSIONS

A simple mathematical model has been developed to assist in the interpretation of thermal-infrared images from aircraft. It should be equally useful in the analysis of thermal data obtained from spacecraft. Previous results obtained at the Mill Creek test in December 1968 are explainable with the model when representative thermal and albedo values are used. Results obtained during the June 1970 overflights, though inconsistent with the initial model predictions, are explainable with the addition of impulsive heating to the model, the explanation being consistent with observations at the time of the overflight.

ACKNOWLEDGMENT

This work was supported by NASA Task 160-75-01-43-10.

REFERENCES

1. Watson, Kenneth, 1971, Introduction and summary [and] Data analysis techniques, Pt. 1 *of* Remote sensor application studies progress report, July 1, 1968, to June 30, 1969: U.S. Geol. Survey Rept. USGS-GD-71-004; available only from U.S. Dept. Commerce Natl. Tech. Inf. Service, Springfield, Va. 22151.

2. Jaeger, J. C., 1953, Conduction of heat in a solid with periodic boundary conditions, with an application to the surface temperature of the moon: Cambridge Philos. Soc. Proc., v. 49, pt. 2, p. 355-359.

3. Rowan, L. C., Offield, T. W., Watson, Kenneth, Watson, R. D., and Cannon, P. J., 1970, Thermal infrared investigations, Mill Creek area, Oklahoma, *in* NASA Second Annual Earth Resources Aircraft Program Status Review: Houston, Tex., Natl. Aeronautics and Space Adm., v. 1, sec. 5, p. 1-25.

4. Rowan, L. C., and Watson, Kenneth, 1971, Multispectral analysis of limestone, dolomite, and granite, Mill Creek, Oklahoma, *in* NASA Third Annual Earth Resources Program Review: Houston, Tex., Natl. Aeronautics and Space Adm., this volume.

5. Clark, S. P., Jr., 1966, Composition of rocks, sec. 1 *in* Handbook of physical constants [revised ed.]: Geol. Soc. America Mem. 97, p. 1-5.

6. National Research Council, 1926-30, International critical tables of numerical data, physical chemistry and technology: New York, McGraw-Hill Book Co., Inc., 7 v.

7. Carslaw, H. S., and Jaeger, J. C., 1959, Conduction of heat in solids [2d ed.]: Oxford Univ. Press, 510 p.

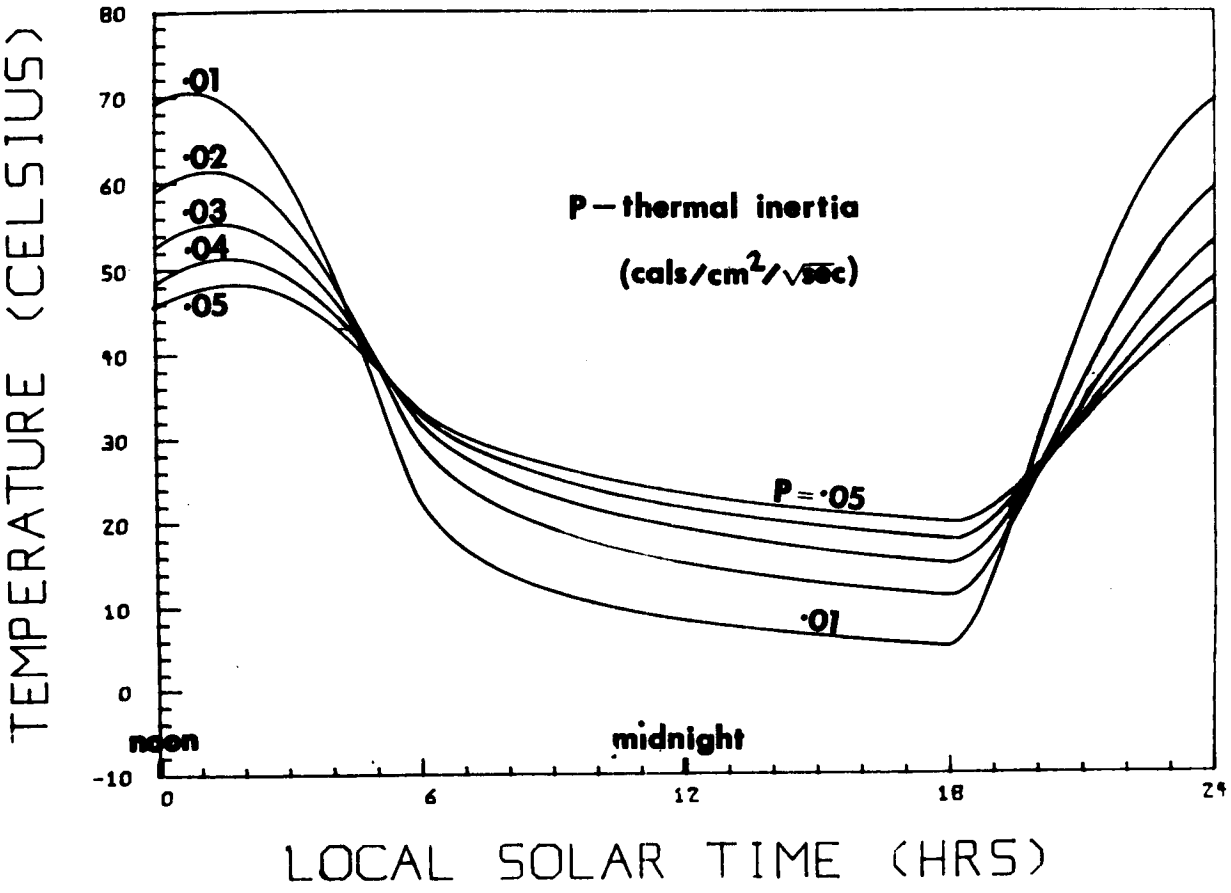

Figure 1.- Diurnal surface temperature variation with local solar time computed from the model for materials with different thermal inertias. Thermal contrast is greatest 1 hour after local noon; maximum nighttime contrast occurs at dawn.

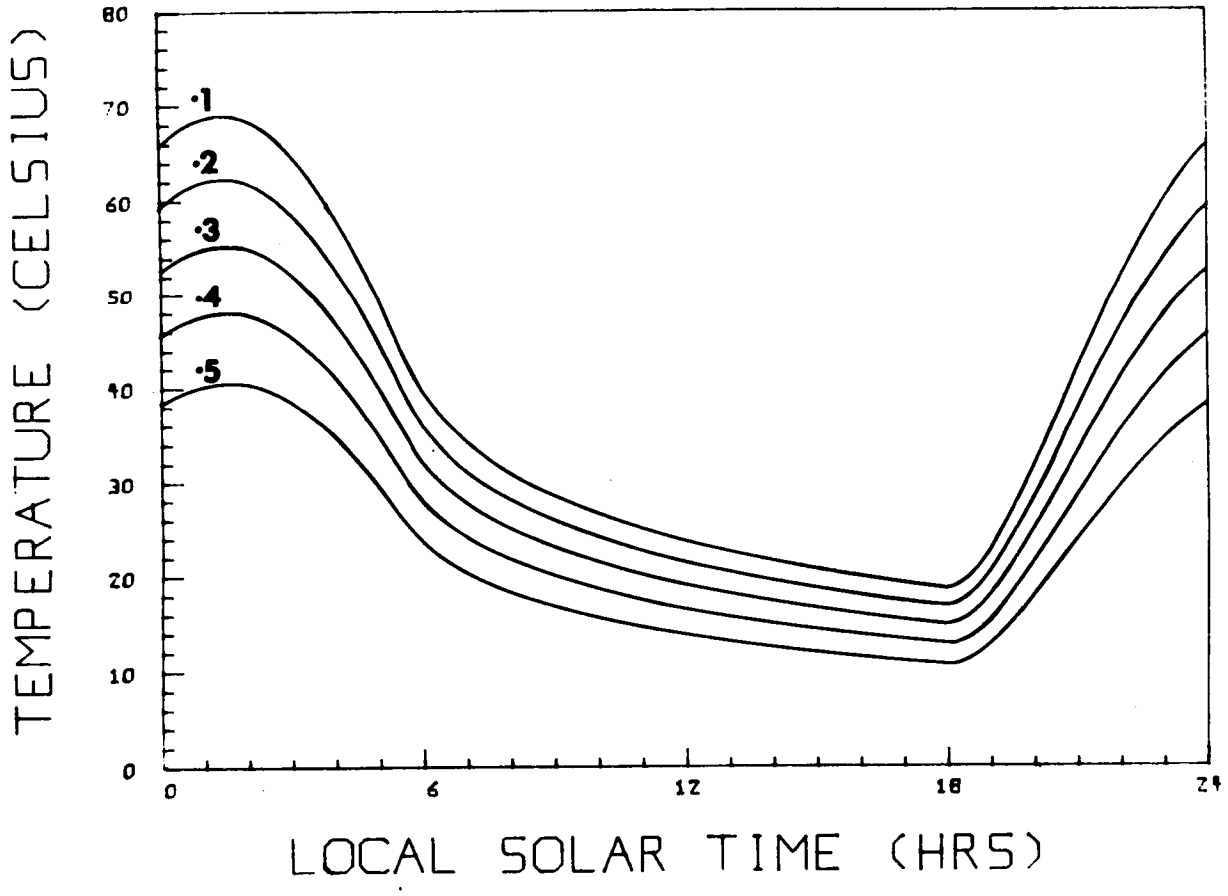

Figure 2.- Diurnal surface temperature variation computed for different albedo values. Because the albedo determines how much incident solar energy is reflected from the surface and consequently how much is absorbed, the temperature contrast is greatest during daytime due to insolation and least at dawn. Noon 0 hours, midnight 12 hours.

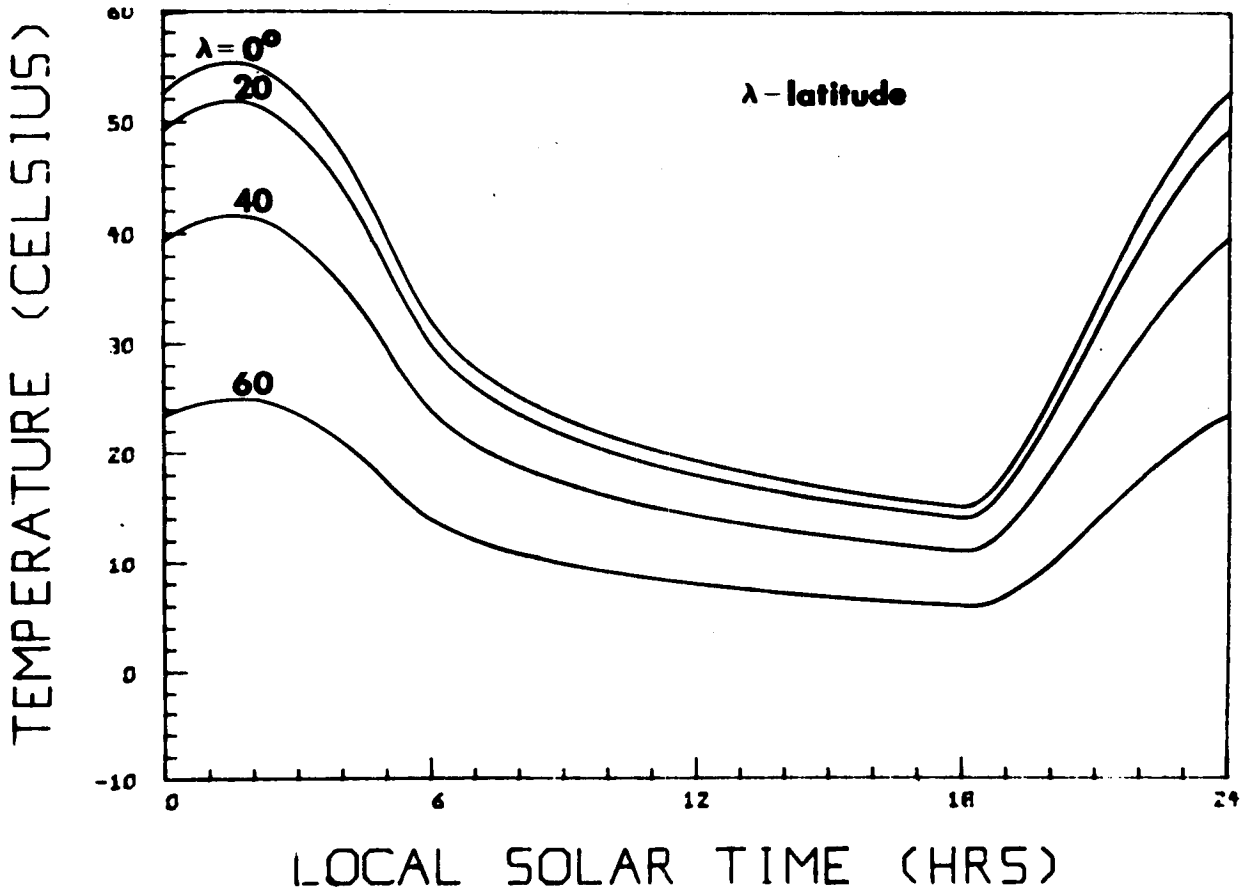

Figure 3.- Diurnal surface temperature variation computed for different site latitudes. Because the net daily insolation received is less at high latitudes the daily temperature change is reduced. Noon 0 hours, midnight 12 hours.

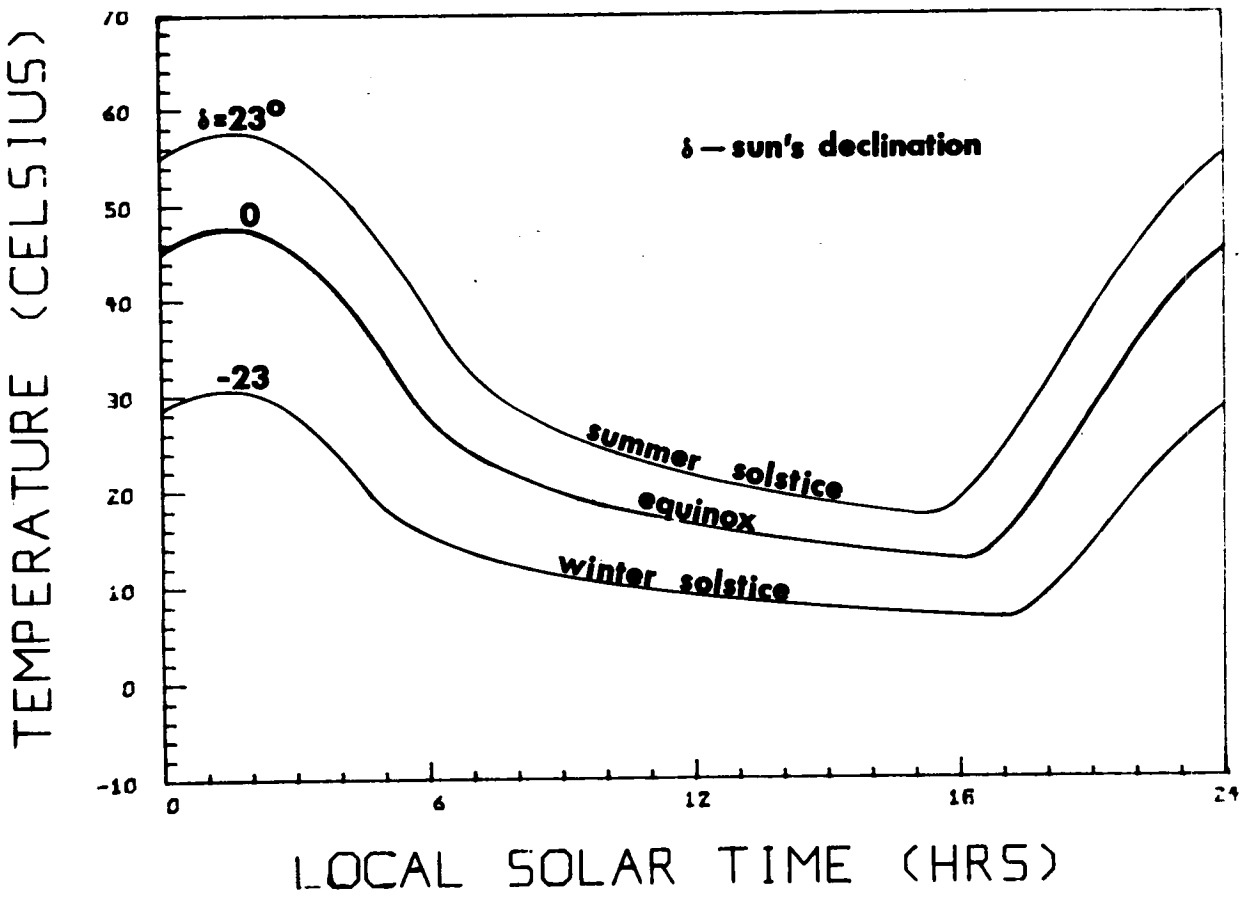

Figure 4.- Diurnal surface temperature variation computed for different seasons. The effect of seasonal change is due to the dependence of insolation of the sun's declination which affects both the amplitude of the incident solar flux and the time of sunrise and sunset. Noon 0 hours, midnight 12 hours.

Figure 5.- Thermal-infrared images of the Mill Creek, Oklahoma, test site obtained in December 1968 at predawn (6 a.m.), midmorning (11 a.m.), and midafternoon (2 p.m.). North is at the top of the images. Dominant rocks on the images are L-limestone, D-dolomite, and G-granite. The predawn thermal contrast between the limestone and dolomite is not observed on the daytime image. The granite appears similar to the limestone.

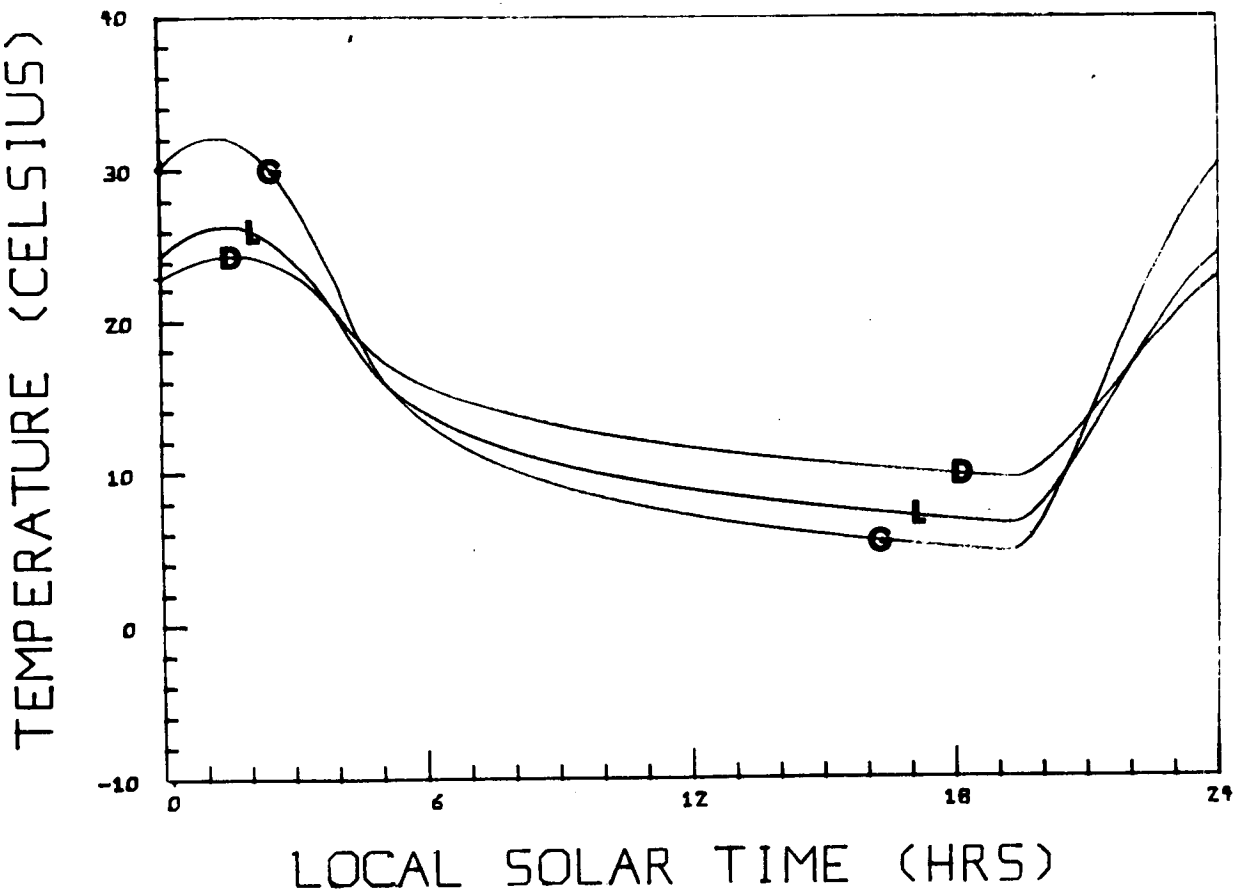

Figure 6.- Diurnal surface temperature variation computed from representative values of the albedo and thermal inertia of the limestone (L), dolomite (D), and granite (G) for the December 1968 overflight. The values were determined from published data, field measurements, and qualitative examination of aerial photographs. Model results are in qualitative agreement with the thermal images shown in figure 5. Noon 0 hours, midnight 12 hours.

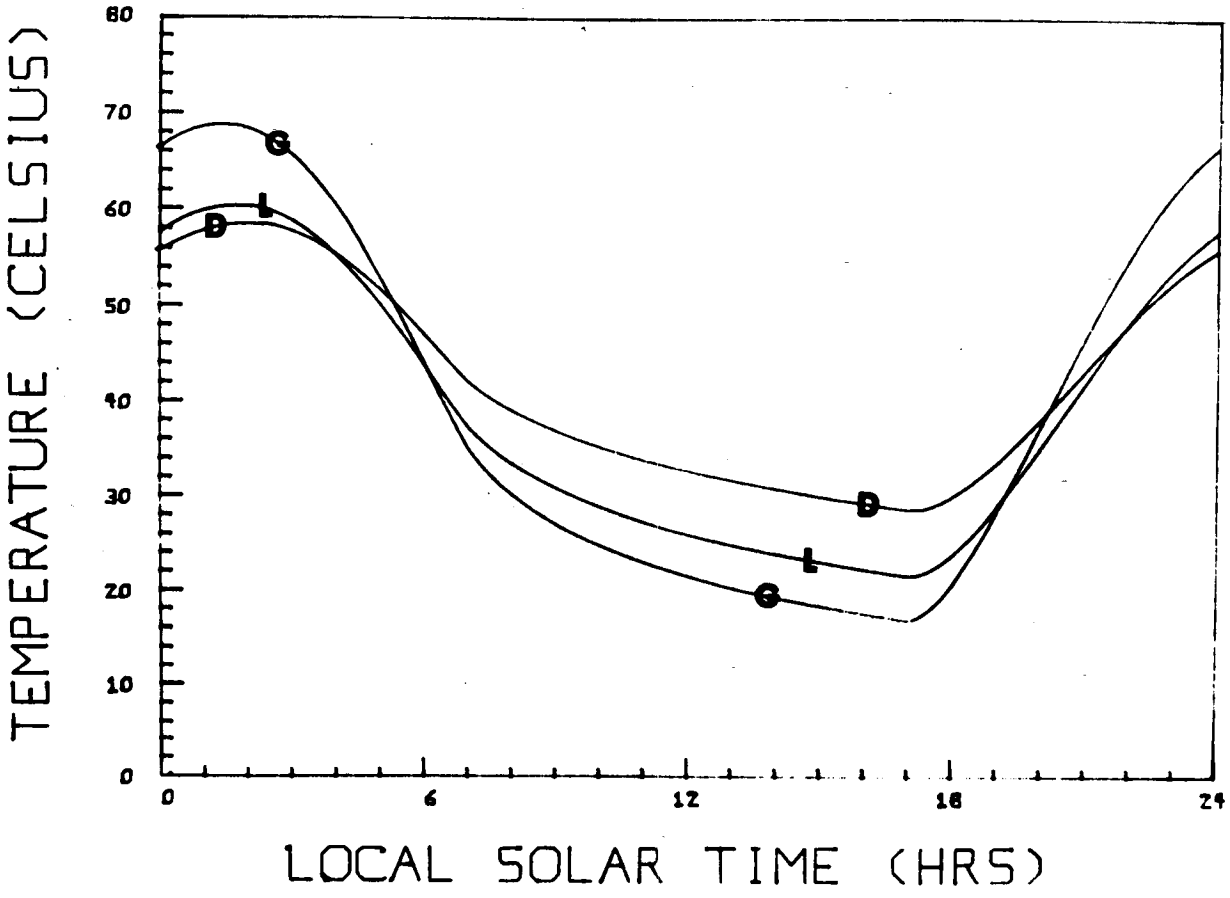

Figure 7.- Predicted diurnal surface temperature variation computed from representative values of the albedo and thermal inertia of the limestone (L), dolomite (D), and granite (G) for the June 1970 overflight. Noon 0 hours, midnight 12 hours.

Figure 8.- Predawn thermal-infrared image of the Mill Creek, Oklahoma, test site obtained in June 1970. L-limestone, D-dolomite, G-granite. The most striking difference in the comparison with the December 1968 image (fig. 5) is the warm granite outcrops. This result is not predicted from the thermal model derived to explain the December data (fig. 7).

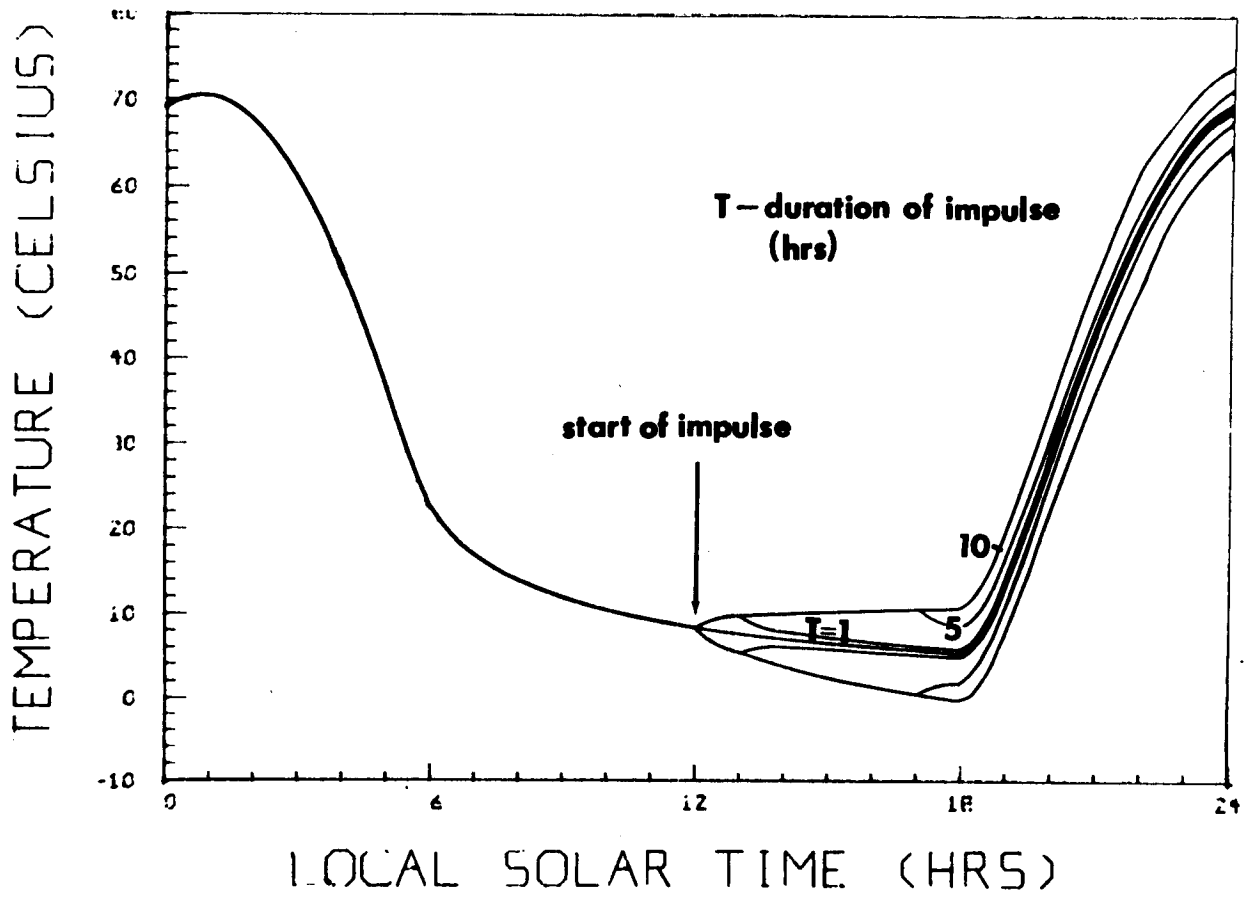

Figure 9.- Diurnal surface temperature variation computed for heating impulses initiated at 12 hours local solar time (local midnight) for time durations (T) of 1, 5, and 10 hours. Noon 0 hours, midnight 12 hours.

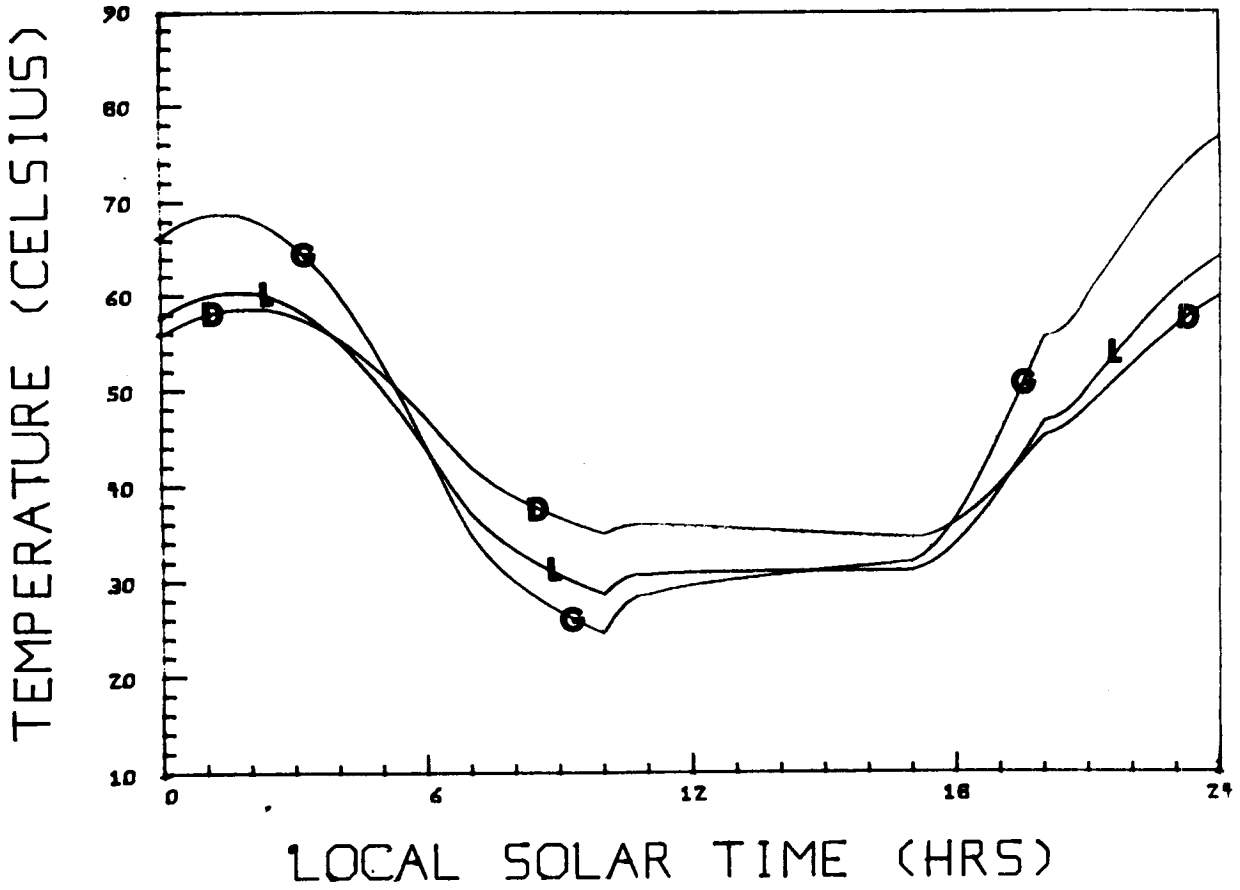

Figure 10.- Diurnal surface temperature variation computed for a heat impulse initiated at 10 hours local solar time for 10 hours' duration on the three materials: limestone (L), dolomite (D), and granite (G). The greatest down heating occurs for the lowest thermal inertia material (granite) and reduces the limestone-dolomite contrast. Both these effects are consistent with the predawn thermal image (fig. 8). Noon 0 hours, midnight 12 hours.

A STUDY OF PASSIVE MICROWAVE TECHNIQUES APPLIED TO GEOLOGIC PROBLEMS

by

A. T. Edgerton
Microwave Division
Aerojet-General Corporation

March 1971

INTRODUCTION

A research program concerning passive microwave techniques applied to geologic problems was conducted by Aerojet-General Corporation. This work, sponsored by the U. S. Geological Survey, was performed to establish the microwave properties of representative rocks and minerals, and to examine the feasibility of using microwave radiometry for various geologic mapping problems. A review of earlier microwave studies pertaining to geology was conducted, coupled with laboratory and field investigations of the microwave emission characteristics of selected geologic features.

The laboratory studies consisted of dielectric constant measurements of representative rocks and minerals. Dielectric measurements were performed with an ellipsometer or precision reflectometer using observational wavelengths of 8 mm and 2.2 cm. Field studies were performed during the fall of 1969 in close cooperation with U. S. Geological Survey and U. S. Bureau of Mines personnel. Field investigations were conducted on numerous sites in the Western United States, utilizing Aerojet's mobile remote sensing field laboratory equipped with four dual-polarized radiometers operating at wavelengths of 0.81, 2.2, 6.0 and 21 cm. The field laboratory, shown in Figure 1, was also equipped with infrared and photographic equipment, along with extensive geophysical and meteorological instrumentation. A majority of the field investigations was concerned with the microwave emission characteristics of representative rock types. A portion of the study was concerned with microwave properties of mineralized areas; experiments were also conducted in the vicinity of a coal seam fire in Colorado and across the San Andreas Fault Zone near the Salton Sea, in Southern California.

LABORATORY RESULTS

Laboratory measurements were made of the dielectric properties of several common rocks and minerals to provide a sound basis for interpreting radiometric observations of similar materials in their natural environment, and to develop a catalog of the microwave properties of rocks and minerals. The real and imaginary parts of the dielectric constants were determined with an ellipsometer or precision reflectometer. Specimens were prepared by cutting a large, flat, smooth surface on each sample.

Figure 2 shows computed values of the real and imaginary parts of the dielectric constant of several minerals and rocks for an observational wavelength of 2.2 cm. The length of the solid line represents the range of values observed for each material. These data show that the dielectric properties of rocks and minerals of similar composition have similar real parts of the dielectric constant. The real part of the dielectric constant ranges from about 2.5 to 9 for the samples examined. The shorter wavelength (8 mm) values were less consistent due to scattering effects associated with mineral fabric and structure within the particular specimens. The density of several of the minerals is also noted on Figure 2. From this it is quite apparent that an increase in the real part of the dielectric constant occurs with increasing density. The trend is more conspicuous at the longer wavelength where scattering from the surface of such specimens as basalt, olivine, and dolomite is less pronounced. The dolomite sample contained minor solution cavities, while the basalt sample was viscular and the olivine was coarse granular. No consistent correlation was noted between the imaginary part of the dielectric constant and sample chemistry or physical characteristics.

FIELD INVESTIGATIONS

REPRESENTATIVE ROCKS

Multiwavelength microwave measurements of outcropping rocks and minerals were taken in localities near Mill Creek, Oklahoma; Goldfield and Tonapah, Nevada; and the Mono Craters and the Anza Borrego areas of California. The radiometric and supporting environmental data were used to compute emissivities of the various rocks and minerals. Correlation was noted between the emissivities and physical characteristics of these materials, including surface roughness (microrelief, particle or fragment size and shape, etc.), moisture content, and specific gravity. No direct association was noted between the chemical composition

of the target materials and the computed emissivities. An examination of both long and short wavelength data permitted an evaluation of the effects of surface roughness. An analysis of these data shows that surface roughness can, in extreme cases, completely mask microwave signatures associated with the bulk properties (e.g., moisture content, density, etc.) of an outcrop. Many examples of this occurrence were noted at the short wavelengths of 8 mm and 2.2 cm. In no case were outcrops encountered in which the long wavelength 21 cm response was completely dominated by surface roughness.

A comparison of calculated emissivities and material density is given on Figure 3 for volcanic rocks outcropping in the Mono Craters area. The data are shown for a wavelength of 21 cm. Densities shown are average values for three samples taken from each scan path. A significant feature of these data is the close correspondence between decreasing emissivity at low antenna viewing angles and increasing rock density. At higher antenna viewing angles, notably 40°, the effects of surface roughness are more pronounced and the relationship is obscured. At the low viewing angles, a change in emissivity of 0.05 corresponds to a density change of 1.0. This amounts to a brightness temperature change of about 15°K.

COAL MINE FIRE

An area near New Castle, Colorado, contains several underground coal seam fires that have been burning for some 50 years. The site is located on the north slope of the Grand Hogback, just south of New Castle, Colorado. The surface trace of the burning coal seam is manifest by an absence of vegetation due to intense heat venting along numerous fractures. Slumps in the overlying sandstone formation, due to consumption of the organic fuel, aid in defining the fire areas. Figure 4 shows a photomosaic of the Grand Hogback and coal seam, along with contour maps of the soil moisture content and soil temperature along the ridge. The burning coal seam is clearly identifiable on both of these contour maps, as evidenced by low moisture content and high surface temperatures. Microwave and infrared images were formed of the ridge and coal seam with 8 mm and 7.5 to 13 micron radiometers, respectively. These instruments were mounted on a motor-driven pan and tilt head enclosed in the back of a van. Both instruments had one-half degree beamwidths and were boresighted. Horizontal line-by-line scans were made of the scene at a 1° per second continuous scan rate $\pm 30^{\circ}$ either side of the center line of the scene. The line scans were initiated 25° above the horizontal plane, 30° to the left of center. After each line scan, the head position was incrementally decreased one-half degree downward. This procedure was followed until 60 steps

had been made, equivalent to approximately 5 degrees below the horizon. Half-degree steps were employed since both radiometers have half-degree resolution. The line-by-line scanning technique permitted computerized reconstruction of the recorded scan data into radiometric images.

Both horizontal and vertical polarization microwave data were obtained from separate measurements by rotating the parabolic dish antenna 90 degrees about the antenna axis. Measurements were performed during both day and night to evaluate diurnal variations in emission at the two wavelengths. These data were processed to remove angular distortion and displayed in pseudo color with Aerojet's color display system. The display technique uses X-Y displacement to describe two dimensions of the scene, and various combinations of color, hue, saturation, and luminescence of the three primary colors to display the radiometric data. The radiometric images are shown in Figure 5. Both day and night images are shown. No attempt was made to provide absolutely calibrated images. Note the excellent delineation of the coal seam outcrop on both day and night infrared imagery. Also note the conspicuous lack of correlation between the outcrop and the microwave data. The near-grazing antenna viewing angles required for the microwave measurements apparently precluded detection of the warm, comparatively dry, fire area. For more modest antenna viewing angles one would expect a microwave brightness temperature contrast of the order of 50 to 80 degrees Kelvin for the moisture content and thermometric temperature distribution observed on the site.

SAN ANDREAS FAULT ZONE

Figure 6 shows a microwave traverse taken across a portion of the San Andreas Fault Zone in an area east of the Salton Sea, near Salton Parkside, California. In this area, rising ground water occurs at intervals along the fault, increasing soil moisture content near the surface.

The microwave traverse was performed along a one-half mile segment of a power-line access road. Thermometric temperature profiles in the alluvium were taken before, during, and after the completion of the traverses, and soil moisture samples were collected at 400-foot intervals along the traverse line. Samples were taken from the surface, and at depth intervals of 0-8 cm, 8-15 cm, and 15-30 cm. The moisture data are compiled on Figure 6. The largest moisture variations occurred in the 16 to 30 cm interval. The point-to-point variability of moisture content values at a particular depth along the traverse must be partly attributed to precipitation which occurred prior to the traverse. The 8 to 15, and 30-cm depth samples are probably most representative of the

equilibrium conditions prevalent at this site. The Cl concentration of soil moisture samples is also indicated on Figure 6. Microwave profile data taken at observational wavelengths of 0.81, 2.2, 6.0 and 21 cm for a view angle of 45° are shown in the lower portion of the figure. Note that the 0.81-cm temperatures are consistently warmer and less polarized than the corresponding longer wavelength temperatures, and that there is little correlation between moisture content and microwave emission at 0.81 cm. Correlation is much better at longer wavelengths, where brightness temperatures decrease with increasing soil moisture conditions. In general, larger brightness temperature anomalies were observed as the observational wavelength increased. This is evident between data frames 130 and 150 where the horizontally polarized brightness temperature changes at wavelengths of 2.2, 6.0 and 21 cm are 36°K, 42°K and 64°K, respectively. The limited correlation with moisture observed at 0.81 cm is largely due to scattering associated with surface roughness. This effect was not evident in the 2.2 cm data. These data provide clear and unambiguous definition of the moisture distribution in the area of the fault trace.

RECOMMENDATIONS

In summary, several potential geologic applications of microwave radiometry were investigated and the microwave emission characteristics of representative rocks and minerals were compiled. On the basis of this work, the following recommendations for additional research are offered:

(1) Detailed investigations of the relationship between density and the dielectric constant/emissivity of geologic materials, including additional analysis of brightness temperature data derived from the reported investigations, additional long wavelength (6 and 21 cm) dielectric constant measurements of samples obtained during the reported effort, and additional field investigations. Data obtained from these activities should be compared with theoretical emissivity values derived from contemporary numerical models.

(2) Detailed microwave radiometric mapping of selected areas of geological significance to evaluate the use of microwave radiometry for mapping soil moisture distribution, and for inferring subsurface features on the basis of soil moisture distribution. This work should be performed in an area containing faulting, geothermal activity, caverns, or other subsurface features.

(3) An experimental evaluation of the effects of layering should be performed with long wavelength sensors, to evaluate the effect of

thin soil/overburden deposits on outcrop signatures. The available data do not permit an evaluation of possible interference phenomena due to layering.

(4) The applicability of microwave radiometry should be examined in other facets of geology such as marine geology, engineering geology, volcanology, etc.

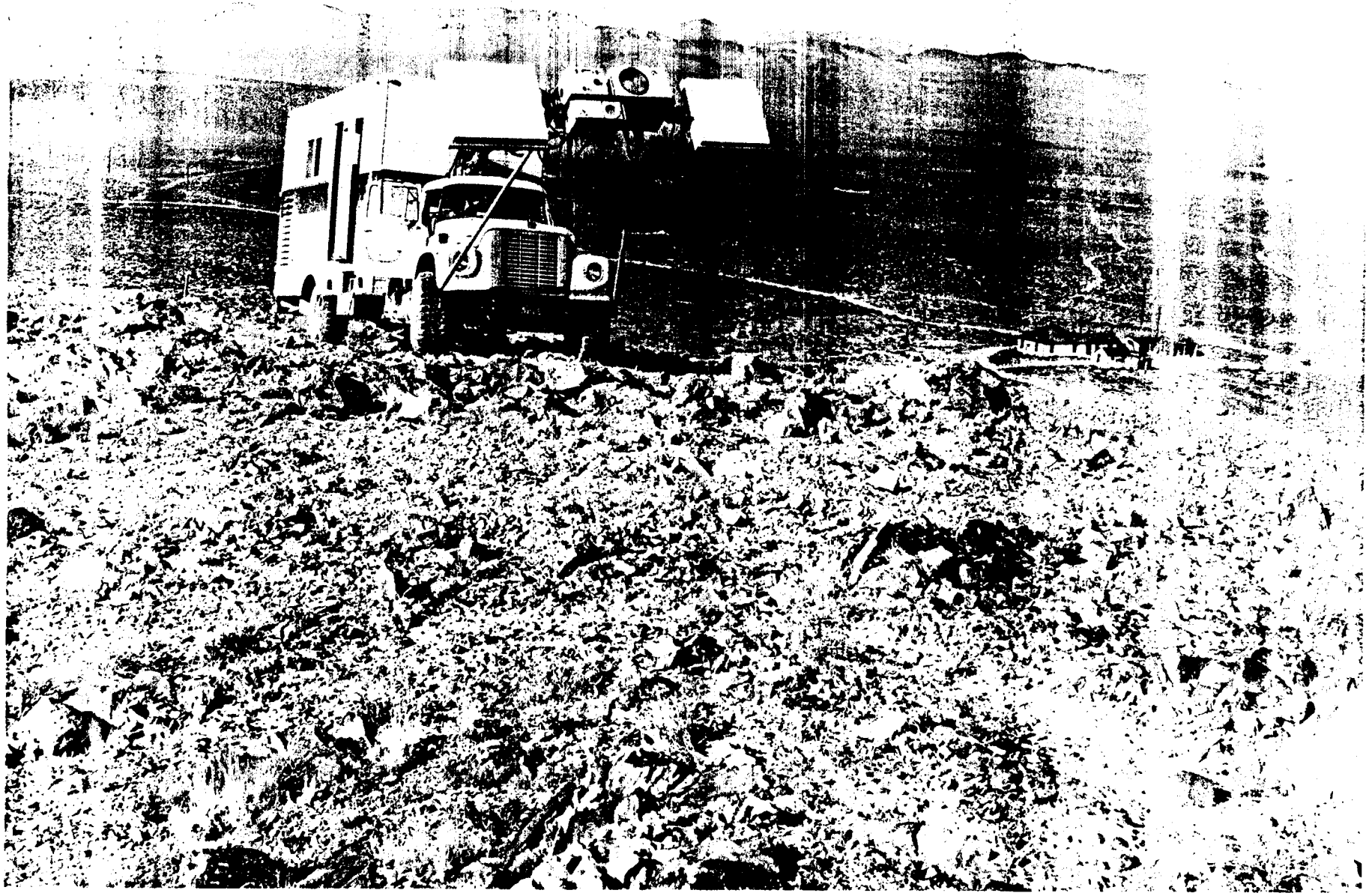

Figure 1. Mobile Field Laboratory

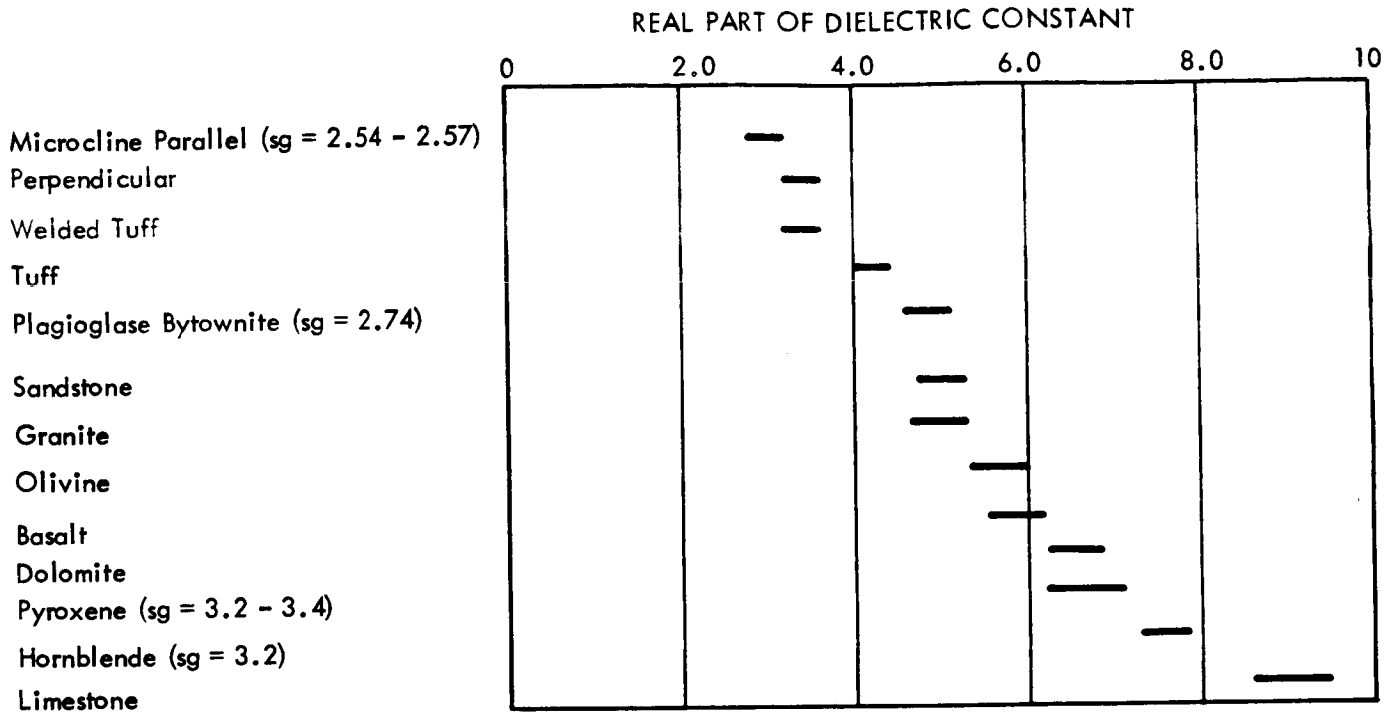

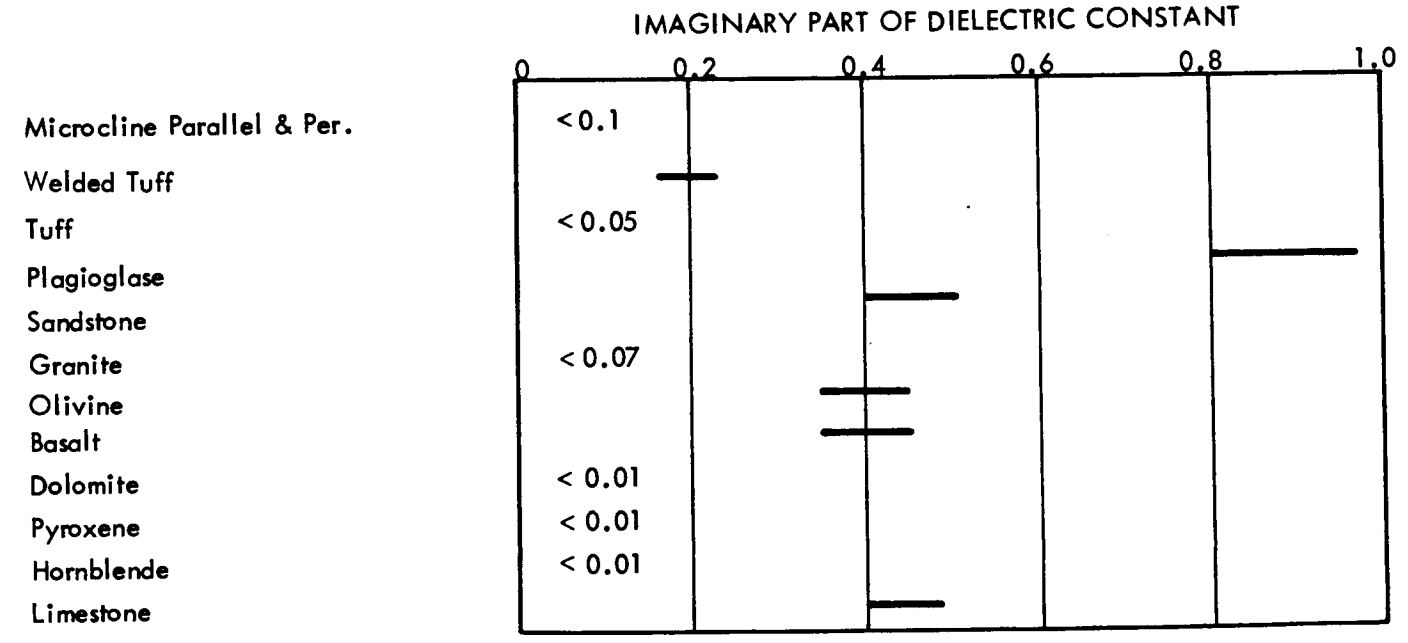

Figure 2. Dielectric Constant of Selected Rocks and Minerals at 13.4 GHz (λ = 2.2 cm)

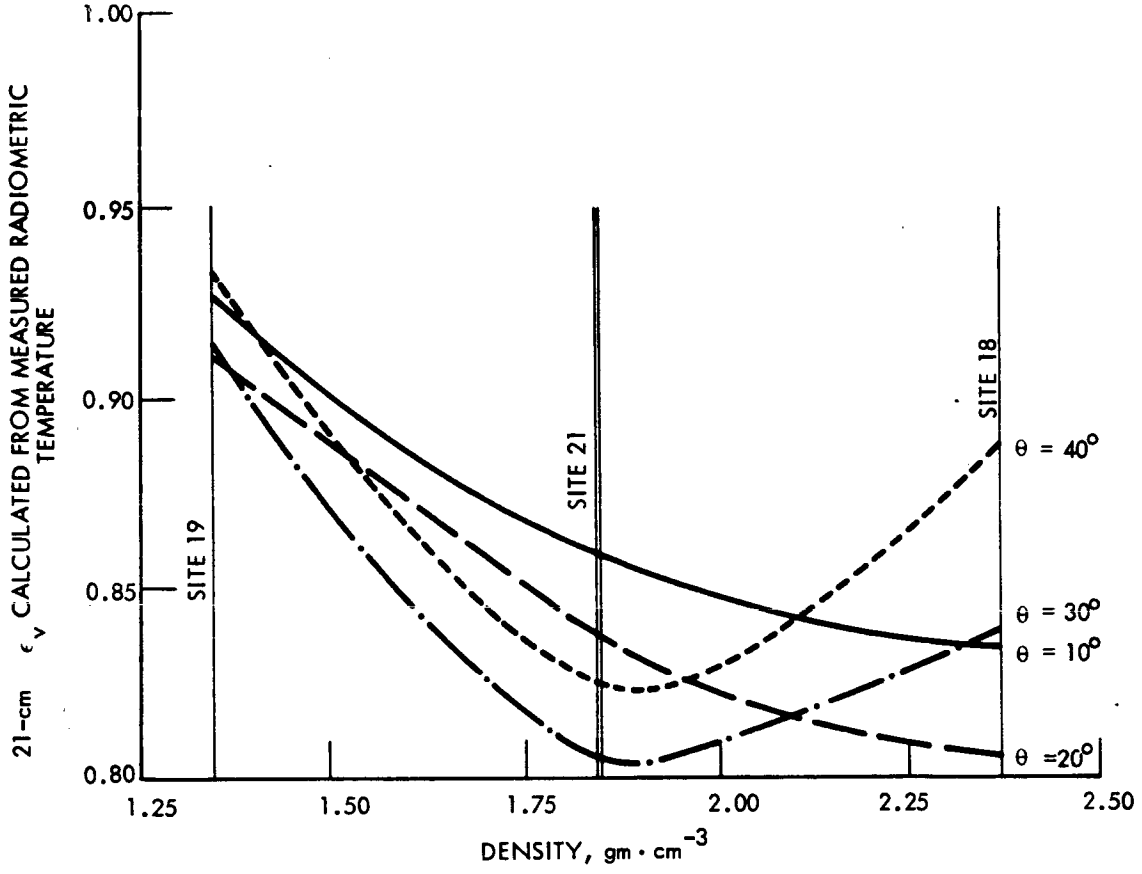

Figure 3. 21 cm ϵ_v as a Function of Density for Acidic Volcano Rocks of the Mono Craters Area, California

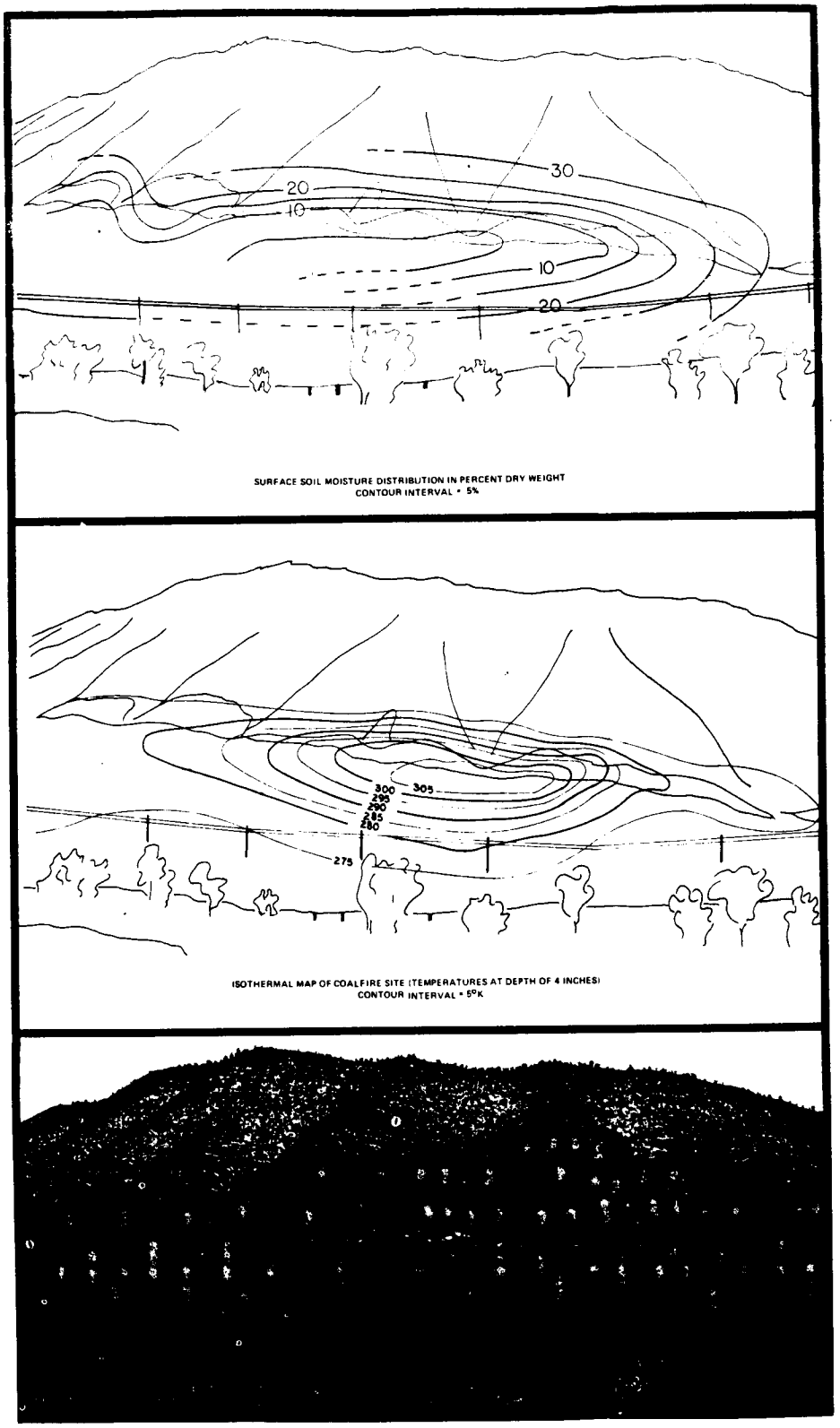

Figure 4. Soil Moisture Distribution and Isothermal Maps of Coal Fire Site, New Castle, Colorado. Map and Photo Scales are Identical.

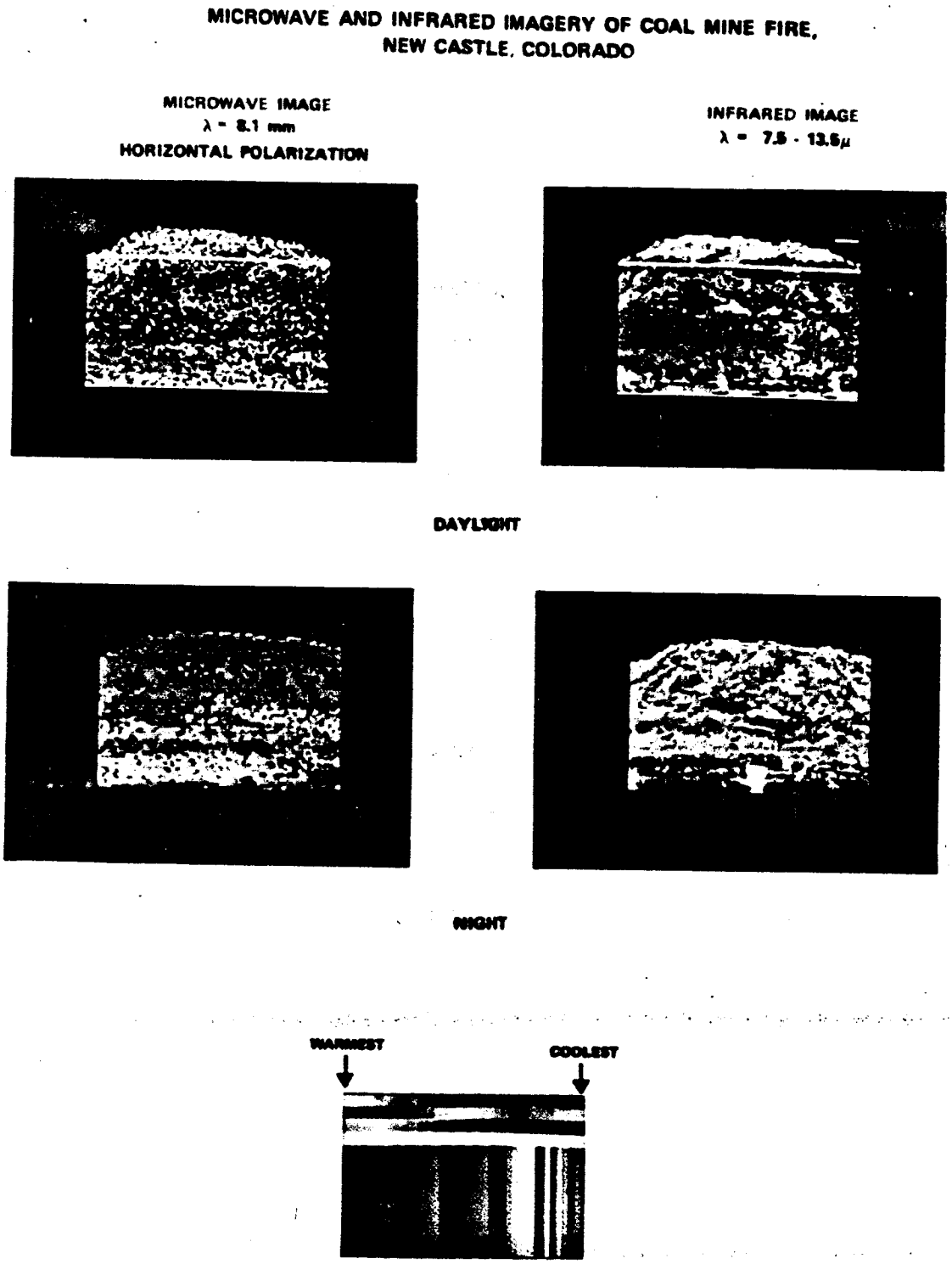

Figure 5. Microwave and Infrared Imagery of Coal Mine Fire, New Castle, Colorado

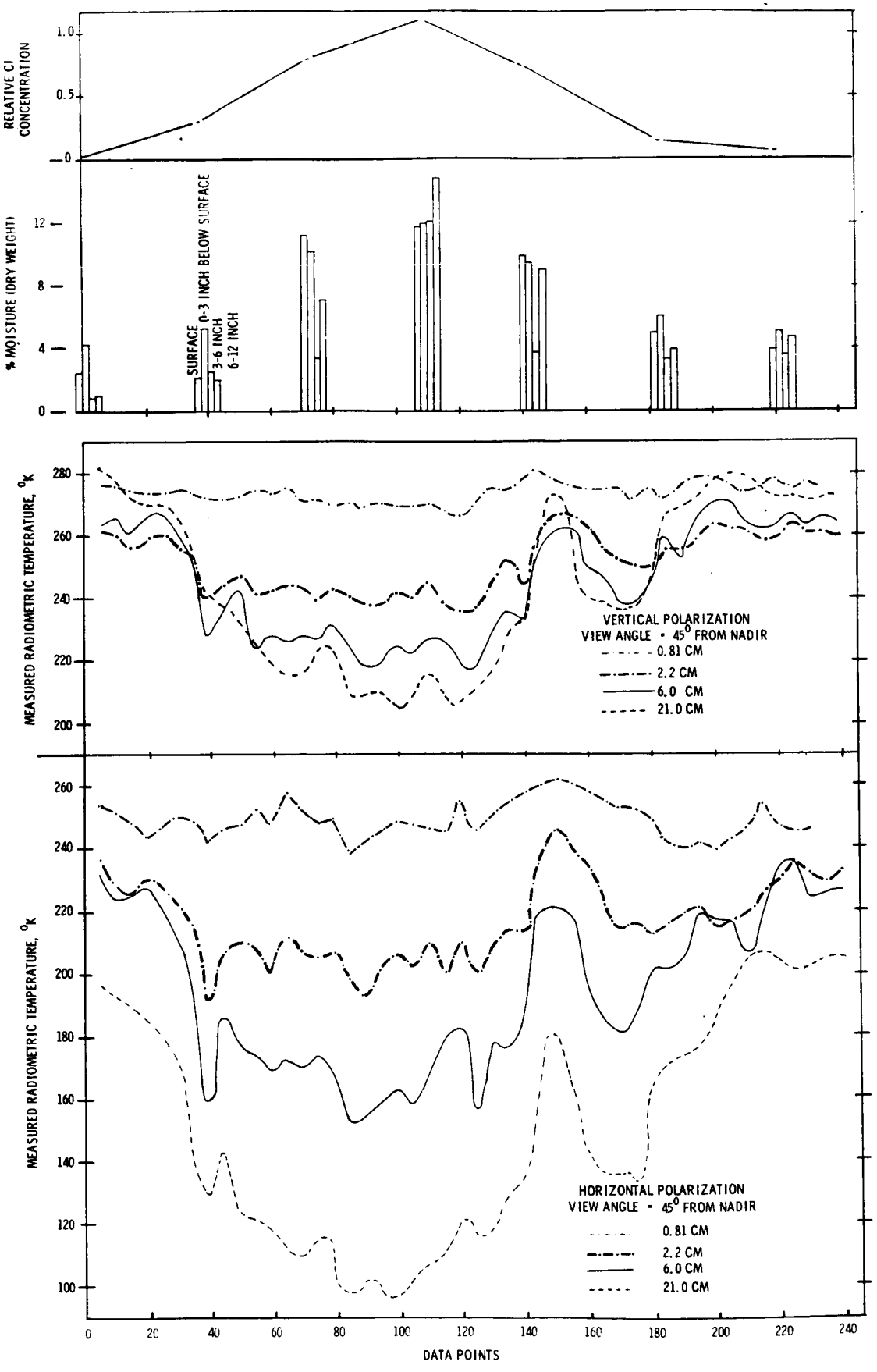

Figure 6. Radiometric Traverse Across Trace of the San Andreas Fault Zone, Salton Sea Area, California

SECTION 15

GEOLOGIC INTERPRETATION OF APOLLO 6 STEREOPHOTOGRAPHY FROM BAJA CALIFORNIA TO WEST TEXAS*

by

STEPHEN J. GAWARECKI
U.S. GEOLOGICAL SURVEY
WASHINGTON, D.C. 20242

INTRODUCTION

Excellent space photography of parts of the southwestern United States and northwestern Mexico (fig. 1) was obtained during the unmanned Apollo 6 spaceflight of April 4, 1968. Two unique features of this photography made it useful for geologic interpretation: 1) its vertical stereocoverage, and 2) its exposure under a relatively low angle of solar illumination through an unusually cloud-free and clear atmosphere. The low angle of illumination made it particularly useful in delineating structural features that affected topographic relief.

The primary objectives of this study were to annotate the structural patterns topographically enhanced by the longer shadows, to analyze their trends with respect to the continental tectonic framework, and to attempt to correlate the pattern with known copper or other base-metal deposits. No attempt was made to systematically define lithologic boundaries because of the small scale of the compilation and the added burden imposed by the limited spectral content of the illumination.

The area studied was a 100- to 105-mile-wide swath of terrain covered by photograph numbers AS6-2-1433 through 1449, a total land area of approximately 60,000 square statute miles. The coverage began from a point centered on Punta Colnett on the Pacific coast of Baja California and extended to the Sacramento Mountains of New Mexico and west Texas (fig. 2).

PHOTOGRAPHIC INSTRUMENTATION AND CONDITIONS

The Apollo 6 photographs were taken with a Mauer 220-G 70 mm camera having a 76-mm focal length f/2.8 Ektar lens. The acquisition format was 5.7 by 5.7 cm, covering a field of view of approximately 41°

*Publication authorized by the Director, U.S. Geological Survey.

edge to edge and 56° diagonally. The film type used was Ektachrome (S.O.121) which produced a positive color transparency. A Wratten 2E filter was used to reduce atmospheric haze by absorbing short wavelength energy below 415 nm. The spacecraft window and its coatings likewise acted as filters, attenuating the visible spectrum (400 to 700 nm) transmission by about 20 percent and the infrared spectrum by more than 90 percent (Kaltenbach, 1969).

The three-layer viewing window in the Apollo capsule probably acted to some degree as a polarizing filter. Because the port was tilted about 32° with respect to the film plane, away from the direction of flight, the polarization probably varied from slight in the direction of flight (east) to strong at the trailing parts of the frames (Space Electronics Systems Div. Staff, 1969). The word "probably" is used because the window layers were effectively anti-reflection coated which would have reduced the degree of polarization. No data on the actual polarization and total filtration involved in the lens system has been reported. Cursory examination of the frames revealed no obvious effects of polarization, but the low solar altitude provided warmer and longer wavelength illumination which is not polarized as much as the shorter wavelength end of the spectrum.

The film exposure, which was set prior to the unmanned flight, was 1/500th of a second at f/5.6. The exposure interval was 8.64 seconds which, in the area of study, produced 61 to 63.5 percent overlap--about optimum for stereoviewing.

The altitude of the spacecraft over Baja California was 224 km and decreased eastward to 212 km over west Texas. Acquisition scale on the 70-mm film was 1:2,946,000 and 1:2,794,000, respectively, for these altitudes. Considering these small scales, it is remarkable that two-lane paved roads as narrow as 11 m were resolvable (Lowman, 1969) on the Apollo 6 photographs.

The low sun angles, or solar altitudes, of 20° on the Pacific coast to 30° in western Texas prevailing during the morning mission passover had two major effects on the photographic results. The first effect was the previously mentioned enhancement of topographic relief by the long shadows. The second effect was the natural filtration of the shorter (blue end) wavelengths of the visible spectrum because of Rayleigh scattering along the greater atmospheric path. The terrain was thus illuminated by the remaining warmer colors in the sunlight, causing a degradation of color contrast. This was especially noticeable in the west where the lowest solar altitude prevailed.

Comparison of Apollo 6 photographs with Gemini and other Apollo mission photographs of the same areas taken during higher solar altitudes shows generally better color rendition in the latter group. Because color contrast generally improves and shadow enhancement of topography decreases with higher solar altitudes, there is enough usable color contrast in the Apollo 6 photographs in the eastern two-thirds of the area to distinguish granitic rocks, some relatively recent mafic volcanic rocks, and some sedimentary rocks. Compensation for the generally decreased color contrast comes from the enhancement of rock textures and characteristic fracture patterns which are also elements of recognition. These factors, together with rock associations and severity of deformation, help to identify metamorphic rocks or relicts thereof in granitic terrain.

The time of day is an important factor in considering the effects of solar altitude on photography. The morning solar altitude is generally better for photography than the same altitude in the afternoon because the latter part of the day normally has a more turbulent atmosphere with accompanying dust and thermal distortion. Cloud buildup due to thermal instability is another frequent problem during the later part of the day. The use of afternoon photography is, nevertheless, not discouraged, because the emphasis of different topographic or drainage alignments by shadows would vary noticeably with different solar azimuths.

Hackman (1967) has noted that the optimum sun angle (solar altitude) for shadow enhancement of terrain is between 20° and 30°. The author found that 30° is optimum for both geologic structure enhancement and for color contrast in this arid terrain. The actual solar altitude optimum for a particular terrain would be a function of the relief of that terrain, the solar altitude being inversely proportional to the relief, up to an ill-defined point where the average terrain slope angle becomes less than the sun angle.

Another important factor in the determination of optimum solar altitude is the atmospheric luminance. Initial studies by Harvey and Myskowski (1965, fig. 1-14) indicated that atmospheric luminance for clear weather conditions should be at a peak between 20° and 30° solar altitude, causing a poor target-to-background contrast ratio. Harvey and Myskowski have restudied the luminance versus solar altitude relationship (D. I. Harvey, oral communication, 1970) and have provided new data which indicate that a broad maximum for atmospheric luminance is centered at 90° (fig. 3).

Other factors are to be considered before a definite generalization can be made regarding optimum solar altitude for space photography. They include such variables as air mass quality, film type and its

intrinsic filtration, extrinsic filtration, exposure, polarization, lens field of view, and terrain color and altitude. The terrain altitude variable may be considered as air mass quantity. Analysis of thes. factors is a study in itself and will not be considered here.

GEOLOGIC INTERPRETATION

The photography was interpreted stereoscopically on 9-inch by 9-inch color prints whose scale was close to 1:718,000. The annotations were transferred to a 1:500,000-scale black and white photomap (fig. 2) prepared by the Geological Survey (U.S. Geol. Survey, 1970) from rectified Apollo 6 photographs of the area. The additional synoptic view afforded by this compilation contributed greatly to the recognition of persistent fracture trends.

From west to east, the physiographic provinces covered by the photography are: the Peninsular Ranges section of the Pacific Border province in Baja California; and the Salton Trough, Sonoran Desert, Mexican Highland, and Sacramento sections of Basin and Range province (Thornbury, 1965; Fenneman, 1931). The approximate boundaries of these physical divisions are shown on figure 1.

The westernmost area is Baja California, separated from the Mexican mainland by the Gulf of California and the Colorado River delta which lie within the Salton Trough. The Sierra Juarez on the north and the Sierra San Pedro Martir on the south form the backbone of the peninsula. Both ranges are essentially westward-tilted fault blocks aligned in tandem to the north-northwest and separated by the major west-northwest-striking Agua Blanca fault (fig. 2). The highest point of this backbone is the summit of Cerro de La Encantada, 3,095 m (10,154 ft), which is close to the steep eastern scarp of the Sierra San Pedro Martir. The two peninsular ranges are part of a granitic batholithic chain of probable mid-Cretaceous age (Wisser, 1954) that contains infolded metasedimentary and metavolcanic rocks and gneisses of questionable origin (Allen and others, 1960; Woodford and Harriss, 1938).

The peninsular ranges afford the highest degree of outcrop per unit area along the Apollo 6 photographic swath. The control of drainage by structure is evident, and many stocks and other centers of intrusion can be distinguished (fig. 2) by the concentric nature of the fracture patterns, relict bedding, and, in many cases, the granitic cores of the unroofed intrusions. Dark metamorphic rocks surround these plutonic cells, and in many places west of the two main ranges these rocks form a steeply dipping discontinuous belt trending north-northwest (M in fig. 2).

The Sierra San Pedro Martir has been raised about 3,000 m (10,000 ft) above the Valle de San Felipe and Valle Chico on the east, and a scalloped eastern range front fault configuration has been produced. The westward convexity of the scallops follows the pattern noted in the Basin and Range province by J. G. Moore (1960) in that it is convex in the direction of the tilted range. Moore (1960, p. B411) stated that "the fault itself is believed to be convex toward the direction of the range, or concave toward the downthrown side of the fault." The major fault bounding the Sierra San Pedro on the east is thus believed to be a normal fault. The main fault probably is closer to the drainage center of the alluvial valley to the east, and the scallops are probably only near-surface gravitational adjustments on the upthrown margin of the main fault. The range salient just east of the summit has concentric drainage concave to the east, also suggesting local large-scale readjustment to gravity. A possible thrust fault may have formed at the toe of this rotated salient block, a feature not uncommon in large landslides.

A strong topographic break forming a rough arc about 21 km west of the summit area is interpreted as a normal fault down to the west (hachured line in fig. 2). It corresponds closely to a large normal fault mapped in reconnaissance near Descanso by Woodford and Harriss (1938) and appears to be the western boundary of the Sierra San Pedro Martir fault block, interrupting the relatively gradual western slope of the range and creating a horst. The southern end of this fault is parallel to the predominantly north-northwesterly lineament direction, which in this area may represent steep metamorphic bedding as well as fracture traces.

The most conspicuous lineament is the Agua Blanca fault that cuts west-northwestward across the peninsula north of the Sierra San Pedro. Allen and others (1960, p. 478) stated that on the basis of across-the-fault matching of plutonic discontinuities, as much as "7 miles of post-Cretaceous right-lateral displacement is very strongly suggested" and that "the possibility of 14 miles...is indicated." Range front offset between the Sierra Juarez and the Sierra San Pedro at the eastern end of the fault is roughly 5 miles.

Except for the extremities of the Agua Blanca fault, the author generally agrees with the fracture pattern shown by Allen and others (1960, figs. 3-8). The splay pattern of the western extremity is slightly different, and the fault is carried through the Paso San Matias into the Valle de San Felipe where it is buried in alluvium. Rusnak and others (1964, pl. 3) and Moore and Buffington (1968, fig. 4) considered extending the Agua Blanca fault across the Valle de San Felipe into the Gulf of California. However, examination of the low basin ranges between the Valle de San Felipe and the gulf on the

photographs shows strong south-southwesterly fracture trends intercepting any east-southeastward extension of the fault. Some short northwest-trending fractures are present, but their orientation and distribution do not support extension, and their relationship to other faults is subordinate. It appears then that the Agua Blanca fault as an entity terminates in the Valle de San Felipe. This in turn suggests that the valley and ranges to the east are in a graben system that parallels the north end of the Gulf of California. This evidence casts some doubt on Moore and Buffington's (1968, p. 1241) contention that the Agua Blanca fault extends into the Gulf of California.

At least two large faults or fracture zones are intercepted by the Agua Blanca fault. One, approximately 15 km long, strikes north-northeast along the Arroyo de Rincon from about the midpoint of the Agua Blanca fault and disappears under the Late Cretaceous and younger marine sedimentary rocks of Punta Colnett on the Pacific coast. The coast north of Punta Colnett may possibly be controlled by this lineament.

North of the Agua Blanca fault, many of the faults have a northwesterly trend, parallel to that of the San Andreas system to the northeast and east in the Salton trough. The Sierra de Juarez is broken up by northwest-, north-northwest-, and north-hortheast-trending faults. The north-northeasterly to easterly trend is represented by generally short fault segments throughout the Baja California area of study.

A roughly triangular anomalous depression whose northwestern apex is at San Vicente (fig. 2) is noticeable between the Agua Blanca fault and the Pacific Coast. This area, which is about 15 km on a side, contains scattered low hills surrounded by reddish flats suggestive of hematite staining. This area is immediately east of the Cerro Colorado iron deposits (Wisser, 1954).

East of the Sierra San Pedro Martir and Sierra Juarez the low basin and range country appears more like the Sonoran desert section of the Basin and Range province than the Peninsular Range to the west or the Salton trough to the northeast. The low ranges opposite the Sierra San Pedro summit area include four small fault blocks tilted toward the northwest and bounded by northeast-trending faults. The inconsistent trends of the ranges contrast with the northwestward trends of the ranges in the Sonoran Desert province across the gulf and adds to the complexity of the structural situation in the Gulf of California.

A coastal feature of interest on the Pacific side is the development of terraces on or in the Upper Cretaceous sedimentary beds. In the Colorado Delta the abnormally straight western boundary at the

playa Salinas de Omotepec (Las Salinas) suggests faulting. Alternatively, the scarplike boundary may only be the result of wave cutting, because the western part of the delta, including the playa area, is occasionally flooded by maximum spring tides (Thompson, 1968).

In the Colorado Delta part of the Salton Trough, there appear to be a few tonal and drainage alignments that may represent recent movements on the San Andreas fault system which passes northwestward through the delta. Along the northeastern side of the delta, the path of the San Jacinto section of the San Andreas fault is easily determined. The San Jacinto fault passes southeastward into older emergent deltaic sedimentary bluffs where alignments suggest development of possible extension fractures with a more northerly component of strike than the main fault. West of the Colorado River, a few alignments are annotated in the San Andreas direction, but the transient nature of the delta surface in this area makes further interpretation tenuous.

The Sonoran Desert section of the Basin and Range province is east of the delta and the Gulf of California. Its eastern boundary, gradational with the Mexican Highland section, is placed by Fenneman (1931) at about the longitude of Tucson. Only about one-fifth of the area is exposed bedrock, which is found mostly in low northwest-trending ranges.

The most conspicuous feature is the Pinacates volcanic field, which is in Sonora between the Mexican border and the Bahia (Bay) de Adair on the Gulf of California. This field of olivine basalt (Jahns, 1959), which covers more than 1,554 sq. km (600 sq. mi.), is observed from space photographs to have at least 250 cinder cones and craters, including 9 of the 10 large craters or maars reported by Galbraith (1959). The highest part of the field is Cerro Pinacate, 1,206 m (3,957 ft) above sea level, which is found in the middle of the southern third of the field. It is part of a strong fissure and cone ridge that strikes close to N. 20° W., forming an incipient shield volcano. The western margin of the field is buried in windblown sand. However, the eastern half contains a few unmantled and relatively fresh-looking basalt flows. According to Jahns (1959, p. 165) "some of the volcanic section may date from late Tertiary time, but most is Quaternary in age." Maximum activity was believed to have occurred during Pleistocene time. An explosive eruption as recently as January 1935 was reported to Ives (1935), but the evidence is hearsay and vague, and there have been no reports of later geothermal activity.

The cinder cones and craters mapped on the space photographs are amenable to alignment analyses in the manner shown by Coulson (1954) in the volcanic field in the Daylesford district, Victoria, Australia. The alignments at the Pinacates (fig. 4) are believed to be structural

trends active during the Quaternary. The strongest alignment set is in the previously mentioned N. 20° W. direction. Other sets average N. 57° W., N. 65° E., N. 17° E., and possibly due north. The N. 57° W. direction contains three of the major craters on one alignment. The N. 65° E. set, which is nearly orthogonal to the N. 20° W. direction, is found in many of the surrounding ranges. The N. 17° E. set is weakly developed, but appears to be present. The due north set is questionable.

The fracture pattern of the area west of the Arizona-New Mexico State line is dominated by a north-northwest trend which controls the orientation of the ranges (see fig. 2). This trend is nearly parallel to the San Andreas fault system but lacks the continuity and strong persistence in strike direction found in the great fault. Subordinate east-northeast to northeast fractures cut or intercept the north-northwest fractures. As the southeast corner of Arizona is approached from the west the ranges become larger in area, more varied in shape and orientation, higher in elevation, both above sea level and above the adjoining basins, and more complex in their fracture patterns. At the Arizona-New Mexico line the dominant fracture trace trends slightly east of north and gives a northerly strike to the long ranges in this region. This trend becomes stronger toward the east in the remaining area of study. The north-northwest, northwest, and east-northeast trends are present but more localized.

Three Quaternary basaltic lava fields in the eastern half of the area of study are aligned to the north-northeast. They are the San Bernardino Valley field in the southeast corner of Arizona, the Las Palomas field in northern Chihuahua, and the West Potrillo Mountains field in southern New Mexico, west of El Paso. (See fig. 2.) Alignment analysis of their craters and cinder cones (figs. 5 and 6) shows that the north-northeasterly trend becomes stronger toward the east and that the north-northwest trend is still recognizable. Immediately north of the West Potrillo field the strong alignment of craters (N. 15° E.) is represented by strong normal faulting of the same trend. Further extension of the alignment northward carries it into the Rio Grande depression, which, according to Kelley (1952, p. 93), is "a series of north-trending grabens arranged in echelon north-northeasterly along the course of the Rio Grande." Kelley (1952, p. 101) further states that this tectonic feature "probably began in late Miocene time and culminated...toward the end of Pliocene time." Woollard (1958, fig. 5) shows a concentration of earthquake epicenters along this depression which indicates that tectonic activity is continuing. Hamilton and Myers (1967) have recognized the Rio Grande rift-valley system that includes the area of the Las Palomas and West Potrillo lava field.

The West Potrillo lava field is cut at its northern end by a N. 59° W. line of craters (fig. 6) whose alignment, when extended to the east-southeast, is nearly on strike with the so-called Texas lineament in west Texas. This lineament, in Hudspeth County east of El Paso, is described by Moody and Hill (1956) as a large scale left-lateral wrench fault that strikes about N. 70° W. A favorably located fracture alignment in the Franklin Mountains north of El Paso which has the same strike as the Texas lineament and the crater alignment may be a link between the two features. West of the lava field, any possible extension of this alignment is hidden under a deep alluvial cover almost to the Arizona State line. Where the projection intercepts a range there is nothing to indicate the presence of the Texas lineament. There are many scattered trends parallel or subparallel to the Texas lineament in the southwest corner of New Mexico, but as an entity the lineament is not in evidence. Sumner (1970) considers the feature as a zone approximately 240 km wide whose northern edge is near the Santa Rita, New Mexico, copper district and whose southern boundary includes the Cananea, Chihuahua, copper deposits. A substantial part of this zone as defined by Sumner (1970) is within the area of study, but fracture trend directions relatable to the Texas lineament "zone" are difficult to trace across northerly-trending ranges near the Arizona-New Mexico line.

The character of the terrain gradually changes across the Rio Grande River basin. The intensely fractured and dissected block mountains give way to mature block mountains of gently tilted strata and cuestaform topography. This part of the Basin and Range province, called the Sacramento section, extends for a short distance beyond the eastern edge of the area of study. The Sacramento Mountains, for which this section was named, trend north-northwest. Accompanying fracture alignments trend in the same direction. The broad uplift, which slopes gradually eastward, has its steep western face bounded with scalloplike scarps convex to the east. This convexity in the direction of the range tilt is consistent with the pattern noted by J. G. Moore (1960) in the Basin and Range province as mentioned earlier in regard to Baja California. Two of the arcuate scarps form the bed of the Sacramento River which drains southeast at the southern end of the range. These arcuate scarps, like those found on the east flank of the Sierra San Pedro Martir in Baja California, are believed to be huge landslips resulting from gravitational readjustments along the main fault just to the west.

On the southeast flank of the Sacramento uplift, the north-northeast fracture trend is strong and includes two structures that are interpreted as grabens. Closely associated with these structures are some east-northeast-trending fracture traces which may be structurally related.

About 20 miles further south is a nearly circular uplift approximately 4 miles in diameter, which, according to the geologic map of New Mexico (Dane and Bachman, 1965), is a raised inlier of the Permian Yeso Formation surrounded by the younger San Andreas Limestone. The presence of the nearby exposed Tertiary volcanic necks or intrusive centers of the Cornudas Mountains strongly suggests that the circular uplift is due to an unexposed, possibly laccolithic, igneous intrusion. If an intrusion is present, it is probably younger than those of the Cornudas Mountains because it is less dissected.

Folding of bedded volcanic rocks and of sedimentary strata is only obvious in the vicinity of the Rio Grande. North of the West Potrillo basaltic lava field, a broad syncline is noticeable in Tertiary volcanic beds. East of the syncline, the Sierra de las Uvas forms a topographically low, highly fractured complementary dome.

North of the Sierra de las Uvas, just across the Rio Grande, a small north-northwest-trending anticline has formed in sedimentary strata. The beds of its eastern flank dip eastward into the basin of the Jornada del Muerto, are buried under alluvium, and are intruded by mafic volcanic rocks before rising to the surface as cuestas on the west flank of the San Andres Mountains. The basin appears to be broadly synclinal, but scattered volcanic remnants along the trough suggest that some graben development may be hidden by the alluvium.

The most important and most widespread mineral deposits found in the area of study are those related to copper. Figure 7 shows the distribution of copper deposits in the southwest, as determined by Burnham (1959), and the major fracture trends within the area of interpretation. An immediate relationship is suggested between many of the fracture trends and the margin trends of the defined copper belt. The two main arms of the belt, north-northwest and north-northeast, are well represented by parallel fracture systems in their respective domains.

It has been presumed that the intersections of major fracture trends were potential loci for ore mineralization (e.g. Billingsley and Locke, 1941; Mayo, 1958; Kutina, 1969). Logically, the intersections could provide the easiest channels of relief for rising magmas containing ore-bearing solutions or other differentiates. Figure 7 shows a few examples of such possible tectonic control of ore deposition. The Tyrone and Santa Rita copper pits in southwestern New Mexico are along a common northeast-trending fracture zone and are at the intersection of this zone with separate north-northwest fracture alignments. The Pima-Twin Buttes copper mining district south of Tucson is near the intersection of strong east-northeast and north-northeast fracture

trends as extended from nearby ranges. The north-northwest trend is very strong in the Bisbee, Arizona, copper district where it intersects with a strong northwest trend.

A comparison of the fracture pattern and copper belt (fig. 7) with contour maps of depths to the Moho and Conrad discontinuities (figs. 8 and 9 respectively) published by Lyons (1970) suggests some significant relationships. In the case of the Moho discontinuity (fig. 8), the two main north-northwest and north-northeast fracture trends and the mineral belt (fig. 7) are nearly parallel to the depth contours. The shallower Conrad discontinuity depth contours (fig. 9) define a broad ridge or platform whose shape conforms quite closely to the mineral belt and the enclosed main fracture alignments.

CONCLUSIONS

The Apollo 6 space photography was found to be especially useful for geologic interpretation because of its vertical stereocoverage and its exposure under a relatively low angle of solar illumination through an unusually cloud-free and clear atmosphere. A low sun angle of about 30° was found to be optimum for shadow enhancement of geologic structures and for color contrasts.

The fracture patterns annotated on the photography showed the regional trends and their distribution. Between Baja California and the Arizona-New Mexico State line the dominant fracture system trends north-northwest, and a subordinate trend strikes on the average east-northeast. From the State line to the eastern margin of the area of study, the north-northeast trend has developed at the expense of the north-northwest trend which becomes subordinate and more localized. This north-northeast trend is also noticeable in vent alignments of the four Quaternary basaltic lava fields that are found between the Gulf of California and central New Mexico. It is strongest in the easternmost West Potrillo field where the extension of vent alignments northward shows their relationship to the Rio Grande depressions, a series of north-trending grabens. At the north end of the West Potrillo field, a N. 59° W. alignment of craters may be related to the Texas lineament. Where westward projection of this alignment through alluvium intercepts a range at the Arizona State line there is no evidence for the lineament. Many scattered trends are parallel or subparallel to the Texas lineament in southwestern New Mexico, but they cannot be carried west of the Arizona line, and the existence of this lineament as a major continental tectonic feature is in doubt.

Support for the idea that intersections of major fracture trends are potential loci for ore mineralization comes from the recognition of such intersections at the Pima-Twin Buttes and Bisbee, Arizona, and the Tyrone and Santa Rita, New Mexico, copper-mining districts. A good correlation exists between the north-northwest and north-northeast fracture patterns and the copper belt as defined in the area of study. In turn, this belt and its fracture zones appear to be related to shallow crustal structures, as shown on recently published depth contour maps of the Moho and Conrad discontinuities.

REFERENCES

Allen, C.R., Silver, L.T., and Stehli, F.G., 1960, Agua Blanca fault--A major transverse structure of northern Baja California, Mexico: Geol. Soc. America Bull., v. 71, no. 4, p. 457-482.

Billingsley, Paul, and Locke, Augustus, 1941, Structure of ore districts in the continental framework: Am. Inst. Mining Metall. Engineers Trans., v. 144, p. 9-64.

Burnham, C.W., 1959, Metallogenic provinces of the southwestern United States and northern Mexico: New Mexico Bur. Mines and Mineral Resources Bull. 65, 76 p.

Coulson, Alan, 1954, The volcanic rocks of the Daylesford district: Royal Soc. Victoria Proc., v. 65, pt. 2, p. 113-124.

Dane, D.H., and Bachman, G.O., 1965, Geologic map of New Mexico: Washington, D.C., U.S. Geol. Survey, 2 sheets, scale 1:500,000.

Fenneman, N.M., 1931, Physiography of western United States: New York, McGraw-Hill, 534 p.

Gailbraith, F.W., 3d, 1959, Craters of the Pinacates, in Arizona Geol. Soc., Guidebook II, Southern Arizona, April 2-6, 1959; Arizona Geol. Soc. Digest, 2d Ann., p. 161-167.

Hackman, R.J., 1967, Time, shadows, terrain, and photointerpretation: U.S. Geol. Survey Prof. Paper 575-B, p. B155-B160.

Hamilton, Warren, and Myers, W.B., 1967, Cenozoic tectonics of the western United States, in World rift system: Canada Geol. Survey Paper 66-14, p. 291-306.

Harvey, D.I., and Myskowski, E.P., 1965, Physics of high altitude aerial photography, in Photographic considerations for aerospace: Lexington, Mass., Itek Corp., p. 1-22.

Ives, R.L., 1935, Recent volcanism in northwestern Mexico: Pan-Am. Geologist, v. 63, no. 5, p. 335-338.

Jahns, R.H., 1959, Collapse depressions of the Pinacate volcanic field, Sonora, Mexico, in Arizona Geol. Soc., Guidebook II, Southern Arizona, April 2-6, 1959; Arizona Geol. Soc. Digest, 2d Ann., p. 165-184.

Kaltenbach, J.F. (compiler), 1969, Science report on the 70 millimeter earth photography of the Apollo 6 mission: U.S. Natl. Aeronautics and Space Admin., Tech. Note MSC S-217, 315 p.

Kelley, V.C., 1952, Tectonics of the Rio Grande depression of central New Mexico, in New Mexico Geol. Soc., Guidebook of the Rio Grande country, central New Mexico, 3d field conference, October 3-5, 1952; p. 93-105.

Kutina, Jan, 1969, Hydrothermal ore deposits in the western United States--A new concept of structural control of distribution: Science, v. 165, no. 3898, p. 1113-1119.

Lowman, P.D., Jr., 1959, Preliminary results from 70 millimeter photographs of North America taken on the Apollo 6 mission, in Kaltenbach, J.F. (compiler), Science report on the 70 millimeter earth photography of the Apollo 6 mission: U.S. Natl. Aeronautics and Space Admin., Tech. Note MSC S-217, p. 155-174.

Lyons, P.L., 1970, Continental and oceanic geophysics, in Johnson, Helgi, and Smith, B.F. (eds.), The megatectonics of the continents and oceans: New Brunswick, N.J., Rutgers Univ. Press, p. 147-166.

Mayo, E.B., 1958, Lineament tectonics and some ore districts of the southwest: Mining Eng., v. 10, no. 11, p. 1169-1176.

Moody, J.D., and Hill, M.J., 1956, Wrench-fault tectonics: Geol. Soc. America Bull., v. 67, no. 9, p. 1207-1246.

Moore, D.G., and Buffington, E.C., 1968, Transform faulting and growth of the Gulf of California since the late Pliocene: Science, v. 161, no. 3847, p. 1238-1241.

Moore, J.G., 1960, Curvature of normal faults in the Basin and Range province of the western United States: U.S. Geol. Survey Prof. Paper 400-B, p. B409-B411.

Rusnak, G.A., Fisher, R.L., and Shepard, F.P., 1964, Bathymetry and faults of Gulf of California, in Marine geology of the Gulf of California--A symposium: Am. Assoc. Petroleum Geologists Mem. 3, p. 59-75.

Space Electronics Systems Division Staff, 1969, Camera system and calibration in Kaltenbach, J.F. (compiler), Science report on the 70 millimeter earth photography of the Apollo 6 mission: U.S. Natl. Aeronautics and Space Admin. Tech. Note MSC S-217, p. 13-42.

Sumner, J.S., 1970, Geophysical aspects of porphyry copper deposits, in Mining and Groundwater Geophysics, 1967: Canada Geol. Survey, Econ. Geology Rept. 26, p. 322-335.

Thompson, R.W., 1968, Tidal flat sedimentation on the Colorado River delta northwestern Gulf of California: Geol. Soc. America Mem. 107, 133 p.

Thornbury, W.D., 1965, Regional geomorphology of the United States: New York, John Wiley and Sons, 609 p.

U.S. Geological Survey, 1970, Apollo 6 photomaps of the west-east corridor from the Pacific Ocean to northern Louisiana: Washington, D.C., 4 sheets, scale 1:500,000.

Wisser, E.H., 1954, Geology and ore deposits of Baja California, Mexico: Econ. Geology, v. 49, no. 1, p. 44-76.

Woodford, A.O., and Harriss, T.F., 1938, Geological reconnaissance across Sierra San Pedro Martir, Baja California: Geol. Soc. America Bull., v. 49, no. 9, p. 1297-1336.

Woollard, G.P., 1958, Areas of tectonic activity in the United States as indicated by earthquake epicenters: Am. Geophys. Union Trans., v. 39, no. 6, p. 1135-1150.

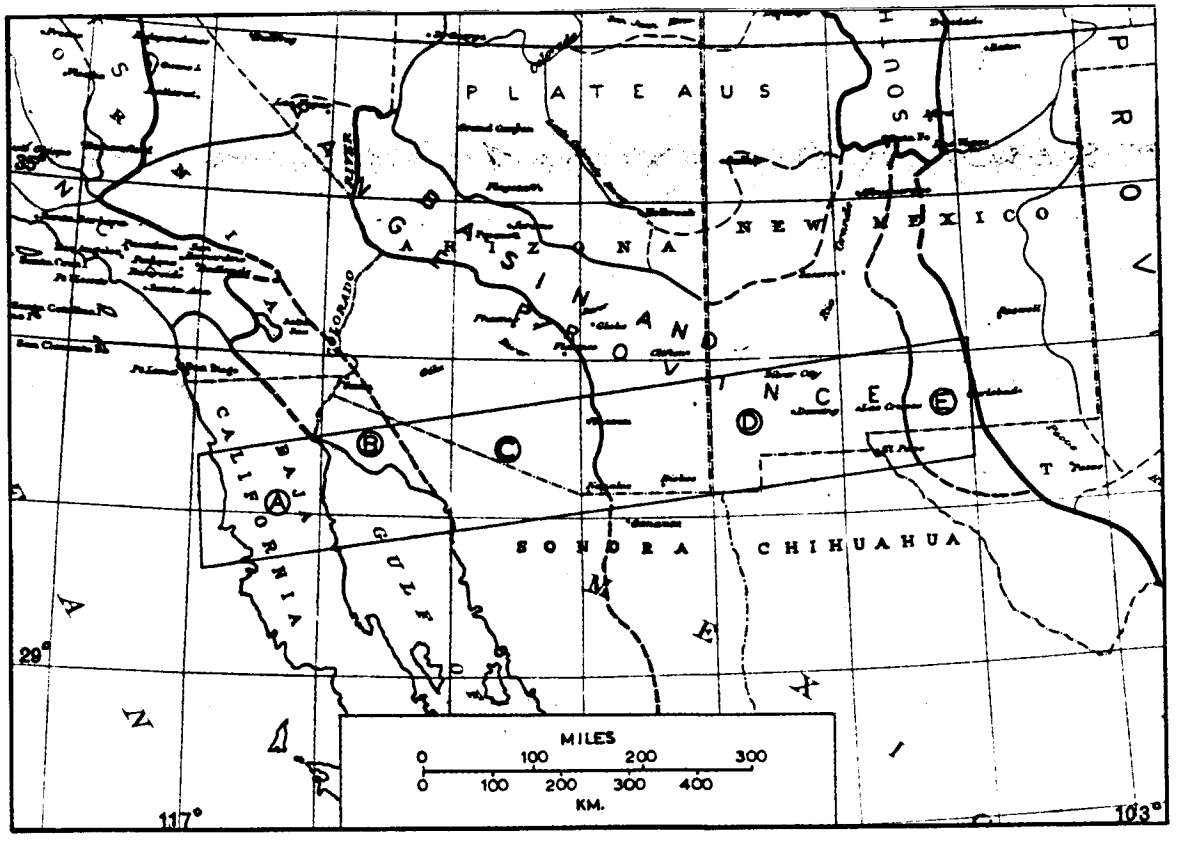

Figure 1 - Index map of southwestern United States and northern Mexico showing area of study and physiographic divisions. (A) The Peninsular Ranges section of the Pacific Border province, and (B) Salton Trough, (C) Sonoran Desert, (D) Mexican Highland, (E) Sacramento sections of the Basin and Range province. (From Fenneman, 1931, and Thornbury, 1965).

APOLLO PHOTOMAP OF THE SOUTHWEST UNITED STATES AND NORTHERN MEXICO

SHOWING GEOLOGIC STRUCTURAL FEATURES

FIGURE 2

SHEET 1 OF 2

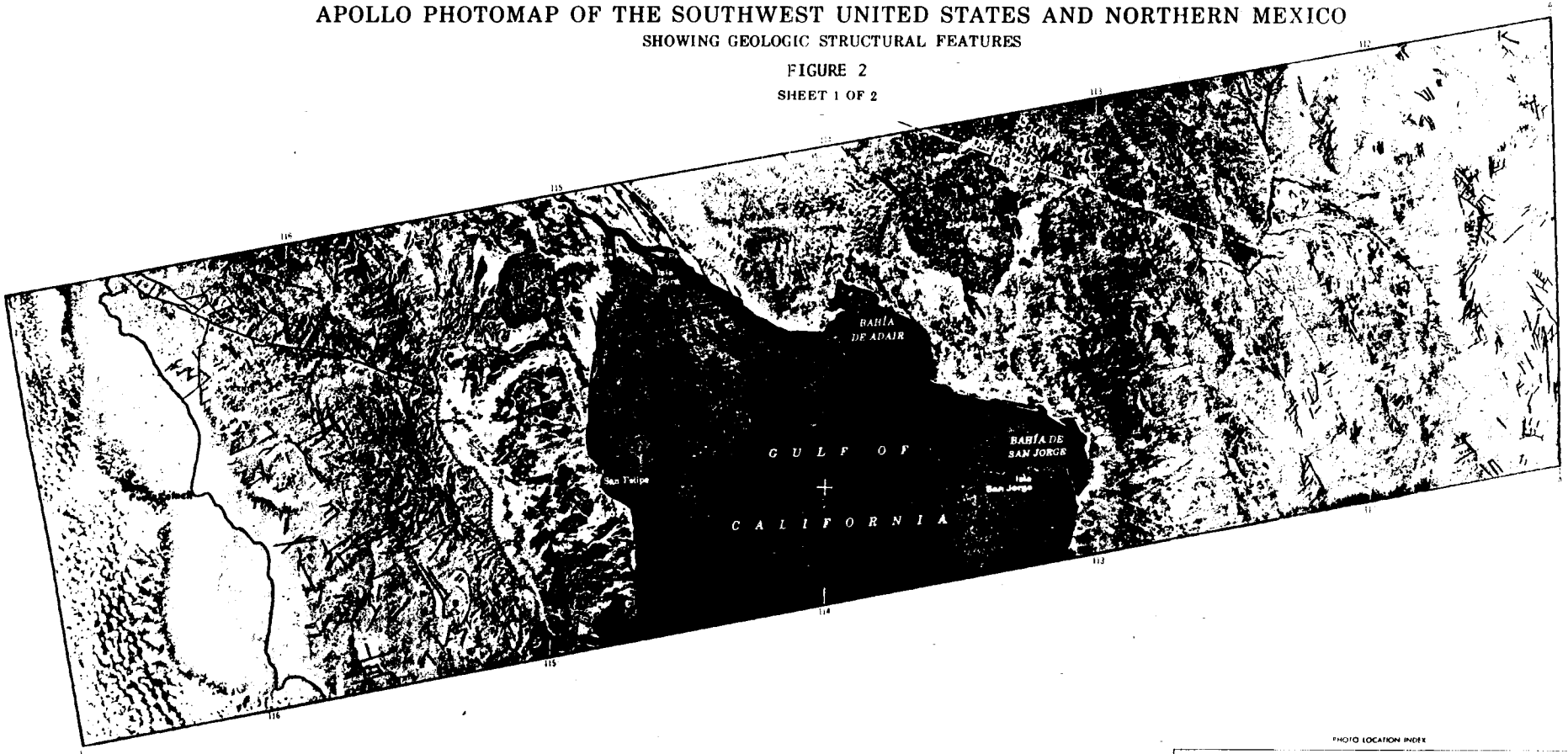

RECTIFIED APOLLO PHOTOGRAPHY

DATE OF PHOTOGRAPHY	APR. 4, 1968
MISSION	APOLLO 6
CAMERA	MAURER 76 MM FOCAL LENGTH
FILM AND FORMAT	70 MM 2 25 IN. SQUARE FORMAT
APPROXIMATE ALTITUDE	115 NAUT. MI (213 KM.)
APPROXIMATE SCALE OF ORIGINAL PHOTOGRAPHY	1 2,790,000

PLOTTED TO THE LAMBERT CONFORMAL CONIC PROJECTION
Based on Standard Parallels of 33° and 45°

0 10 20 30 40 50 MILES
0 10 20 30 40 50 60 70 80 Km

PREPARED BY THE U.S. GEOLOGICAL SURVEY
IN COOPERATION WITH THE NATIONAL AERONAUTICS AND SPACE ADMINISTRATION

THE DISPLACEMENT OF BOUNDARIES, GRID, SCALE, ETC. ON THIS PHOTOMAP IS APPROXIMATE AND MUST NOT BE CONSIDERED AUTHORITATIVE

N

PHOTO LOCATION INDEX

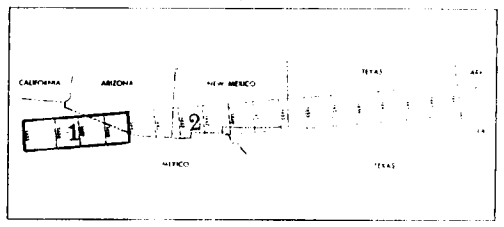

APOLLO PHOTOMAP OF THE SOUTHWEST UNITED STATES AND NORTHERN MEXICO

SHOWING GEOLOGIC STRUCTURAL FEATURES

FIGURE 2 CONT'D

SHEET 2 OF 2

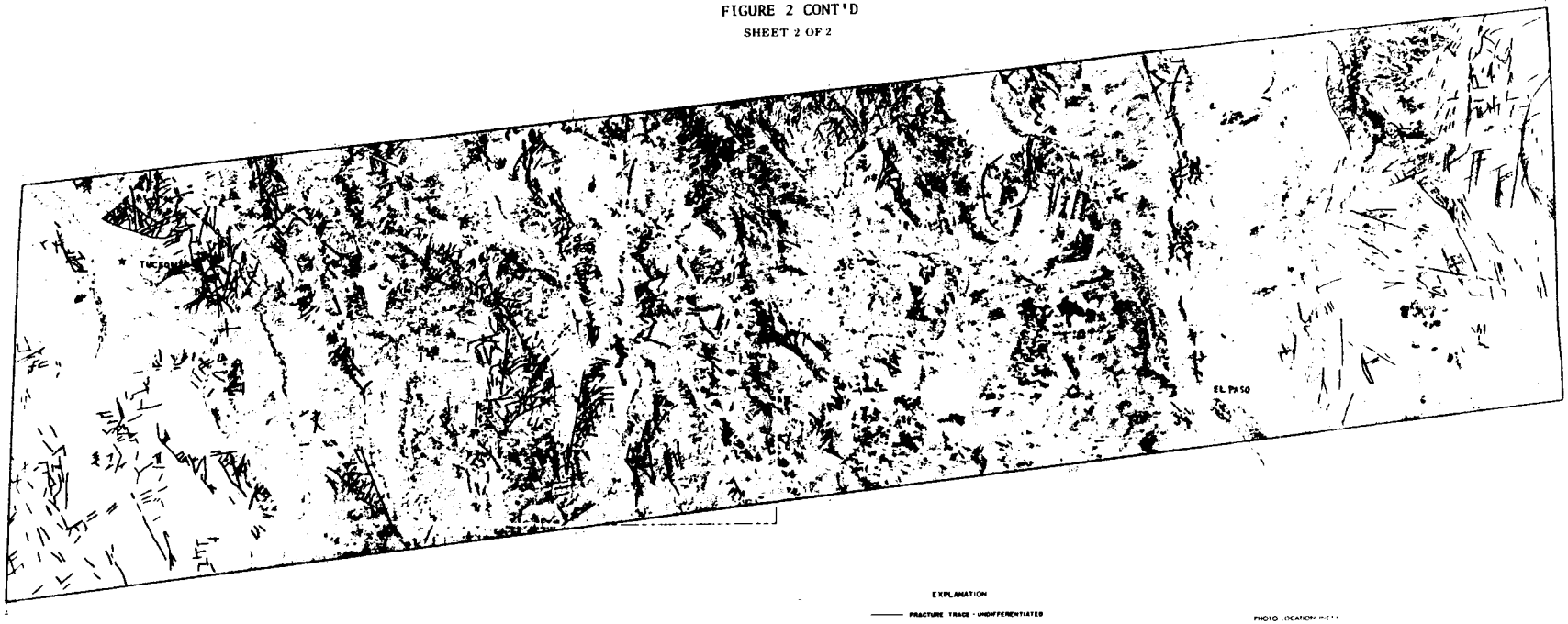

RECTIFIED APOLLO PHOTOGRAPHY

DATE OF PHOTOGRAPHY	APRIL 4, 1968
MISSION	APOLLO 6
CAMERA	MAURER 76 MM FOCAL LENGTH
FILM AND FORMAT	70 MM 2 25 IN SQUARE FORMAT
APPROXIMATE ALTITUDE	115 NAUT MI (213 KM)
APPROXIMATE SCALE OF ORIGINAL PHOTOGRAPHY	1 2 790 000

GEOLOGIC INTERPRETATION
BY
STEPHEN J GAWARECKI
U S GEOLOGICAL SURVEY
1971

0 10 20 30 40 50 60 70 80 90 MILES
0 10 20 30 40 50 60 70 80 KM

N

EXPLANATION

- FRACTURE TRACE - UNDIFFERENTIATED
- HIGH ANGLE FAULT, SHOWING RELATIVE MOVEMENT
- NORMAL FAULT, HACHURES ON DOWN SIDE
- ANTICLINE, SHOWING DIRECTION OF PLUNGE
- SYNCLINE, SHOWING DIRECTION OF PLUNGE
- DOME IN SEDIMENTARY ROCKS
- INTRUSIVE CENTER AND ASSOCIATED STRUCTURAL ARCS
- STEEP METAMORPHIC BEDS AND/OR RELICT BEDDING IN GRANITIC ROCKS
- VOLCANIC VENTS - CINDER CONES OR CRATERS
- MAAR CRATERS, SOME ENCLOSING LATER VENTS

PHOTO LOCATION INDEX

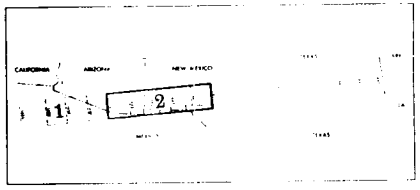

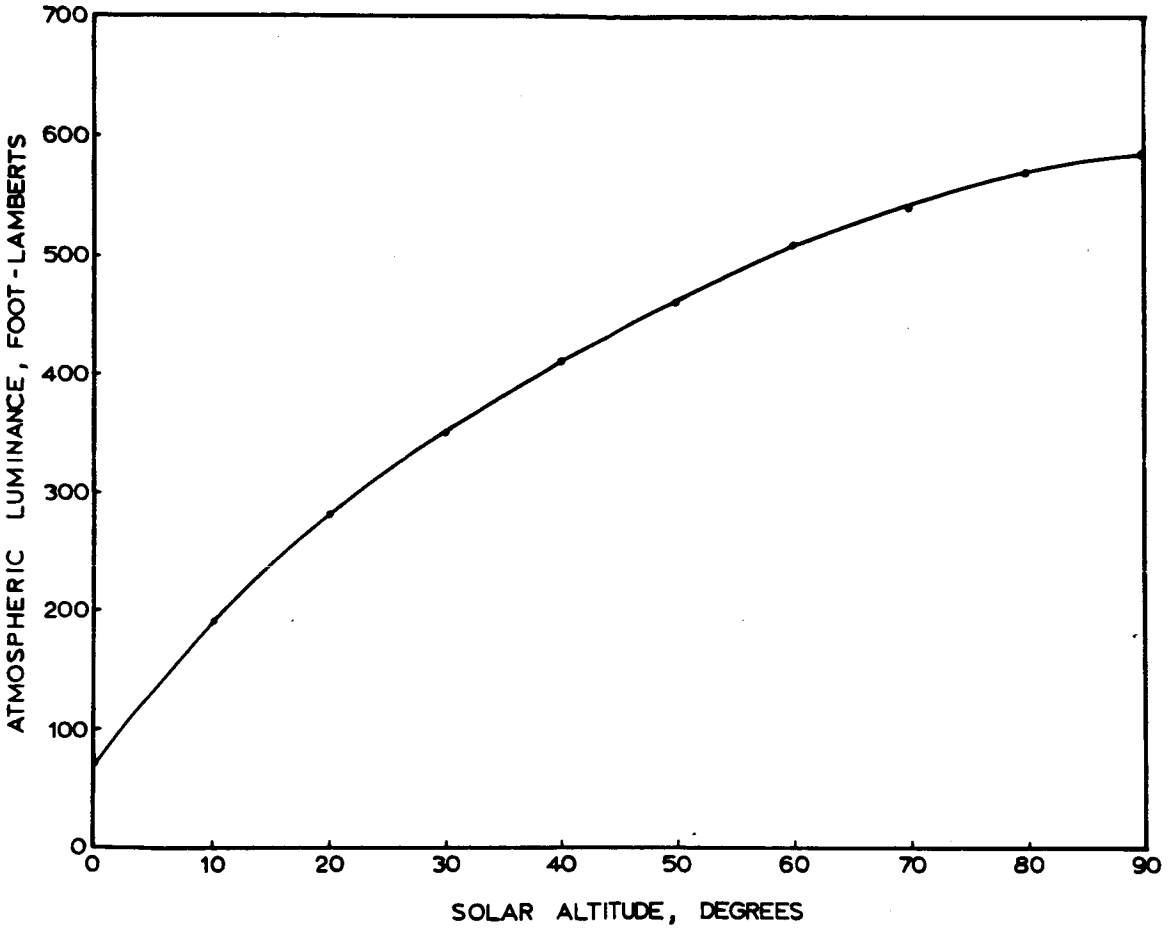

Figure 3 - Atmospheric luminance versus solar altitude for clear weather conditions. (From D.I. Harvey and E.P. Myskowski, personal communication, 1970).

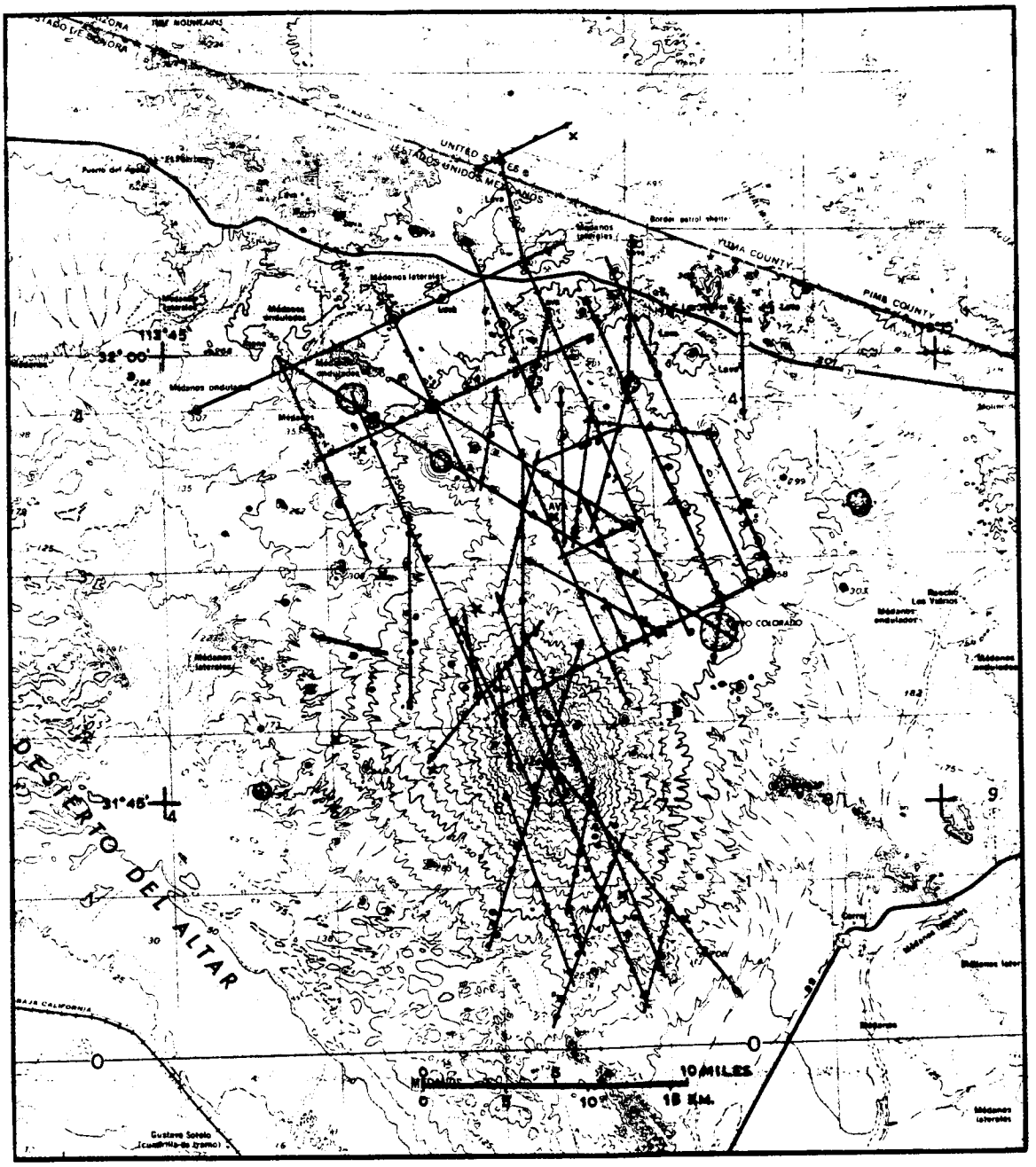

Figure 4 - Alignment analysis of craters at the Pinacates basaltic lava field, Sonora, Mexico. Solid dots are recognized craters, Xs are possible craters, and maars are shown with internal hachuring.

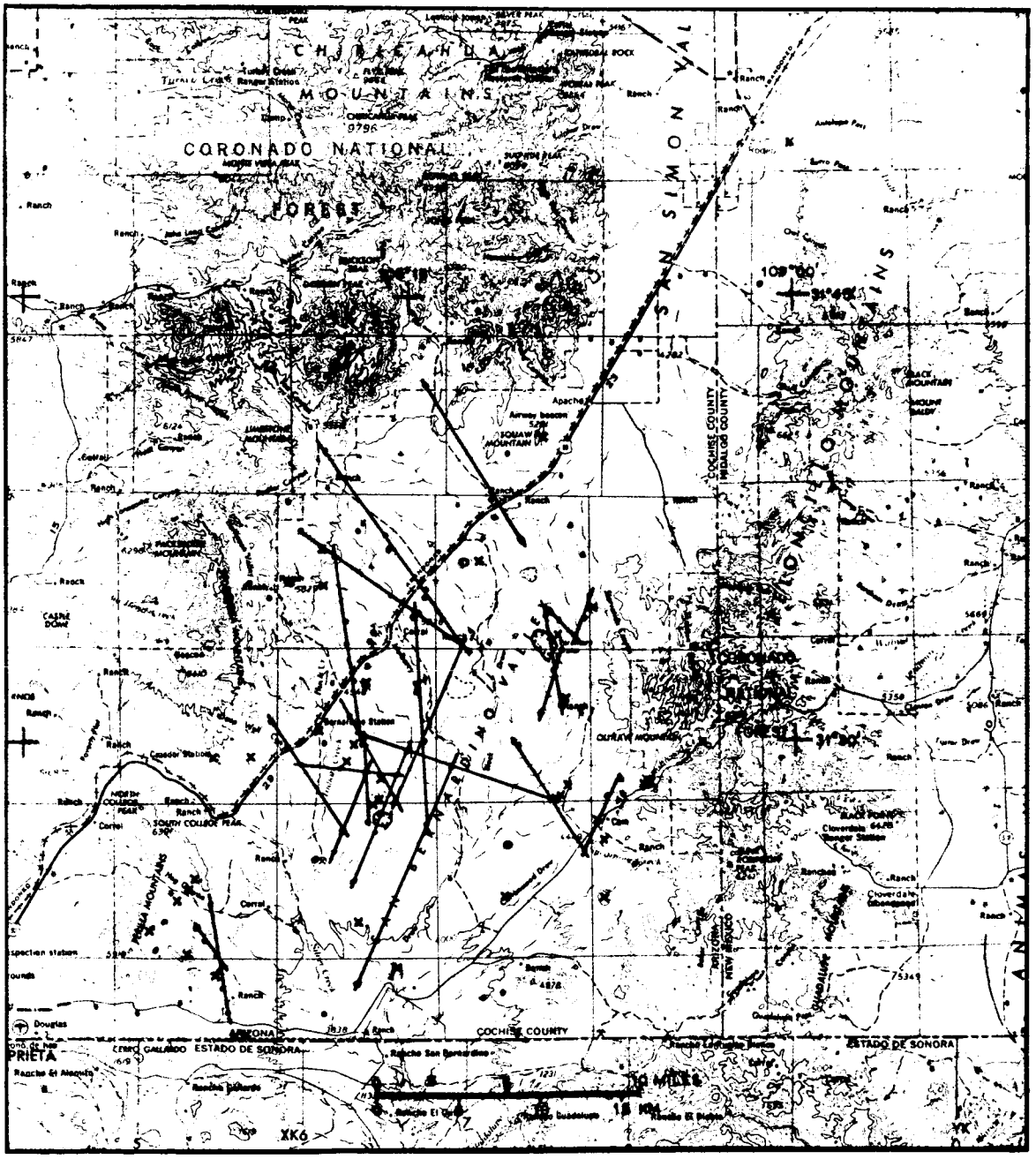

Figure 5 - Alignment analysis of the San Bernardino Valley basaltic lava field, southeastern Arizona. Solid dots are recognized craters, Xs are possible craters, and maars are shown with internal hachuring.

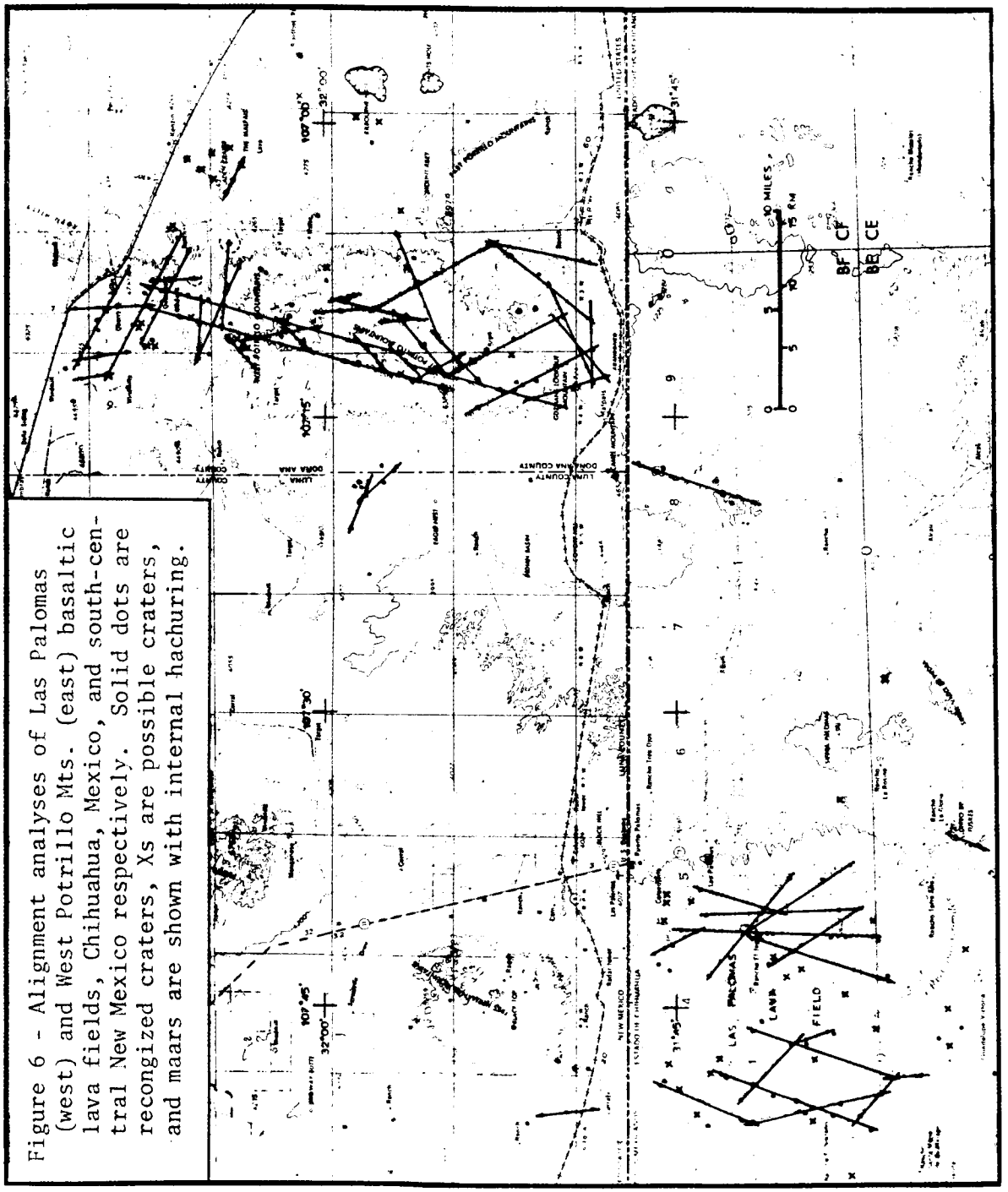

Figure 6 - Alignment analyses of Las Palomas (west) and West Potrillo Mts. (east) basaltic lava fields, Chihuahua, Mexico, and south-central New Mexico respectively. Solid dots are recongized craters, Xs are possible craters, and maars are shown with internal hachuring.

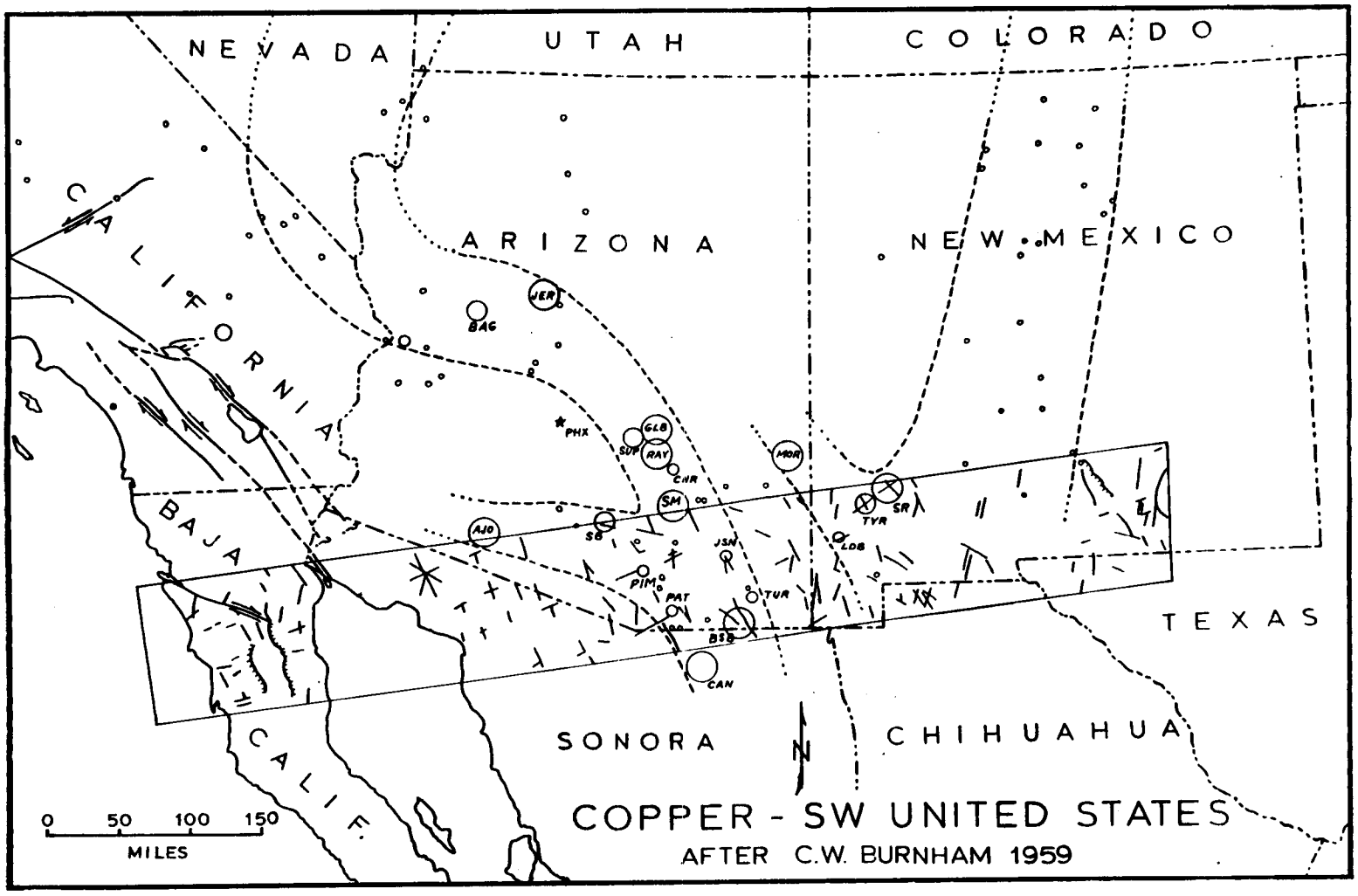

Figure 7 - Copper belt in the southwestern United States (from Burnham, 1959), and its relationship to fracture trends in area of study. Mining districts covered by the Apollo 6 photography include Silver Bell (SB), Pima-Twin Buttes (PIM), Patagonia (PAT), Johnson (JSN), Bisbee (BSB), Turquoise (TUR), Lordsburg (LDB), Tyrone (TYR), and Santa Rita (SR).

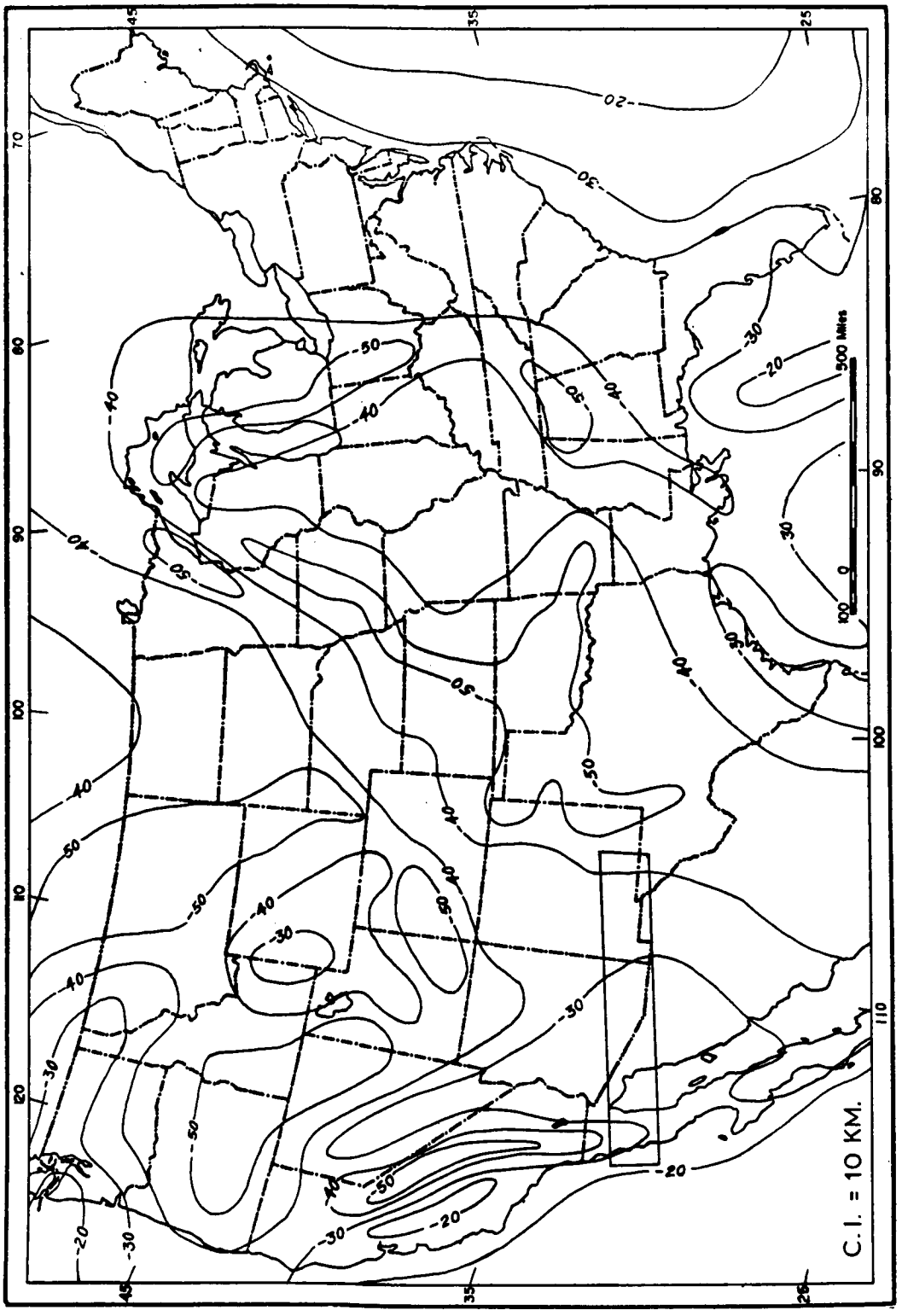

Figure 8 - Moho discontinuity depth contour map of the United States and northern Mexico. (From Lyons, 1970). Area of study is outlined.

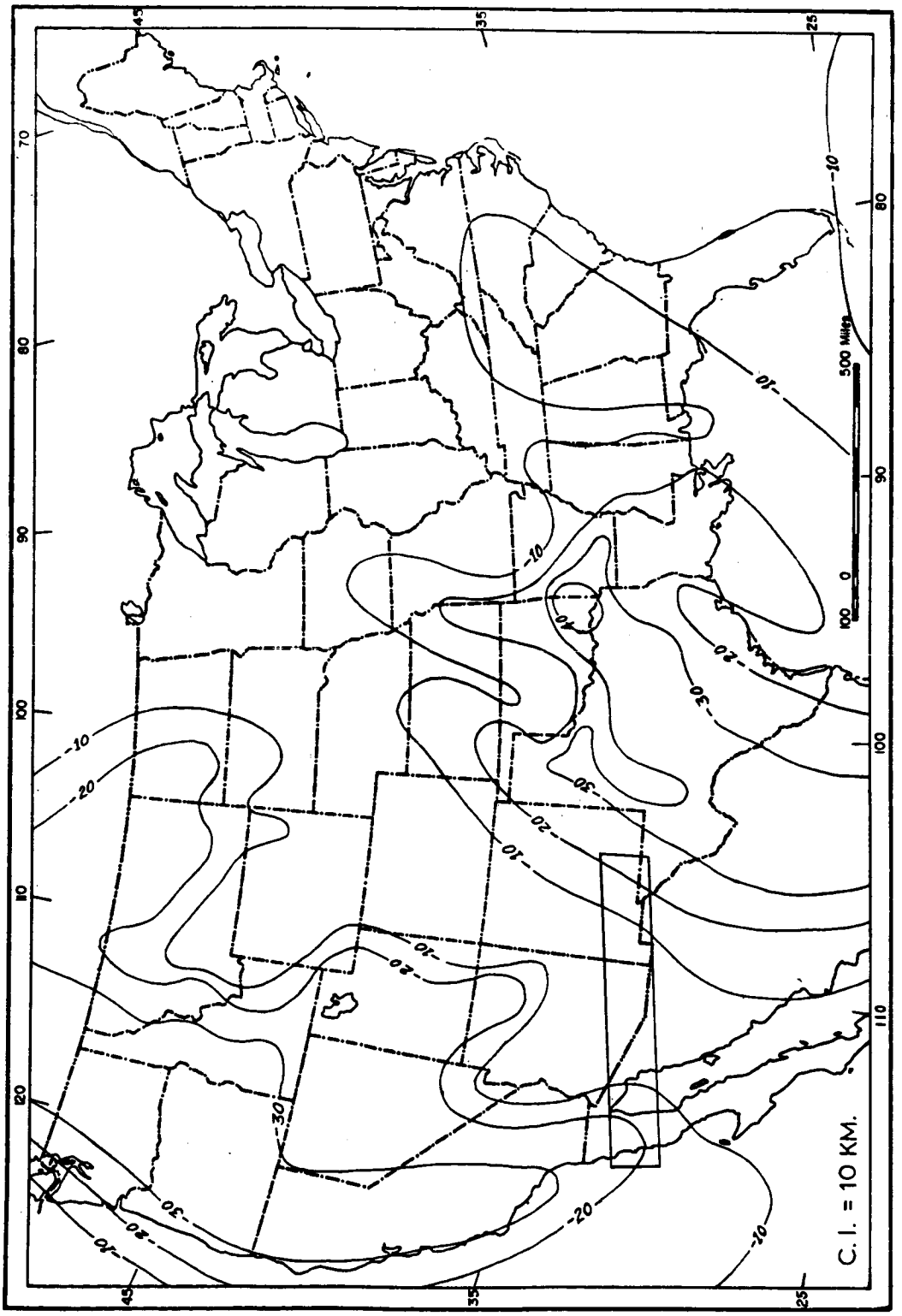

Figure 9 - Conrad discontinuity depth contour map of the United States and northern Mexico. (From Lyons, 1970). Area of study is outlined.

SECTION 16

Geology

GEOLOGIC TERRAIN MAPPING FROM EARTH-SATELLITE AND ULTRA-HIGH AERIAL PHOTOGRAPHS

by

R. B. Morrison
U.S. Geological Survey
Denver, Colorado

My project under the EROS Program of NASA-USGS involves using earth-satellite and ultra-high aerial photographs for geologic terrain mapping in the southwestern U. S. An important objective, in addition to producing various kinds of terrain maps, is to improve the techniques of photointerpretation that can be used with these small-scale photographs, thereby reducing the amount of field checking necessary to maintain suitable accuracy.

The mapping experiments are synoptic in two respects: they cover large regions, and they are multidisciplinary. They utilize the synoptic "megaviews" provided by the space photos and also, to an appreciable degree, by the ultra-high aerial photos. Such small-scale photographs, with their uniformly illuminated coverage of large areas, create exceptional opportunities for integrative interpretation of both strongly and subtly imaged terrain features without the noise of distracting detail.

The other synoptic aspect is the systematic mapping of three important kinds of terrain data: (1) geomorphic (landform) features, which are classified as to type, age, and degree of dissection/local relief; (2) soils, classified in terms of their profile development and particle-size, and (3) the surficial geologic deposits, such as Quaternary alluvium, eolian sand, and lacustrine sediments--the "soils" of common parlance. All three kinds of terrain data are interdependent to a large degree and information on one kind helps in the interpretation of the other two kinds.

In the latest mapping experiment, these three kinds of maps are being prepared at 1:250,000 scale for an 8,000-square-mile area between Tucson and Ajo, Arizona, using aerial photography obtained with the RB57F aircraft during Mission 101, Site 30, on August 10 last year. The nine cameras on this airplane provided color, color-infrared, and multispectral air photos from about 60,000 feet above the terrain and with photo scales ranging from 1:60,000 to 1:240,000.

The Tucson-Ajo study area, shown by the rectangle on figure 1, is two degrees of longitude long by one degree of latitude wide and extends from the west edge of Tucson to a few miles past the mining town of Ajo. It is in the SW corner of the Arizona Regional Ecological Test Site. This area has relatively low mountain ranges alternating with broad desert plains. It is one of the warmest and driest parts of the United States, and much of it is very sparsely populated. It includes about two-thirds of the Papago Indian Reservation and a like proportion of the Organ Pipe Cactus National Monument. Yet about ten percent of it, mainly along the Santa Cruz River valley, is irrigated farmland interspersed with several small cities and numerous suburban and industrial centers. This highly developed portion, as well as areas adjacent to it, is undergoing the rapid expansion of population, commerce, and industry that is dramatically in progress in southern Arizona.

This area was selected not only because it provides a good sample of the desert terrain of southwestern Arizona, but especially because it is admirably suited for improving and testing the photointerpretive techniques for mapping geologic terrain features with small-scale air and space photos. Because of the aridity, the screening effect of atmosphere and vegetation is minimal, and color air and space photos provide accurate information of the color and minute details of configuration of the ground surface. This is very useful for interpreting the distribution of various kinds of soils and surficial deposits.

Interpretation of landform type and the degree of dissection/local relief is the easiest, involving the least amount of inference. Interpretation of soils, surficial geology, and the age of landforms is considerably more difficult, and requires secondary and even tertiary levels of inference--and consequently, much more need for control by field data. We have found that the most efficient procedure is to maintain a rather intimate feedback between office photointerpretation and field checking. This insures that the field work is done in the right places, and yet is kept to the minimum consistent with maintaining suitable standards of mapping accuracy.

The impending deluge of space and air photographs from the ERTS and ultra-high aircraft missions makes urgent the need for simplifying and speeding up the interpretive process, utilizing as far as practicable such aids as image enhancement and computer processing. The two main uses of image enhancement are (1) to accentuate subtle differences in tonal density, that are at or below the threshold of ready visibility by the human eye, and (2) (the opposite) to clear up the clutter of small details in order to accentuate the major elements within a complex system. I recently tested the possibilities of image enhancement of space and ultra-high air photos with two types of digital density slicing machines. I concluded that, at their present stage of development, these machines are of marginal utility for the types of mapping

I am doing: they may be of some assistance in certain types of terrain, generally in quite limited areas, but by no means can they entirely supplant the work of a skilled photointerpreter.

One of the RC8 metric cameras aboard the RB57F was supplied with Aeroneg 2448 color film. This film was developed to a negative, and then color positive transparencies and paper prints were made from it. We find that these color air photos provide much more information useful for mapping soils and surficial geology than do color-infrared photos. Only with the Aeroneg photos are we able to make many of the soil and other discriminations.

The Aeroneg color transparencies show remarkable detail considering their 1:120,000 scale. With a precision magnifying stereoscope it is possible to distinguish comparatively small rock outcrops along washes that dissect the bajada surfaces, and thus to map the extent of hardrock pediments that are generally covered by thin alluvium. Our geomorphic map is the first attempt to show the distribution of buried pediments throughout this region. This information has practical value in giving a better understanding of the configuration of the ground-water basins, and also delimits the areas where bedrock is readily accessible for mineral exploration by geochemical, geophysical, and drilling methods. The resolution of these photos is good enough that they show the arroyos caused by so-called "post-white-man erosion." These arroyos started developing less than 100 years ago, and are actively growing in many places in the desert lowlands, seriously impairing rangelands and some farmlands. If the ERTS satellite photos can attain the resolution of these air photographs, their repetitive coverage will afford a splendid opportunity to determine the distribution of these arroyos throughout the Southwest, and to find out the rates of their headward growth, the degree of success of corrective measures, and any vegetative or cultural changes that may accelerate or retard the gullying. Information of this kind will be highly significant for attacking a key ecological problem in the Southwest.

From the three basic-data maps (soils, landforms, and surficial geology) we expect to prepare a map or maps of the potential land uses, showing both the capabilities and the limitations for various uses. The land use map will attempt to communicate the geologic terrain information in a practical, readily understandable way so that it can be utilized for regional environmental planning and development.

The Tucson-Ajo study is proving remarkably successful in quickly producing a series of comprehensive, integrated maps that display many of the fundamental geologic terrain characteristics of a large area. The soils, geomorphology, and surficial geology of this area previously were unmapped or mapped only in small bits and pieces with widely differing, relatively uncoordinated approaches. The three basic maps will

be fully compiled and field checked within 1 1/2 years after the start of the mapping, involving only about 2 1/2 man-years of professional time. This is an unprecedentedly short time for completing a job of this scope. Normally each map would require several teams of specialists working over a much longer period. Each team probably would differ somewhat in its approach and interpretation, and consequently the results from the various teams would have to be coordinated in order to arrive at a coherent, integrated map of the whole area--which in itself involves considerable effort. The rapid, indeed explosive, growth of southern Arizona has created an urgent need for data of the type provided by these maps--there just isn't time to map by traditional methods. The ERTS imagery, combined with the ultra-high aerial photography for the Arizona Regional Ecological Test Site, will come just in the nick of time to provide the wherewithal for efficient terrain mapping of this region. These maps will provide information necessary for avoiding the sort of "quiet crisis" that is confronting so many of our urban and suburban areas--a crisis compounded partly of misuse of land, bad planning, and uncoordinated real estate and industrial developments--all containing the seeds of future decay and environmental deterioration.

In closing, I'll point out that the geologic terrain maps are quite cheap to prepare. The set for the Tucson-Ajo study area will cost less than $8.00 a square mile at the project level, without the costs of overhead and NASA's support, such as the RB57F aircraft mission.

REMOTE SENSING IN MARINE GEOLOGY: ARCTIC TO CARIBBEAN

by

Paul R. Carlson
U.S. Geological Survey
Menlo Park, California

INTRODUCTION

The Office of Marine Geology, U.S. Geological Survey, has participated in the cooperative NASA program since 1968. The main emphasis of the program has been to evaluate the applications of remote sensing to coastal dynamics of both nearshore and estuarine waters. The study areas include the Arctic, the Pacific Northwest, the Gulf of Mexico adjacent to Texas, the New England coast, San Francisco Bay, and islands of the northeastern Caribbean (Puerto Rico and the Virgin Islands).

This paper will illustrate briefly some of our studies in four of these areas--the Arctic, the Pacific Northwest, the Caribbean, and San Francisco Bay.

ARCTIC (BEAUFORT SEA)

Since the discovery of oil near Prudhoe Bay and the resulting plans for exploitation, concern has been expressed about the lack of information on the Arctic environment. A study being conducted by Erk Reimnitz is concerned with the processes operating in the nearshore zone of the Beaufort Sea. This area is dominated by ice movement, ice gouging, and freeze-up/break-up phenomena, and the resulting nearshore water circulation and sediment movement are poorly known. Arnborg, Walker, and Peippo (1967) suggested that most of the sediment being carried to the sea by the melt-water laden rivers is carried down in the first few weeks of the discharge season. At the beginning of this time, the ice is still shore-fast, and as a result the water runs out on the ice. This ice, however, was found to have very little sediment resting on it, thus posing the question of the whereabouts of the sediment. An answer may be that much of the initial sediment may be flushed rapidly through small thaw holes or moulins (figure 1). Evidence of violent flushing action is indicated by the presence of scour depressions on the sea floor below the moulins. Some of these scour depressions, measured with a sounding line from a small

fiberglass boat, had a relief of more than a meter. Continued work is planned in this harsh environment, and it is hoped that the ERTS-A imagery may provide some of the needed coverage of nearshore circulation patterns.

PACIFIC NORTHWEST

The coastal zone of Oregon and Washington, which is subject to continuous change caused by geologic, oceanographic, and meteorologic processes, has undergone accelerated changes in recent years because of increasing population pressures and man-made modifications. Monitoring these changes lends itself very well to aerial remote sensing techniques, especially on a repetitive basis as planned for ERTS-A and B.

Geologic mapping of the Oregon-Washington Coast Range, an area of high annual rainfall, lush vegetation, and thick soil profile, has been underway for several years (Snavely and Wagner, 1963; Snavely and Wagner, 1964; Snavely, MacLeod and Rau, 1969), and much of the mapping has been completed. Conventional aerial photography, while useful, shows considerably less detail than images obtained with a high-frequency side-looking radar (MacLeod and Snavely, 1968). Although the radar image is somewhat distorted, some linear features not readily observed on conventional photos can be easily delineated on the radar image (figure 2). Norman S. MacLeod and Parke D. Snavely, Jr., are currently preparing a geologic map of a 10-mile-wide coastal strip of northern and central Oregon utilizing surface geology and radar imagery. A preliminary portion of this map from the northern Oregon coastal area showing numerous faults and formation contacts is shown in figure 2. Similar structural features are being investigated on the adjacent continental shelf using marine seismic techniques.

Marine geologic investigations are being conducted in the nearshore zone off southern Oregon (Clifton, 1968; Hunter, Clifton and Phillips, 1970). Aerial reconnaissance and photography combined with SCUBA diving are providing synoptic overviews necessary for a proper understanding of sediment movement in this dynamic high-energy environment. Rip currents (figure 3), which are generated by storm waves striking the beach at an oblique angle, are a very important transport mechanism in the littoral zone, and their effects on sedimentation are far from being thoroughly understood. However, the combination of SCUBA "ground truth" and aerial photography, especially on a repetitive basis, shows great promise in developing the relation of large rips to the overall pattern of longshore sediment transport.

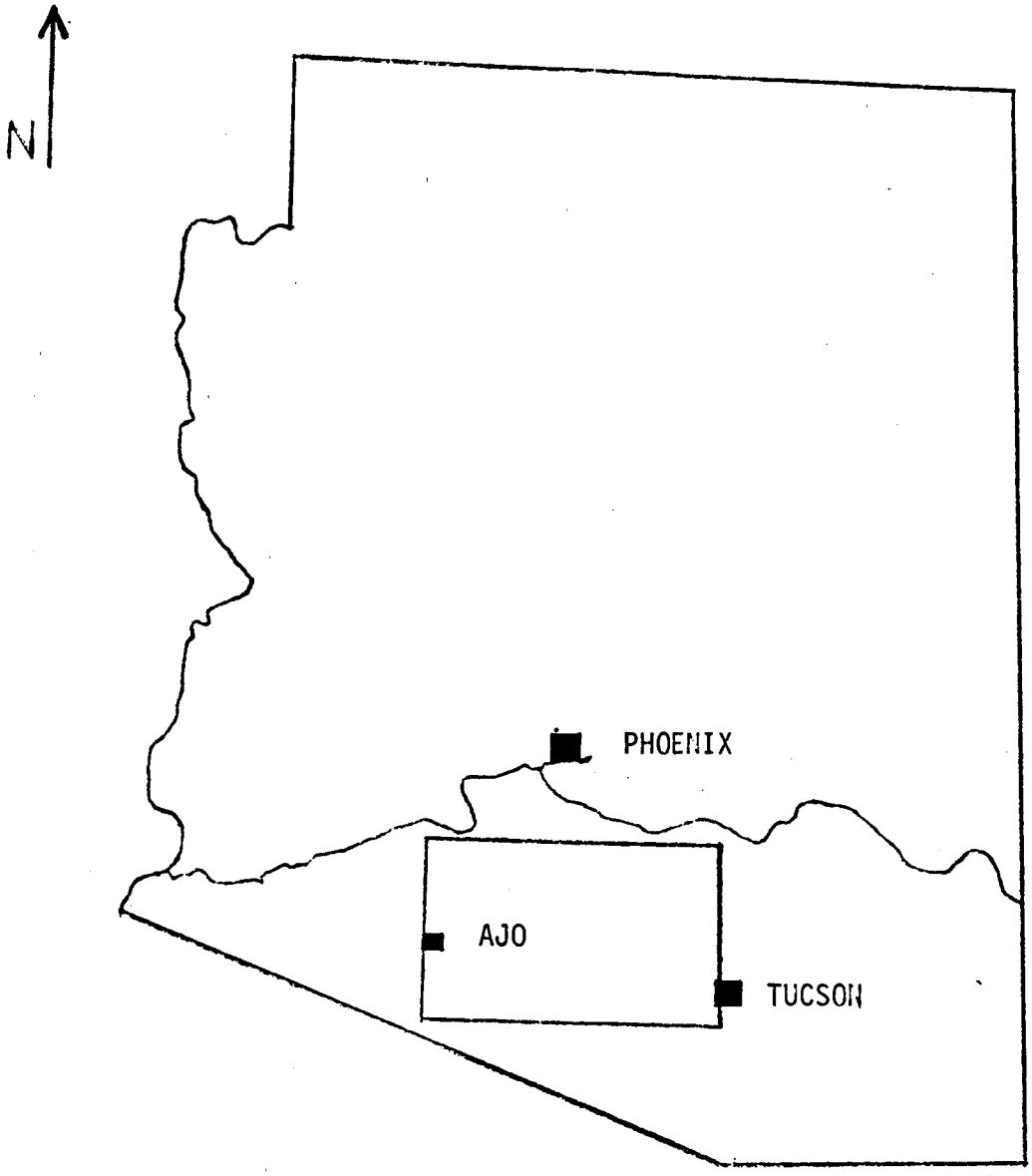

Figure 1.- Outline map of Arizona with inner rectangle showing the Tucson-Ajo study area.

CARIBBEAN-TEKTITE

Project TEKTITE, located in Lameshur Bay on the south side of St. John, U.S. Virgin Islands, housed USGS marine geologist H. Edward Clifton during TEKTITE I in 1969 (Clifton, 1969; Clifton et al., 1970) and Clifton, Ralph E. Hunter and R. Lawrence Phillips during TEKTITE II in 1970. They found the clear water admirably suited to mapping coral reef distribution and related sedimentary facies in water depths of up to 20 meters. To map the reefs they used color aerial photos from a U.S. Air Force (Cambridge Research) overflight conducted shortly before TEKTITE I began (figure 4). The aerial photography provides the needed broad view to the diver whose area of coverage is quite restricted on any given dive. The diver in turn can check in great detail the intricacies of the various facies of reef and detrital sediments (see figure 5). A combination aquanaut-astronaut view of the tropical nearshore zone shows great promise for providing the kind of data needed for a better understanding of the complex reef environment.

SAN FRANCISCO BAY

The San Francisco Bay system has very complex circulation which, in addition to being influenced by tidal forces and wind stress, is greatly affected by seasonal variations in discharge from the Sacramento-San Joaquin River system (Peterson and Carlson, 1968; McCulloch et al., 1970). We are presently studying the circulation of the bay waters in order to determine net transport of suspended and bottom sediments. Because of the complexity of the circulation, water cruises have been combined with occasional aerial photographic missions to provide a synoptic view of the waters being sampled (Carlson et al., 1970).

During the winter season, the high discharge from the Sacramento River system results in a very large volume of fresh, turbid water entering the bay. Figure 6 shows a plume of this low-salinity high-turbidity water entering south San Francisco Bay. The rather smooth well-defined plume front is typical of winter conditions after about a month of very high discharge (5 million acre feet during January 1970) from the Sacramento River system. Data from a water-sampling cruise conducted simultaneously with the overflight illustrate the differences in salinity, turbidity, and suspended-sediment content between the plume water and south bay water (figure 7). Measurements of the physical properties of the water masses provide a vertical "picture" of stratification. These data, combined with aerial photos which delimit the surface configuration, are being used to evaluate semiquantitatively the effects of fresh-water discharge on the circulation of the south bay.

In the summer, when discharge is greatly reduced, the plume becomes much less distinct (figure 8), and the shape of the plume front changes from smoothly lobate to intricately digitate. The great complexity of these waters illustrates the importance of synoptic coverage in order to evaluate water measurements properly. The much lower volume of fresh water being added to the bay by the Sacramento River system (1.5 million acre feet during July 1969) results in much higher salinities and about one-fifth the amount of suspended sediment being introduced into the south bay at the north end (Bay Bridge) (figure 9).

Recently acquired sampling gear includes an in situ salinity, temperature, and depth probe and a towable pumping system. The water is pumped on board and measured continuously for the properties specified in figure 10. This continuous printout from a traverse through Carquinez Strait (northern part of bay system) shows the good inverse correlation between chlorophyll and light transmission. This pumping system will be towed across plume boundaries (figures 6 and 8) and across other water patterns in the bay (figure 11) at the time of NASA overflights and during ERTS orbits. Combining air coverage with water truth improves the synoptic view of the detailed patterns of water types in San Francisco Bay and the adjacent Pacific Ocean. Through the use of density separation techniques (figure 11) or isodensitometer scans of aerial negatives, we hope to quantify the suspended sediment budget of the San Francisco bay system.

SUMMARY

The remote sensing program of the Office of Marine Geology has expanded to eight target areas. These areas include the coastal zones of the Beaufort Sea, Oregon and Washington, Texas and New England; the littoral zone off southern Oregon and northern California; the San Francisco Bay estuary system; the Virgin Islands (Project TEKTITE) and the island of Puerto Rico.

Aerial coverage of these areas has included the use of available aerial photos, NASA overflights whenever possible, and contract aircraft, which includes a considerable amount of photo reconnaissance by the principal investigators flying in light planes using hand-held 35 mm cameras. Ground truth for the target areas was obtained in a variety of ways: shipboard monitoring using a towable pumping system, SCUBA diving in the surf zone, living and working in an undersea habitat, and mapping faults and other structural features in the coastal zone and projecting these features offshore to relate to those structures mapped by marine seismic techniques.

We are looking forward to the improved synoptic coverage attainable with the ERTS imagery. Such coverage is necessary in the study of dynamically changing zones. These zones contain some of the most critical environmental problems this nation will be called upon to deal with in the very near future.

REFERENCES

Arnborg, Lennart, Walker, H. J., and Peippo, Johan, 1967, Suspended Load in the Colville River, Alaska, 1962: Geografiska Annaler, v. 49, Ser A., p. 131-144.

Carlson, P. R., Peterson, D. H., Conomos, T. J., and McCulloch, D. S., 1970, Aerial and in situ observation of a fresh-water plume in San Francisco Bay and adjacent Pacific: EOS (Am. Geophys. Union Trans.), v. 51, p. 767.

Clifton, H. E., 1968, Beach lamination: nature and origin: Marine Geology, v. 7, p. 553-559.

_____, 1969, TEKTITE I - 60 days under the sea: Geotimes, v. 14, no. 4, p. 10-12.

Clifton, H. E., Mahnken, C. V., Van Derwalker, J. C., and Waller, R. A., 1970, TEKTITE I, Man-in-the-sea project: Marine Science Program: Science, v. 168, p. 659-663.

Hunter, R. E., Clifton, H. E., Phillips, R. L., 1970, Geology of the stacks and reefs off the southern Oregon Coast: Ore Bin, v. 32, no. 10, p. 185-201.

MacLeod, N. S., and Snavely, P. D., Jr., 1968, Radar and infrared imagery, Oregon and Washington coasts: NASA Earth Resources Aircraft Program Status Review, v. 1, p. 17A-1-8.

McCulloch, D. S., Peterson, D. H., Carlson, P. R., and Conomos, T. J., 1970, Some effects of fresh-water inflow on the flushing of South San Francisco Bay: A preliminary report: U.S. Geol. Survey Circular 637A, p. A1-A27.

Peterson, D. H., and Carlson, P. R., 1968, Influence of runoff on seasonal changes in salinity in San Francisco Bay, California: Am. Geophys. Union Trans., v. 49, p. 704.

Snavely, P. D., Jr., MacLeod, N. S., and Rau, W. W., 1969, Geology of the Newport Area, Oregon: Ore Bin, v. 31, no. 2, p. 25-48.

Snavely, P. D., Jr., and Wagner, H. C., 1963, Tertiary geologic history of western Oregon and Washington: Washington Div. Mines and Geology Rept. Inv. 22, 25 p.

_____, 1964, Geologic sketch of northwestern Oregon: U.S. Geol Survey Bulletin 1181-M. p. M1-M17.

Figure 1.- Moulin-like opening in shore-fast ice of the Bering Sea. This oval opening, just below the center of the photo, is approximately 20 meters long. Photo by Erk Reimnitz using a hand-held 35 mm camera and Ektachrome film from an altitude of about 3000 ft. June 1970.

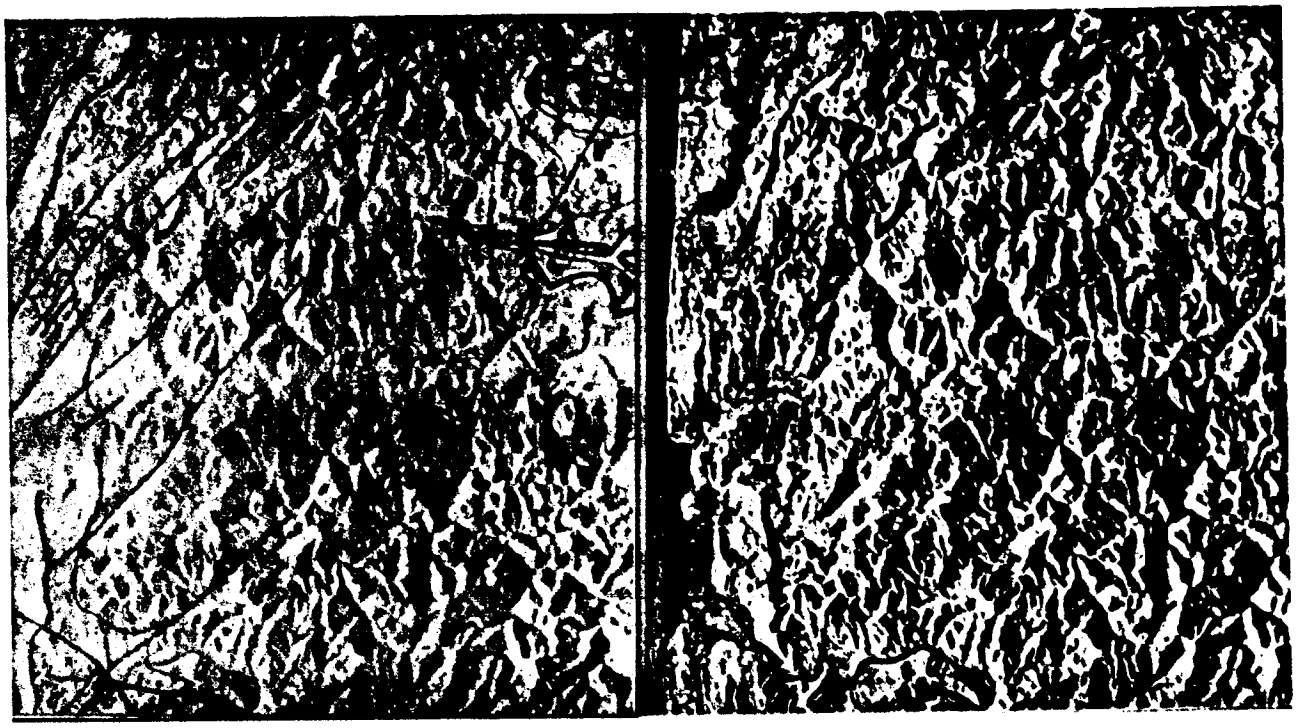

Figure 2.- Right: Radar image of northern Oregon coastal zone. Lincoln City is at left Center of the 10-mile-square area. Left: Geologic map overlies duplicate radar image. Dashed lines indicate faults, most of which were mapped by field study and corroborated by radar imagery obtained after much of the field mapping had been done. Some of the faults are best seen on the radar images. Solid lines edged with colors are formation contacts. Radar imagery was flown on October 25, 1965.

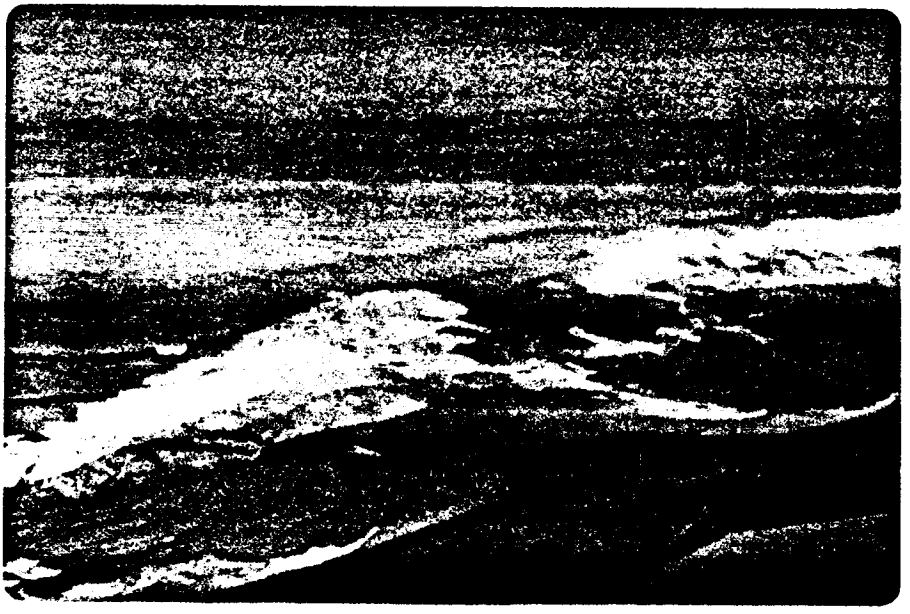

Figure 3.- Rip current on the southern Oregon coast. Distance across the sand barrier in foreground about 300 ft. Photo by H. E. Clifton with a 35 mm camera and Kodachrome film from an altitude of about 500 ft.; summer 1970.

Figure 4.- Cabritte Horn Pt. and Lameshur Bay, St. John, U.S. Virgin Islands, near the site of project Tektite. North is toward the upper left corner. U.S.A.F. photo, November 1968, altitude 4000 feet, camera K-17, focal length 12 inches, color film-Kodak 8442.

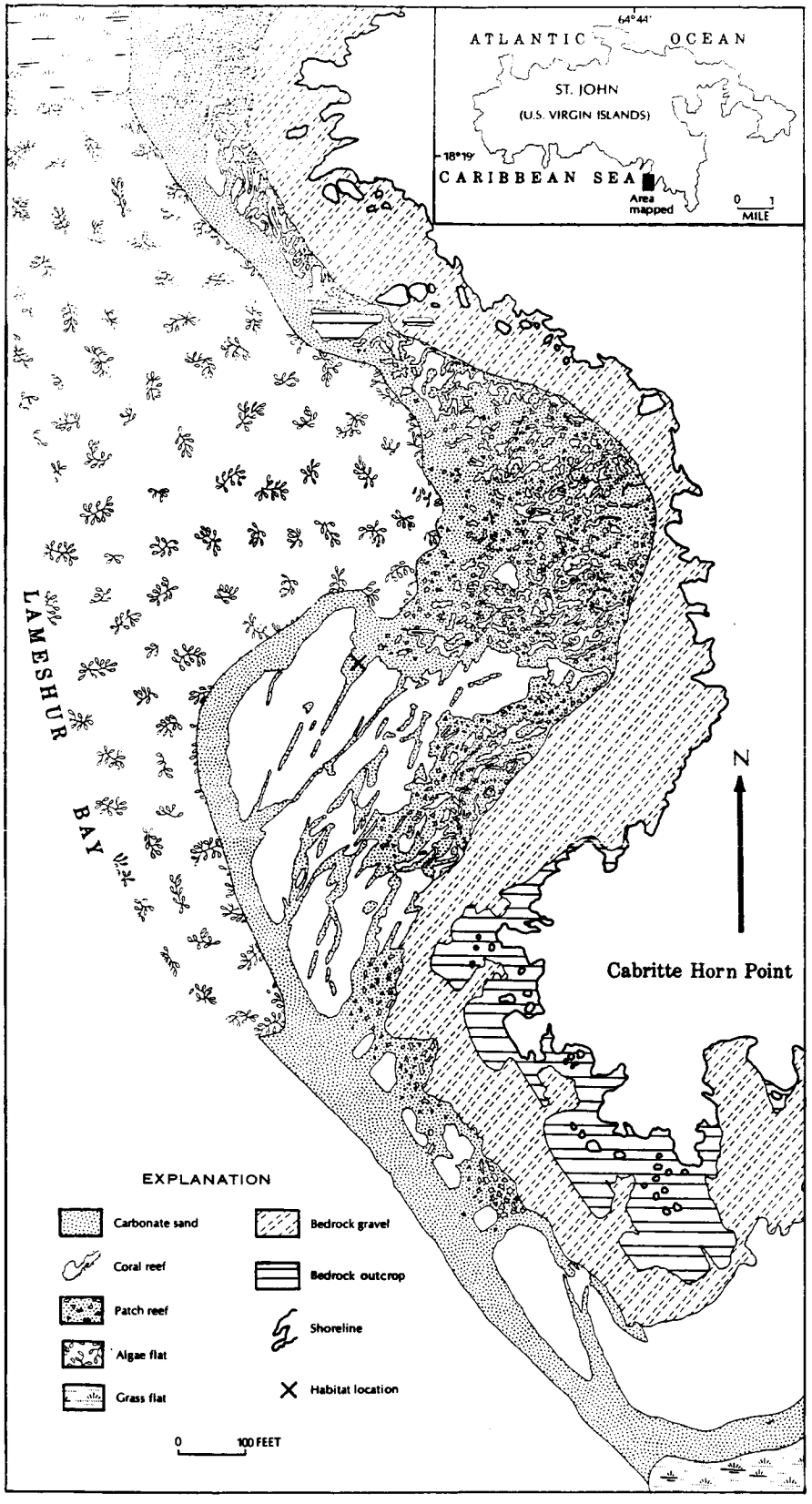

Figure 5.- Sedimentary facies in the vicinity of the Tektite habitat (from Clifton et al., 1970). Clifton used aerial photographs including that shown as figure 4 to make this map of bottom types.

Figure 6.- South San Francisco Bay during winter conditions of high discharge from the Sacramento-San Joaquin River system (view north, January 28, 1970). A plume of turbid, low-salinity water has advanced about 10 km into the south bay. The light-blue color is due to the large amount of suspended sediment in the water. San Francisco is at left center and Oakland at right center. Infrared color photo taken with a hand-held 35 mm camera from an altitude of 6000 ft.

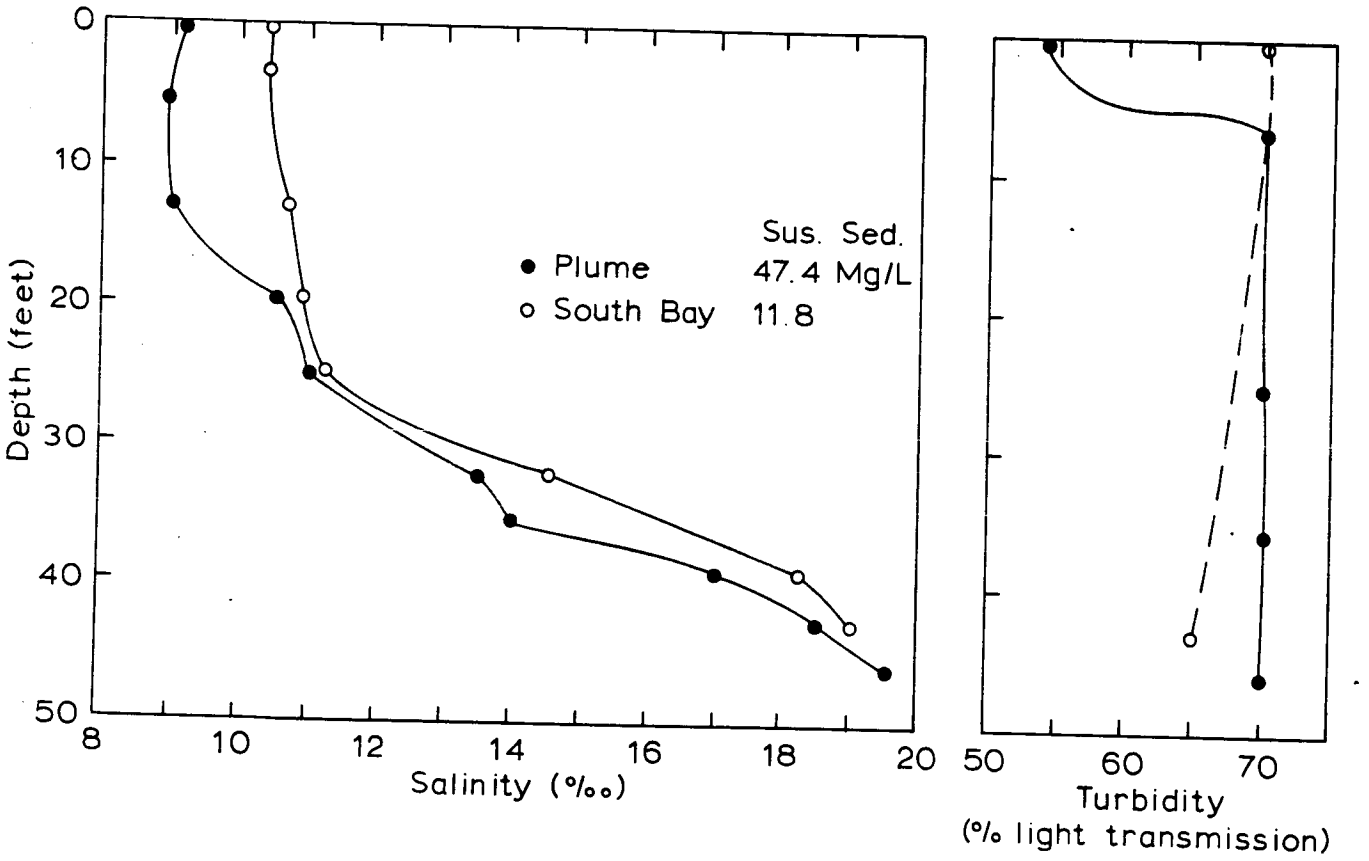

Figure 7.- Vertical salinity and transmissometer casts within and in front of the plume shown in figure 6. Suspended sediment values in milligrams per liter from water samples collected at approximately 1-meter depth.

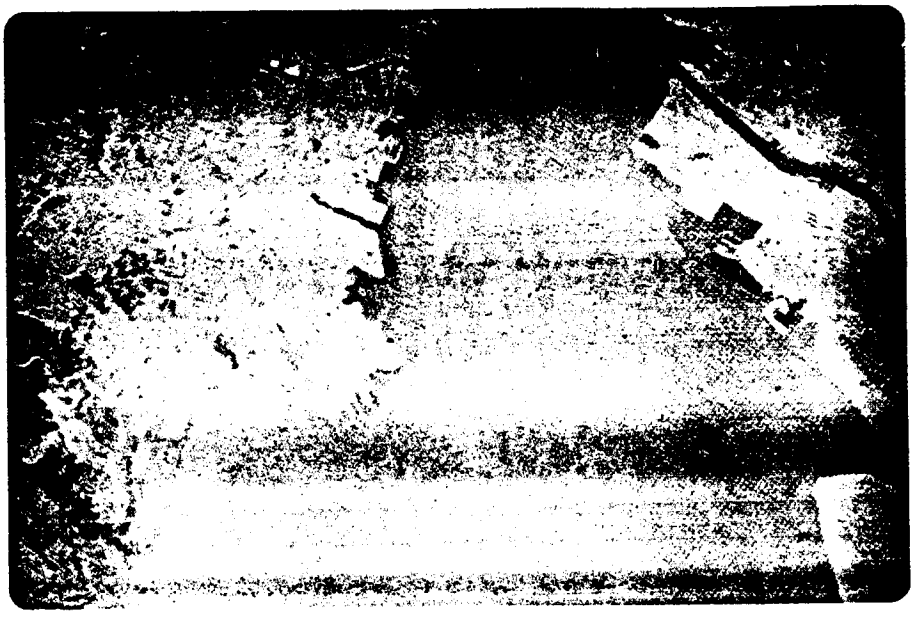

Figure 8.- South San Francisco Bay during summer conditions of low discharge from the Sacramento-San Joaquin River system (North is toward the upper right corner). Plume is much less distinct than during high discharge, and the lighter blue color indicating larger amounts of suspended particulate matter is south of the plume front, the reverse of the winter flow situation (figure 6). San Francisco Peninsula on left. NASA Mission 100, Test site 48, IR color photo, altitude 60,000 ft., RC-8 camera.

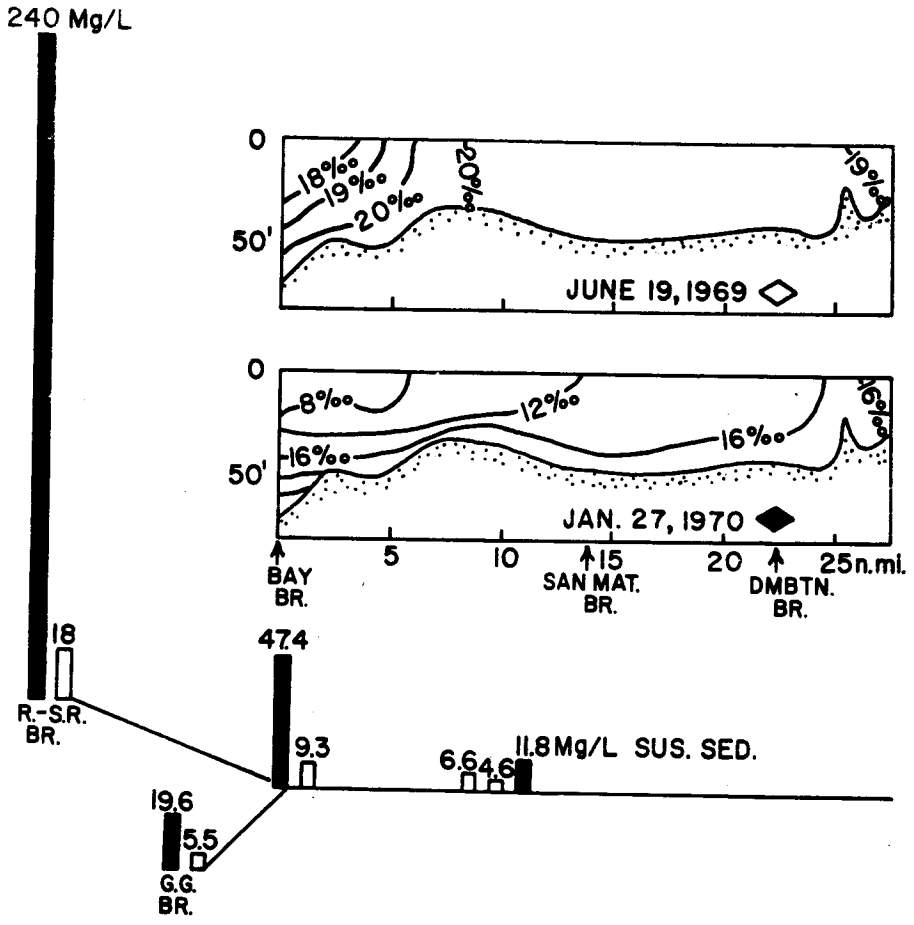

Figure 9.- Comparison of summer and winter salinity and suspended sediment distributions in south San Francisco Bay. Salinity is shown by parts per thousand (o/oo) contours on the two profiles. Suspended sediment is indicated in milligrams per liter (Mg/L) by the vertical bars: solid bars represent data collected Jan. 27, 1970, and open bars data of June 19, 1969: The distance scale for suspended sediment is the same as that for the salinity profiles. Locations listed are the main bridges crossing San Francisco Bay: R. - S.R. Br. = Richmond - San Rafael Bridge; G.G. Br. = Golden Gate Bridge; Bay Br. = San Francisco-Oakland Bay Bridge; San Mat. Br. = San Mateo Bridge; and Dmbtn. Br. = Dumbarton Bridge.

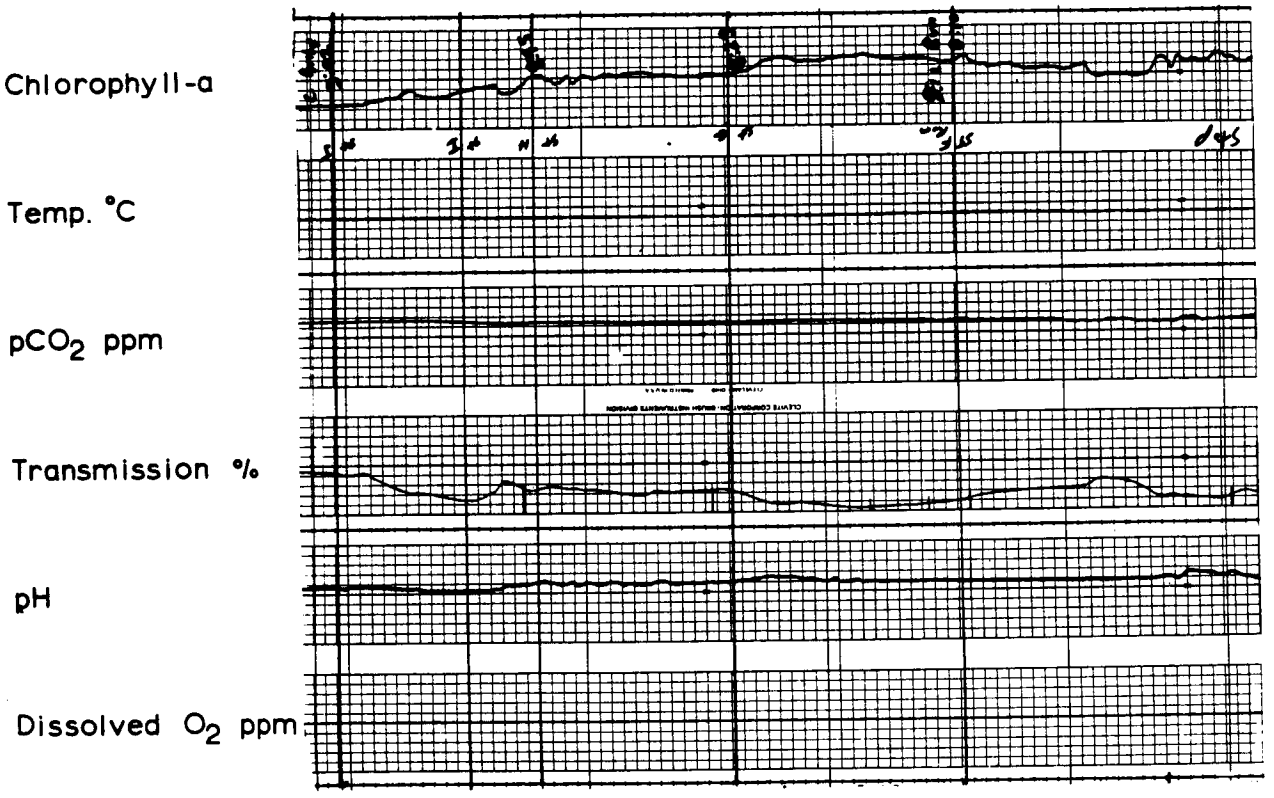

Figure 10.- Horizontal profile of continuously monitored water characteristics at one meter depth through Carquinez Strait. Profile runs from east (right) 0745 hrs. to west 0902 hrs.

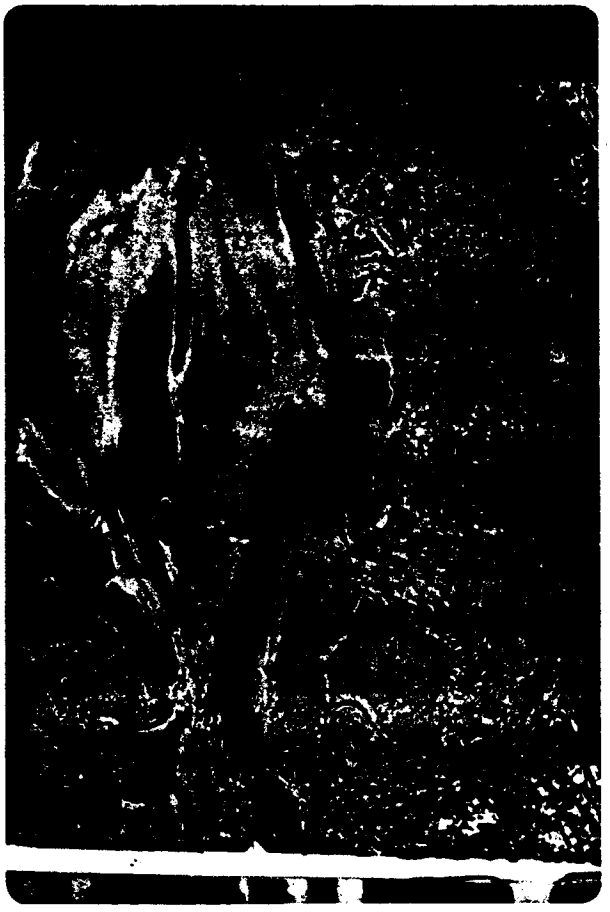

Figure 11.- False color density slice composite of south San Francisco Bay. San Francisco Peninsula on left. Prepared by International Imaging Systems from a USAF black and white, high altitude photo (>60,000 ft).

RELATIONSHIP BETWEEN VEGETATION REFLECTANCE SPECTRA AND SOIL GEOCHEMISTRY: NEW DATA FROM CATHEART MOUNTAIN, MAINE*

by

F. C. Canney
U.S. Geological Survey
Denver, Colorado

and

Sondra Wenderoth, and Edward Yost
Long Island University
Greenvale, New York

ABSTRACT

Studies in 1968 at Catheart Mountain, Maine (where a copper molybdenum deposit is concealed beneath soil on a forested mountainside), suggested that measurement of the spectral reflectance of vegetation might be a useful tool in exploration for concealed mineral deposits from aircraft and, possibly, from spacecraft. The spectral-reflectance curves for red spruce and balsam fir in the 350- to 1100-nanometer region showed differences between specimens growing over and away from the mineral deposit. However, the inferences that could be drawn from the data were limited by the small number of samples (19) and the relatively large variance of the spectroradiometric data. Thus, when improved instrumentation became available in 1969, the experiment was repeated on a larger sample group (15 anomalous spruce, 9 background spruce, 10 anomalous fir, and 10 background fir). Measurements of copper and molybdenum contents in the supporting soil were used to categorize the trees as anomalous or background.

Analyses using parametric and nonparametric statistical tests were performed to establish whether significant differences existed between the anomalous and background groups. At the 95-percent confidence level, significant differences were found to exist for both species, generally in the chlorophyll band centered at about 550 nanometers and in the region from 700 to 900 nanometers. In general, these results confirmed the 1968 study but at a much higher level of confidence.

---

*Publication authorized by the Director, U.S. Geological Survey

INTRODUCTION

The basic long-range objective of our work is to attempt to develop more efficient ways of prospecting for mineral deposits. Traditional prospecting methods, wherein geologists roam across the countryside and examine rocks visible at the surface, can no longer be expected to produce many important mineral discoveries. Most areas of the world amenable to this way of prospecting have been examined repeatedly by several generations of prospectors. However, in large areas of the world, rocks favorable for the occurrence of ore lie concealed beneath a mantle of soil. It is in such areas that many important ore discoveries have been made by utilizing the newer geochemical and geophysical techniques. For example, the discovery of an area of soils abnormally rich in metals--a geochemical anomaly--furnishes a strong clue to the possible presence of a nearby concealed mineral deposit. But to find such geochemical anomalies on the ground requires painstaking and expensive ground surveys. We simply have to develop cheaper techniques of finding such anomalous zones by appropriate sensors mounted on aircraft or space platforms if the world's needs for an increased supply of critical minerals are to be met.

At the last program review I reported on the feasibility of using the reflectance spectra of trees to detect such soil anomalies. Interrelationships between a tree and its environment are complex, and many parameters affect plant health, growth, and trace-element composition; the geological environment is one of the more important environmental parameters. In recent years, it has occurred to a number of individuals that trees growing in an abnormally metal-rich soil should be in a stressed condition and that this stressed condition and, hopefully, the cause of the stress--a mineral deposit--could be detected by analysis of vegetation spectra.

PREVIOUS WORK

Two years ago the U.S. Geological Survey and the Science and Engineering Group of Long Island University under Prof. Edward Yost collaborated in a feasibility study on this supposition. The site used to test the hypothesis was Catheart Mountain, Maine, where a copper-molybdenum deposit is largely concealed beneath soil on a completely forested mountainside. The soils contain anomalous amounts of metal, mostly copper and molybdenum, and these metals, especially molybdenum, are also concentrated in the trees.

As I reported last year, the reflectance spectra of balsam fir and red spruce trees were measured by placing a spectroradiometer on a "cherry-picker" to get the instruments above the tree level and thus look at the tree as an aerial camera or scanner would see it. Simultaneous measurements of reflected and incident radiation were obtained. The results indicated that a difference existed between the spectra of balsam fir and red spruce growing in soils with anomalous copper-molybdenum contents and the same species growing in soils of normal metal contents. However, although the differences noted were highly encouraging, we could not claim, in general, that they were significant at the 95-percent confidence level. This was due principally to the small number of samples used--(19)--and by the relatively large variance of the data in the 750- to 1100-nanometer region.

Thus, when improved equipment became available the following year it seemed advisable to repeat the experiment on a larger sample group. This was done in August 1969.

1969 FIELD WORK

The equipment employed for measuring incident and reflected radiation in the near-ultraviolet, the visible, and the near-infrared portions of the spectrum was modified considerably for the second test. A truck equipped with a 36-foot periscope tower replaced the cherry-picker, both reflectance spectroradiometers were located within the truck, and the data were recorded automatically on paper tape. The use of this truck greatly increased the efficiency of the operation because, as the upper mirror could be angularly adjusted and the entire tower itself could be rotated, five to ten trees could generally be scanned from one setup.

Two incident spectrometers were set up in a clear area close to the equipment van. These instruments were calibrated separately, and the resultant data were then averaged and treated as one reading.

All reflectance measurements consisted of three scans per target; each scan included 27 data points of three readings each measured at every 25 nanometers from 350 to 750 nanometers and at every 50 nanometers from 750 to 1250 nanometers. At the start of each day the reflectance spectroradiometers were calibrated against a white diffusing plate. Also, because a cooled detector was used, the precision of the infrared measurements was much better in 1969 than in 1968.

Great care was taken in the experiment that several important variables did not influence the data appreciably. Measurements were

made in fully illuminated areas of the tree, and extraneous reflectance from background objects such as other trees, patches of ground, or dead branches was kept minimized by careful selection of the tree area to be measured.

Samples of soil at the base of each tree, as well as samples of tree needles, were collected and chemically analyzed. The division of trees into background and anomalous groups was made on the basis of the metal content of the soil. In this second experiment, 44 trees were measured--15 anomalous spruce, 9 background spruce, 10 anomalous fir, and 10 background fir. The average directional reflectance spectra of each of the 44 trees was computed from the in situ measurements of incident and reflected radiation using the calibrated reflectance standard.

RESULTS

These data were analyzed for significant differences between tree groups using both parametric and nonparametric statistical tests. I am glad to be able to report that differences again appeared between anomalous and background groups, and that this time the differences were generally significant at the 95-percent confidence level.

Figure 1 shows data for red spruce and balsam fir. For red spruce the obvious increase in spectral reflectance of the anomalous group in the visible part of the spectrum (400-700 nanometers) and decrease in the infrared (IR) part of the spectrum (700-1100 nanometers) is evident. The black band at the top shows where the differences are significant. In 1968 our data revealed the decrease in the infrared for the anomalous group but not the increase in the visible. In 1968, however, our anomalous group was growing in soil only slightly anomalous in metal in contrast to the 1969 group. The increase at about 550 nanometers probably indicates a lower chlorophyll content in the needles of the anomalous group caused by the effect of the abnormal chemical environment on the metabolism of the trees. The decrease in IR reflectance undoubtedly reflects some alteration in the mesophyll cell structure.

For balsam fir you note the anomalous group is more highly reflective in both the visible and IR. This is also what we found in 1968 although at a lower level of significance. For balsam fir, as for spruce, the higher reflection in the visible is probably indicating an incipient chloratic condition, although the anomalous trees appeared quite healthy to the eye. Why anomalous fir should show an enhanced IR

reflectance whereas anomalous spruce shows a decrease is most interesting, but we have no good explanation at the moment. One of us (FCC), however, plans to make some studies of needle-cell structure and these may provide some clues.

In order to determine to what extent the soil geochemistry was related to the reflectance spectra, a multiple regression analysis was performed for both tree species using the soil mineralization as the independent variable and the reflectance spectra as the dependent variable. These data are shown in table 1. You can see that, in general, balsam fir shows the greatest multiple correlation between all elements and the reflectance spectra--about 0.8 at a number of wavelengths. The coefficients of red spruce show the same general relationship between soil geochemistry and spectra although the values of these coefficients are somewhat less.

The correlations between reflectance data and metal content in the plant tissue itself have not as yet been studied in detail, but I thought these data (fig. 2) worth showing. You will note the rather good relationship between molybdenum content and reflectance; the copper points, on the other hand, are rather erratically distributed. One may speculate that, at least for balsam fir at Catheart Mountain, molybdenum may be the more important element affecting reflectance.

Of course, in these complex natural environments, it is really quite difficult to evaluate the influence on reflectance of any one element. To do this I think it will be necessary to go to controlled greenhouse studies, and the Geological Survey has plans to get such studies underway very soon.

FUTURE PLANS

Where do we go from here? Obviously, after the successful second Catheart ground experiment, aerial experiments were indicated and these were done the last week in August by the Michigan aircraft. We were plagued by bad weather and could not fly all scheduled lines and runs, but the more important ones were successfully flown. I have not yet received any data from this mission. Provided the results of the Michigan flight are encouraging, the Catheart site will be suggested for an ERTS-type experiment because the size of the anomalous area is about a mile square.

Additional Catheart-type ground experiments for different metals and vegetation species in different geological environments should be

done. A group in the Geological Survey has, in fact, just completed last week one such study in the Front Range in Colorado. There the reflectance of Pinus Ponderosa in the near IR was found to be significantly greater for sites of high copper content--in the 800-1,900 ppm range in the soil--than for sites of low copper content--40-170 ppm.

The Geological Survey also has plans to study a site in the Republic of Panama where a copper-molybdenum deposit occurs in a tropical rain-forest environment.

Repetitive coverage of one or more sites is sorely needed to ascertain changes in reflectance during a growing season. It seems that this could be accomplished easily from ERTS, and such an experiment will be proposed.

In conclusion, I am still highly optimistic that continuation of research in this field will ultimately result in a dramatic new way of prospecting for mineral deposits from aircraft or space platforms.

TABLE I.- CORRELATION OF REFLECTANCE WITH TRACE-ELEMENT CONTENT OF SOIL

WAVE LENGTH (nm)	MULTIPLE CORRELATION COEFFICIENT	
	RED SPRUCE	BALSAM FIR
380	0.688	0.777
400	0.738	0.769
425	0.719	0.790
450	0.718	0.800
475	0.717	0.782
500	0.726	0.778
525	0.706	0.828
550	0.680	0.823
575	0.705	0.822
600	0.646	0.810
625	0.650	0.813
650	0.663	0.818
675	0.726	0.348
700	0.667	0.432
725	0.690	0.776
750	0.587	0.839
800	0.651	0.816
850	0.640	0.819
900	0.423	0.833
950	0.703	0.737
1000	0.719	0.765
1050	0.676	0.739
1100	0.510	0.786

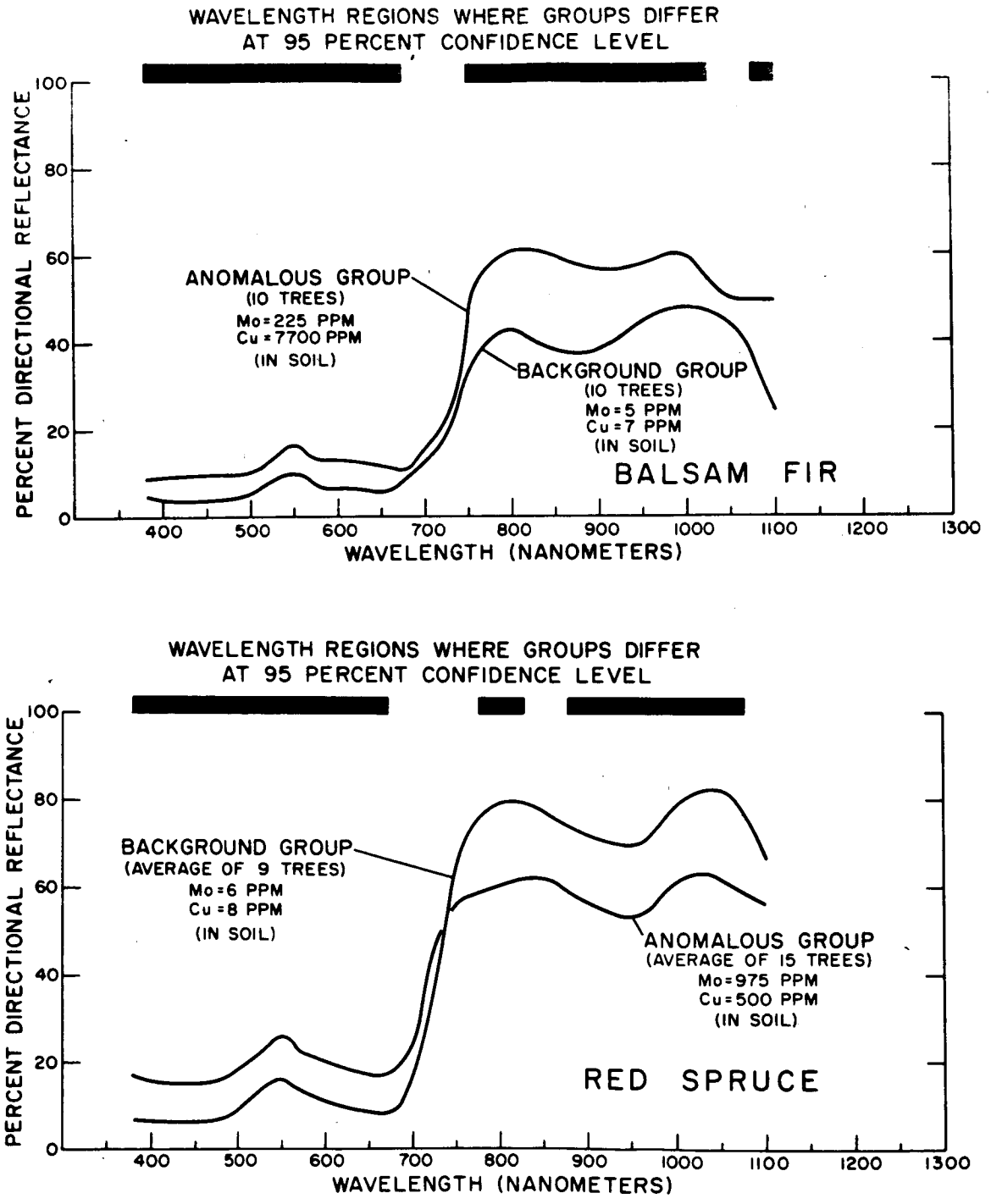

Figure 1.- Reflectance of balsam fir and red spruce

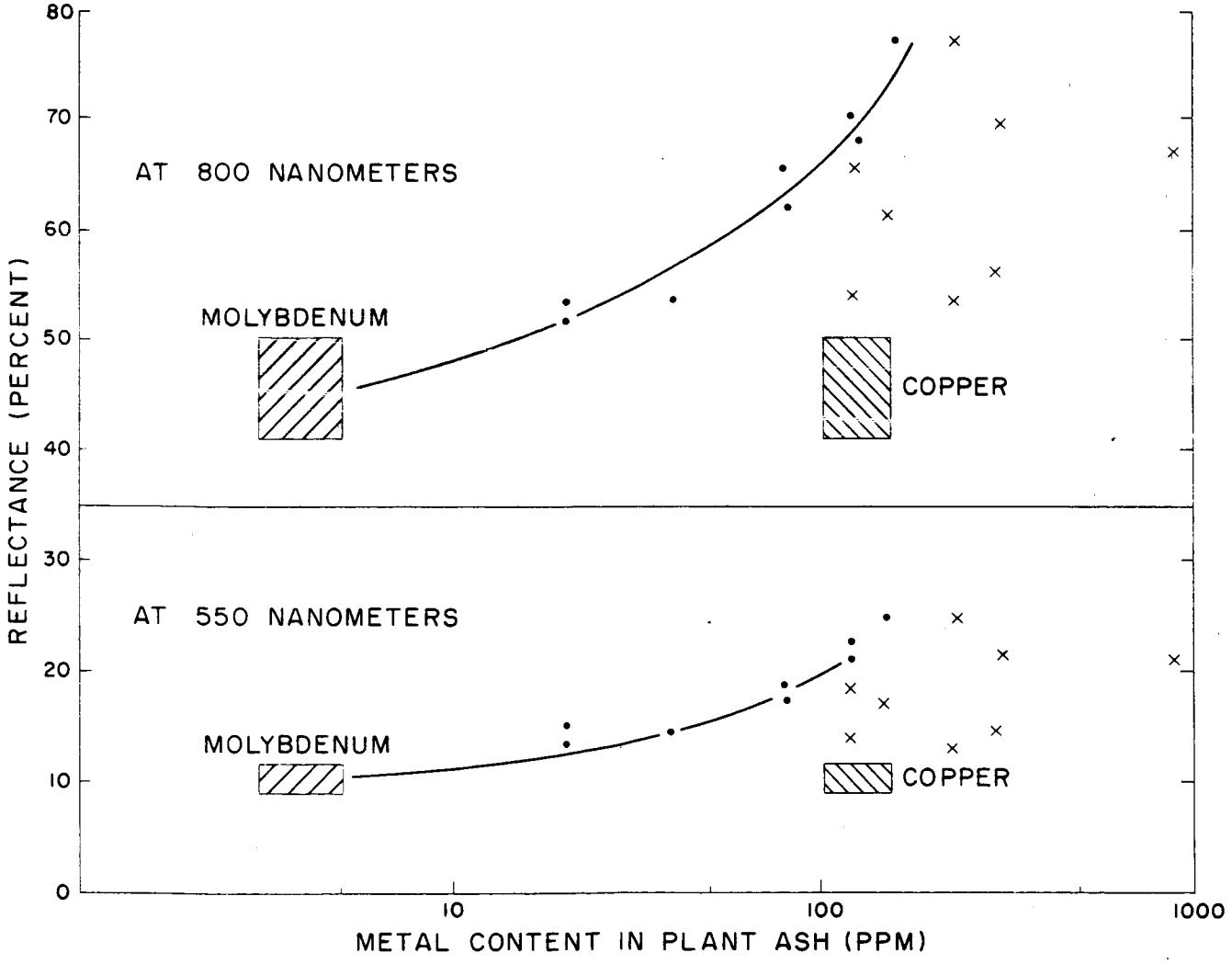

Figure 2.--Relationship between molybdenum (solid dot) and copper (X) contents of balsam fir needles and directional reflectance at 550 and 800 nanometers.

GROUND TRUTH VS. NO GROUND TRUTH

by

Grover B. Torbert
Bureau of Land Management
Department of the Interior
Washington, D. C.

INTRODUCTION

The Bureau of Land Management was created by a merger of the General Land Office and the Grazing Service in 1947. It manages approximately 450 million acres of public domain lands, and the leasing for minerals on the Outer Continental Shelf, and is one of the major revenue producing agencies of the Federal Government.

The basic program of disposing of the public domain lands, which aided in the development of the country in its early history is no longer applicable under the heavy demands on lands by today's public. The program today in the BLM is one of applying multiple use principals in order to obtain the maximum benefit for the greatest number of the public. Because of the greater awareness of problems of pollution by the general public, all resource programs in the Bureau are being more carefully reviewed to include environmental statements to assure a minimal change in the ecology which would result when harvesting the natural resources.

Where there is such a great difference in the character of lands, from semi-tropical islands (omitted lands of Florida), deserts, mountains, heavily forested coastal areas, and arctic slopes, there is also a great diversity of natural resources and management techniques. The Bureau's responsibility in resource management cuts across the broad spectrum of all natural resources.

METHOD OF ANALYSIS

The area of study was the southeastern Arizona test site, and within the test site three specific areas were studied in detail, Safford Area, Point of Pines Area, and Fort Apache-White River Area. The three specific areas are of great contrast from flat arid areas to high alpine mountains.

Data was obtained from the Apollo 9 photographic missions, high altitude aerial photography, and simulated ERTS-A data from high altitude aircraft. Various monoscopic and stereoscopic devices were used to analyze the features, and machines such as the microdensitometer were used to study film density variation. The Giannini additive color viewer was also used. However, no "ground truth" was permitted the contractor.

A complete detailed description of the method is contained in the report "Application of Space and High Altitude Photography to Interior Department Functions," by Raytheon/Autometric.

Thematic maps were prepared for the various disciplines--geology, geomorphology vegetation, hydrology, and soils. Interpreted boundaries were delineated. No collaborative data was used in the interpretation. However, both the BIA and BLM gathered "ground truth" during the overflight of high altitude aerial photography.

After the first report was completed and accepted a further study was made using the "ground truth," obtained by the agencies and a field trip by the contractor. A second report entitled "Ground Observations and Utility Evaluations of Space and High Altitude Photography" is to be published on this phase of work and will be available in the near future.

RESULTS

These studies proved conclusively that certain responsibilities of the Department of the Interior could be executed by use of ERTS A type data. It is possible to monitor gross features of the vigor of crop lands and vegetative cover, type soils, classify geological features, and determine hydrological condition.

Although no new thematic maps were prepared after visits to the test site, the data gathered on the ground was compared with the original mapping. A conservative estimate shows that 80 to 85% of the interpretation in the areas checked were correct and small shifts in the location of boundaries would result in a greater percentage of correct mapping.

Vegetative cover, crops, and soils types were generalized because of the scale of the imagery. Such generalization is necessary when mapping at a scale 1:250,000. As many as 12 to 15 variations in soils texture were observed in a ten-mile stretch, and in an isolated area rock outcrops in a grassland area were interpreted as scrub oak or brush. This type of mistake may have been avoided had the interpreter been familiar with the areas or if a greater resolution imagery had been available.

The geological features interpretated from the imagery were more detailed than that shown on the geological maps of the area.

The mistakes in the hydrological mapping were due primarily to trying to map stream courses monoscopically. It is suggested that stereoscopic imagery be used when possible.

There is a definite relationship between vegetation vigor and ground moisture content. This is of great interest to our range land managers.

Cultural features, such as, fence lines, towns, villages, roads (in high contrast areas) were interpreted easiest from the red band of the electro-magnetic spectrum.

CONCLUSIONS

The two studies, one detailed with maps and tables showing the extent of each resource, and the second a summary of the utilization of ground observations, show that a knowledge of an area is a quality to be desired when interpreting an area.

A better study could have been performed had funds been available to remap the area completely after the "ground truth" was observed.

Although it was shown that repetitive cover was of value, this value of repetitive coverage could have been strengthened if all 8 flights had been usable and received on time. The studies did not allow for an inquiry into the effect of the lack of correlation between ground observations and over flights. There is need for more and better communications between the flights and ground observer if this factor is to be usable in the future.

Because of the high percentage of correctly interpreted features, it should be possible to extrapolate much of the known data on resources, over large areas of BLM responsibility. This does not repeat not imply, suggest, nor recommend the discontinuing of "Ground Truth." We know the more intelligence we have the better will be any interpretation.

BLM FUTURE PLANS

A proposal is being prepared for submission to the "Water Resources Working Group," the EROS Program, to delineate the limits of high and low water lines along the southwest coast of Florida. These two boundary lines are indicators of the limits of BLM's responsibility for omitted lands and the leasing on the Outer Continental Shelf. This project is of interest to the State of Florida and National Ocean Surveys, formerly USG&GS.

A REVIEW OF APPLICATION STUDIES ON INDIAN LANDS USING NASA AEROSPACE IMAGERY

by

Arthur M. Woll
Bureau of Indian Affairs
Department of the Interior
Washington, D.C.

INTRODUCTION

The American Indian lands are receiving a lot of attention in remote sensing, through the EROS and NASA programs. We have recently completed the report by Raytheon, "Applications of Space and High Altitude Photography to Interior Department Functions." Much of the area studied is Indian country (Figure 1). The sketch shows that a large amount of the area in eastern Arizona belongs to the Indians.

We have three ongoing remote sensing projects on three different Indian Reservations. On the Fort Apache Reservation, we are conducting a multiband thermal and "false color" sensing of an Englemann Spruce beetle infestation on Mount Baldy, adjacent to a U. S. Forest Service proposed wilderness area. On the San Carlos Reservation, we have a joint project by USGS, EROS, and the San Carlos Tribe. This is an intensive examination of a circular topographic feature, noted by W. Douglas Carter, USGS, on the Apollo 9 imagery. On the Papago Reservation, Doeringsfeld, Amuedo and Ivey, Petroleum, Mineral and Engineering Geologists of Denver, Colorado, have an EROS funded contract to provide the Papago Tribe with a report showing potential mineral areas, by comparing and correlating space imagery with high-resolution imagery and aeromagnetic data.

FORT APACHE

On the Fort Apache Reservation, the basic objective for collecting the thermal imagery is to assist in the control of the beetle, by detection of sick trees during the first year of the beetle's life cycle. The foliage of an infested tree during this period does not exhibit any discoloration, so that the only practical means of detection by remote sensing is to scan the hot, sick trees that appear to have a 4 to 5 degree centigrade temperature. Effective control measures, such as logging or burning of trap trees, require the elimination of infested hot spots during this first year of the cycle.

Efforts in obtaining the necessary thermal data have met with several difficulties. We started with a NASA mission request early in 1970. The first request was denied, but was given reconsideration when a resubmission expanded the test area, and justified the uniqueness of this project, as compared to a thermal sensing beetle study, which the U. S. Forest Service is conducting in the Black Hills. On August 24, we were notified that the request was being processed; but we have not received a schedule date. Then, Herbert E. Skibitzke, of USGS Water Resources Division in Prescott, Arizona, attempted to obtain the data by flying a Survey aircraft, but was not successful. The last resort - only partially successful - was the use of the Bendix scanner in an Intermountain Aviation Inc. aircraft. On November 5, they flew the test area, but had a malfunction with the thermal scanner. We are presently examining the results of a November 16 reflight.

The success of this project is dependent on receiving timely data. Once the data are received, we plan to use a visual densitometer on the transparencies to extract the thermal data, in advance of running the magnetic tape through the computer for image characteristic analysis. Mr. Morrison of the Bell Aerospace Company in Tucson, has been our advisor on the instrumentation system, data conversion system and needed computer facilities. Upon receiving information from a successful analysis, the Bureau will lay out a series of trap trees situated within the infested hot spots, to destroy as many beetles as possible. With early detection and successful analysis, we feel that a control program can be developed to save these 40,000 acres of Englemann Spruce from the ravages of this insect.

SAN CARLOS

On the San Carlos Reservation, there is a circular topographic feature first recognized on the Apollo 9 imagery (Figure 2). The Bureau of Indian Affairs and the San Carlos Tribe are interested in the formation, especially as to its water and mineral resource possibilities. The feature is about 4 miles in diameter and is cut on the west side by two tangent lineaments bearing N20W and N50W, respectively. Both lineaments are represented by warmer valleys and the N50W extending valley contains the Dry Lake Reservoir. After a brief field examination in June 1970, a joint study by the USGS, EROS, the San Carlos Tribe and the BIA was started that developed detailed geologic mapping, supported by airborne and ground-based geophysical surveys.

Two men conducted a 2-week field mapping program to better define the surface geology, structure, and stratigraphy of the area. The high-altitude imagery, large-scale aerial photographs, and topographic maps at a scale of 1:24,000 were used.

The aeromagnetic survey included approximately 400 line miles at 1/2-mile spacing. A gravity survey was conducted on foot to support the aeromagnetic work. The lunar rover vehicle was tested as to its magnetometer's utility on subsurface formations. As of the middle of November, all the field work had been completed and the gravity and magnetic data are being compiled. January 1 is the target date for the report.

Preliminary results indicate that: (1) there is a magnetic high in the area; and (2) no evidence of mineralization was encountered in the geologic mapping.

This project is a fine example of remote sensing - of imagery at small scale, with poor resolution, being used as a management tool to define a limited area, where an intensive resource inventory could be conducted. The EROS program was the mechanism by which the expertise and financial support of several agencies were joined together in an excellent effort. The land owner, in this case the San Carlos Indians, will benefit from this investigation for possible water or mineral resources.

PAPAGO

The third reservation with action is the Papago. The main objective of this project is to test the utility of small-scale aerospace imagery (Apollo 6 and 9, and high-altitude photography from NASA test site 4) for mineral exploration, when used in conjunction with large-scale imagery and aeromagnetic data. The Papago Reservation has limited mineral development within its boundaries, but is surrounded by many open pit copper mines, such as the Ajo, Silver Bell, Mission, Pima, and Twin Buttes. The Indians have accumulated a large quantity of geophysical data, because several exploration firms have worked the reservations, and as a requirement of their leases, given the Indians their raw data. With this large amount of ground and aerospace data available, there is a great opportunity to develop target areas with mineral deposits.

The contractor, Doeringsfeld, Amuedo and Ivey, will prepare stereo geophysical maps for two different aeromagnetic surveys of the area. The mineralization target areas will be based on intrusive masses, zones of hydrothermal alteration, and aeromagnetic lineaments. The contract calls for a final report by June 1971, with a confidential supplement to the Papago Tribe, indicating high-potential target areas. The Tribe, in turn, may use these findings to obtain higher mineral leasing rates from interested exploration firms.

Again, this project uses the synoptic overview of aerospace imagery to control large quantities of raw data that have not been adequately compiled or correlated to date.

A review of these on-going projects brings us to a subject on which the Mineral and Land Resources Working Group (EROS program) is concentrating effort at the present time. That is, the design of a comprehensive management information system for natural resources, using remote sensing as a management tool to control the data and information in place.

The information requirements in Agencies today with their PPB systems (or PPE, as it is more properly called, for Planning, Programming, and Evaluation) and the realization that ERTS-A will give us a large amount of real time data, dictate that we find an effective system to convert this raw data into meaningful and usable information. We, therefore, are developing an operational demonstration of a resource information system using the latest aerospace technology. Again, eastern Arizona will be our work area. We will start at the top with in-place regional and gross data from high-altitude aircraft and spacecraft.

In our target areas, for example the forest, we will concentrate our multidiscipline sampling in problem and high-potential areas. For the first attempt, we can use existing data, both remote sensing and ground data, to locate these areas and define our data need to complete the system. This approach will require the land manager to accept the concept that a great portion of the forest is significantly similar in content and management needs, so that a rather simple data bank, with updating by real time, in-place data, will fill his information needs. This will replace many of the old concepts, such as: (1) The more data we collect, the better the information; (2) Collect the same data on all forest stands; or (3) We cannot give the administrator or manager the information until it's proven 110% correct, and this may require a resurvey of the entire forest.

We are presently preparing an RFP to contract for the development of an operational demonstration of a resource information system that will give the manager information useful in handling the practical problems of management.

The Bureau (BIA) and the Indians look to the EROS and NASA programs to help them with their natural resource problems. We are pleased to see the eastern Arizona, south Florida and Dakota multidiscipline test sites in Indian country, and look forward to a great deal more remote sensing action.

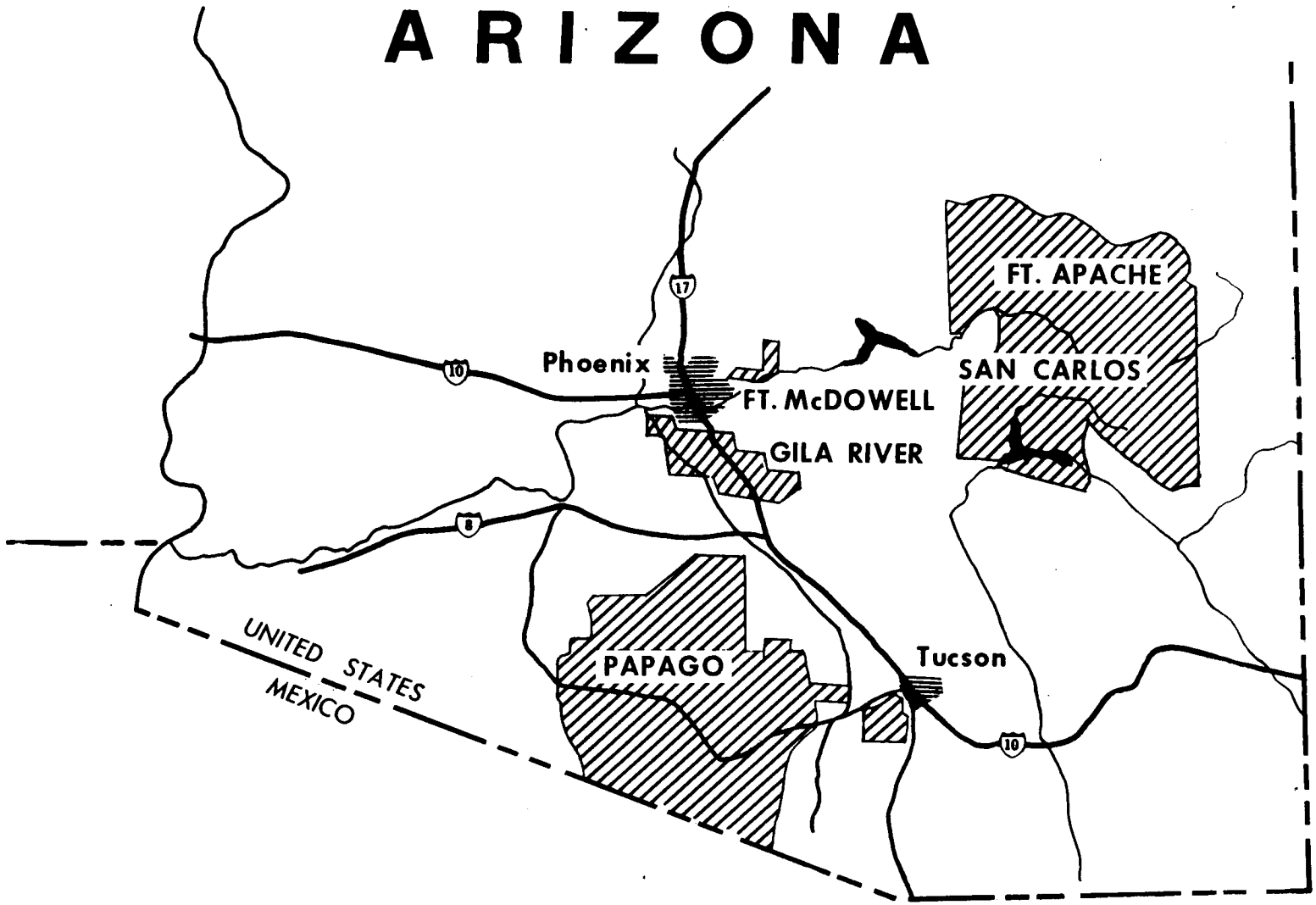

Figure 1. Indian lands in eastern Arizona.

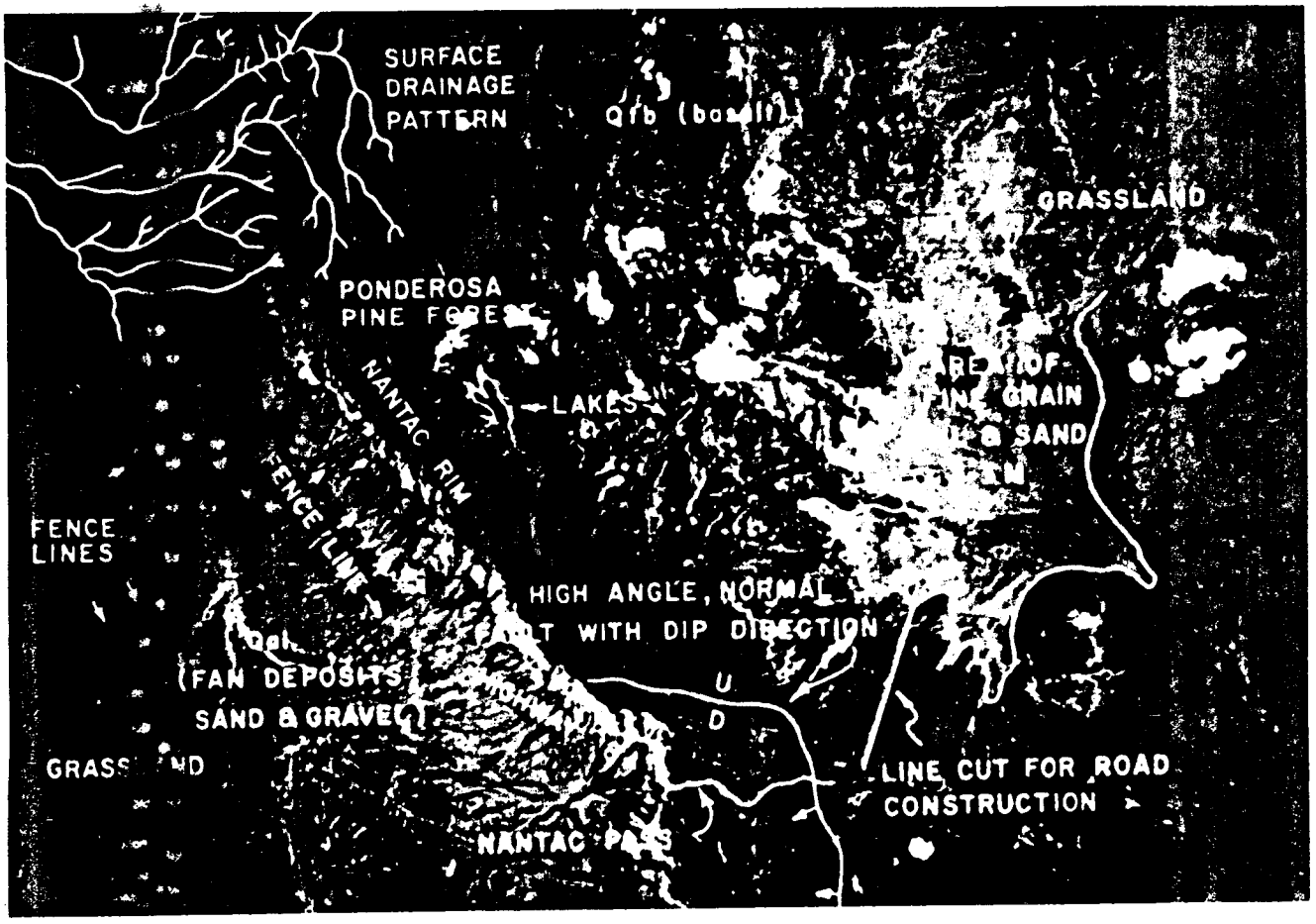

Figure 2. - Interpretations of Remote Sensor Imagery

Point of Pines (Nantac Rim) Area, San Carlos Indian Reservation, Arizona